(NASA-CR-155566) EVALUATION OF STOL NAVIGATION AVIONICS Final Technical Report (Santa Clara Univ.) 276 p HC A13/MF A01 CSCL 01D
N78-17051
Unclas
G3/06 02520

ELECTRICAL ENGINEERING AND COMPUTER SCIENCE

THE UNIVERSITY OF SANTA CLARA

FINAL TECHNICAL REPORT

NASA Grant NGR 05-017-031

Evaluation of STOL Navigation Avionics

December 1, 1977

PREFACE

This final technical report covers work performed under NASA-Ames Grant NGR 05-017-031, Evaluation of STOL Navigation Avionics.

Inquiries regarding the contents of this report should be directed to:

Dr. W. R. Dunn, Principal Investigator
c/o Department of Electrical Engineering & Computer Science
University of Santa Clara
Santa Clara, California 95053

TABLE OF CONTENTS

I. INTRODUCTION AND SUMMARY

The following summarize the research projects undertaken on NASA Grant NGR 05-017-031. Detailed research results are presented in Sections II through V.

PROJECT: Application of Vector Magnetometer to Aircraft Control and Navigation.

INVESTIGATORS: W. R. Dunn and R. Pietila

Recent technological improvements and corresponding cost reductions in 3-axis (i.e., vector) magnetometry led to investigation by Ames and University of Santa Clara researchers into use of this device in avionics flight control and navigation applications. Early analytical work showed that vector magnetometer outputs could be used to determine aircraft change provided that one attitude angle was known. These results were confirmed by successful correlation of attitude computed from magnetometer data taken during a NASA Convair 880 test with actual aircraft attitude. To demonstrate the viability and uncover the limitations of the theory, development of a solid state remote magnetic indicator was undertaken. The effort involved development of a microprocessor based system employing a 3-axis magnetometer and evaluation of the system using test apparatus constructed at the University. The background and results of this work are described in detail in Section II of this report. Results of the research were also published in [1] and [2].

PROJECT: Application of Earth Electric Field Phenomena to Aircraft Control and Navigation.

INVESTIGATORS: W. R. Dunn, C. Keller, W. Keller, R. Wilson, R. Yarbrough

Hill's [3] late 1972 paper on use of the earth's electric field in flight control prompted NASA and University researchers to undertake investigation of earth field applications to large aircraft control and navigation.

The principle underlying Hill's work is the fact that in clear weather, the earth's surface terminates a large (approximately 300v/m at the surface) electric field which is close to the local vertical. Hill then successfully demonstrated that airborne (RPV) measurements of this field could be used to provide pitch/roll control.

University investigations were undertaken to evaluate the use of this phenomena in bad (e.g. IFR) weather conditions. The principal finding of this investigation was that this field (direction) can be significantly altered in and near cloud structures particularly the cumulonimbus cloud structure. Section III provides a review of the basic earth electric field phenomena and develops the basic field model for the cumulonimbus structure. The basic conclusion of this work is that the variability of the effects of the cumulonimbus on the clear weather electric field made navigational use of this field in all flight conditions a highly unreliable proposition. It is further proposed that electric field measurements might possibly better serve in a low cost system for identifying the direction and change intensity of cumulonimbus clouds during flight.

PROJECT: Electronic Aircraft Cabin Noise Suppression

INVESTIGATORS: W. R. Dunn and W. Keller

Section IV describes an extension of Olson's [4] pioneering work in the use of active compensation as a means of reducing acoustic noise. This extended work provides a theoretical basis on which wide band acoustic noise can be significantly reduced in aircraft cabins.

PROJECT: SIRU (Strapdown Inertial Reference Unit) Technical Support.

INVESTIGATORS: W. R. Dunn, W. Keller, C. Keller

University researchers worked with government and (government) contractor personnel in the installation and checkout of the Carco motion simulator facility developed for use in the SIRU program. This effort consisted of Carco table orthogonality measurements, adjustment and calibration of recording electronics, and specification of Carco Table/Sigma 7 computer interface.

Section II

Aircraft Attitude Measurement
Using a Vector Magnetometer

PRECEDING PAGE BLANK NOT FILMED

TABLE OF CONTENTS

Table of Contents (Continued)

CHAPTER I

A VECTOR AUTOPILOT SYSTEM

1-1 INTRODUCTION

An essential requirement of an aircraft attitude control system is that deviation of the body axes relative to a reference axes frame must be sensed. In addition, to overcome the ever-present possibility of errors or failure of the sensors, various configurations of redundant sensors are usually employed to assist in detection and correction of errors. To this end, there has been a continuing effort to improve existing sensors, to develop new sensor configurations, and to develop new sensor devices.

This chapter discusses the role of a vector magnetometer[1] as a new instrument for aircraft attitude determination. Although magnetometers have played a role in the attitude measurement of missiles and satellites [Ref. 1-1], there is an apparent lack of application in aircraft systems. By providing independent measures of attitude, the solid state vector magetometer sensor system can not only assist in improving accuracy and reliability of existing systems but can also reduce component count with obvious benefits in weight and cost. Additionally, since a large number of aircraft heading reference systems depend on measurement of the Earth's magnetic field, it can be shown that by substituting a three-axis magnetometer for the remote sensing unit; both heading and attitude measurement functions can be derived using common elements, thereby further reducing the component count.

---

[1]Aviation use to date has been essentially scalar magnetometry.

To investigate the feasibility of the above system, this chapter will proceed by developing a technique to determine attitude given magnetic field components. Sample calculations are then made using the Earth's magnetic field data acquired during actual flight conditions. Results of these calculations are compared graphically with measured attitude data acquired simultaneously with the magnetic data. The role and possible implementation of various reference angles are discussed along with other pertinent considerations. Finally, it is concluded that the Earth's magnetic field as measured by modern vector magnetometers can play a significant role in attitude control systems.

1-2 ATTITUDE DETERMINATION

Coordinate systems are usually defined by orthogonal right-handed sets of three unit vectors. An example of such a set is illustrated in Fig. 1-1 where the orientation of the body fixed frame used in this paper is delineated. Angular rotations are conventionally defined as rotations in the plane normal to a unit vector with the positive sense of rotation defined by the right-hand rule [Ref. 1-2].

To derive relationships of attitude variations as a function of magnetic vector component variation, we can proceed by considering matrix representations of an orthogonal transformation. If Hx, Hy, and Hz are the magnetic components measured at a desired airframe attitude and Hx', Hy', and Hz' are the components measured after any rotation of the body, vector $H' = [Hx' \; Hy' \; Hz']^T$ can be related to vector $H = [Hx \; Hy \; Hz]^T$ by an orthogonal linear transformation $H' = AH$. Here A must satisfy the orthogonality condition $AA^T = I$, where A^T is the transpose of A; additionally, the determinant of A must be unity [Ref. 1-3, 1-4].

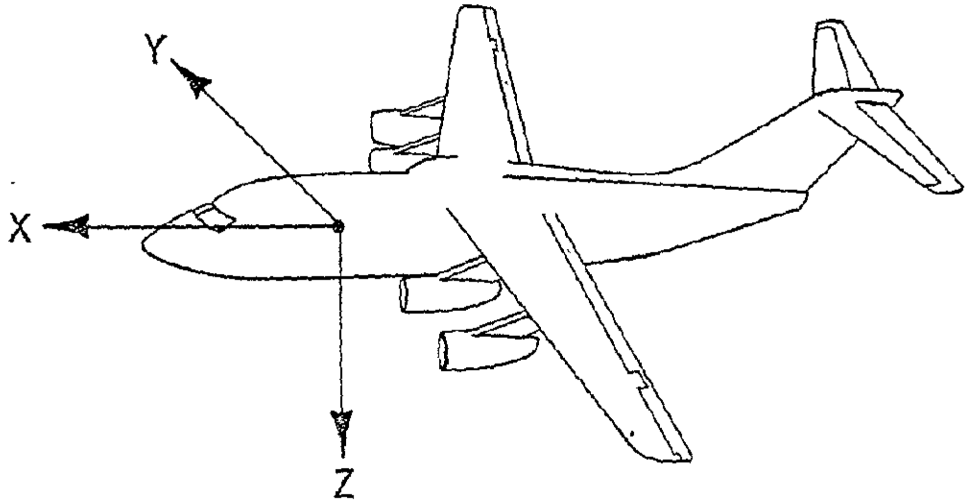

Fig. 1-1 AXIS ORIENTATION

Rotations about the z axis in Fig. 1-1 result in yaw deviations (ψ) and in new components (H'), as shown by

$$\begin{bmatrix} Hx' \\ Hy' \\ Hz' \end{bmatrix} = \begin{bmatrix} \cos\psi & \sin\psi & 0 \\ -\sin\psi & \cos\psi & 0 \\ 0 & 0 & 1 \end{bmatrix} \begin{bmatrix} Hx \\ Hy \\ Hz \end{bmatrix} \tag{1-1}$$

Similarly, independent rotations about the y axis and the x axis result in pitch (θ) and roll (ϕ) dependent variations in the measured H components, as shown by

$$\begin{bmatrix} Hx' \\ Hy' \\ Hz' \end{bmatrix} = \begin{bmatrix} \cos\theta & 0 & -\sin\theta \\ 0 & 1 & 0 \\ \sin\theta & 0 & \cos\theta \end{bmatrix} \begin{bmatrix} Hx \\ Hy \\ Hz \end{bmatrix} \quad (1\text{-}2)$$

$$\begin{bmatrix} Hz' \\ Hy' \\ Hz' \end{bmatrix} = \begin{bmatrix} 1 & 0 & 0 \\ 0 & \cos\phi & \sin\phi \\ 0 & -\sin\phi & \cos\phi \end{bmatrix} \begin{bmatrix} Hx \\ Hy \\ Hz \end{bmatrix} \quad (1\text{-}3)$$

The effect of a combined rotation can be expressed by using the product of the transformation matrices. In addition, if the rotations are small, the total rotation experienced by applying sequential rotations is independent of the order in which the rotations are performed [Ref. 1-3,1-4].

$$\begin{bmatrix} Hx' \\ Hy' \\ Hz' \end{bmatrix} = \begin{bmatrix} \cos\psi & \sin\psi & 0 \\ -\sin\psi & \cos\psi & 0 \\ 0 & 0 & 1 \end{bmatrix} \begin{bmatrix} \cos\theta & 0 & -\sin\theta \\ 0 & 1 & 0 \\ \sin\theta & 0 & \cos\theta \end{bmatrix} \begin{bmatrix} 1 & 0 & 0 \\ 0 & \cos\phi & \sin\phi \\ 0 & -\sin\phi & \cos\phi \end{bmatrix} \begin{bmatrix} Hx \\ Hy \\ Hz \end{bmatrix} \quad (1\text{-}4a)$$

$$\begin{bmatrix} Hx' \\ Hy' \\ Hz' \end{bmatrix} = \begin{bmatrix} \cos\psi\cos\theta & \sin\psi\cos\phi + \sin\theta\cos\psi\sin\theta & \sin\phi\sin\psi - \sin\theta\cos\psi\cos\phi \\ -\sin\psi\cos\theta & \cos\psi\cos\phi - \sin\phi\sin\psi\sin\theta & \cos\psi\sin\phi + \sin\psi\sin\theta\cos\phi \\ \sin\theta & -\cos\theta\sin\phi & \cos\phi\cos\theta \end{bmatrix} \begin{bmatrix} Hz \\ Hy \\ Hz \end{bmatrix} \quad (1\text{-}4b)$$

Assume that the angular variations θ, ψ, and ϕ are small enough so that the small angle approximations

$$\sin\theta \approx \theta,\ \sin\psi \approx \psi,\ \sin\phi \approx \phi,$$
$$\cos\theta \approx \cos\psi \approx \cos\phi \approx 1$$

can be made. Then, if the products of small angles (in radians) can be assumed to be much smaller than the angles alone, the expression reduces to

$$\begin{bmatrix} Hx' \\ Hy' \\ Hz' \end{bmatrix} = \begin{bmatrix} 1 & \psi & -\theta \\ -\psi & 1 & \phi \\ \theta & -\phi & 1 \end{bmatrix} \begin{bmatrix} Hx \\ Hy \\ Hz \end{bmatrix} \tag{1-5}$$

Further modifications in the form of the matrices result in

$$\begin{bmatrix} Hx' \\ Hy' \\ Hz' \end{bmatrix} = \begin{bmatrix} -Hz & Hy & 0 \\ 0 & -Hx & Hz \\ Hx & 0 & -Hy \end{bmatrix} \begin{bmatrix} \theta \\ \psi \\ \phi \end{bmatrix} + \begin{bmatrix} Hx \\ Hy \\ Hz \end{bmatrix} \tag{1-6}$$

By subtracting, we arrive at an expression for the difference in H components as functions of angular deviation.

$$\begin{bmatrix} Hx' \\ Hy' \\ Hz' \end{bmatrix} - \begin{bmatrix} Hz \\ Hy \\ Hz \end{bmatrix} = \begin{bmatrix} \Delta Hx \\ \Delta Hy \\ \Delta Hz \end{bmatrix} = \begin{bmatrix} -Hz & Hy & 0 \\ 0 & -Hx & Hz \\ Hx & 0 & -Hy \end{bmatrix} \begin{bmatrix} \theta \\ \psi \\ \phi \end{bmatrix} \tag{1-7}$$

It is significant to note at this point that the transformation matrix is singular implying that solutions for θ, ψ, and ϕ are not independently available.

1-3 ATTITUDE DETERMINATION EMPLOYING MAGNETIC FIELD COMPONENTS

A given orthogonal set of three unit vectors can be displaced in Euclidean space by rotating the system through any angle δ about a directed rotation axis. It is also customary to represent this rotation vectorially as a directed line segment whose length is proportional to the rotation angle. This rotation is analogous to the rotation experienced by the body fixed frame of Fig. 1-1 as the aircraft experiences combined pitch, yaw, and roll variation. During flight the body fixed set rotates about this rotation axis assuming new (possibly erroneous) attitudes in space. The task of the attitude sensing system is to provide measures of compounded pitch, yaw, and roll that would result in the same attitude assuming that the rotations occurred sequentially about the x, y and z axes rather than the actual rotation axis.

It was shown in the previous section that a compounded rotation of an orthogonal set can be described by a product of respective transformation matrices. Additionally it was noted that for small angular rotations the order of multiplication is unimportant. Using the relationships of (1-7), expressions for the angular deviations in terms of measured magnetic vector components can be derived.

$$\Delta Hx = -Hz\theta + Hy\psi \qquad (1\text{-}8a)$$

yields

$$\theta = (Hy\psi - \Delta Hx)/Hz \qquad (1\text{-}8b)$$

$$\psi = (\Delta Hx + Hz\theta)/Hy \qquad (1\text{-}8c)$$

Similarly,

$$\Delta Hy = -Hx\psi + Hz\phi \qquad (1\text{-}9a)$$

yields

$$\psi = (Hz\phi - \Delta Hy)/Hx \qquad (1\text{-}9b)$$

$$\theta = (\Delta Hy + Hx\psi)/Hz \qquad (1\text{-}9c)$$

and

$$\Delta Hz = Hx\theta - Hy\phi \qquad (1\text{-}10a)$$

yields

$$\theta = (\Delta Hz + Hy\phi)/Hx \qquad (1\text{-}10b)$$

$$\phi = (Hx\theta - \Delta Hz)/Hy \qquad (1\text{-}10c)$$

Assuming that Hx, Hy and Hz are nominal vector components as measured in a reference attitude and that Hx', Hy' and Hz' are new field components at the new attitude, then $\Delta Hx = Hx' - Hx$, $\Delta Hy = Hy' - Hy$, $\Delta Hz = Hz' - Hz$ are expressions of the incremental changes in field components. Additionally, before using (1-8), (1-9) or (1-10) to solve for attitude variations (pitch, yaw, or roll), one additional angle from an auxiliary sensor[2] must be supplied. Using one additional angle of rotation (about any one axis) the remaining two rotations can then be calculated.

To illustrate this point, flight data acquired during the flight of a NASA flown Convair 900 instrumented with a three-axis magnetometer and a Litton inertial navigation system were used to calculate roll, pitch, and yaw.

---

[2]It was noted following (1-7) that a unique solution for attitude variation is not possible using magnetic field data alone.

Attitude variation about each of the three axes was calculated using measured magnetic field components supported by one angle from the inertial system. The results of these calculations are plotted in Figs. 1-2 through 1-4.

It is significant to note that the rotations shown occurred simultaneously (i.e., time base is the same for all three figures). The flight was at an altitude of approximately 5000 ft at an airspeed of approximately 250 nmi/h.

Although the data used to plot the attitudes shown in Figs. 1-2 through 1-4 were not acquired specifically for this purpose, the correlations in measured and calculated attitude clearly show that, within the limits of instrument accuracy, signals proportional to attitude variation can be derived using flight data.

1-4 A POSSIBLE SYSTEM CONFIGURATION

Since the intent of this chapter is to introduce the notion that magnetometer technology has advanced to the point where three-axis magnetometers can be incorporated in aircraft attitude sensing systems on a cost effective basis, the system discussion will be limited in scope to describing a possible combined heading and attitude measurement method.

Heading references fall into three classes; 1) those that depend on the Earth's magnetic field, 2) those that depend on the use of low-drift gyroscope to retain a preset azimuth, and 3) those (gyrocompasses) that depend on sensing the Earth's rotation [Ref.1-5]. By far the greatest number of aircraft heading systems depend on the Earth's magnetic field, although many of these include gyroscopes to improve the performance characteristics.

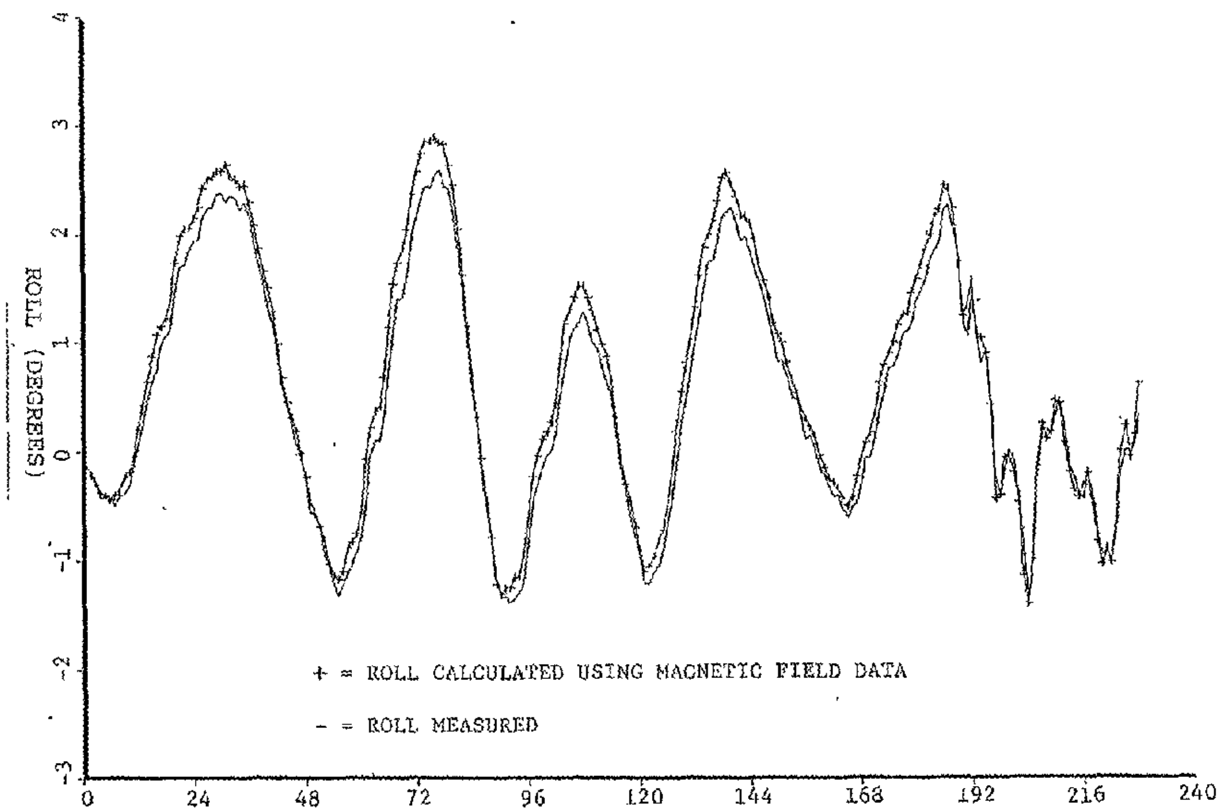

FIGURE 1-2 ROLL AXIS

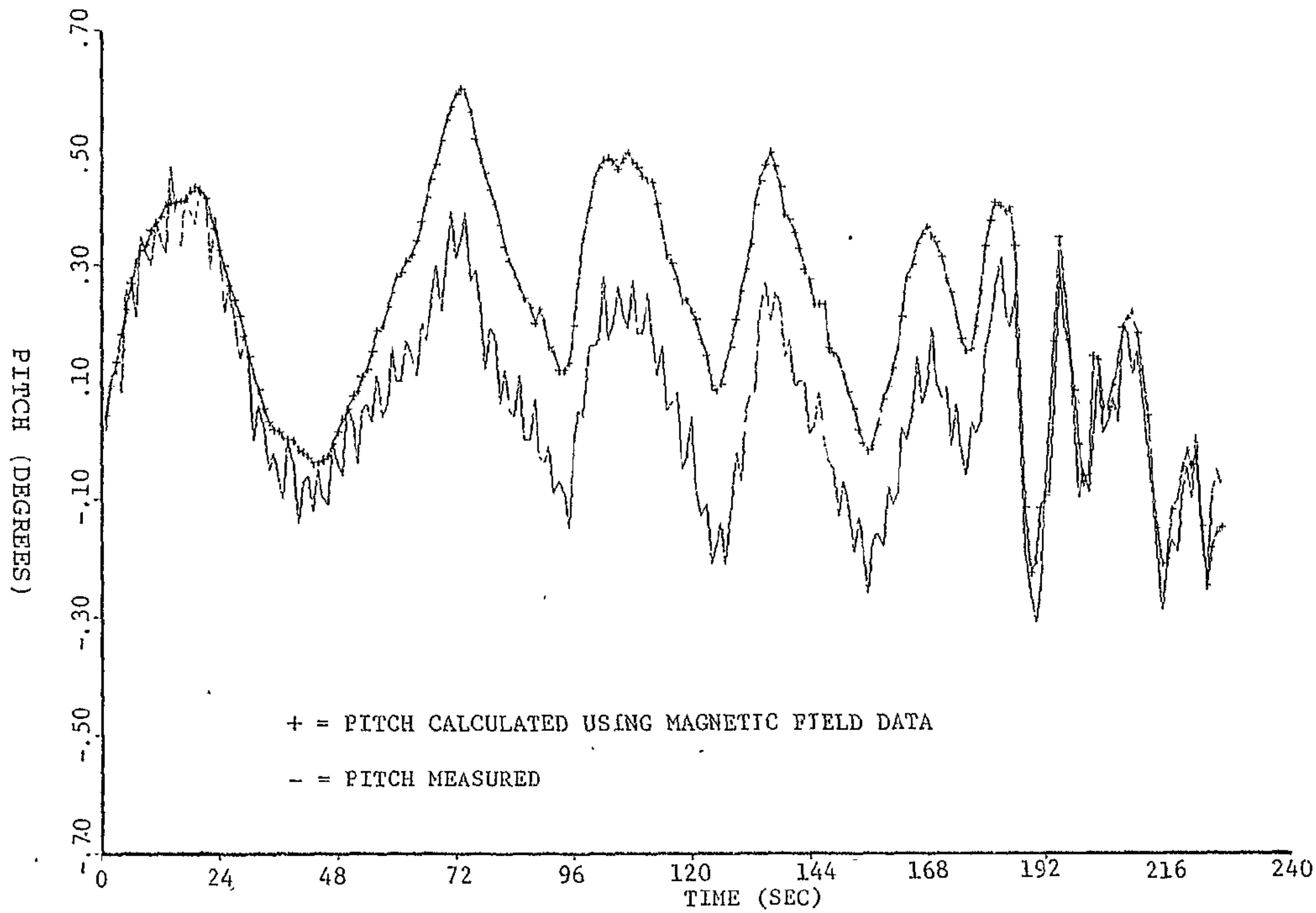

FIGURE 1-3 PITCH AXIS

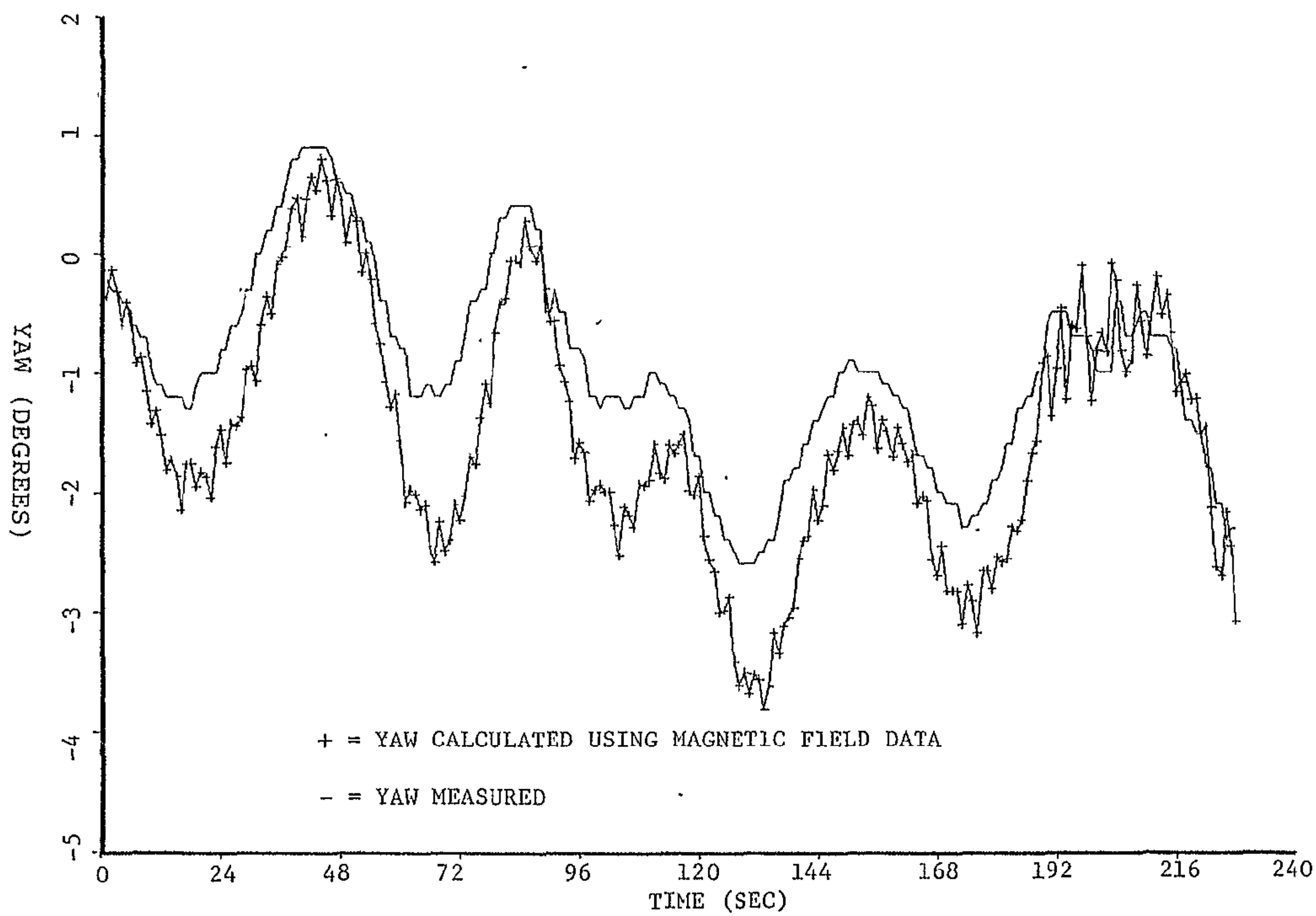

FIGURE 1-4 YAW AXIS

A popular system combination (with no gyro) is to combine a pendulous remote magnetic sensor and a synchro receiver in a null seeking circuit. The philosophy being to attempt to measure only the horizontal component of the Earth's magnetic field and to swing the receiver into alignment with it. Under acceleration, departures of the sensor unit from the horizontal result in angular heading errors ε [Ref. 1-5].

$$\varepsilon = (aH/g) \tan\gamma \sin\theta$$

where aH is the horizontal acceleration, g is the acceleration due to gravity, θ is the angle between the acceleration vector and magnetic north, and γ is the magnetic field dip angle; arctan (vertical field/horizontal field).

Accuracy of this system can be improved by incorporating a strapped-down solid state magnetic sensing unit (free of acceleration errors) that measures and displays the angle of the Earth's horizontal magnetic component relative to the aircraft. This system can be implemented as follows:

1) Determine the direction of the magnetic vector F relative to the sensors (and the airframe), by measuring the x, y and z components (Figs. 1-1 and 1-5). The direction cosines $\cos\alpha$, $\cos\beta$, $\cos\gamma$ are the cosines of the angles α, β, γ between the magnetic vector and the positive x, y and z axes. Additionally,

$$\cos\alpha = x/(x^2 + y^2 + z^2)^{\frac{1}{2}}$$

$$\cos\beta = y/(x^2 + y^2 + z^2)^{\frac{1}{2}}$$

$$\cos\gamma = z/(x^2 + y^2 + z^2)^{\frac{1}{2}}$$

2) Using either a vertical reference[3] or knowledge of aircraft attitude, we can effectively rotate the body axes such that the x-y plane is horizontal (see Chapter II).

3) Simple application of direction cosines will yield the direction of magnetic north in the aircraft's x-y plane.

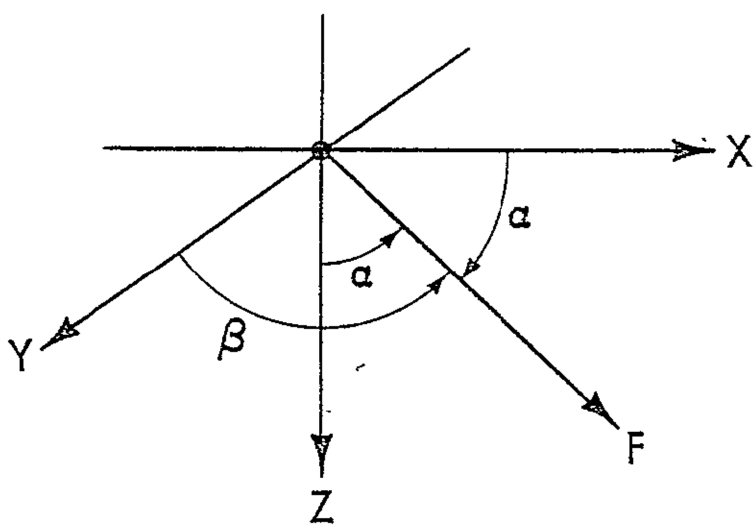

Fig. 1-5 FIELD VECTORS AND DIRECTION COSINES

Although the preceding discussion implies that heading can be determined by using a strapped-down magnetometer, there remains the problem of attitude determination. Another widely used system for obtaining a heading reference

[3]Not necessarily derived inertially [Ref. 1-11].

is to combine the relatively excellent short term stability of a directional gyroscope with the long term stability of magnetic field measurements. By slaving the directional gyroscope to the magnetic field [Ref. 1-5, sec. 10.4.7], gyroscopes with relatively large free drift error can be used to provide an excellent heading reference.

Replacement of the pendulous remote sensing unit of this type of system with a strapped-down vector magnetometer would result in both heading and attitude information on a continuous basis. This combination would operate as follows:

1) The system is initialized by determining a reference attitude (perhaps by using a primary inertial attitude system).

2) The angular position of the horizontal magnetic field component is computed as above and used to slave the directional gyroscope.

3) The directional gyroscope, with relatively good short term stability (devices with free drift of less than 0.5 deg/h have been designed), is used to determine yaw (ψ) errors.

4) For small angle deviations, (1-8), and (1-9), and (1-10) can be employed to recalculate aircraft attitude. The process loops back to step 2) closing the loop on a combined attitude and heading reference system.

The sampling frequency required to maintain an acceptable level of error is of course determined by the aircraft performance expected (angular rates) and by the gyro error (drift rate plus errors due to additional sources such as gyroscope tilt from vertical). The overall system is such that heading can be determined as before with errors due to sensor departures from horizontal substituted for long term accumulation of attitude uncertainty (this can be corrected by looping to step 1) at a frequency dependent on error rates). Additionally one gains measurements of attitude with minimal computation and replacement of a mechanical remote sensing unit with a solid state strapped-down magnetometer sensor.

1-5 OTHER CONSIDERATIONS

The characteristics of the Earth's magnetic field and its variations have long been established [Ref. 1-6-1-10]. Since the field is to be used as a reference in the attitude measurement scheme, there is a need here to discuss its adverse characteristics. Although the field does experience variation, most of the variation is either in amplitude (ionospheric contributions) or has time constants that make the variation negligible (secular variation).

In traversing local anomalies, there will, however, be deflections in the ambient field due to the additive effect of local dipoles or monopoles. The effect of local terrain caused anomalies can be visualized by picturing the main field vector oriented in space with a second modulating vector rotating at its tip. Maximum angular error would occur when this modulating vector has maximum magnitude and is positioned at right angles to the main vector.

To illustrate the effect of local anomalies one can calculate the level of anomaly required to cause an error. Since the Earth's main field is typically in the order of 0.50 G it is readily apparent that a local anomaly of approximately 0.01 G at right angles to the local field is required to cause an error of 1 deg. Furthermore, the local anomaly would have to be aligned with one of the aircraft body axes to result in one degree of attitude error in any one axis. Fortunately, anomalies with components of this magnitude positioned at right angles to the main field are extremely rare. In addition, the anomalies are localized over ore bodies or other geophysical irregularities, have magnitudes that diminish as the cube of altitude, and tend to average to zero over relatively short distances. In summary, the probability of encountering an anomaly that would cause as much as a 1 degree error is relatively small. The error, if introduced, will be short lived and, unlike drift error, will average to zero.

Fundamental to a magnetic field referenced system is the ability to measure orthogonal components of the field vector. Precision and accuracy of measurement of the components is of course specified by the desired control specifications.

Since the Earth's magnetic field varies in magnitude on a global basis between 0.3 G and 0.6 G (30,000 gamma to 60,000 gamma), it is apparent that full scale measurements of 0.6 G can be expected. Sensors mounted at right angles to the field will monitor no measureable field and thus define the lower limit of measurement to be zero. For the continental United States the declination varies between 60 and 80 deg, resulting in a range in horizontal component of 0.15 to 0.25 G with vertical component in the range of 0.4 to 0.55 G. Heading variations (yaw) result in changes of the horizontally sensed field components and would specify the maximum precision required. In addition, flight at 45 deg ± (n x 90 deg) (where n is any whole number) with respect to magnetic north results in minimum sensitivity of the x and y axes measurements. In this case sensor inputs would range between 0.106 and 0.177 G with minimum field at the north. Assuming the preceding ambient measurements, variations in component magnitude of approximately 0.0180 to 0.0305 G/deg for small angle variations can be expected.

A brief survey of commercial magnetometer manufacturers reveals that triaxial magnetometers that measure from zero to 0.6 G with linearities of 0.5 percent, noise less than ±1 mG and sensitivies of at least 2.5 V per 600 mG are currently available. In addition, these devices have a bandwidth of direct current to at least 500 Hz and are rated to have less than 1 deg error in orthogonality.

From a precision standpoint, it is apparent that variations in yaw for this worst case situation can be sensed to better than 0.1 deg with currently available magnetometer technology. The sensor technology required to implement an attitude sensing system of reasonable specifications is available (more detailed analysis is presented in Chapter III).

Although the preceding calculations indicate that for small angular variations attitude can be calculated using measured magnetic data, there is a need to consider the effects of larger finite rotations. In this case the small angle assumptions would not be valid and an Euler transformation would have to be made. Measurement of three axes of field components could be used to develop the direction cosines required to determine the orientation of the axis of rotation, the angular rotation about it, and the three angular rotations of pitch, roll, and yaw.

For the special case where the axis of rotation aligns with the magnetic vector, there would of course be no measured component changes.[4] By measuring the attitude of a second vector (not in alignment with the magnetic vector), we could resolve the ambiguous situation cited above and provide additional redundancy.

The optimum auxiliary vector would be one that could be sensed without using inertial devices. The Earth's electric field can be considered. The main reason for considering this field as a means of providing an auxiliary angular reference is that the resultant system has the potential of being completely solid state. The electric field vector can be used to determine attitude variation in a manner analogous to the magnetic vector system. Inherent limitations of each single vector system can be obviated if the vectors are not coincident.

Although Hill [Ref. 1-11] reported success in controlling pitch and roll using the electrostatic field alone, comments by Markson [Ref. 1-12] indicate that the electrostatic field is not always a reliable vertical reference. Employment of the electrostatic field for this attitude measurement system is limited to augmenting the magnetic field measurements by eliminating ambiguity of motion around the magnetic vector. The requirement of vertical electrostatic field is thus removed and replaced by a requirement that the field direction is relatively stable.

By using two independently derived vectors we have sufficient data to obviate the ambiguity just cited and we have the potential of providing redundancy as well.

---

[4]An example of this would be yaw rotation while flying straight and level over the magnetic poles or roll rotation while flying towards a pole at the magnetic equator.

1-6 CONCLUSION

This chapter has identified a novel method of measuring aircraft attitude using relatively inexpensive, well developed instrumentation. It has recognized that magnetic field sensing systems have been used to some extent in attitude sensing and control of space vehicles; it has also suggested, however, that with appropriate support, magnetometers can find increased application in aircraft attitude measurement systems.

This claim is corroborated by actual flight test data. Magnetometers have evolved to a point where three axis measurements of the Earth's magnetic field can be made with sufficient precision and accuracy to enable measurement of small angle attitude variations.

This chapter has also discussed a possible system configuration combining heading determination and attitude measurement functions. By replacing the conventional remote sensing unit with a three-axis magnetometer, it has been suggested that both functions can be obtained with the hardware required previously for heading measurement alone.

As with any system, there are limitations imposed. The main limitation for a vector magnetometer system seems to be the inability to sense rotations around the magnetic vector itself. This problem is not unlike the ambiguity experienced by magnetic heading systems at high latitudes. By judiciously incorporating auxiliary instruments, not only can the ambiguities be removed but a degree of redundancy can be added while still maintaining a cost and weight advantage over comparable systems.

CHAPTER II

AN ATTITUDE INDEPENDENT REMOTE MAGNETIC INDICATOR

2-1 INTRODUCTION

Preliminary investigation [Ref.2-1] revealed that aircraft attitude can be calculated using measurements of earth's magnetic field vector and a single auxiliary rotation angle. An algorithm to compute the two remaining aircraft rotational angles was developed. Using flight data, it was demonstrated that an excellent correlation in computed versus actual aircraft attitude could be achieved. In addition to providing measurements of the magnetic field for redundant attitude computations (to improve accuracy and reliability of existing autopilot systems), it was noted that the vector magnetometer could substitute for the remote magnetic sensing unit. In this manner both heading and attitude measurements could be derived using common elements with obvious benefits in weight and cost.

This chapter discusses the mechanization of a microprocessor based computer system that uses a three axis magnetometer plus gyro data to compute heading. The magnetometer is a three axis solid state device that can be mounted in a strapped down configuration resulting in an attitude independent remote magnetic indicator. Gyro measurements of pitch and roll angle plus three axis magnetic measurements are used by the algorithm to compute aircraft heading. The system can function independently to compute heading or by simply increasing the stored program could implement the attitude computing algorithm of [Ref. 2-1] as well.

The chapter proceeds by developing an algorithm to compute aircraft heading using the strapped down magnetometer and two gyro measured angles. Practical aspects of designing the system including both hardware and software are then presented. In addition, the limitations in instrument accuracy and operation as determined by sensor errors, signal processing errors, arithmetic precision and computation speed are discussed. Considerable computational capability inherent in the system enables minimization of systematic errors. It is demonstrated that inexpensive sensors can be employed with offset and orthogonality errors compensated by microprocessor programming. Finally, it is concluded that a microprocessor based computer with a solid state magnetometer can play a significant role in aircraft instrumentation.

2-2 AN ALGORITHM TO COMPUTE AIRCRAFT HEADING

Coordinate frames are usually defined by orthogonal right-hand sets of three unit vectors. An example of such a set is illustrated in Fig. 1-1 where the orientation of the body fixed frame used in this chapter is delineated. The reference coordinate frame referred to in this chapter is oriented with axes x and y in the horizontal plane and axis z vertical (z down is positive). Pitch attitude angle (Θ) of an aircraft is defined [Ref. 2-2] as the angle between some preferred longitudinal axis and the horizontal reference. In this chapter, pitch angle is the angle between the x axis of the aircraft and the x-y plane of the reference axis set. Since angular rotations are conventionally defined as rotations in the plane normal to a unit vector with the positive sense of rotation defined by the right-hand rule [Ref. 1-2], we will define positive pitch angle (Θ) as the "nose up" or positive rotation about the y axis when the y axis is horizontal. The roll and yaw angles (ϕ and Ψ) will then simply be rotations about the x and y axes respectively.

By aligning the three magnetometer axes with the respective x, y and z axes of the aircraft, we can measure magnetic field components of the aircraft at any attitude. For the trivial case where pitch (Θ) and roll (Φ) are both zero degrees, Hx and Hy are the horizontal field components and we can compute yaw from the horizontal vectors as follows:

$$\Psi_1 = \cos^{-1}(Hx/(Hx^2 + Hy^2)^{\frac{1}{2}} \qquad (2\text{-}1a)$$

or

$$\Psi_1 = \sin^{-1}(Hy/(Hx^2 + Hy^2)^{\frac{1}{2}} \qquad (2\text{-}1b)$$

We select either (2-1a) or (2-1b) based on the relative magnitudes of Hx and Hy. By minimizing the numerator of the argument we guarantee that the inverse trigonometric operation results in an angle between zero and forty-five degrees with maximum sensitivity ensured. Heading is then computed using the signs of Hx and Hy to select the appropriate equation from Table 2-1.

Hy \ Hx	NEGATIVE	POSITIVE
Negative	$\Psi = 180 - \Psi_1$	$\Psi = \Psi_1$
Positive	$\Psi = \Psi_1 + 180$	$\Psi = 360 - \Psi_1$

Table 2-1. Formulae to Compute Heading

For most cases, the pitch and roll angles are not zero and inverse rotations are required to determine the actual horizontal field components Hx and Hy. Since any aircraft attitude can be represented as a sequence of rotations about each axis beginning at some reference attitude, we can determine the reference Hx and Hy field components by performing an inverse roll followed by an inverse pitch computation[1].

The inverse roll computation can be developed by considering vector components of an arbitrary vector $\overline{H}$ in Fig. 2-1. The first set (x_2, y_2, z_2) represents the vector components measured in a reference orientation. The second set has common origin and aligns with common x axis component. It is rotated (rolled) about the x axis resulting in new y and z values. We can describe vector $\overline{H}$ in both coordinate frames as

$$\overline{H} = x_2 \cdot \hat{i}_2 + y_2 \cdot \hat{j}_2 + z_2 \cdot \hat{k}_2 \tag{2-2}$$

and

$$\overline{H} = x_3 \cdot \hat{i}_3 + y_3 \cdot \hat{j}_3 + z_3 \cdot \hat{k}_3 \tag{2-3}$$

Since the vector $\overline{H}$ is unique, we note that equations (2-2) and (2-3) are equal. Furthermore if we form dot products we solve for the horizontal components x_2, y_2, and z_2 in terms of the rotated values and the roll angle (Φ).

From (2-2) we obtain

$$\overline{H} \cdot \hat{i}_2 = x_2(\hat{i}_2 \cdot \hat{i}_2) + y_2 (\hat{j}_2 \cdot \hat{i}_2) + z_2(\hat{k}_2 \cdot \hat{i}_2) \tag{2-4a}$$

$$\overline{H} \cdot \hat{i}_2 = x_2 \tag{2-4b}$$

and from (2-3) we obtain

$$\overline{H} \cdot \hat{i}_2 = x_3(\hat{i}_3 \cdot \hat{i}_2) + y_3 (\hat{j}_3 \cdot \hat{i}_2) + z_3(\hat{k}_3 \cdot \hat{i}_2) \tag{2-5a}$$

$$\overline{H} \cdot \hat{i}_2 = x_3 \tag{2-5b}$$

---

[1]Since pitch is defined as the angle between the x axis and the horizontal plane we can assume that at any heading, aircraft attitude results due to a pitch followed by a roll.

then

$$x_2 = x_3 \tag{2-6}$$

Similarly,

$$\bar{H} \cdot \hat{j}_2 = y_2 = x_3(\hat{i}_3 \cdot \hat{j}_2) + y_3(\hat{j}_3 \cdot \hat{j}_2) + z_3(\hat{k}_3 \cdot \hat{j}_2) \tag{2-7a}$$

$$y_2 = y_3 \cos \Phi - z_3 \sin \Phi \tag{2-7b}$$

and

$$\bar{H} \cdot \hat{k}_2 = z_2 = x_3(\hat{i}_3 \cdot \hat{k}_2) + y_3(\hat{j}_3 \cdot \hat{k}_2) + z_3(\hat{k}_3 \cdot \hat{k}_2) \tag{2-8a}$$

$$z_2 = y_3 \sin \Phi + z_3 \cos \Phi \tag{2-8b}$$

These expressions can be summarized as

$$\begin{bmatrix} x_2 \\ y_2 \\ z_2 \end{bmatrix} = \begin{bmatrix} 1 & 0 & 0 \\ 0 & \cos \Phi & -\sin \Phi \\ 0 & \sin \Phi & \cos \Phi \end{bmatrix} \cdot \begin{bmatrix} x_3 \\ y_3 \\ z_3 \end{bmatrix} \tag{2-9}$$

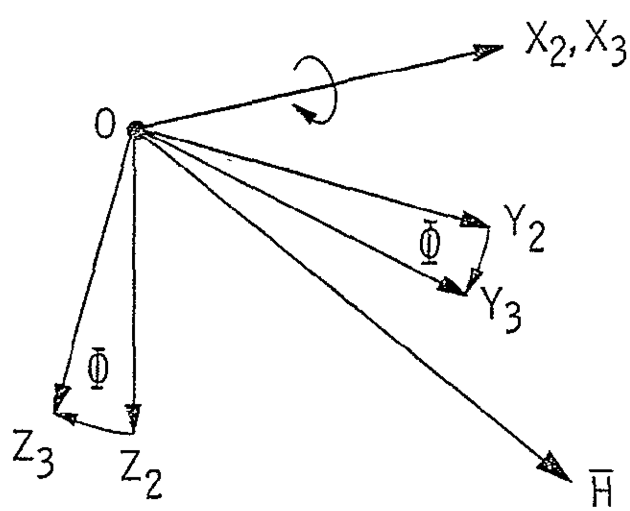

Fig. 2-1 AXES ROTATED IN ROLL

Similarly, considering an axis set rotated in pitch as shown in Fig. 2-2, we can express the reference set x_1, y_1, z_1 in terms of the rotated set x_2, y_2, z_2 as follows

$$\begin{bmatrix} x_1 \\ y_1 \\ z_1 \end{bmatrix} = \begin{bmatrix} \cos\theta & 0 & \sin\theta \\ 0 & 1 & 0 \\ -\sin\theta & 0 & \cos\theta \end{bmatrix} \cdot \begin{bmatrix} x_2 \\ y_2 \\ z_2 \end{bmatrix} \qquad (2\text{-}10)$$

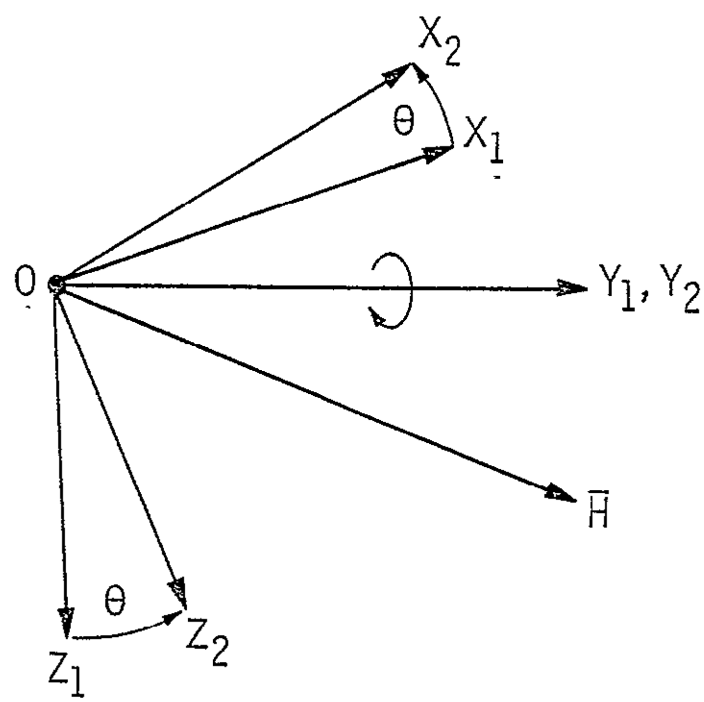

Fig. 2-2 AXES ROTATED IN PITCH

Finally, if we assume that the axis set subscripted with 3 represents components of Earth's magnetic vector measured at an arbitrary aircraft attitude, we can derive the magnetic components (Hxh, Hyh, Hzh) in the horizontal plane for a given heading

$$\begin{bmatrix} Hxh \\ Hyh \\ Hzh \end{bmatrix} = \begin{bmatrix} \cos\Theta & 0 & \sin\Theta \\ 0 & 1 & 0 \\ -\sin\Theta & 0 & \cos\Theta \end{bmatrix} \begin{bmatrix} 1 & 0 & 0 \\ 0 & \cos\Phi & -\sin\Phi \\ 0 & \sin\Phi & \cos\Phi \end{bmatrix} \bullet \begin{bmatrix} Hx_3 \\ Hy_3 \\ Hz_3 \end{bmatrix} \tag{2-11a}$$

$$\begin{bmatrix} Hxh \\ Hyh \\ Hzh \end{bmatrix} = \begin{bmatrix} \cos\Theta & (\sin\Theta\sin\Phi) & \sin\Theta\cos\Phi \\ 0 & \cos\Phi & -\sin\Phi \\ -\sin\Theta & (\cos\Theta\sin\Phi) & \cos\Phi\cos\Theta \end{bmatrix} \bullet \begin{bmatrix} Hx_3 \\ Hy_3 \\ Hz_3 \end{bmatrix} \tag{2-11b}$$

The algorithm to be implemented with the microprocessor would therefore require operations as outlined in Fig. 2-3. Details of programming method, modifications to the above equations to facilitate programming and computation speed versus accuracy tradeoffs are discussed in following sections.

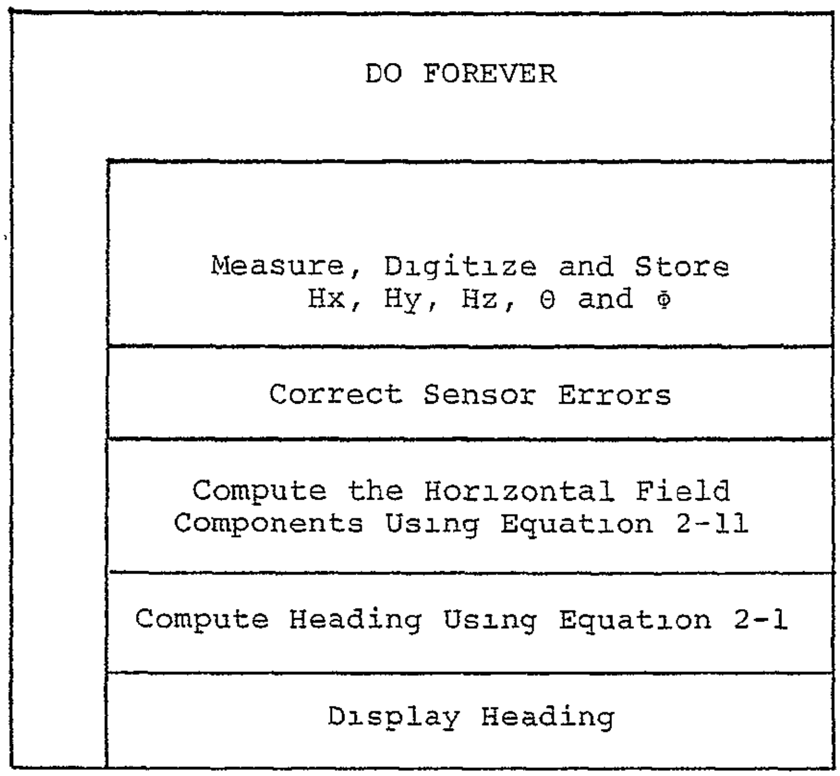

Fig. 2-3 LOGICAL OPERATIONS REQUIRED TO COMPUTE HEADING

2-3 MECHANIZATION OF THE HEADING ALGORITHM

A. General Considerations

To evaluate the performance of an integrated system experimentally, an instrument was designed to implement the algorithm developed above. Several approaches were considered to implement the heading instrument for experimentation:

1) A minicomputer implementation incorporating an HP-2100 minicomputer supported by peripheral interface and analog circuitry. Programming of the HP-2100 would have enabled the computer to control multiplexing and processing of sensor data as suggested by Parish and Lee [Ref. 2-3].

2) A hybrid system composed of a remote data acquisition system to collect data from sensors for subsequent processing by a computer (possibly an HP-2100).

3) A digital/analog electronic implementation incorporating the design of a special purpose computer to perform the required functions of a heading instrument.

The first two approaches were abandoned since it was desirable to perform the experiments at various locations remote from a computer facility and to have data available immediately without having to rely on off-line computations at a later date. The design task then evolved to the design of a special purpose computer system to implement the algorithm, provide a means for evaluating the performance of the proposed algorithm and to allow modifications to the system if required.

B. Design Criteria

Having decided on the general approach to implementing the algorithm it became necessary to consider the performance criteria desired of the instrument.

1) Accuracy
   As a design goal, an absolute accuracy of ±1.0° in heading uncertainty was selected for the laboratory implementation. This accuracy is compatible with commercially available heading systems.

2) Computation Speed
   The bandwidth of the system is determined mainly by the computation speed of the computer[2]. As a design goal, complete heading updates once per second was established.

3) Flexibility
   A desirable feature of the laboratory evaluation instrument was considered to be flexibility. Revisions or additions to the algorithm as predicted by experimental data should be incorporated with minimal redesign of the instrument.

2-4 CONCLUSIONS

An instrument designed to implement the heading algorithm developed above uses a three axis magnetometer to measure magnetic field data in the vicinity of an aircraft. Since the magnetometer proposed is a solid state three axis fluxgate device and is permanently mounted in a strapped down configuration, the implementation results in an attitude independent

[2]The response times of the various sensors and analog circuitry are orders of magnitude greater than the desired one second sample interval.

remote magnetic indicator[3].

Several factors will contribute to system inaccuracy. Although the major error sources can be evaluated mathematically (Chapter IV), there is a need to evaluate the implementation experimentally. Systematic errors that arise can be reduced by instrument computation. This capability (inherent with a computer based system) enables incorporation of less expensive sensors in the heading instrument with less concern with factors such as temperature regulation, sensor orthogonality and sensor offset[4].

Since the algorithm can be implemented using a microprocessor as the major computer element, the resulting instrument will have inherent computation capability, be small in size and consume relatively little power. These factors make the instrument an ideal device for aircraft application where the need for redundant distributed processing capability is invaluable.

[3] Current remote magnetic indicators are pendulous and rely on gravity to enable measurements of the horizontal magnetic vector (not attitude independent).

[4] Assuming that the sensors have repeatable or measurable characteristics, algorithms can be developed to correct previously measured erroneous data.

CHAPTER III

DESIGN OF A MICROPROCESSOR BASED HEADING INSTRUMENT

3-1 INTRODUCTION

Progress in device and component technologies during the 1970's has led to an assortment of sophisticated integrated circuits (IC) devices [Ref. 3-1] which enable the design of instruments with a high degree of sophistication and accuracy. Of these devices, the microprocessor has to date been the most exploited component in industrial control and instrumentation applications [Ref. 3-2 through 3-7]. There have been many papers presented addressing the general application and feasibility of applying microcomputers to particular design tasks [Ref. 3-8 through 3-21].

Although much of the literature to date on microprocessors has addressed the design of commercial products (usually the final result of a carefully orchestrated effort beginning with a market survey), the design of a laboratory instrument for algorithm evaluation differs in design philosophy. In particular, the laboratory instrument is designed to evaluate a proposed algorithm under laboratory conditions. The traditional benchmark evaluations and attempts to match the microprocessor to the application is not only difficult but unnecessary. If the processor is much more powerful than necessary, the "overkill" is little noticed; but if an insufficiently endowed microprocessor is selected, the effects can be devastating. Not only will the program be difficult to write and voracious of memory, it would be difficult to change to a more powerful microprocessor part way through the project. With these considerations in mind, a general purpose, flexible microprocessor with powerful architecture and instruction set the Signetics 2650 microprocessor [Ref. 3-22] was selected.

3-2 HARDWARE DESIGN CONSIDERATIONS

The design of a microprocessor based system begins by considering the total system level block diagram to be implemented (Fig. 3-1). Inputs from five sensors including x, y and z axis magnetic data plus pitch and roll angles (Hx, Hy, Hz, Θ and Φ) are to be multiplexed, sequentially sampled and converted to a digital representation prior to processing (executing the algorithm developed above). The main subsystem of Fig. 3-1, the central processing unit (CPU), operates under control of instructions stored in the system memory and interfaces with the input and output subsystems via data ports.

At this early stage in the design, it is significant to note that the block diagram of Fig. 3-1 differs slightly from that of a classical discrete hardware solution. The input subsystem (composed of analog multiplexer, sample and hold, and analog to digital converter) differs from a conventional data acquisition in that it is devoid of a control section. The microprocessor will control the data acquisition sampling and conversion in addition to performing the arithmetic function associated with the algorithm.

Having established a tentative block diagram of the instrument, the design continues by addressing relevant characteristics and limitations of each subsystem. These characteristics will then in term be considered in configuring the final system and program to be executed.

1) The Analog Subsystem

Composed of the analog multiplexer, sample/hold and analog to digital converter, the analog subsystem of Fig. 3-1 affects both system accuracy and throughput rate. The

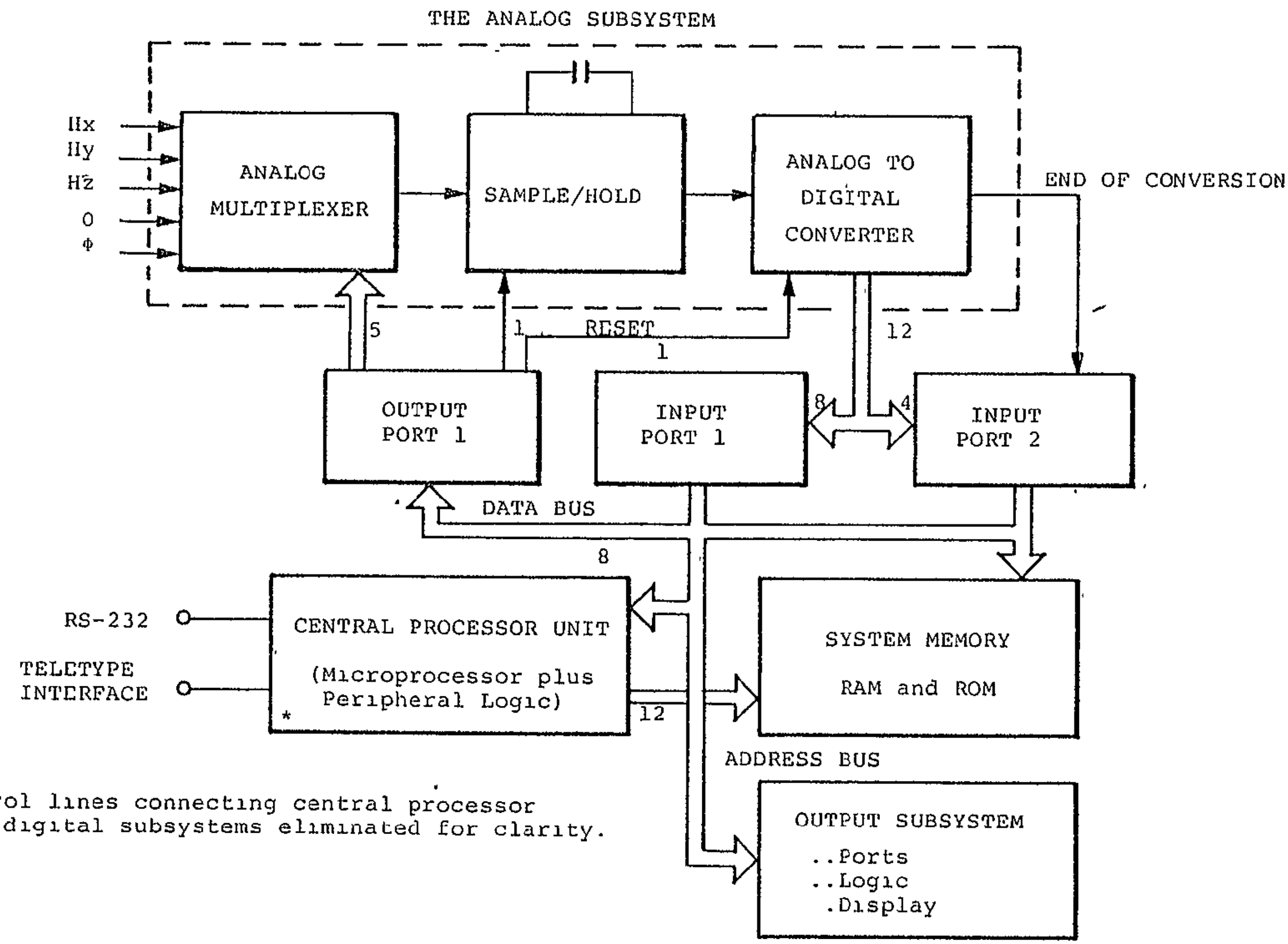

*Control lines connecting central processor to digital subsystems eliminated for clarity.

Fig. 3-1. SYSTEM BLOCK DIAGRAM

well-known Shannon theorem [Ref. 3-23, 3-24] on sampling theory defines one of the basic limits on throughput rate stating that the minimum frequency for sampling must be double the highest significant frequency of the signal, including the noise on the signal. This minimum frequency is necessary, the theorem states, if the sampled signal is to contain all of the information needed for undistorted reconstruction. At a lower sampling frequency ailiasing can occur[1]. The minimum sampling rate for data to be used in this heading instrument (based on the design goal of Chapter II) then results in a system bandwidth of 30 hertz. The analog signals from each sensor are low pass filtered to reduce frequency content above 60 hertz. A survey of commercially available multiplexers, sample and hold modules and analog to digital convert modules (ADC) [Ref. 3-25 to 3-28] reveals that subsystems with throughput characteristics exceeding the requirements of a system sampled at one second intervals are readily available (pertinent specifications are discussed in more detail in Chapter IV). The limiting parameter determining total system speed performance will then be the execution time of the algorithm (a programming consideration). A further system consideration is the ability to adjust analog system offset and gain. These adjustments are made using variable resistors (trim pots) connected to appropriate leads on the sample and hold and analog to digital converter modules.

2) The Central Processing Unit (CPU)

The central processing unit (Fig. 3-2) is composed of the microprocessor (Signetics 2650) supported by peripheral logic elements (Fig. 3-2). Design of this subsystem involved medium

---

[1]That is, the sampled data derived from a sine wave of frequency f sampled at a frequency less than 2f can be fitted with sine waves of a frequency other than f.

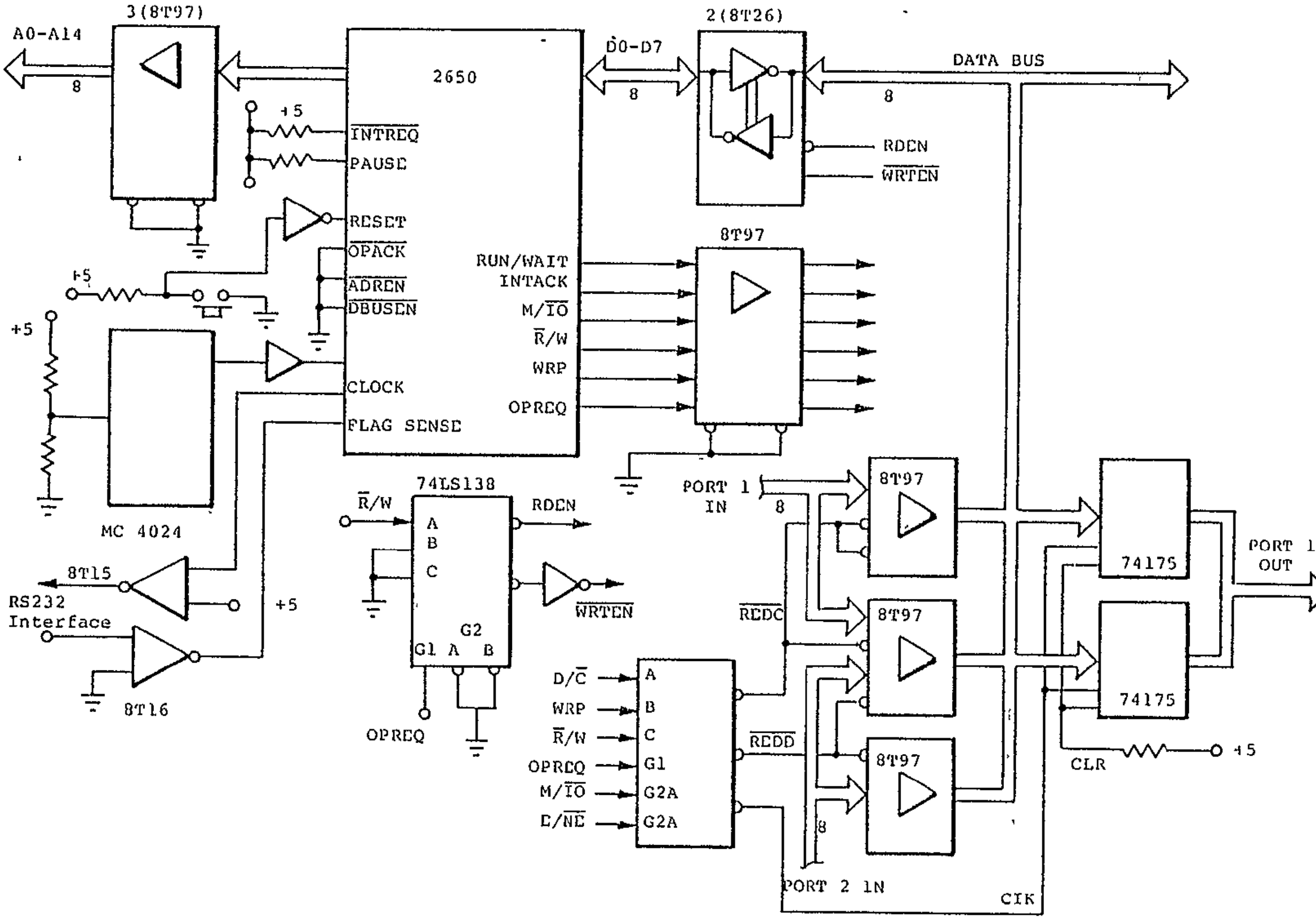

Fig. 3-2. THE CPU SUBSYSTEM

and small scale integrated circuits using well-known [Ref. 3-29 through 3-31] design techniques. To facilitate system development several features were included in the design of the CPU subsystem (features that would not necessarily be required in a production instrument). These include:

a) System reset, single step and normal run mode operation controlled by switches and logic elements.

b) An RS-232 teletype interface is included to enable manual intervention and development capability during program development. The program was developed by loading and executing instructions into the random access memory (RAM) under control of the PIPBUG[2] program.

3) The Memory Subsystem

The memory subsystem (Fig. 3-3) was organized onto cards each with two thousand byte capability. In this manner system memory could easily be expanded (or reduced) in increments of 2K bytes. The memory chips selected were organized as 256 four bit words and feature pin for pin compatibility with commercially available random access (RAM) and programmable read only memory (PROM) chips. Program segments could then be developed in RAM and finally "burned" into PROM chips for a permanent, nonvolatile operation. In this manner the system development begins with 1K bytes of memory devoted to the resident PIPBUG program (in ROM chips) with the remainder of memory allocated as RAM for both program and scratch pad usage.

[2]Signetics tradename for the 2650 resident loader and monitor program.

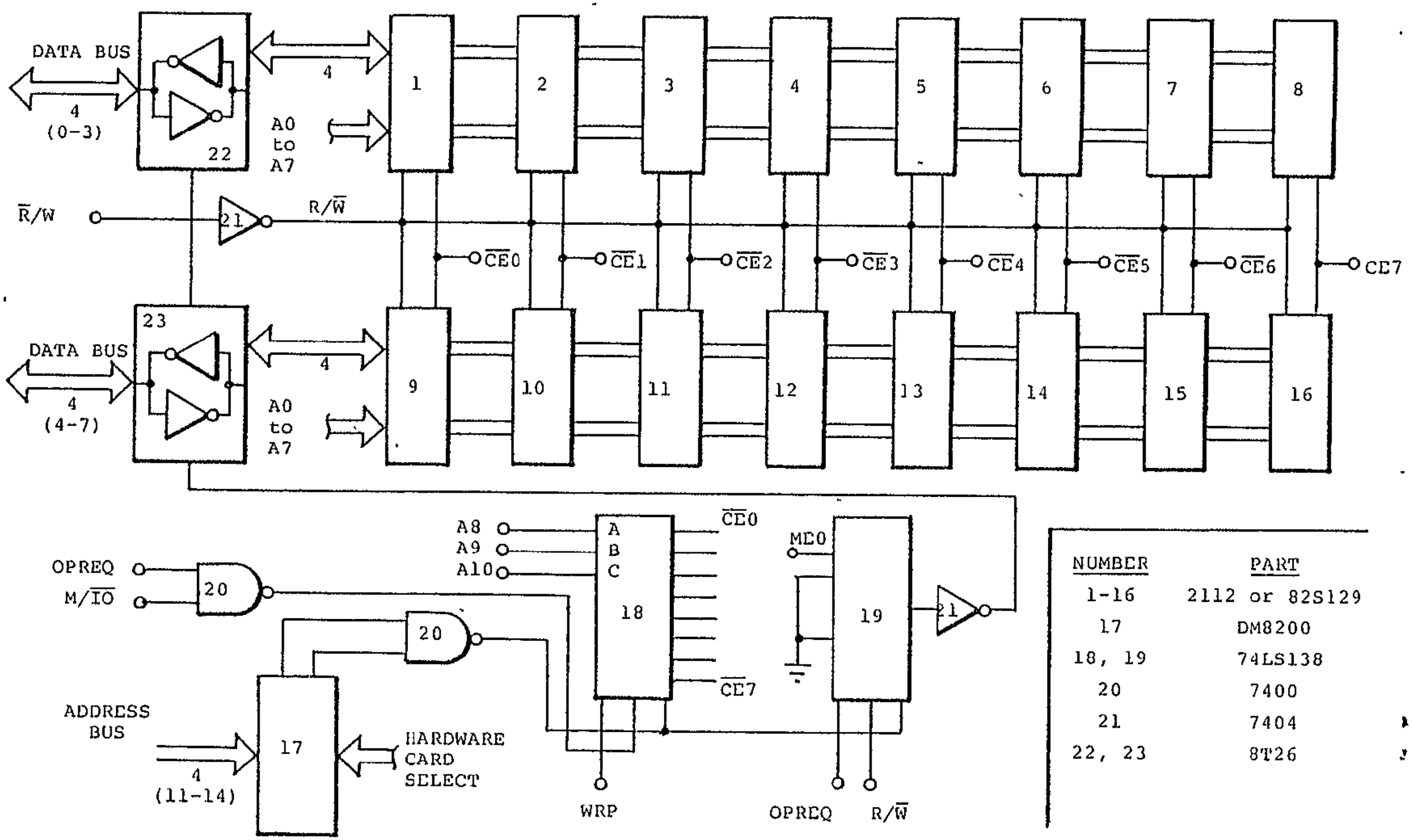

NUMBER	PART
1-16	2112 or 82S129
17	DM8200
18, 19	74LS138
20	7400
21	7404
22, 23	8T26

Fig. 3-3. MEMORY SUBSYSTEM (1 Card)

As the program is developed, additional memory is added in increments of 2K bytes per card or 256 bytes on the card. Modifications to the program can be easily made using the PIPBUG program and teletype.

4) The Output Subsystem

For laboratory development the output subsystem of Fig. 3-4 was designed to provide seven segment visual output of the aircraft heading with three significant digits displayed. To expediate the design cycle and to enhance system throughput rate, the outputs were designed as ports with latches and decoder driver functions provided by hardware. In other applications a hardware/software tradeoff could be made with the data decoding and driving implemented using table lookup and multiplexing controlled by the CPU.

3-3 SOFTWARE DESIGN CONSIDERATIONS

The general purpose processor selected to implement the CPU was designed to implement programmed logic and to perform conventional computer operations. This heading instrument takes advantage of both areas. Since the instrument is actually a special purpose computer under control of a stored program, the functional specialization resides in the program rather than the hardware logic. Modifications can be made relatively easily, satisfying the flexibility design goal of Chapter II.

Having decided on the tentative hardware structure described in Section 3-2 above, the program development leading to the final listing in Appendix B proceeded as follows:

1) Structured flow charts were developed depicting the total system operation as an ordered sequence of operations. Each

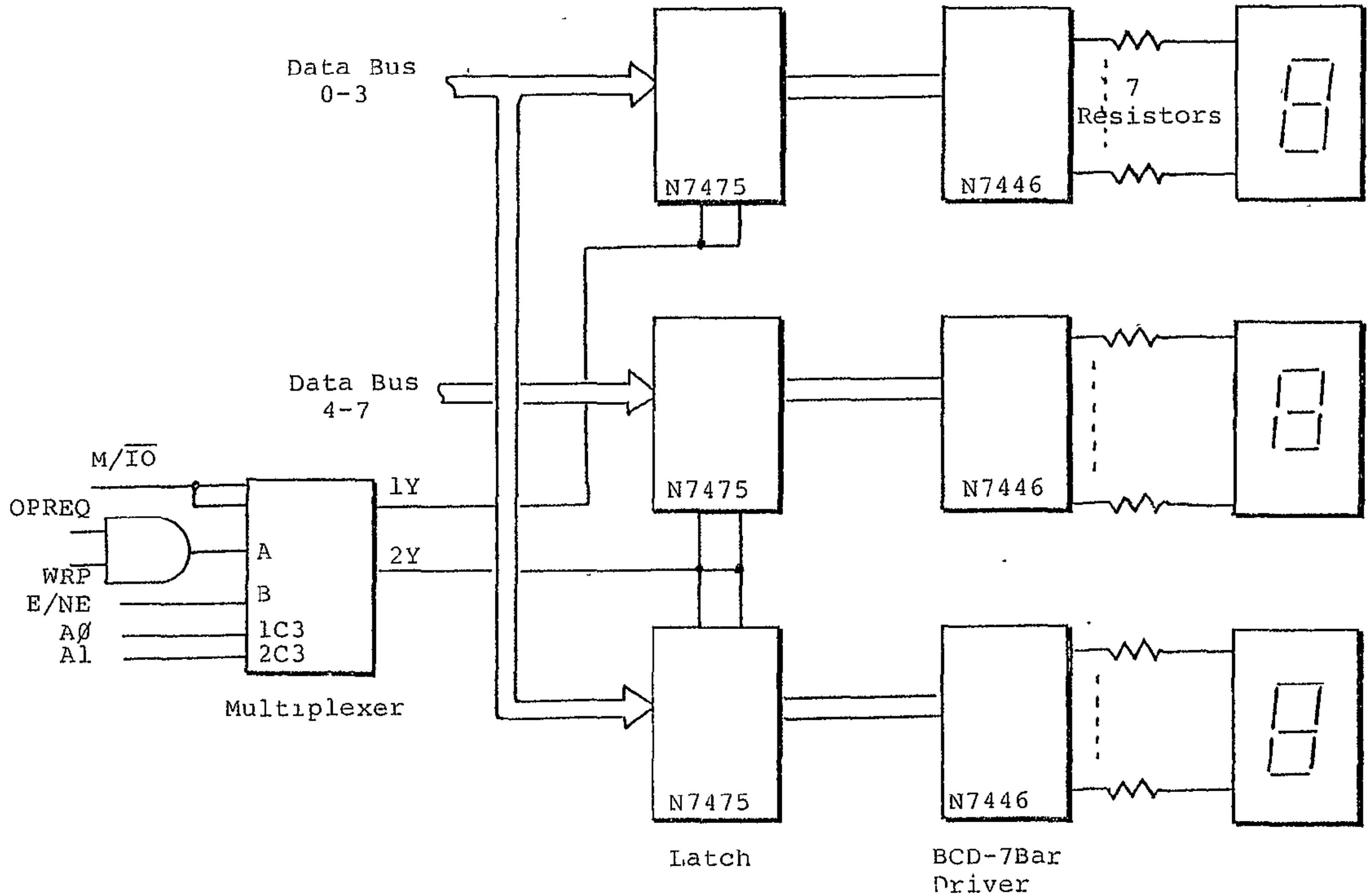

Fig. 3-4   THE OUTPUT SUBSYSTEM

operation is identified as a separate subroutine which in turn can have "nested" subroutines of its own (Fig. 3-5).

2) System accuracy requirements were next investigated (discussed in detail in Chapter IV) to ascertain the precision requirements[3] of the various subroutines.

3) The respective subroutines outlined in 1) above were developed and implemented using a cross assembler program [Ref. 3-32]. Each subroutine was then loaded into the development hardware and "debugged" prior to total program integration. The above program development depicts a top down strategy of program development [Ref. 3-33] and leads to an expedient system development with subroutines being individually developed to yield a modular program construction.

3-4 DESIGN OF SUBROUTINES

The total program consists of an overall system program composed of nested subroutines. The discussion in this section is limited in scope to the design of the more-complex subroutines required to implement the solid state remote magnetic heading algorithm.

1) Subroutine "SAMP" (Fig. 3-6a)

The first portion of this subroutine is dedicated to the control function of selecting an analog channel via the multiplexer, sampling and holding the data, resetting and reading data from the analog to digital converter (ADC). Prior to or during the programming of this section, data fields in

---

[3]This step is vital to determine whether the operations outlined in 1) above are to be carried out in a single or multi-precision manner.

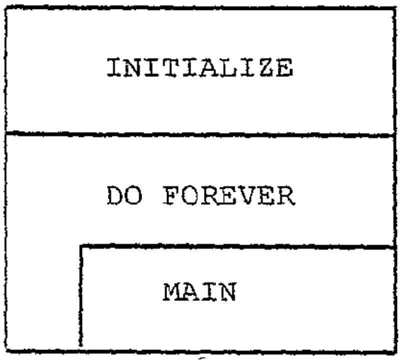

Power on reset of all registers and subsystems

Compute the aircraft heading

Fig. 3-5a. SYSTEM PROGRAM

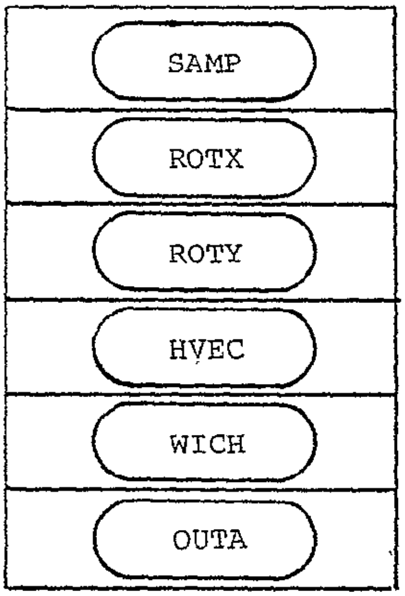

Sample all analog channels

Compute the horizontal Hx field

Compute the horizontal Hy field

Compute the horizontal field vector

Compute heading

Output the data

Fig. 3-5b. SUBROUTINE "MAIN"

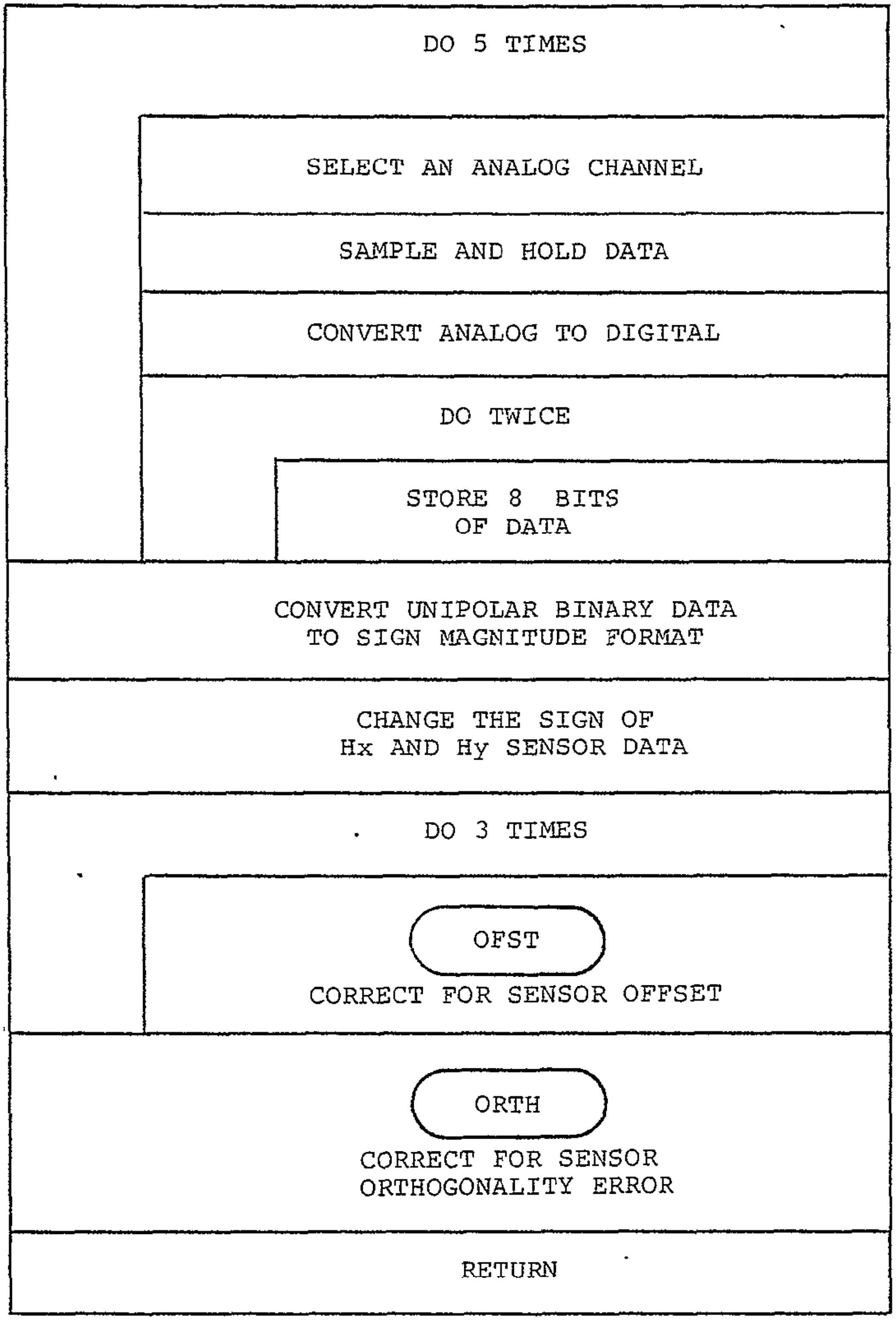

Fig. 3-6a. SUBROUTINE "SAMP"

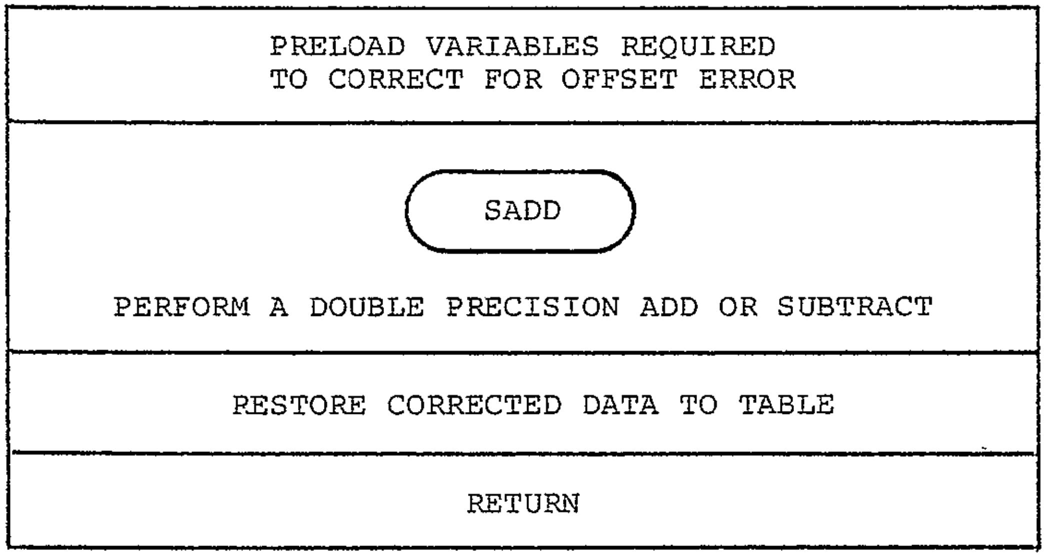

Fig. 3-6b. SUBROUTINE "OFST"

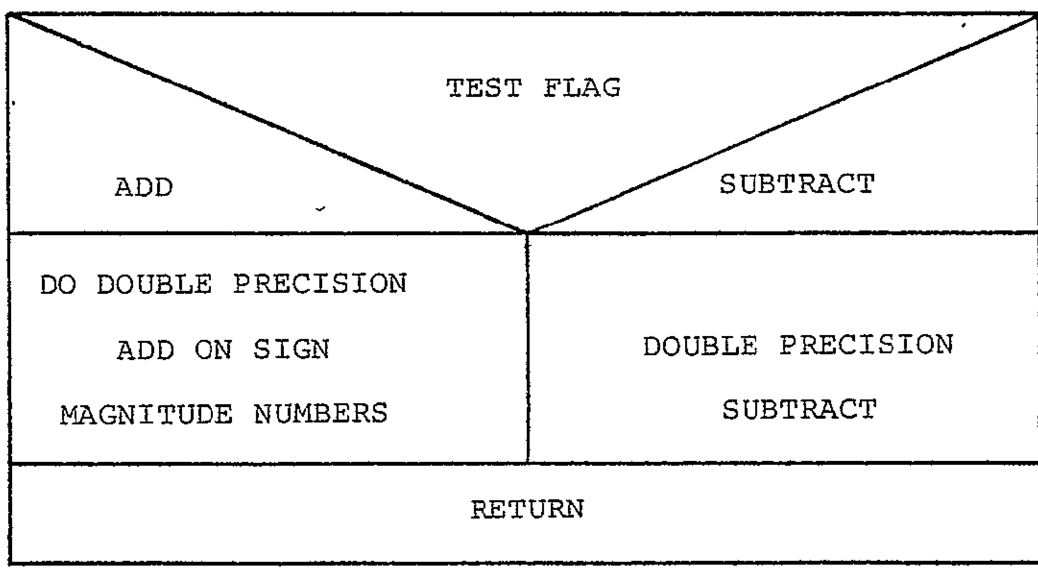

Fig. 3-6c. SUBROUTINE "SADD"

input ports 1 and 2 and output port 1 of Fig. 3-1 are allocated. Control information is then passed to the peripheral module by writing control words to output port 1. Analog to digital converter status and the 12 bit data field are sampled by reading input ports 1 and 2.

Sensor outputs were biased at +2.5 Volts with transfer characteristics as depicted in Fig. 3-7a [Ref. 3-34]. The ADC selected for this laboratory instrument had a binary output data format related to analog input as shown in Fig. 3.7b [Ref. 3-35]. The second function of the sampling subroutine "SAMP" was to convert data from a unipolar binary format to a sign magnitude format. Since the total transfer function from sensor input to ADC output (Fig. 3-7a and b) indicates an offset of 2.5 Volts or 1/2 the ADC output range, the sign magnitude format can be generated as shown in Fig. 3-8.

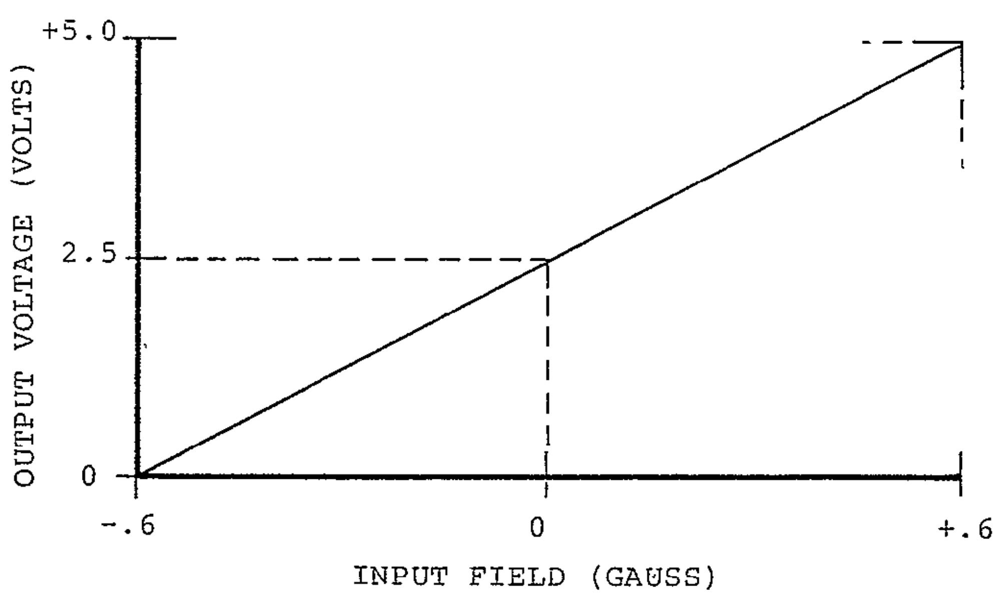

Fig. 3-7a. SENSOR TRANSFER CHARACTERISTIC

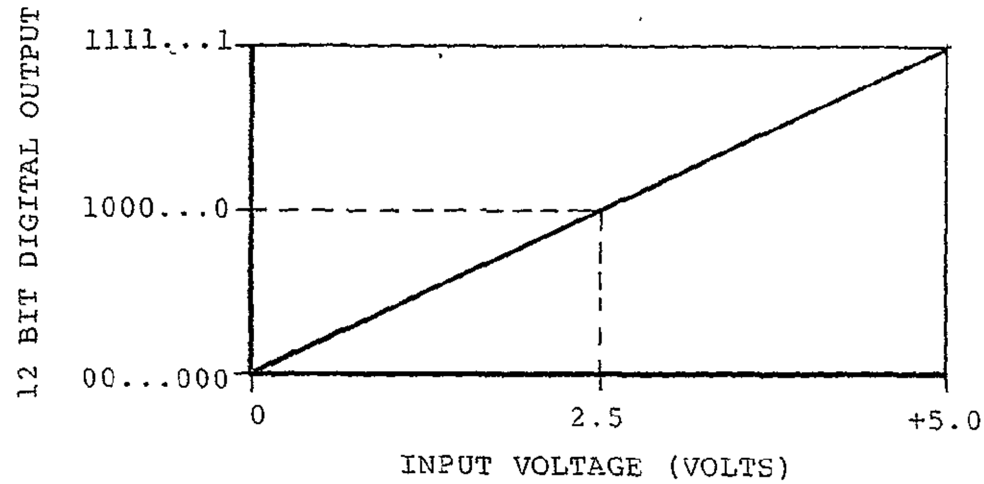

Fig. 3-7b. VDC TRANSFER CHARACTERISTICS

SIGN BIT

?

1	0
$x = x_0 + \sum_{i=1}^{11} x_i \cdot 2^i$ $(x = x_0 + x^*)$ Where: $x_0 = 0$ x^* = The 11 least significant bits of the binary number	$x = x_0$ + 2's complement of the 11 least significant bits $x_0 = 1$ (indicating negative quantity)

Fig. 3-8 CONVERSION OF DATA

The third function of the "SAMP" subroutine was to reverse the sign of the Hx and Hy data (to correct a test fixture problem) and to correct for sensor offsets. Although analog subsystem offsets are corrected by adjusting either the sample and hold module or the ADC, the independent sensors themselves have offsets[4]. Offset errors for the laboratory instrument were compensated by determining the offset correction term for each sensor (method described in detail in Chapter V) and then either adding or subtracting the term to the respective data during the sample subroutine. By characterizing the sensor errors[5], actual datum could be improved further during this step.

The final function of the "SAMP" subroutine was to correct for sensor orthogonality error (subroutine "ORTH"). Although the sensors were physically aligned and specified to have orthogonality characteristic [Ref. 3-34] less than ± 1 degree relative to the base coordinates, this nonorthogonality contributes appreciably to total system error (see error analysis in Chapter IV). The physical misalignment of the sensors was determined experimentally (Chapter V) and determined to be mainly a misalignment of sensor x in the x-y plane as illustrated in Fig. 3-9.

The actual data measured with the x axis sensor is then related to the true Hx and Hy values as

$$Hx^1 = Hx \cos \varepsilon - Hy \sin \varepsilon \ .$$

---

[4]With zero stimulus applied the sensors have a finite nonzero output. This error in the fluxgate magnetometer is a function of temperature, voltage and magnetic remanence in the sensor magnetics [Ref. 3-36].

[5]Sensor characteristics relating the temperature and power supply coefficients of offset error and nonlinearity can be derived empirically.

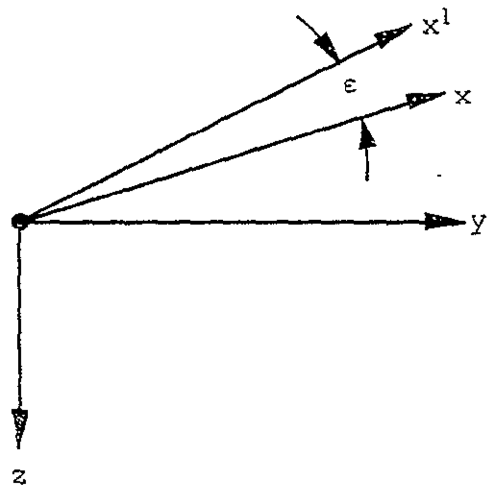

Fig. 3-9 X AXIS NONORTHOGONALITY

Using small angle approximations, we can solve for the desired true value of Hx

$$Hx^1 \simeq Hx - Hy \sin \varepsilon \qquad (3\text{-}1a)$$

$$Hx = Hx^1 + Hy \sin \varepsilon \qquad (3\text{-}1b)$$

By measuring ε (Chapter V) and storing the angle as a constant, the x axis data was then restored using equation 3-1b above in subroutine "ORTH".

2) Subroutines ROTX and ROTY

These subroutines compute arithmetic values for Hxh and Hyh of equation 2-11b using sign magnitude quantities and table lookup to determine solutions for the transcendental functions. Subroutines "SADD" and "SMPY" are nested and used to perform double precision add and multiply as required.

3) Subroutine HVEC

Following computation of the horizontal X and Y axis magnetic vector, the subroutine "MAIN" calls subroutine "HVEC" to compute the square of the horizontal vector. Vectors Hx and Hy are squared by calling subroutine "SQU" then added, yielding H(HORIZONTAL)^2.

4) Subroutine WICH

To compute heading, equation 2-1 (or a similar form) must be solved using the horizontal magnetic field vector and either the x or y axis horizontal field component. Although the square root operation implied in equation 2-1 could be implemented using a numerical technique [Ref. 3-37, 3-38], the computation time is decreased by using a table lookup method. Subroutine "WICH" (Fig. 3-10) compares the absolute magnitude of the two horizontal field vectors Hx and Hy to determine the relative heading of the aircraft[6] with respect to the north-south and east-west axes (Fig. 3-11).

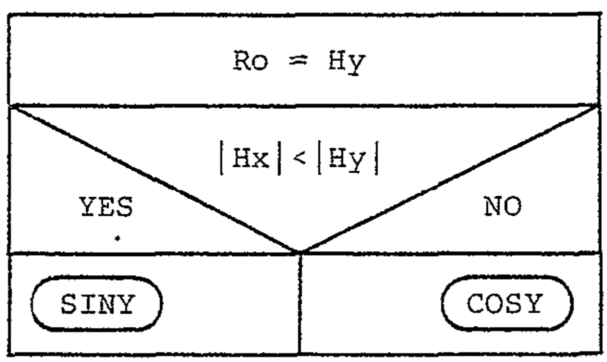

Fig. 3-10. SUBROUTINE "WICH"

[6] If $|Hx| < |Hy|$, then an equation similar in form to 2-1a must be used.

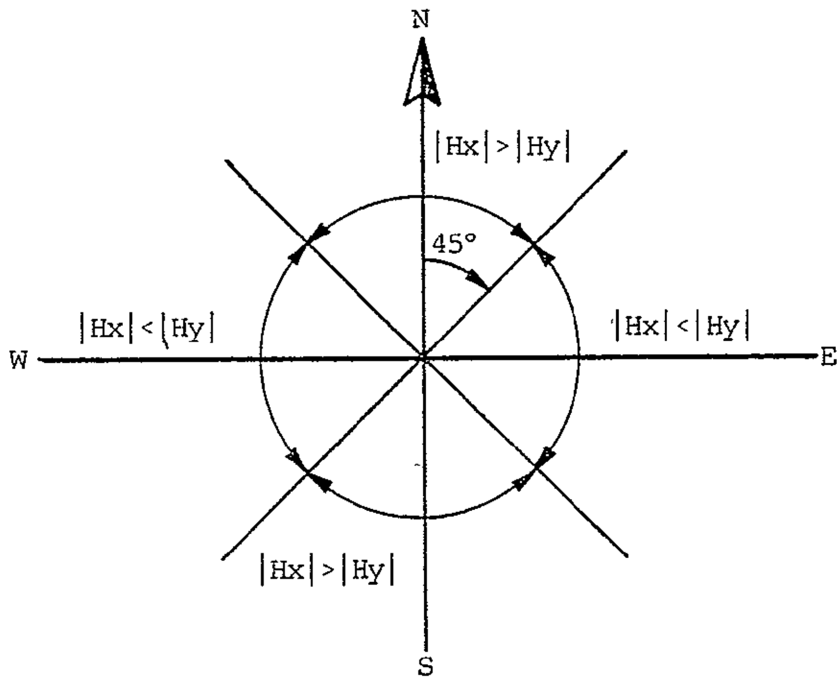

Fig. 3-11. MAGNITUDES OF Hx AND Hy RELATED AIRCRAFT HEADING

5) Subroutines COSY and SINY (Fig. 3-12, 3-13)

Depending on the relative absolute magnitudes of Hx and Hy, either "COSY" or "SINY" is called to compute aircraft heading. These subroutines invoke subroutine "DIVI" to form the quotient of the axis vector squared and the horizontal field vector squared (a double precision operation). Subroutine "ANGL" is then called to perform an associative table lookup operation using successive approximation and interpolation to complete the inverse cos squared operation. The double precision binary quantity is then converted to three digit binary coded decimal format (BCD) prior to computation of aircraft heading (subroutine "HDG").

The subroutine "SINY" of Fig. 3-12 includes a subtraction of the computed angle from 90 degrees following conversion to BCD format. This operation ensures that the angle passed to

	Ro, Rl = Hx^2
DIVI	A = Hx^2/Hh^2
ANGL	B = $\arccos^2(A)$
BCDA	Convert B to BCD Format
HDG	Compute Heading
	RETURN

Fig. 3-12. SUBROUTINE "COSY"

	Ro, Rl = Hy^2
DIVI	A = Hy^2/Hh^2
ANGL	B = $\arccos^2(A)$
BCDA	Convert B to BCD Format
	B = 90 - B
HDG	Compute Heading
	RETURN

Fig. 3-13. SUBROUTINE "SINY"

the calling subroutine upon exiting either "SINY" or "COSY" is an aircraft heading angle relating sensor x to the north-south axis.

6) Subroutine HDG (Fig. 3-14)

The function of this subroutine is to compute aircraft heading having established the angle between the x axis sensor and the north-south geodetic axis. Determination of the actual heading is accomplished by comparing the signs of both the x and y axis horizontal vectors prior to computing heading (Fig. 3-15). It should be noted that all of the preceding computations leading to horizontal vector data were on sign magnitude quantities preserving the correct horizontal vector polarities[7].

3-5 CONCLUSIONS

This chapter has outlined the practical aspects of designing an instrument to evaluate both the heading algorithms and solid state magnetic indicator proposed in previous chapters. The chapter outlined a design approach that can be used to implement a microprocessor based instrument. In particular, the need to consider the total system hardware requirements while simultaneously considering the programming requirements was identified. Design proceeded by outlining a system block diagram (Fig. 3-1) with major subsystems considered. The instrument required a special purpose computer with an analog subsystem to sample and digitize five sensor signals. Timing and control of the analog subsystem plus digital processing of data was controlled by a microprocessor based central processing unit (CPU). Memory for permanent storage of

[7]It is possible at certain attitudes to require sign reversals when computing horizontal vectors.

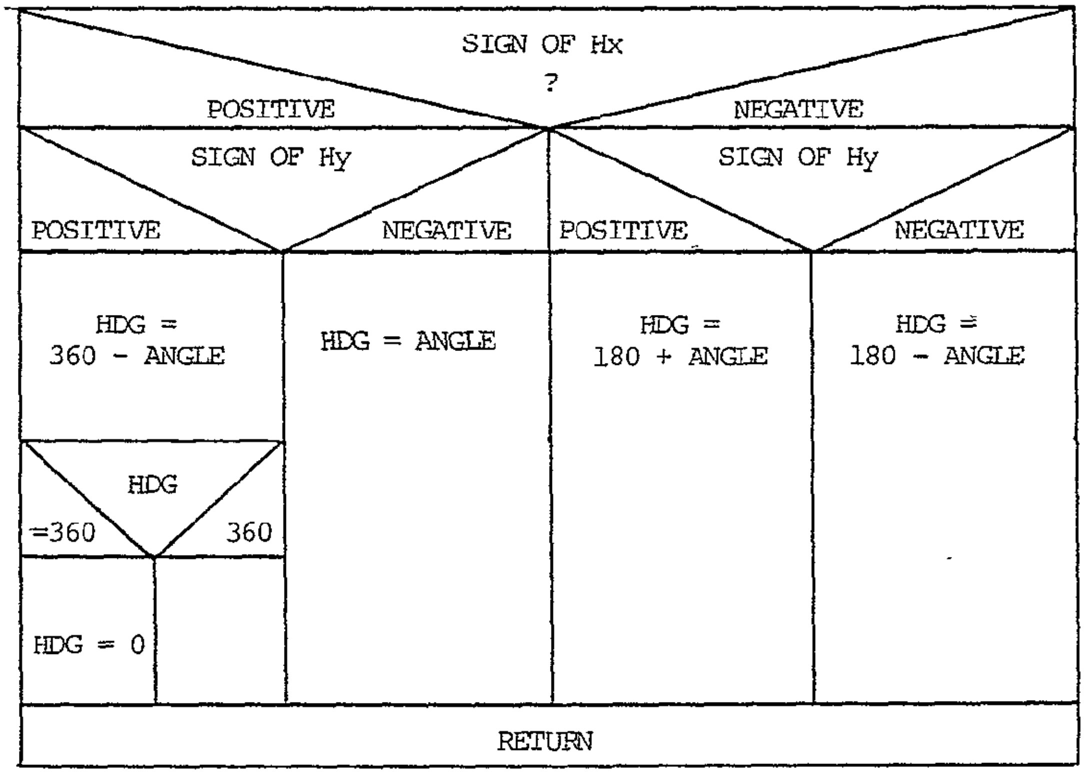

Fig. 3-14. SUBROUTINE "HDG"

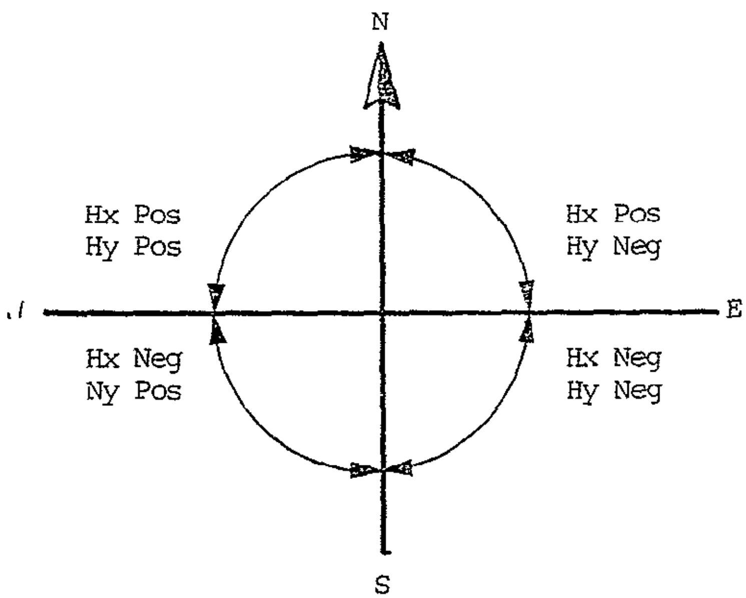

Fig. 3-15. POLARITIES OF HORIZONTAL VECTORS RELATED TO AIRCRAFT HEADING

instructions and temporary storage of data was implemented using memory chips organized on cards with 2048 byte capacity. The particular memory chips selected feature pin compatibility[8] with both read only and volatile random access versions. System inputs consisted of sensor signals from a three axis solid state fluxgate magnetometer plus two analog signals simulating gyroscope outputs. System outputs consist of visual seven segment readout displaying computed heading. In addition, an RS-232 teletype interface was provided to facilitate system development and experimentation.

By identifying the total system in block diagram form at the very beginning, the role and requirements of each subsystem as well as the supporting software were identified. The design then evolved on a modular basis with each subsystem and its supporting program developed in parallel. In this manner pin assignments for input/output ports and critical timing requirements that involved both hardware and software consideration were handled efficiently. By outlining the program requirements in flow chart form (analagous to the block diagram of the hardware subsystem), subroutines were identified facilitating a modular program development. Where possible, subroutines were shared in a nested manner avoiding replication of programming and waste of memory.

Details of error analysis and calculation of overall system throughput rate were deferred to Chapter IV. It was pointed out however, that errors induced by imprecision of data plus truncation and roundoff during processing of the algorithm were to be considered early in the design phase. These data were required to select the sensors and the analog to digital

---

[8]Memory integrated circuit (IC) devices of both types can be used in the same mechanical sockets with actual chip type being used transparent to the remainder of the system.

converter as well as to design the supportive software for the analog subsystem. In addition, the data precision requirements were necessary prior to programming the algorithm[9].

By incorporating a microprocessor as the main CPU element, considerable sophistication in both control and computing performance was achieved. The overall system was designed relatively quickly, provided a convenient laboratory instrument for evaluation of the proposed algorithms and featured inherent flexibility.

[9]Some of the subroutines required double precision manipulations to maintain overall system accuracy.

CHAPTER IV

HEADING INSTRUMENT ERROR ANALYSIS

4-1 INTRODUCTION

The heading instrument designed to evaluate the heading and solid state remote magnetic indicator algorithms is prone to error from many sources. These errors will accumulate and degrade the accuracy of aircraft heading or yaw angle computations. This chapter addresses the various error sources to determine their relative magnitudes and effects on the overall computation.

Prior to beginning the hardware design of the microprocessor based instrument many of these potential error sources were considered. Their effects were considered in establishing parameters such as word lengths, A/D converter precision, computation speeds, sampling rates, magnetometer sensor accuracies, system noise tolerance, etc. As the design of the microprocessor based system evolved, the error analysis refined. Ultimately, important limitations in instrument design and operation were identified by combined error analysis and empirical data. By carefully analyzing the source and extent of the limiting parameters (such as sensor offset and nonorthogonality), the magnitude of errors unique to this laboratory sensor array were identified. Specialized software was then added (with empiracally derived constants) to correct for the otherwise limiting sensor irregularities improving the total system performance.

In this manner, it is apparent that error analysis is an integral part of instrument design. Not only are important parameters identified early in the design cycle (prior to system block diagram development), but shortcomings in conventional sensors can be improved by judicial application of error correcting algorithms. In this case, data constants were determined after the final instrument became operational. The sensor peculiarities were analyzed empirically using the instrument itself.

The chapter begins by first identifying and carefully analyzing potential error sources in the sensors. This analysis is followed by a similar consideration of errors originating in the analog subsystem. Processing errors that originate due to the finite word length and precision of the microprocessor along with the effects of simplifications made to the algorithms are finally analyzed. The chapter then concludes with a summary of measurement errors, a sample error analysis, a comparison of predicted to measured error and a summary.

4-2 SENSOR ERRORS

The heading computation algorithm employing the remote magnetic indicator (Chapter II) is prone to error proportional to both fluxgate magnetometer sensor and gyroscope measurement errors. Errors inherent in the fluxgate magnetometer are summarized on the data sheet [Ref. 3-34]. Since the experimentation employed simulated gyroscope sensors with voltage levels accurately represented, the analysis of sensor errors will assume ideal gyroscope sensors to predict experimental data.

A) Sensor Offset Error

Magnetometer sensors exhibit error caused by both electronic and magnetic phenomena. Errors in the Develco sensors were outlined by Workentine [Ref. 4-1]. These offset errors are induced in the Develco sensors by both electronic offset voltages and currents in the respective sensor electronics and by residual magnetic fields in the magnetic mass of the sensor assemblies. Although the physical and electronic design attempts to reduce offset error, a finite non-zero output can exist when a zero input is applied.

Offset error for each sensor in the Develco model 9200C three axis magnetometer assembly is specified [Ref. 3-34] as "Zero Field Bias +2.5 Volts $\pm$1.0%". This offset translates into a worst case maximum error voltage of

$$EOFFSET = \pm(2.5V \times 0.01) = \pm 25mV$$

Since the offset error is sensor dependent, correction cannot be made at a single physical point (as for analog subsystem offsets described in Section 4-3). Corrections can however be made to the measured data by simply adding or subtracting a constant equal to the offset magnitude following each data measurement[1].

Offset values for each sensor used in the experiment were obtained by rotating the sensor into alignment with earth's magnetic field vector to measure both positive and negative maximum values. The difference in magnetic measurement (assuming negligible analog subsystem error) is related to system offset error composed of sensor electronic and sensor plus test fixture induced magnetic offset error. The actual offset error can be calculated using these two measurements

[1]Offset corrections were made in the sample subroutine "SAMP" illustrated in Fig. 3-6a.

$$|Emax| = Ef + Eo$$
$$|Emin| = Ef - Eo$$
$$|Emax| - |Emin| = (Ef + Eo) - (Ef - Eo) = 2\ Eo$$
$$Eo = (1/2)\ \ (|Emax| - |Emin|)$$

where

Emax = The maximum positive voltage recorded when the sensor aligns with earth's field vector.

Emin = The maximum negative voltage recorded when the sensor aligns 180° with earth's field vector.

Ef = The magnitude of earth's magnetic vector represented in volts.

Eo = The sensor offset voltage due to both electronic and magnetic phenomena

Data recorded during x, y and z axis offset measurements as described above are recorded in Table 4-1. Since the offset error is a function of sensor magnetic permeability, the actual offset value will vary with time depending on induced magnetic fields[2].

Final offset correction values were determined by rotating two sensors in the horizontal plane around the third vertical axis and measuring offsets in two sensors at a time. Recorded data for each sensor was previously corrected for orthogonality error by the sample subroutine "SAMP" (discussion

---

[2]For example, magnetized screwdrivers or other tools used near the sensor will alter the residual magnetic field.

SENSOR AXIS	DATA RECORDED (HEXADECIMAL)		OFFSET (HEXADECIMAL PLUS SIGN)
	|Emax|	|Emin|	
X	628	E78	+40
Y	640	E5D	-15
Z	637	E68	-25

Table 4-1 OFFSET DATA DERIVED BY MEASURING EARTH'S FIELD

of this correction follows in Section 4-2B). Data recorded in this manner appears in Tables 4-2 and 4-3. Final correction terms for correcting sensor offset error were calculated using these data. Offset terms to be added or subtracted from respective data channels are tabulated in Table 4-4.

By correcting system offset errors in this manner, the effective error contribution can be reduced appreciably (see final data discussion Chapter V). For a flight instrument, sensor offset characteristics as a function of temperature variation and supply voltage can be derived empirically and appropriate offset corrections made by computing the value of the correction term variable. Magnetically induced offsets can be reduced by degaussing the sensor assembly periodically.

B) Axis Alignment Errors

The error specification of [Ref. 3-34] indicates that the maximum axis alignment error is ± 1 degree relative to base referenced coordinates. This error results in sensor directional uncertainty as illustrated in Fig. 4-1. Each sensor is located within a right circular cone with axis along the true sensor axis and vertex at the common sensor origin. Although this alignment uncertainty contributes no error in determining the total magnetic vector

$$\overline{H} = (\overline{H}x^2 + \overline{H}y^2 + \overline{H}z^2)^{\frac{1}{2}},$$

there is considerable uncertainty in attempting to resolve the true magnetic field component along any axis of the reference coordinate system. This alignment uncertainty of magnetic sensors limits system performance of conventional field direction measuring apparatus [Ref. 4-1].

Protractor Heading Measurement (Degrees)	Data Measured Hx (Units)	Data Measured Hy (Units)	Protractor Heading Measurement (Degrees)	Data Measured Hx (Units)	Data Measured Hy (Units)	Error Due To Offset X (Units)	Error Due To Offset Y (Units)
0	8	-759	180	83	720	75	-39
345	199	-743	165	-112	704	87	-39
330	383	-677	150	-292	638	91	-39
315	540	-569	135	-448	527	92	-42
300	666	-421	120	-573	381	93	-40
285	749	-249	105	-658	206	91	-43
270	783	- 62	90	-696	14	87	-48
255	770	132	75	-681	-179	89	-47
240	706	314	60	-616	-362	90	-48
225	597	473	45	-504	-521	93	-48
210	449	601	30	-359	-645	90	-44
195	273	687					
180	(DATA UNAVAILABLE DUE TO TEXT FIXTURE LIMITATION)						
165							
	TOTAL OFFSETS					978	477
	AVERAGE OFFSETS					88.9	43.4

Table 4-2 X AND Y AXIS ERROR MEASURED BY ROTATING X, Y AROUND Z IN THE HORIZONTAL PLANE

Protractor Heading Measurement (Degrees)	Hz Data Measured (Units)	Protractor Heading Measurement (Degrees)	Hz Data Measured (Units)	Offset Error (Units)
0.5	0	180.5	-56	-56
315.5	-527	135.5	469	-58
270.5	-763	90.5	707	-56
225.5	-571	45.5	513	-58
		TOTAL OFFSET		-228
		AVERAGE OFFSET		-57

Table 4-3 Z AXIS OFFSET ERROR MEASURED BY ROTATING THE Z AXIS AROUND THE VERTICAL X AXIS

Sensor Axis	Total Average Offset (Units)	Required Correction	Amount of Correction Decimal	Binary	Hex
X	88.9	Subtraction	45	00101101	02D0
Y	43.4	Addition	22	00010110	0160
Z	47.0	Addition	29	00011101	01D0

Table 4-4 OFFSET CORRECTION VALUES

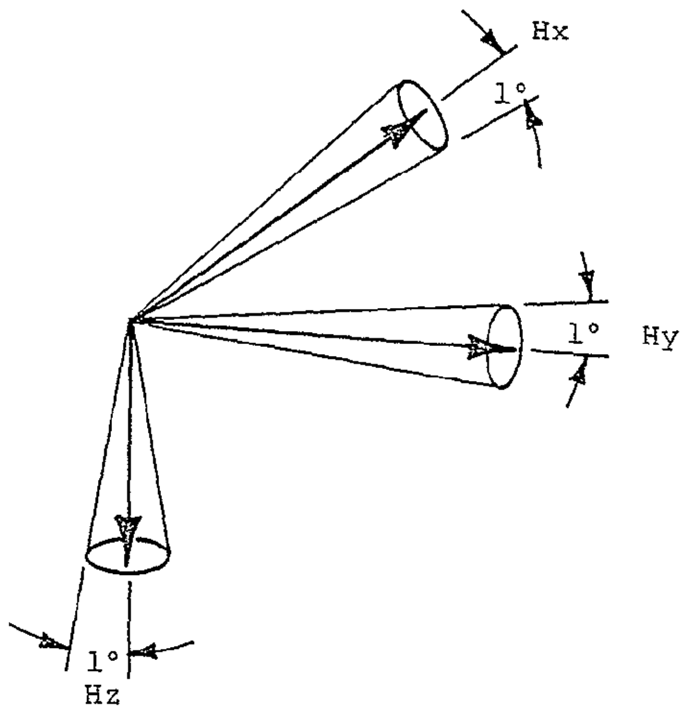

Fig. 4-1 SENSOR ALIGNMENT UNCERTAINTY

Although this error source can be reduced by physically aligning the sensors more accurately during assembly, cost of the sensors increases. Ultimately, directionality of the magnetic sensors becomes a function of the physical sensor itself and more accurate sensors are required as pointed out by Gise [Ref. 4-2]. A heading system that tolerates sensor misalignment is therefore a very desirable alternative to requiring precise alignment or more elaborate sensors.

During assembly of the Develco fluxgate magnetometer sensor array, sensor misalignment is determined by using earth's magnetic field and a precision mechanical rotation assembly. A sensor (assume the X axis) is aligned with earth's magnetic vector by positioning the sensor to maximize electrical output[3]. One of the other sensors (assume the y axis) is aligned with the rotation axis of the precision calibration assembly (Fig. 4-2) and perpendicular to the first by rotating the sensor array around the second sensor axis (y axis in this case) and adjusting its relative position until a null output is achieved at all rotation angles. Mechanical orthogonality of the sensors is then limited only by the mechanical imprecision of the calibration device (orthogonality within ±0.01 degrees can be easily achieved in the calibration tool) and by the directional characteristics of the physical sensors.

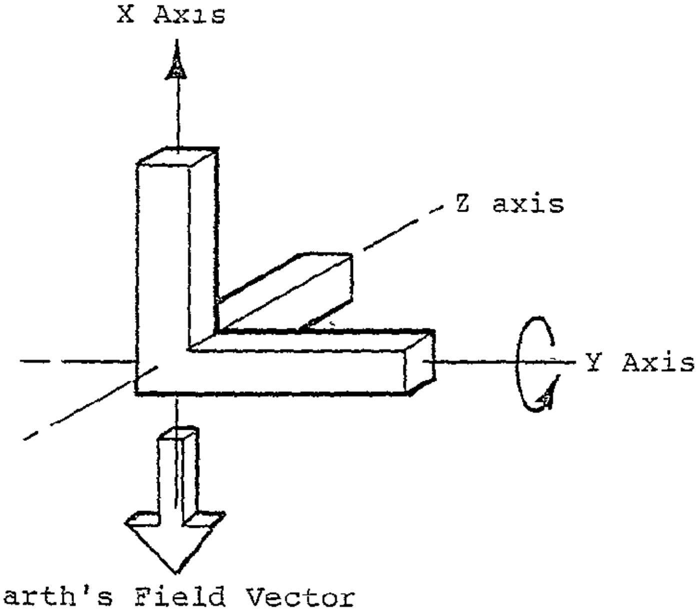

Fig. 4-2 MECHANICAL ORIENTATION OF THE MAGNETOMETER SENSORS DURING CALIBRATION

In addition to functioning as an alignment apparatus, the calibration device described above provides a convenient means

[3]By maximizing or nulling a measurement, the mechanical positioning is a function of only the field and the resolution of the voltage measuring device obviating errors due to physical position measurement.

to characterize sensor assemblies after final assembly adjustments are made. Any misalignment of the second sensor relative to the first results in a coning of the second sensor around the rotation axis[4] with a sinusoidal output voltage that is a function of total earth's magnetic field and axis alignment error. The peak to peak voltage resulting from sensor coning is recorded during the final alignment test and made available to sensor purchasers. Coning voltages developed for the sensor assembly used with this experiment were obtained from Develco [Ref. 4-3] and are recorded in Table 4-5. Sensor misalignment for each axis can be derived using additional data provided by Develco along with additional empirical data derived by experimentation.

The total ambient magnetic field at the Develco laboratory is measured using the three sensors (applying equation 4-1) and is supplied as digital data. In our case, the total field measured was 1573 units or

$$\frac{1573 \text{ units}}{\begin{array}{l}2048 \text{ units}\\ \text{Full Scale (F.S.)}\end{array}} \times 60{,}000 \text{ gamma F.S.} = 46{,}084 \text{ gamma } (\gamma)$$

$$\text{Sensitivity of the sensor} = \frac{2.5 \text{ Volts F.S.}}{60{,}000\ \gamma\text{F.S.}} = 42\ \mu\text{Volts}/\gamma$$

Considering the X axis sensor, coning resulted in a signal of 38 mV peak to peak (or 19mV peak). Misalignment of the X axis sensor from the Y-Z plane can then be calculated as

[4]Assume that the first axis is initially adjusted for maximum output to align it with earth's field and the rotation axis is perpendicular to the field.

SENSOR ASSEMBLY NO. S/N 1043-013

Rotation Axis	Coning Voltage (Peak-Peak mV)	Orthogonality Error (Degrees)
X	38	0.57
Y	8	≈0
Z	51	0.76

Table 4-5 MAGNETOMETER ORTHOGONALITY MEASUREMENTS

Peak Signal = 19 mV or 456 gamma angular misalignment

$$\varepsilon_x = \sin^{-1} \frac{456}{46{,}084}$$

$$\varepsilon_x = 0.57 \text{ degrees}$$

Similarly, the Y and Z axis have misalignment errors of $\varepsilon y \approx 0$ and $\varepsilon z = 0.76$ degrees with respect to the X-Z and X-Y planes respectively (sensor orthogonality errors are tabulated in Table 4-5).

Having established that sensor orthogonality errors exist, the remaining task is to identify the direction that the sensor axis points relative to the other two sensor axes. Since the Y axis has relatively little orthogonality error, it will be assumed to be perpendicular to the X-Z plane. In addition, since the Hz data enters into the algorithm in a second order manner relative to the Hx and Hy measured data, correction and characterization of the Hx sensor was considered to be of primary concern. Orientation of the X axis sensor relative to the Y and Z axes was determined empirically.

Angular position of the X axis sensor can be described using the error angles εxy and εxz as delineated in Fig. 4-3. Characterization of sensor orthogonality error in terms of these two angles would enable algorithmic corrections of measured data.

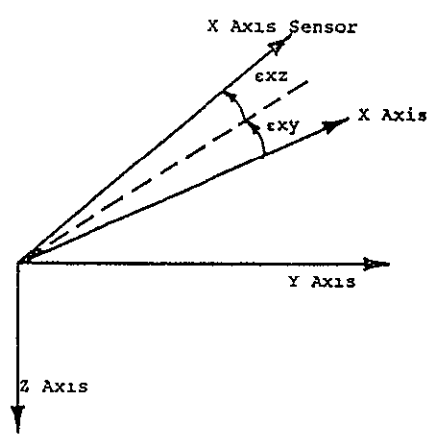

Fig. 4-3 X AXIS SENSOR ORIENTATION

1) Empirical Determination of εxz

The angle εxz (angle between the x axis sensor and the z axis of the geodetic coordinate system) was determined in several steps using the test apparatus described in Chapter V.

i) The x and y sensors were oriented in the horizontal plane with the z axis sensor vertical downward.

ii) The x and y sensors were rotated around the z axis with magnetic data measurements (corrected for sensor offset error as described in Section 4-2A) recorded in Table 4-6 for incremental rotation angles.

iii) The total horizontal field at each angular position was calculated

$$Hht = (Hx^2 + Hy^2)^{\frac{1}{2}}.$$

iv) Average horizontal field Hav was computed by averaging the results of iii) above.

v) The horizontal field deviation Hd was computed for each angular position; tabulated in Table 4-6 and plotted on Fig. 4-4.

$$Hd = (Hav - Hht)$$

The horizontal field deviation or error (as shown on Fig. 4-4) was now examined. An angular error εxz should cause the horizontal field error curve to peak at 90 and 180 degrees. Since this obviously was not the case, it was concluded that major error in x axis orthogonality was due to the component εxy.

Physical* Heading (Degrees)	Displayed** Heading (Degrees)	Measured Data (Units) Hx	Hy	Total Computed Horizontal Field (Hht) (Units)	Hd (Hav-Hht) (Units)
355	90	12	-727	727	-3
335	70	258	-682	729	-1
315	50	477	-555	732	2
295	30	637	-362	733	3
275	10	720	-127	731	1
255	350	718	127	729	-1
235	330	628	363	725	-5
215	310	464	569	734	4
195	290	242	687	728	-2
175	270	-10	731	731	1
155	250	-258	686	733	3
135	230	-476	557	733	3
115	210	-635	362	731	1
95	190	-721	123	731	1
75	170	-718	-133	730	0
55	150	-628	-371	729	-1
35	130	-460	-565	729	-1

Total Hht = 12415

Average (Hav) = 730

*Measured using a protractor on the test apparatus.
**Computed and displayed digitally by the instrument.

Table 4-6 MEASUREMENT OF HORIZONTAL FIELD

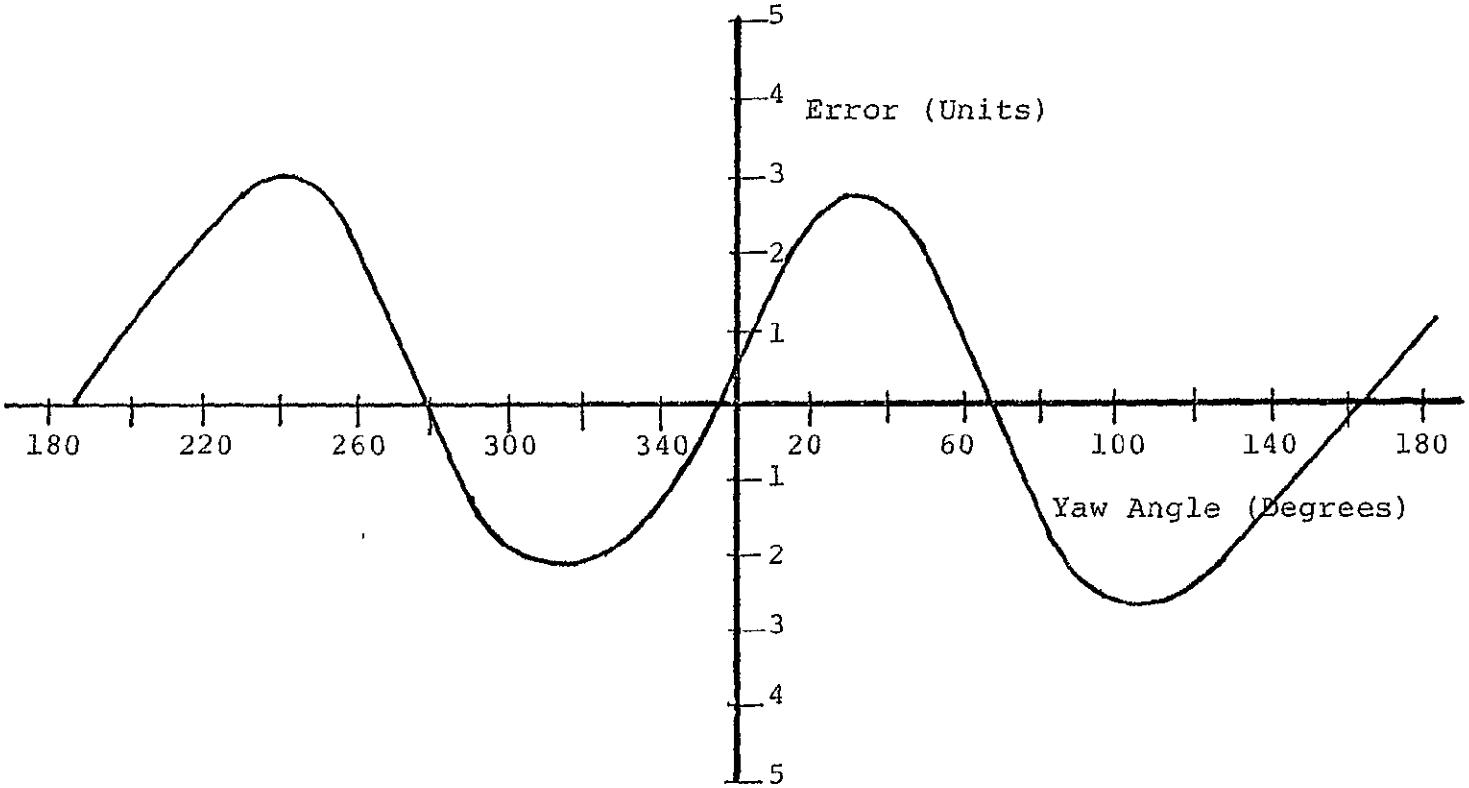

Fig. 4-4 DEVIATIONS OF THE HORIZONTAL FIELD MEASUREMENT FROM THE MEAN

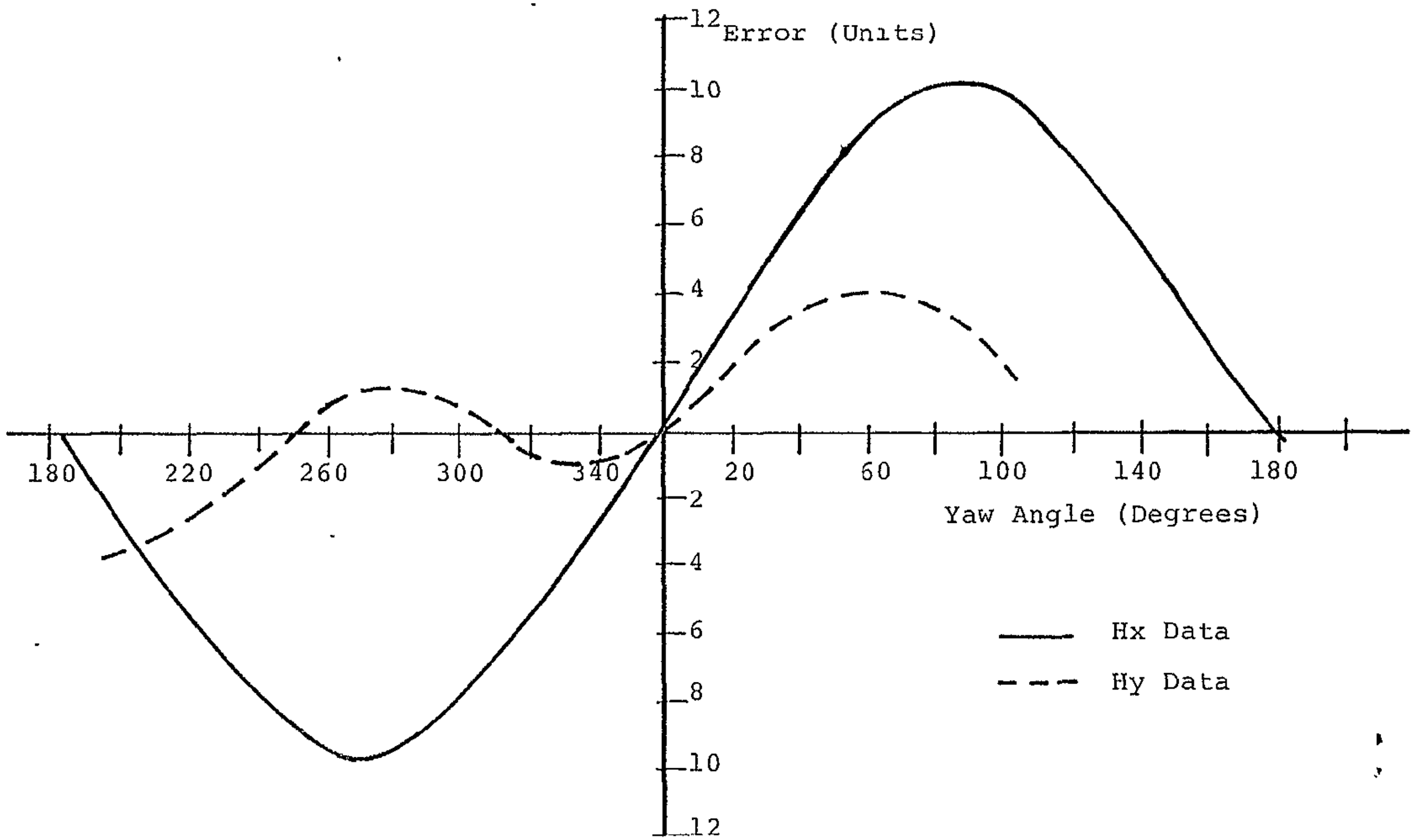

Fig. 4-5 DEVIATION OF Hx AND Hy DATA FROM THE COMPUTED FIELD COMPONENTS AS A FUNCTION OF YAW

2) Empirical Determination of εxy

The angle εxy representing x axis sensor misalignment relative to axis y was measured as follows:

Steps i) and ii) above were repeated with the exception that the calculated values for Hx and Hy (Hxc and Hyc respectively) were recorded with measured Hx and Hy data (Hxm and Hym respectively) in Table 4-7. The calculated values were obtained by assuming that the angle εxz as determined above was negligible and that the y axis sensor was perpendicular to the x-z plane. With these assumptions, we note that at the heading of zero degrees (extrapolated between display of 10 and 350 degrees of Table 4-7 and Fig. 4-5), there is no error in yaw due to either Hx or Hy. By physically rotating the sensors in fixed intervals from yaw = 0 degrees and noting that the horizontal field Hh = 730 units, we can then compute expected Hx and Hy data at respective yaw orientations.

Physical orientation of the x axis sensor is easily determined by considering orientation at the maximum error excursions. These observations are illustrated in Fig. 4-6. We note that the only possible orientation of the x axis sensor satisfying the data in Fig. 4-5 is that of Fig. 4-6.

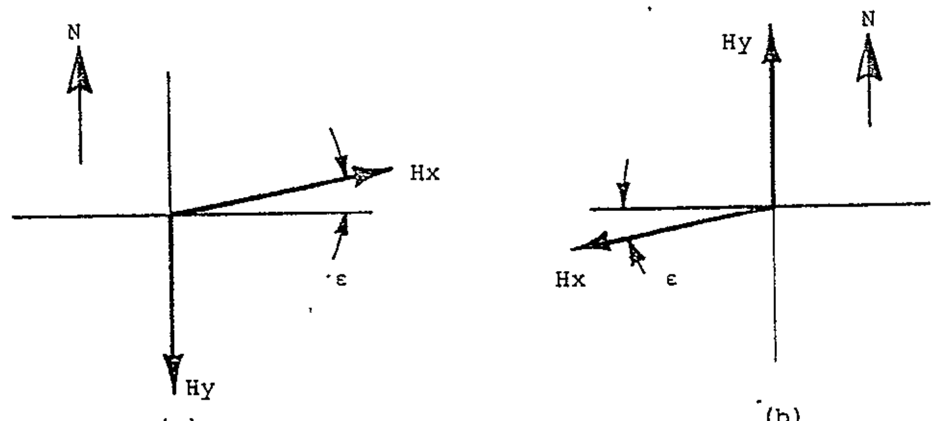

Fig. 4-6 (a) SENSORS ORIENTED AT YAW = +90 degrees
(b) SENSORS ORIENTED AT YAW = +270 degrees

Physical* Heading (Degrees)	Displayed** Heading (Degrees)	Measured Data (Units)		Computed Data (Units		Deviation (Units)	
		Hxm	Hym	Hxc	Hyc	(Hxm-Hxc)	(Hym-Hyc)
355	90	12	-727	0	-730	+12	+ 3
335	70	258	-682	250	-686	+ 8	+ 4
315	50	477	-555	469	-559	+ 8	+ 4
295	30	637	-362	632	-365	+ 5	+ 3
275	10	720	-127	719	-127	+ 1	0
255	350	718	127	719	+127	- 1	0
235	330	628	363	632	365	- 4	- 2
215	310	464	569	469	559	- 5	10
195	290	242	687	250	686	- 8	1
175	270	-10	731	0	730	-10	1
155	250	-258	686	-250	686	- 8	0
135	230	-476	557	-469	559	- 7	- 2
115	210	-635	362	-632	365	- 3	- 3
95	190	-721	123	-719	+127	- 2	- 4
75	170	-718	-133	-719	-127	1	- 6
55	150	-628	-371	-632	-365	4	- 6
35	130	-460	-565	-489	-559	9	- 6

* Measured using a protractor on the test apparatus.
** Computed and displayed digitally by the instrument.

Table 4-7 MEASURED AND COMPUTED Hx AND Hy DATA IN THE HORIZONTAL PLANE

Magnitude of the angle ϵxy can be computed as follows using data from Fig. 4-5

Max. delta from Fig. 4-5 = 10 units
Average horizontal field = 730 units

$$\epsilon xy \max = \sin^{-1} \frac{10}{730}$$

$$= 0.79 \text{ degrees}$$

We note that the angle of 0.79 degrees is approximately the same as determined by Develco during manufacture of the sensors (Table 4-5). The added error is due to test set inaccuracy.

C) Fluxgate Sensor Noise Induced Error

The analog output from the fluxgate sensors can exhibit an error due to signal uncertainty resulting from noise. Although the data sheet [Ref. 3-34] indicates that 5mV peak to peak of ripple can exist on the output, the frequency content centers in the 550 kHz range (driver frequency of the fluxgate magnetometer) and no appreciable ripple[5] exists below 60 Hz (especially when the sensor output is filtered prior to data sampling). The noise specification of less than 1 gamma peak to peak in the 1 Hz bandwidth region is also negligible. In summary, no appreciable error due to noise on the magnetometer signal lines is evident.

D) Magnetometer Gain Error

The magnetometer is specified to have gain (sensitivity) of 2.5 Volts/600 milligauss, $\pm 1\%$ which translates into a maximum signal uncertainty of

[5]Verbally confirmed by Workentine of Develco [Ref. 4-1].

$$\pm(2.5V \times 0.01) = \pm 25 \text{ mV}.$$

This represents a sensor transfer function of 4.16 Volts/gauss or 0.24 gauss per volt. The uncertainty then can be expressed as

$$\pm(0.24 \text{ gauss} \times 0.01) = \pm 2.4 \text{ milligauss}$$
$$= \pm(2.4 \times 10^2) \text{ gamma}$$

Since this error is not corrected in the laboratory instrument it will be considered in total in the final error analysis. It is worth noting however, that should the magnetometer gain uncertainty be characterized, gain corrections for each sensor could be made during computation by the computer. In addition the error term is proportional to actual signal level applied.

E) Magnetometer Linearity Error

D.C. linearity of the magnetometer is specified to be $\pm 0.5\%$ of signal level. This uncertainty at full scale can be expressed as $\pm(2.5 \text{ Volts} \times 0.005) = \pm 12.5\text{mV}$. Alternately, linearity error can cause a signal uncertainty of ± 1.2 milligauss or $\pm(1.2 \times 10^2)$ gamma. Linearity error is also not corrected during computation and is considered in the final error analysis. By simply characterizing and correcting the linearity characteristics of each sensor, considerable improvement in system accuracy could be achieved.

4-3 ANALOG SUBSYSTEM ERROR ANALYSIS

The analog subsystem of the instrument is outlined in block diagram form in Fig. 4-7. This subsystem accepts analog signals from magnetometer and gyroscope transducers, performs a time division multiplexing between the signals and digitizes

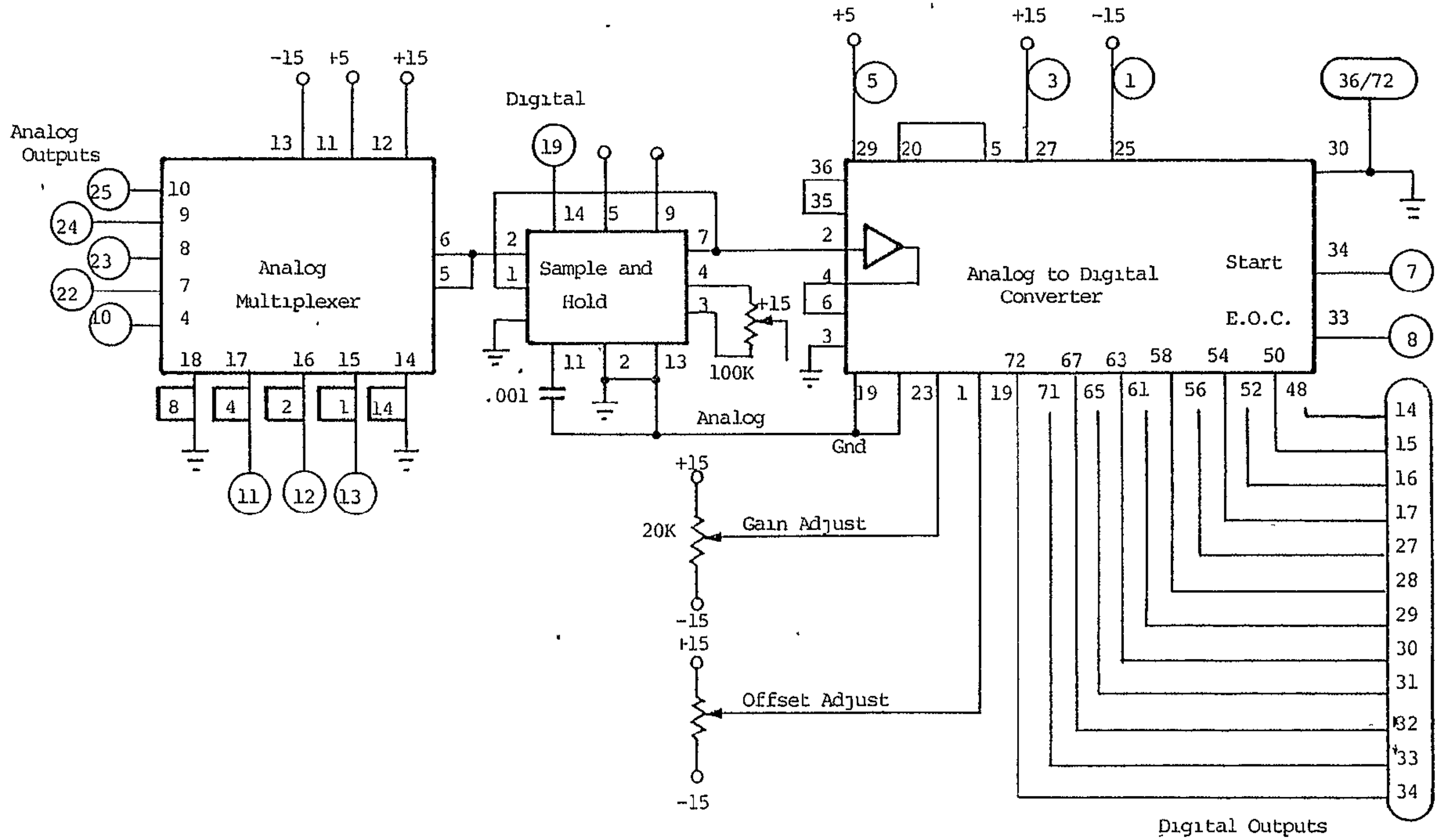

Fig. 4-7 THE ANALOG SUBSYSTEM

the respective signals prior to subsequent processing by the computer. During this data acquisition and conversion process, errors are introduced into each of the signals. This section addresses the potential error sources and computes the respective error contributions to be expected during operation of the instrument.

Although the multiplexer and sample and hold blocks of Fig. 4-7 could be eliminated (eliminating possible error sources) by digitizing each signal with a unique analog to digital converter, it can be shown that such a system would be expensive and difficult to implement. The analog to digital converter (A/D) quantizes an analog signal in a finite amount of time. Speed of conversion is predicted in a finite amount of time by both the resolution of the converter and the frequency of the signal to be converted. Time required to perform a conversion is generally called the "aperature time".

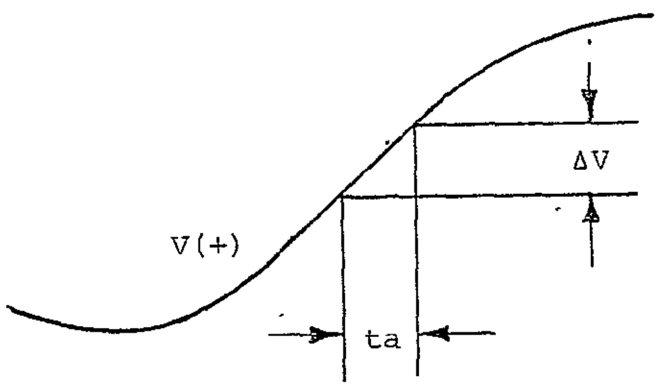

Fig. 4-8 APERATURE TIME AND AMPLITUDE UNCERTAINTY

As illustrated in Fig. 4-8, aperature time and amplitude uncertainty are related by the time rate of change of the analog signal. For the particular case of a sinusoidal signal to be converted, the maximum rate of change occurs at the zero crossing of the waveform and the amplitude change is:

$$\Delta V = \frac{d}{dt} (V \sin wt)_{t = 0} \times ta \qquad (4\text{-}1a)$$

$$\Delta V = V\ w\ ta \qquad (4\text{-}1b)$$

$$\text{giving } \frac{\Delta V}{V} = w\ ta = 2\ \pi f\ ta. \qquad (4\text{-}2)$$

From this result we can determine the aperature time required to digitize a 30 Hz signal to 12 bits resolution (a resolution of 1 part in 4096 or 0.0244%).

$$ta = \frac{V}{V} \times \frac{1}{2\ f} = \frac{.000244}{6.28 \times 30} = 1.3 \times 10^{-6}$$

This result indicates that to remain within 1 bit of resolution (0.0244%) we require an aperature time of 1.3 microseconds to process analog signals varying at a rate of 30 Hertz. It can be seen that the system would require fast A/D converters plus extremely fast computational capability to accommodate this configuration of sensors and analog subsystem. By using multiplexing and sample and hold circuitry we can however reduce the number of A/D converters required to one and alleviate the aperature and processing requirements imposed above.

The operation of sampling to be used by the instrument is illustrated in Fig. 4-9 which shows an analog signal and a train of sampling pulses. The pulses are provided by the central processing unit. A switch connects the analog signal for a very short period of time to the hold circuitry charging a capacitor and storing the sampled voltage until the next sample is required. This type of sampler is called sample and hold.

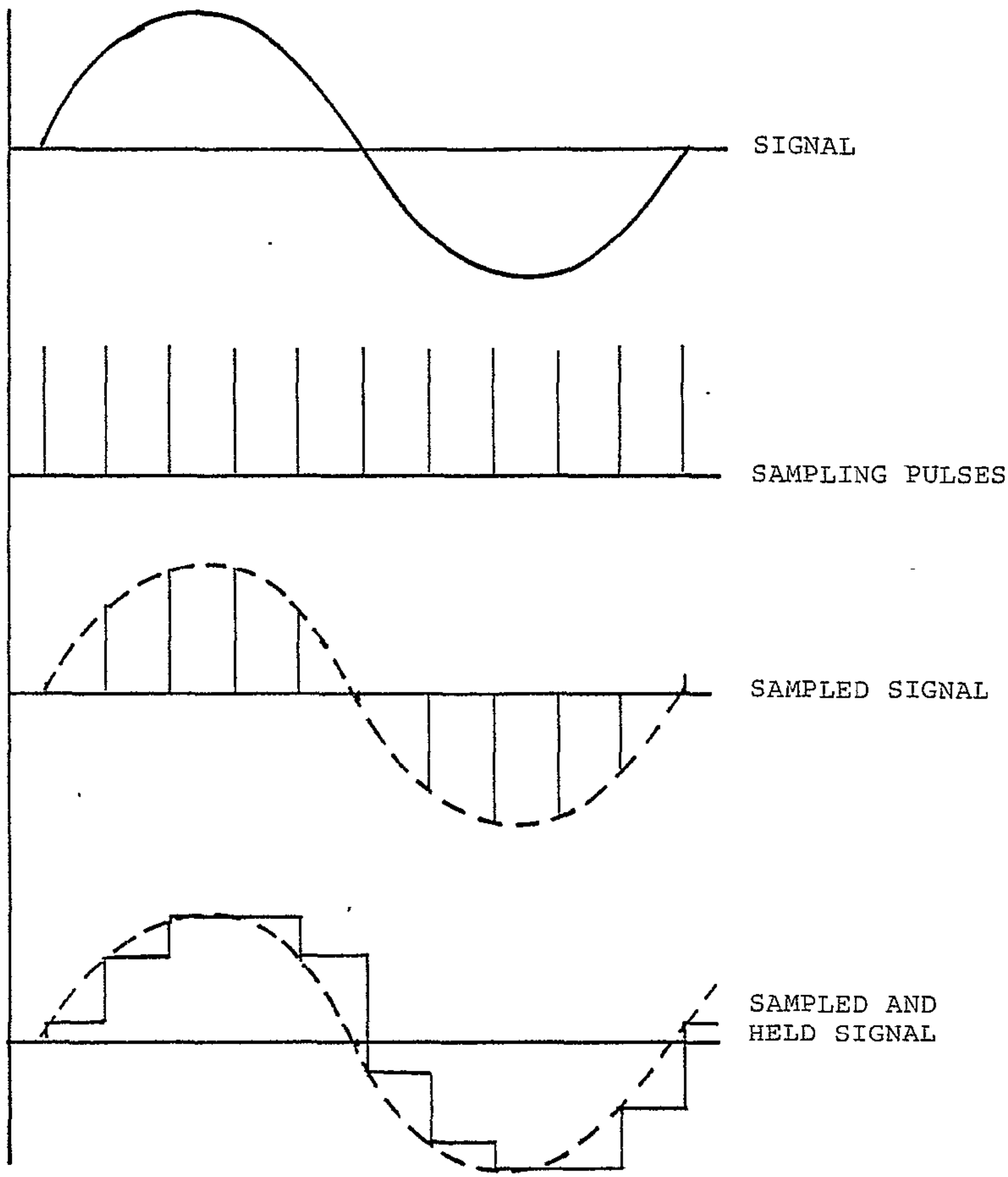

Fig. 4-9   SIGNAL SAMPLING PROCESS

A) Sampling Rate Errors

The process of uniformly sampling a function of continuous time can yield a significant source of error if the sampling period T is selected too large [Ref. 4-4, 4-5]. This error can be illustrated by considering an analog signal xa(t) that has the Fourier representation [Ref. 4-6]

$$xa(t) = \frac{1}{2\pi}\int_{-\infty}^{\infty} Xa(j\Omega)e^{j\Omega t}d\Omega \tag{4-3a}$$

$$Xa(j\Omega) = \int_{-\infty}^{\infty} xa(t)e^{-j\Omega t}dt \tag{4-3b}$$

The sequence x(n) with values x(n) = xa(nT) is said to be derived from xa(t) by periodic sampling and T is the sampling period. The reciprocal of T is called the sampling frequency or sampling rate. In order to determine the sense in which x(n) represents the original signal xa(t), it is convenient to relate Xa(jΩ), the continuous-time Fourier transform of xa(t), to $X(e^{j\Omega})$, the discrete-time Fourier transform of the sequence x(n). From (4-3a) we note that

$$x(n) = xa(nt) = \frac{1}{2\pi}\int_{-\infty}^{\infty} Xa(j\Omega)e^{j\Omega nt}d\Omega \tag{4-4}$$

From the discrete-time Fourier transform we also obtain the representation [Ref. 4-4]

$$x(n) = \frac{1}{2\pi}\int_{-\pi}^{\pi} X(e^{j\omega})e^{j\omega n}d\omega \tag{4-5}$$

To relate the equations (4-4) and (4-5) we can express (4-4) as a sum of integrals over intervals of length 2π/T, as in

$$x(n) = \frac{1}{2\pi}\sum_{r=-\infty}^{\infty}\int_{(2r-1)\pi/T}^{(2r+1)\pi/T} Xa(j\Omega)e^{j\Omega nT}d\Omega \tag{4-6}$$

Each term in the sum can be reduced to an integral over the range $-\pi/T$ to $+\pi/T$ by a change of variables to obtain

$$x(n) = \frac{1}{2\pi} \sum_{r=-\infty}^{\infty} \int_{-\pi/T}^{\pi/T} Xa\left[j(\Omega+\frac{2\pi r}{T})\right] e^{j(\Omega+\frac{2\pi r}{T})nT} d\Omega \tag{4-7a}$$

$$x(n) = \frac{1}{2\pi} \sum_{r=-\infty}^{\infty} \int_{-\pi/T}^{\pi/T} Xa(j\Omega+j\frac{2\pi r}{T}) e^{j\Omega nT} e^{j2\pi rn} d\Omega \tag{4-7b}$$

If we now change the order of integration and summation and note that $e^{j2\pi rn} = 1$ for all integer values of r and n, we obtain

$$x(n) = \frac{1}{2\pi} \int_{-\pi/T}^{\pi/T} \left[\sum_{r=-\infty}^{\infty} Xa(j\Omega+j\frac{2\pi r}{T})\right] e^{j\Omega nT} d\Omega \tag{4-8}$$

By substituting $\Omega = \omega/T$ we get

$$x(n) = \frac{1}{2\pi} \int_{-\pi}^{\pi} \left[\frac{1}{T} \sum_{r=-\infty}^{\infty} Xa(\frac{j\omega}{T}+j\frac{2\pi r}{T})\right] e^{j\omega n} d\omega \tag{4-9}$$

which is identical in form to equation (4-5). We can therefore make the identification (equating like terms of (4-5) and (4-9)

$$X(e^{j\omega}) = \frac{1}{T} \sum_{r=-\infty}^{\infty} Xa(\frac{j\omega}{T}+j\frac{2\pi r}{T}) \tag{4-10}$$

We can also express (4-10) in terms of the analog frequency variable Ω (where $\Omega = \omega/T$) as

$$X(e^{j\omega T}) = \frac{1}{T} \sum_{r=-\infty}^{\infty} Xa(j\Omega+j\frac{2\pi r}{T}) \tag{4-11}$$

The last two equations clearly reveal the relationship between the continuous-time Fourier transform and the Fourier transform of a sequence derived by sampling. For example, if Xa $(j\Omega)$ is as depicted in Fig. 4-10a then $X(e^{j\omega})$ will be as shown in Fig. 4-10b when the sampling period T is too long and as shown in Fig. 4-10C if T is short enough.

From Fig. 4-10c it is obvious that if $\frac{\Omega oT}{2} < \pi$, i.e., we sample at a rate at least twice the highest frequency of $Xa(j\Omega)$, then $X(e^{j\omega})$ is identical to $Xa(\omega/T)$ in the interval $-\pi \leq \omega \leq \pi$ and can be recovered from the samples $xa(nT)$ by an appropriate interpolation formula.

For the remote magnetic indicator instrument designed in previous chapters, the analog signals are filtered with a low pass section reducing frequency content above 30 Hz. The sampling rate must therefore exceed 60 Hz (T<16.67 m.s.) to enable accurate dynamic operation of the system.

Laboratory measurements of sampling rates on the functional microprocessor based instrument revealed that the analog subsystem operated at a sampling rate of 62.5 Hz (16 m.s.) indicating that the algorithm execution rate supported a system bandwidth of 31.25 Hz. If frequency content of the analog signals is less than 31.25 Hz there is no error due to sampling.

B) Analog Multiplexer Induced Error

The analog multiplexer of Fig. 4-7 selectively connects one analog transducer output at a time to the input of the sample and hold subsystem. The Datel Systems, Inc., multiplexer [Ref. 4-7] selected for the remote magnetic indicator experiment features eight MOS-FET switches with associated driver circuits,

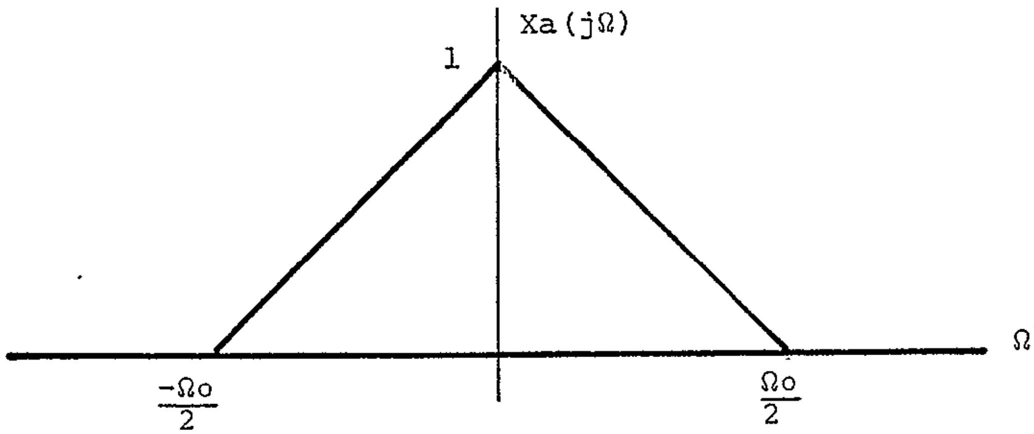

(a) Fourier transform as a continuous-time signal

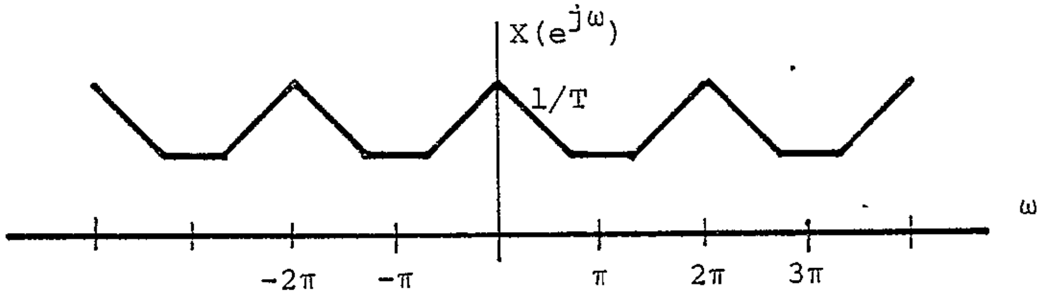

(b) Fourier transform of the discrete-time signal obtained by periodic sampling (T is too large)

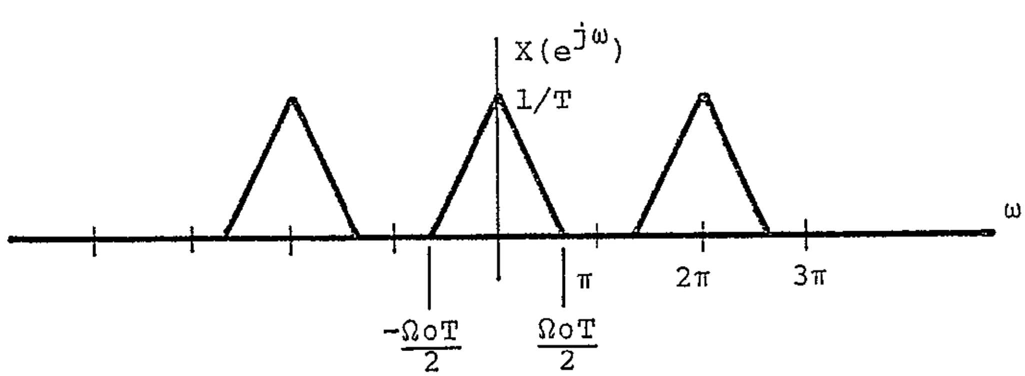

(c) Same as (b) except T is short enough

Fig. 4-10 FOURIER TRANSFORMS OF CONTINUOUS AND DISCRETE-TIME SIGNALS

FET pull-up to reduce propogation delays and all of the necessary decoding logic to enable random channel addressing with a four bit parallel binary input.

Several important parameters are used to characterize analog multiplexers and can contribute error.

1) Transfer Accuracy

Transfer accuracy is a function of the source impedance, switch resistance, load impedance (if the multiplexer is not buffered) and the signal frequency. It expresses the input to output error as a percentage of the input. In our case the system configuration predicates a maximum error due to transfer accuracy of ($\pm$0.01%) yielding an error term of

$$\pm 0.0001 \times 2.5 \text{ Volts} = \pm 25 \text{ mV}$$

2) Settling Time

This parameter defines the time elapsed from the application of a full scale step input to the time when the output has entered and remained within a specified error band around its final value. In our case the selected multiplexer has a maximum settling time of 1 microsecond to $\pm$0.01% full scale (F.S.) Since the control system selecting channels is implemented using a microprocessor, the minimum time between analog subsystem commands will always be greater than 3.0 microsecond[6]. The multiplexer will therefore always have settled to the final value before the sample and hold circuit (following this subsystem) can be activated with no error due to the settling time parameter.

[6]One machine cycle time for the 2650 microprocessor with 1 mHz clock frequency.

3) Throughput Rate

The highest rate at which the multiplexer can switch from channel to channel at its specified accuracy is in this case 500 kHz. Since this rate is more than four orders of magnitude greater than the operational rate of the subsystem there is no error due to throughput rate limitations.

4) Input Leakage Current

The amount of signal coupled to the output as a percentage of input signal applied to all OFF channels together can be calculated by considering the maximum leakage current specified from OFF channels to the ON channel. In our case the maximum error signal can be calculated

$$\text{Error} = \left[\, 4\ (8\ \text{na} \times 2000\ \text{ohms source imped.})^2 \,\right]^{\frac{1}{2}}$$

$$\text{Error} = 32\ \text{microvolts}$$

Note that in this case the voltage levels are statistically independent allowing an R.S.S. of error sources to calculate total error [Ref. 4-8, 4-9].

C) Sample and Hold Circuit Induced Errors

The sample and hold subsystem consists of a switch and capacitor arrangement as shown in Fig. 4-11. The Datel Systems, Inc., model SHM-IC-1 integrated circuit sample and hold device [Ref. 4-10] features a self-contained high gain differential input amplifier, a digitally controlled electronic switch and a high input impedance buffer amplifier. The external components used with the sample and hold circuit in the solid state remote magnetic indicator instrument consisted of the 0.001μf holding capacitor and a 100K offset trimpot. By connecting the output back to the negative input of the input amplifier (Fig. 4-11), the sample and hold subsystem operated in a unity gain, noninverting mode. When the switch is closed, the unit is in the sampling or tracking mode (Digital Control = 0 Volts), and will follow a changing input signal.

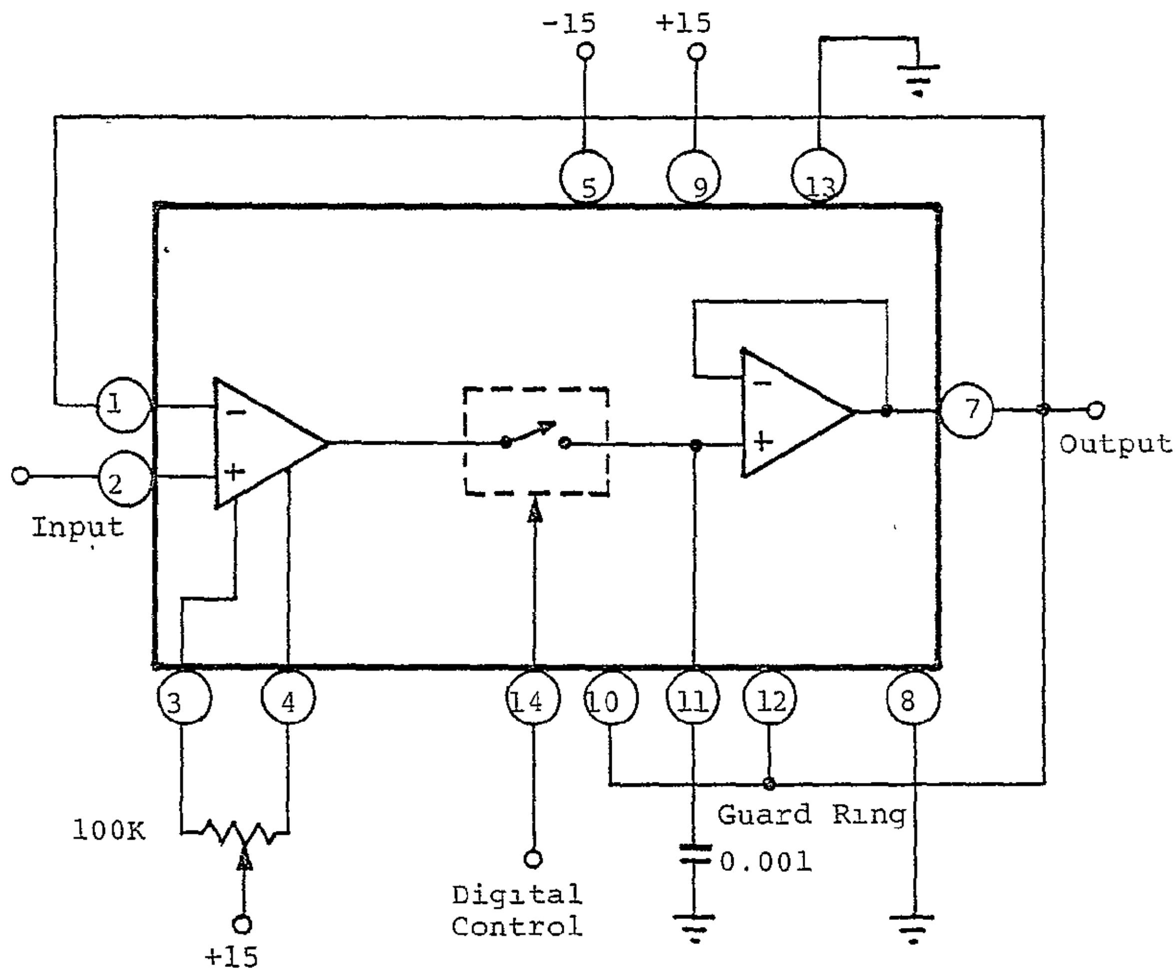

Figure 4-11 SAMPLE AND HOLD SUBSYSTEM

When the switch opens the unit is in the hold mode and retains a voltage on the capacitor for some period of time depending on capacitor and switch leakage. Sample and hold devices are characterized by a number of important parameters that must be considered in the design of a data acquisition subsystem.

1) Acquisition Time

The time lapse between the time that the sample command is given to the point where the output enters and remains within a specified error band around the input value is specified to be less than 4 microseconds time to transit from 0 to 0.1% of 10 Volts with C = 0.001 μf [Ref. 4-10]. This implies that the control signals emanating from the central processor should allow at least 4 μs acquisition time prior to entering the hold mode. We note that the sample and hold subroutine (Appendix B) executes the instruction

IORI, R3 H'80' READY TO HOLD,

a two machine cycle instruction prior to sending the hold control signal. This instruction delays control signal transmission by (2 x 3 μs) = 6 μs allowing the sample and hold circuit ample time to settle with no appreciable error due to the acquisition time parameter.

2) Hold Mode Voltage Droop

The maximum change in output voltage as a function of time is specified to be 50 mv/sec maximum using a 0.001 μf polystyrene capacitor. Since the maximum total accumulated time to completion of the analog to digital conversion can be calculated as

5 Instructions (11 machine cycles)	= 33 μs
1 Analog to Digital Conversion	= 20 μs
3 Instructions if Conversion not synchronized with instructions (7 machine cycles)	= 21 μs
	74 μs

we can then compute droop error to be 50 mv/sec x (74 x 10^{-6}) sec = 3.73 mv.

3) Aperature Delay

The maximum time lapse between the time of hold signal receipt to opening of the switch is specified to be 50 nsec, an insignificant length of time in the instrument. There is therefore no error due to aperature delay.

4) Offset Error

Although the maximum offset error is specified to be 20 mv maximum [Ref. 4-10], the error was eliminated using the 100K trimpot offset adjustment. There was no appreciable offset error contribution due to the sample and hold circuit.

5) Gain Error

The gain error of a sample and hold circuit is apparent during the sample mode when the transfer function of the total amplifier deviates from the ideal unity slope condition (Fig. 4-12). In the noninverting unity gain mode, the specified gain error is $\pm 0.05\%$ maximum yielding a signal error of

$$(\pm 0.0005) \times 5.0 \text{ V} = 250 \text{ mV}$$

This error can, however, be eliminated with the gain

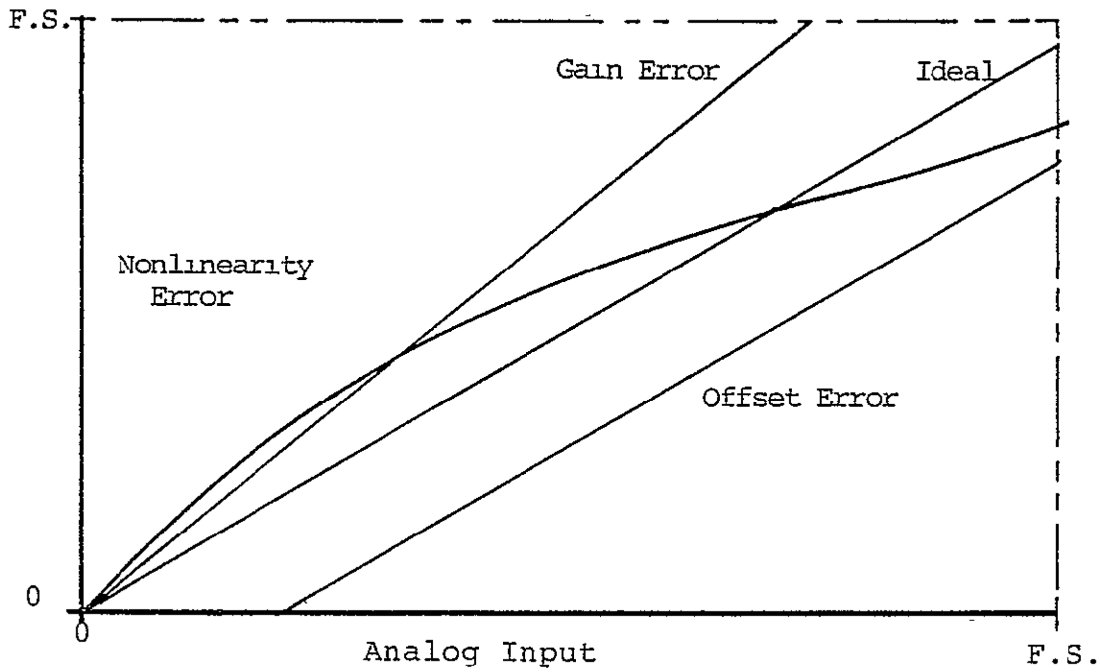

Fig. 4-12 GAIN, OFFSET AND LINEARITY ERRORS

adjustment available at the analog to digital converter. There will therefore be no appreciable net gain error due to the analog subsystem.

6) Nonlinearity Error

Nonlinearity error is apparent in the sample and hold circuit if the transfer function departs from a linear curve (Fig. 4-12). In the noninverting unity gain mode with a 0.001 µf holding capacitor the maximum nonlinearity is 0.01% resulting in a worst case signal uncertainty of (.0001) x 2.5 Volts = 25 mV.

7) Hold Mode Feedthrough

This error appears due to input signal appearing at the output when the unit is in the hold mode. Although the feedthrough varies with signal frequency and the expected signal frequencies are substantially lower than the upper frequency limits of the sample and hold device (30 Hz max. versus several kiloHertz), we consider the worst case feedthrough of 0.01% [Ref. 4-10] or 25 mV.

D) Analog to Digital Converter Induced Errors

The A/D Converter selected for the solid state magnetic indicator instrument (Datel ADC-MA12B1B) [Ref. 4-11] uses the successive approximation technique to achieve excellent linearity and speed. Important parameters that potentially contribute errors are addressed below.

1) Resolution Error

The smallest analog change that can be distinguished by the A/D converter is

$$\text{Least Significant Bit (LSB)} = \frac{\text{Full Scale}}{2^n}$$

$$\text{LSB} = \frac{5}{2^{12}} = 1.22 \text{ mV}$$

this uncertainty manifests itself as an error in computing by limiting the precision of any calculation.

2) Linearity Error

The maximum deviation from a straight line drawn between the end points of the converter transfer function are specified in [Ref. 4-11] to be $\pm$ 1/2 LSB (in our case $\pm$1.22 mV of analog signal).

C-2

3) Accuracy Error

The input to output error of the A/D converter is specified in [Ref. 4-11] to be $\pm 0.012\%$ F.S. $\pm 1/2$ LSB or

$$\pm(0.00012) \times 5.00\text{V} \pm 1.22 \text{ mV} = \pm 1.82 \text{ mV Worst Case}$$

In reality, the two error terms are unrelated and the

$$\text{Rss Error} = \pm \left[(.00012 \times 5\text{V})^2 + (1.22\text{mV})^2\right]^{\frac{1}{2}}$$

$$\text{RSS Error} = \pm 1.36 \text{ mV}$$

4) Offset Error and Gain Error

Both the offset error and gain error were adjusted to zero using the trimming potentiometers (Fig. 4-7) and the calibration procedure outlined in Ref. 4-11. A reference signal of plus 1/2 LSB (1.22 mV) was applied to the converter and the offset trimming potentiometer adjusted until the output flickered equally between logic "0" and logic "1". The gain was then adjusted by setting the converter input to full scale minus 1-1/2 LSB (4.99817 Volts) and the gain trimming potentiometer was adjusted until the output flickered between logic "111...110" and logic "111...111". The above steps were repeated until no appreciable error in gain or offset was evident.

4-4 PROCESSING ERRORS

Errors in processing data accrue due to several sources including imprecision and truncation. Since the microprocessor selected for the instrument is inherently an eight bit device, single precision calculations are conducted with eight bits and double precision calculations are conducted with a total of sixteen bits. This section addresses the effects of computational precision and truncation in the various subroutines and relates these to overall computational accuracy. The various subroutines are analyzed in chronological order as they appear in the main program.

A) Subroutine "SAMP"

The sample subroutine (delineated in Fig. 3-6a) selects and digitizes analog signals by controlling respective analog subsystem modules. During the first portion of this subroutine, A/D converter data bits are stored in two consecutive bytes[7] in the computer memory. The A/D conversion precision of 12 bits is thereby preserved.

The second, third and fourth operations of the sample subroutine convert the unipolar binary format of the data to sign magnitude format, adds offset quantities and merely changes the signs of the Hx and Hy data. The operations are conducted in a double precision manner and precision of the data remains unaltered.

Correction of x axis orthogonality error is the final operation of the sample subroutine. Equation (3-1) is implemented at this point using a table lookup (for the sin function), multiplication and addition. The final result can be expressed as

$$Hx = Hx' + Hy \text{ Sin } \varepsilon$$

[7]A byte is accepted terminology for an eight bit data quantity.

where the respective quantities have the following forms

$$Hx^1 = x_1 + \sum_{i=1}^{11} a_i 2^i$$

$$Hy = x_2 + \sum_{j=1}^{11} a_j 2^j$$

$$\text{Sin } \varepsilon = \sum_{k=1}^{8} a_k 2^{-k}$$

and

x_1, x_2 are sign bits

$a_{i,j,k}$ equal 0 or 1 depending on whether the respective term is to exist or not

We can analyze the effects of imprecision and truncation by noting that the sin function has eight significant binary bits resulting in a resolution of 1/256 or 90°/256 = 0.352°.

The relative error in sin ε is computed by Dahlquist [Ref. 4-12] as follows

let $\tilde{a}$ = the approximate value of sin ε

a = the exact value of sin ε

then the relative error in $\tilde{a}$ is

$$(\tilde{a} - a)/a \text{ if } a \neq 0$$

Since data in the sin table has been truncated, maximum relative error can be as large as $\pm(1/2^{12})$ or $\pm 0.02\%$.

From the definition of relative error we obtain the following relationships between exact, estimate and estimated relative error

$$\tilde{a} = a + ar = a(1 + r)$$

If a_1, and a_2 have relative errors of $\pm 0.39\%$ and $+0.02\%$, respectively, then

$$\tilde{a}_1\tilde{a}_2 = a_1(1 \pm 0.0039)\ a\ \ (1 \pm 0.00024)$$
$$= a_1a_2(1 \pm 0.0039)(1 \pm 0.00024)$$

Thus, the relative error in $\tilde{a}_1\tilde{a}_2$ is

$$(1 \pm 0.0039)(1 \pm 0.00024) - 1 =$$
$$\pm(0.0039)\ \pm(0.0039)(0.00024)\ \pm(0.00024)$$
$$\cong \pm(0.0041)$$

Since the maximum value of Sin ε to be encountered occurs when the orthogonality error (ε) is 1 degree, sin ε = 0.017 maximum. The maximum value for Hy can be 0.6 gauss or 2048 units. Maximum error due to imprecision in the product HySinε is then

$$\text{Er Max} = (2048 \times 0.017)(1 + .0041) - (2048 \times 0.017)$$
$$= 0.1427 \text{ units}$$

Since only the integer portion is retained in the final product, insignificant error can be attributed to imprecision of the sin ε term in this case. Orthogonality error will be adequately corrected.

B) Subroutines ROTX and ROTY

These subroutines were developed in Chapter III and implement the equation of 2-11 required to compute horizontal x and y magnetic field components. Equations to be implemented by the respective subroutines are

$$Hx = Hxm \text{ Cos (pitch)} + Hym \text{ Sin (pitch) Sin (roll)} + Hzm \text{ Sin (pitch) Cos (roll)} \tag{4-12}$$

and

$$Hy = Hym \text{ Cos (roll)} - Hzm \text{ Sin (roll)} \tag{4-13}$$

where Hxm, Hym and Hzm are measured field components made available from the magnetometer via the analog subsystem.

Since the transcendental functions are implemented using table lookup and are limited in precision to 8 bits, imprecision in these variables will dominate in generating error. In particular, the sin/cos terms will have relative error in the order of $\pm 1/256$ or $\pm 0.39\%$ while the measured field data has relative uncertainty of only $\pm 1/4096$ or $\pm 0.02\%$. Multiplications will result in addition of the bounds for the relative error as illustrated in section 4-4A above.

The transcendental terms above are limited in magnitude to 1.0 maximum while the field measurements can be 0.60 gauss max. In this case the individual product terms of (4-12) and (4-13) can have maximum errors of

$$Er = (2048)(1 + 0.0041) - (2048) = 8.4 \text{ units}$$

Errors in Hy and Hx (4-12 and 4-13) will be maximum when roll and pitch are at 45 degrees and the fields are equal. In this case the error in Hy will be

$$EHy = [(0.707)(2048)(1 + 0.0041) - (0.707)(2048)] -$$

$$[(0.707)(2048)(1 - 0.0041) - (0.707)(2048)]$$

$$EHy = 4.94 - 5.94 = 11.87 \text{ units}$$

Similarly, maximum error in Hx can be calculated as

$$EHx \cong [(0.707)(2048)(1.0041) - (0.707)(2048)] \times 3$$

$$EHx \cong 17.8 \text{ units maximum}$$

It should be noted that these error terms are worst case and peak at multiples of 45 degrees in yaw.

C) Subroutines COSY and SINY

These two subroutines compute the angle between the x axis sensor (when projected onto the horizontal plane) and the north-south horizontal vector of earth's magnetic field. The first two opeations of these subroutines perform double precision multiplication and division. Since the data variables involved are 12 bits in length and the computations performed preserving 16 bits, no error is introduced.

The "ANGL" subroutine called by the above two subroutines computes the desired (x axis to horizontal vector) angle by completing an associative table look up procedure. The task required is to match a given data quantity either (Hx^2/Hh^2 or Hy^2/Hh^2) with the contents of a memory cell. The address of this cell is then the required angle.

Since the table is limited in precision to 16 bits there are obviously cases where an interpolation is required to ascertain the true address[9]. The function stored in tabular form is $\cos^2\theta$ where θ varies from 45 to 90 degrees. Maximum error will therefore be induced while attempting to locate solutions (angles near 90 degrees if inadequate precision is provided. Error in this region due to resolution of tabular data can be examined by noting the entries in Table 4-8

θ	$\cos^2\theta$	Most Significant Binary Bit (2^{-x})
90	0	-
89	0.000305	12
88	0.001218	9
87	0.00274	8

Table 4-8 $\cos^2\theta$ AND MOST SIGNIFICANT BINARY DIGITS

provided to indicate the relative magnitudes of $\cos^2\theta$ in the region of $\theta = 90$ degrees. We observe that the most significant binary digit affected at 89 degrees is binary decimal digit 12 implying that the resolution of Hx^2/Hh^2 or Hy^2/Hh^2 (the argument of $\cos^2\theta$) must be accurate to at least $1/2^{12}$ or 0.024%.

Considering the horizontal field of earth's magnetic vector as observed in laboratory experimentation at this latitude, we note that Hh is 730 units. At a heading of 89 degrees, $Hx = 730 \cos 89 = 12.7$ units. The argument would therefore be

$$ARG = Hx^2/Hh^2 = \frac{(12.7)^2}{(730)^2} = 0.000305$$

[9]The procedure determines the relative address by linear interpolation, then selects the closest address as the required angle for the solution.

Since, the squaring and division operations are conducted in double precision, precision is preserved and the algorithm should be able to resolve heading to at least one degree over all portions of the compass.

D) Errors Due to the Remaining Subroutines

Since all of the remaining subroutines work with data that has been rounded to a precision representing 1 degree or better and the computations involve addition or subtraction in double precision binary or binary coded decimal (BCD) format, we note that there will be no further appreciable error due to truncation or rounding.

4-5 MEASUREMENT ERROR SUMMARY

Errors due to sensors and measurement of their respective outputs were discussed in sections 4-2 and 4-3 above. Before proceeding with the analysis of errors, the total signal inaccuracy due to contribution from the many sources above will be summarized in Table 4-10. Total instrument error can then be computed by considering the propagation and enhancement of these errors during the computation process.

Since the errors in Table 4-9 are stochastically independent, we can compute error for any given signal level by finding the RSS of respective error sources. In this manner, the instrument error can be evaluated by considering all input signals with errors superimposed to produce an erroneous computation of heading.

PARAMETER	ERROR	COMMENT
1. Magnetometer		
Offset	≈0	Corrected by software
Orthogonality	≈0	Corrected by software
Noise	Negligible	
Gain	±0.01%	Proport.to signal level
Linearity	±0.01%	
2. Analog Subsystem		
Sampling	Negligible	Sampling rate & filtering adequate
Multiplexer		
Transfer Accuracy	±0.01%	Proport.to signal level
Settling Time	≈0	
Rate	≈0	
Input Leakage	≈0	
Sample and Hold		
Acquisition	≈0	
Hold	4mV	
Aperature Delay	≈0	
Offset	≈0	Corrected by software
Gain	≈0	Corrected by software
Nonlinearity	±0.01%	Proport.to signal level
Feedthrough	±0.01%	Proport.to signal level and frequency
A/D Converter		
Resolution	±1.2mV	
Accuracy	±1.4mV	
Offset	≈0	
Gain	≈0	

Table 4-9 SENSOR AND ANALOG SUBSYSTEM ERROR SUMMARY

4-6 SAMPLE ERROR ANALYSIS

Orthogonality correction using the algorithmic method can be verified by computing expected error prior to correction and comparing measured system output with the error predicition. Assuming that the angle between the x and y sensors exceeds 90 degrees as in Fig. 4-13, we can proceed to compute error by noting the following relationships

$$Hx = Hh\ \mathrm{Cos}\ (+\psi)$$
$$Hy = Hh\ \mathrm{Sin}\ (\psi)$$
$$Hx_1 = Hx\ \mathrm{Cos}\ \varepsilon - Hy\ \mathrm{Sin}\ \varepsilon$$
$$\text{True Yaw} = \psi T = \mathrm{Cos}^{-1}\left(\frac{Hx}{(Hx^2+Hy^2)^{\frac{1}{2}}}\right)$$

Computed yaw

$$\psi m = \mathrm{Cos}^{-1}\left[\frac{Hx\mathrm{Cos}\varepsilon - Hy\mathrm{Sin}\varepsilon}{(Hx\mathrm{Cos}\varepsilon - Hy\mathrm{Sin}\varepsilon)^2 + Hy^2)^{\frac{1}{2}}}\right]$$
$$= \mathrm{Cos}^{-1}\left[\frac{Hh\mathrm{Cos}\psi\mathrm{Cos}\varepsilon - Hh\mathrm{Sin}\psi\mathrm{Sin}\varepsilon}{[(Hh\mathrm{Cos}\psi\mathrm{Cos}\varepsilon - Hh\mathrm{Sin}\psi\mathrm{Sin}\varepsilon)^2 + H^2h\mathrm{Sin}^2\psi]^{\frac{1}{2}}}\right]$$

Using small angle approximations with $\varepsilon \cong 0.79°$

$$\mathrm{Cos}\varepsilon \cong 1 \text{ and } \mathrm{Sin}\varepsilon \approx 0.014$$

then

$$\psi m = \mathrm{Cos}^{-1}\left[\frac{Hh\ \mathrm{Cos}\psi - 0.014\ \mathrm{Sin}\psi}{[Hh^2\ (\mathrm{Cos}\psi - 0.014\ \mathrm{Sin}\psi)^2 + Hh^2\mathrm{Sin}^2\psi]^{\frac{1}{2}}}\right]$$

Computed error

$$\text{Error} = \psi m - \psi$$

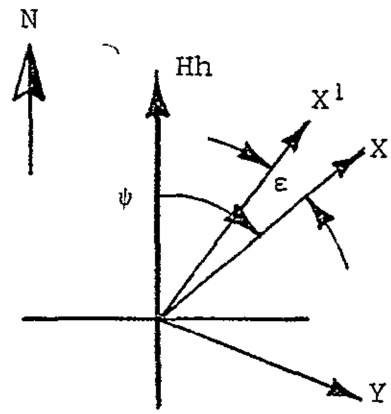

Fig. 4-13 ANGLE (X - Y)>90°

We can now evaluate computed yaw angle (ψm) given a particular yaw (ψ) and the horizontal field vector (Hh). Heading error for horizontal field vector of 730 units at various yaw angles with pitch and roll angles of zero degrees is tabulated in Table 4-10 and plotted along with actual measured yaw error (data taken during experimentation of Chapter V) in Fig. 4-14.

Heading (Degrees)	Computed Error (Degrees)	Heading (Degrees)	Computed Error (Degrees)
90	0.8	290	0.7
70	0.7	270	0.8
50	0.5	250	0.7
30	0.2	230	0.5
10	0.0	210	0.2
350	0.0	190	0.0
330	0.2	170	0.0
310	0.5	150	0.2
		130	0.5

Table 4-10 COMPUTED HEADING ERROR WITH Hh = 730 UNITS

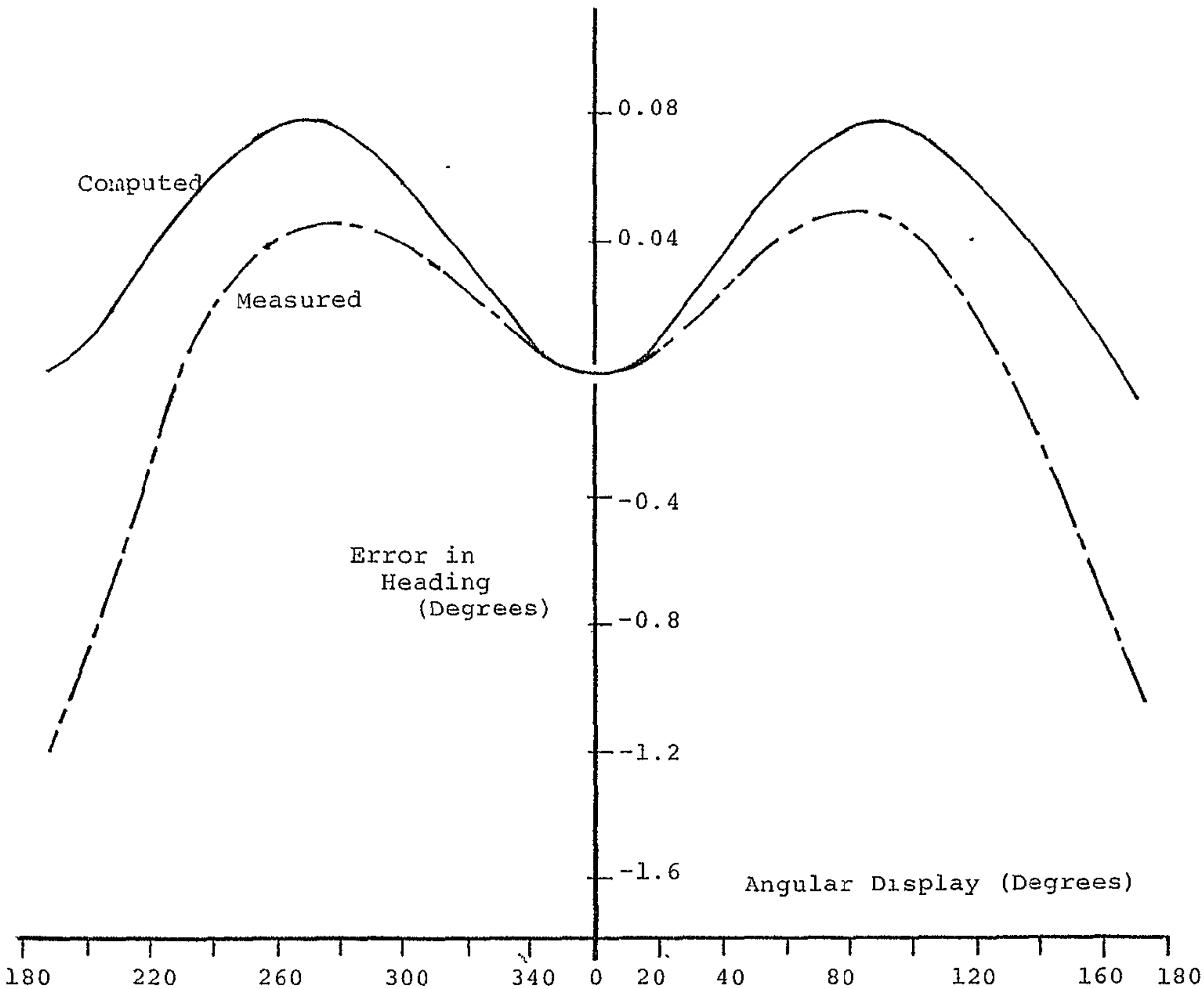

Fig. 4-14 COMPARISON OF COMPUTED AND MEASURED ORTHOGONALITY INDUCED ERROR

4-7 CONCLUSIONS

The preceeding error analysis has identified potential error sources along with relative magnitudes of error to be expected. Magnetometer sensor and analog subsystem errors were identified and analyzed individually. During this analysis it became apparent that errors due to sensor offset and nonorthogonality dominated and would severely limit total instrument performance. The relative magnitudes of these errors and their mode of contribution would have degraded system capacity.

By carefully characterizing the offset and orthogonality error it was determined that these systemmatic errors could be reduced by appropriate programming. A need to identify the extent of each error unique to the laboratory instrument imposed a need to evaluate the instrument empirically. Using earth's magnetic field and the laboratory test fixture (described in Chapter V) to provide control inputs each of the parameters was identified and measured. An algorithm with the empirically determined correction coefficients was included in the final system to reduce the error and to improve final system performance. The remaining potential error sources were tabulated and relative magnitudes noted.

Processing errors due to register precision and truncation were analyzed by considering pertinent subroutines individually. It was noted that the relative error bounds add when multiplying variables with relative error. In addition, it was noted that error accrued during processing is proportional to sensor signal levels involved. The final uncertainty is then proportional to actual aircraft attitude with error increasing as displacement from level flight occurs. Computational error is also noted to increase at particular headings causing the error function to peak at specific yaw angles.

The sample error analysis clearly shows that a correlation between sensor nonorthogonality induced error and measured (uncorrected) data exists. By predicting and computing an error function prior to experimentally verifying the result we gain confidence that the sensor characteristics derived empirically in previous sections are correct.

CHAPTER V

LABORATORY EVALUATION OF THE ATTITUDE INDEPENDENT REMOTE MAGNETIC INDICATOR AND HEADING INSTRUMENT

5-1 INTRODUCTION

This chapter addresses laboratory evaluation of the microprocessor based computer designed to implement the heading measurement instrument. An integral part of this instrument was the three axis fluxgate magnetometer used to implement the attitude independent remote magnetic indicator of Chapter II. The laboratory evaluation was designed to investigate empirically the effects of physical parameters that would otherwise be impossible to assess.

Although phenomena such as noise, magnetic field gradient, sensor orthogonality errors and offset errors can be predicated, combined effects on the proposed instrument and remote magnetic indicator are best evaluated in the laboratory. In addition, it was noted that errors due to sensor offset and nonorthogonality could be corrected by software included with the sample subroutine. Determination of the effectiveness of this correction technique necessitated laboratory measurements of the errors (to determine correction constants) and comparison of data prior to and following corrections.

The chapter begins by discussing laboratory test apparatus designed to evaluate the instrument. Actual data measured and recorded during experimentation is then presented in both tabular and graphic form to facilitate comparison and evaluation. Finally, the laboratory data is discussed and it is concluded that the remote magnetic indicator used with the heading measurement instrument results in a viable alternative to conventional heading measurement systems. The microprocessor based computer implentation of the instrument has added unique sensor measurement correction ability that enhances performance of otherwise marginal sensors. In this manner limitations in systems performance that now exist due to sensor inadequacy can be minimized without incurring the burden of using more expensive sensors.

5-2 TEST APPARATUS

A) Electronic Subsystem

The microprocessor based computer (illustrated in photos 5-1 and 5-2) was constructed on printed circuit boards consisting of a central processing card, two memory cards (2K bytes capacity each) and an output board. A separate analog subsystem card contained the multiplexer, sample and hold, analog to digital converter and trimming potentiometers. The circuit cards were all organized with edge connectors and mounted vertically into a hand wired backplane assembly as shown in photos 5-1 and 5-2.

The card in the left foreground of photo 5-1 served as the output display with three seven-segment displays displaying significant figures of system heading. A small printed circuit in the right foreground of photo 5-1 contained potentiometers used to generate analog signals proportional to roll and pitch signals (simulating gyroscope outputs). Cards shown vertically mounted in photo 5-2 can be identified from right to left as the analog subsystem, two memory cards and the central processing card. The large integrated circuit shown on the CPU card is the Signetics 2640 microprocessor.

B) Sensor Assembly

To evaluate the effects of combined aircraft pitch, roll

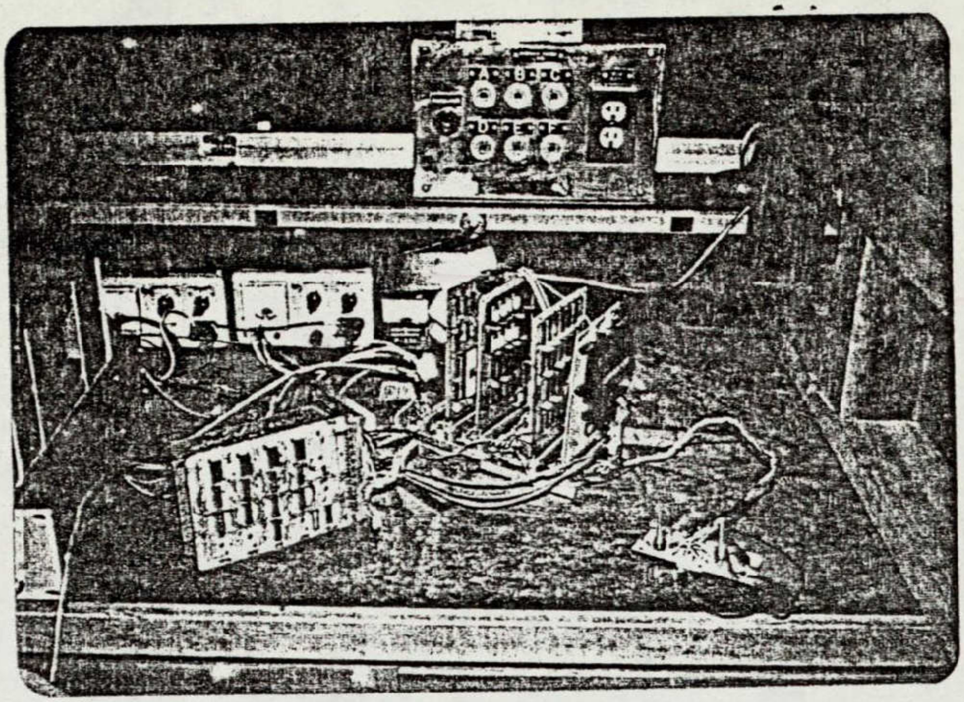

Photo 5-1 . MICROPROCESSOR BASED HEADING COMPUTER

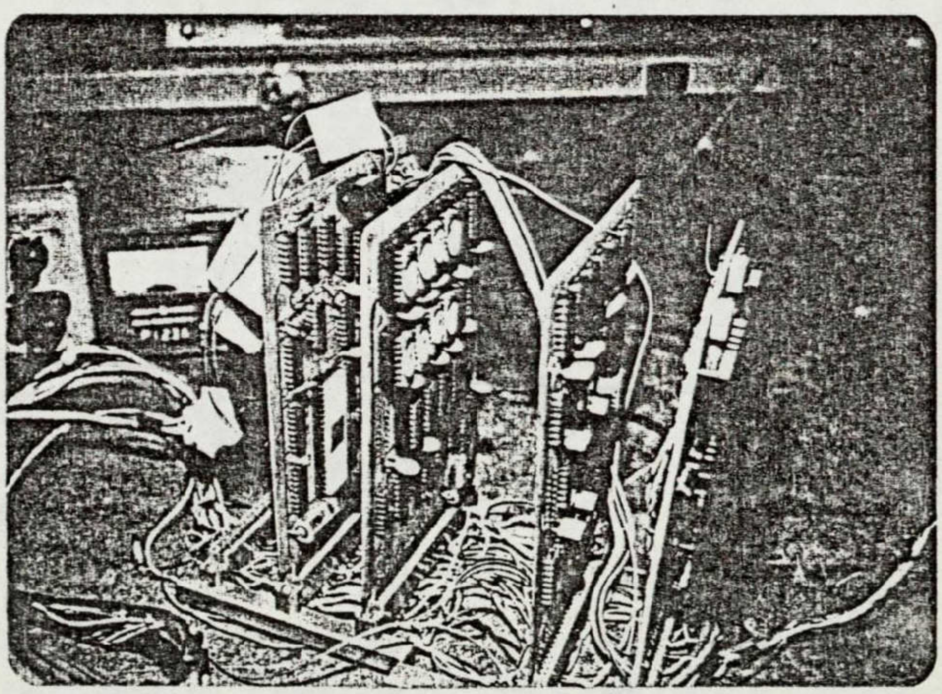

Photo 5-2 CENTRAL PROCESSOR, MEMORY AND ANALOG SUBSYSTEM

and yaw a three axis gimbal apparatus was required. In addition, since angular measurements were required, a means of measuring angular rotation in each of the three exes was provided. The gimbal apparatus as illustrated in photos 5-3 and 5-4 was fitted with large protractors centered on the rotation axes. Pointers were provided to enable angular rotation measurements on the respective protractor scales. Since the angular precision on each protractor scale resolved angular position to 0.5 degrees, angular measurements to a resolution of at least 0.5 degrees were possible. Angular position was measured by estimating the decimal place of each measurement with accuracy to ± 0.5 degrees ensured.

Since the three axis magnetometer (housed in the rectangular block of photos 5-3 and 5-4) measured ambient magnetic fields the test apparatus was constructed of nonferrous material. This ensured that local fields due to residual magnetic fields in the test apparatus would be minimized. In addition, since the material had low permeability, there would be little deformation of the local field causing error due to changing field gradient.

The sensor package shown in photos 5-3 and 5-4 was physically mounted such that the sensors were centered as close to the center of the gimbal as possible. This precaution ensured that measurement error due to sensor translation was minimized[1]. During instrument evaluation, the entire gimbal assembly and sensor were leveled and mounted in a Helmholtz coil assembly as illustrated in photo 5-5. Although the coils were not activated during experimentation, the rotations in heading were

---

[1]Since the local magnetic field has a nonzero gradient, field measurements include a component due to translation of the sensor axes. This component of measurement produces unacceptable error in a system designed to measure field components that change due to rotation.

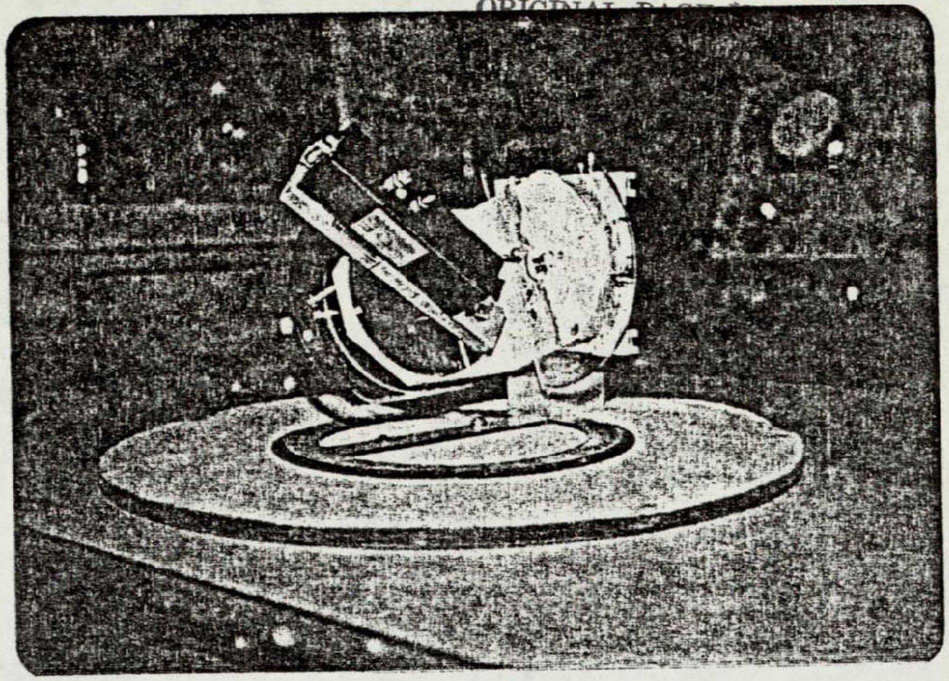

Photo 5-3 MAGNETOMETER SENSOR MOUNTED ON GIMBALLED TEST FIXTURE

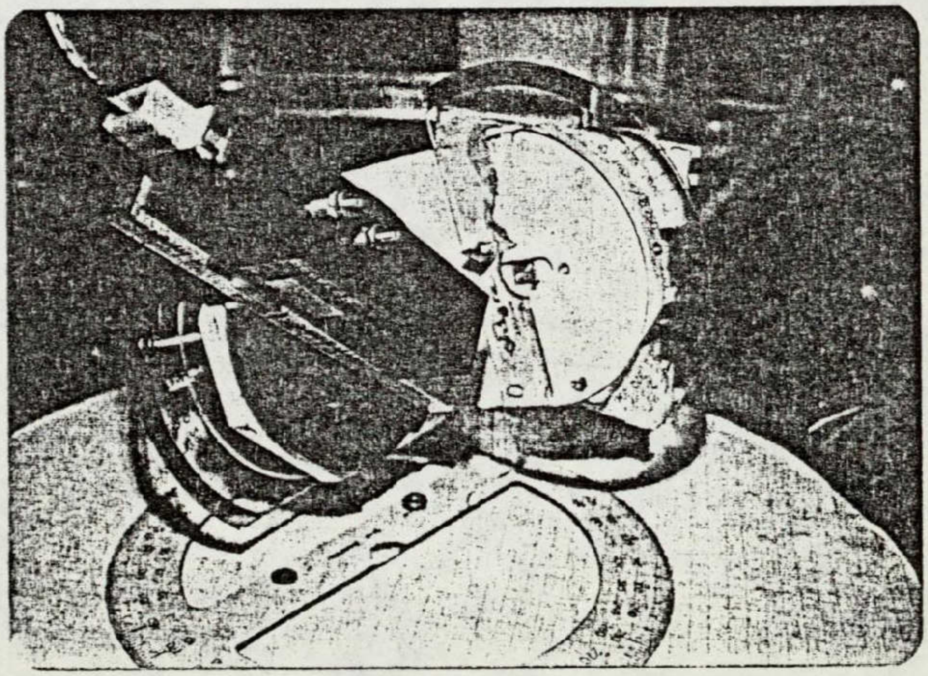

Photo 5-4 SENSOR AND GIMBAL ASSEMBLY WITH PROTRACTORS

carefully controlled since the gimbal assembly was an integral part of the Helmholtz coil fixture with the vertical rotation axis serving as the system yaw axis.

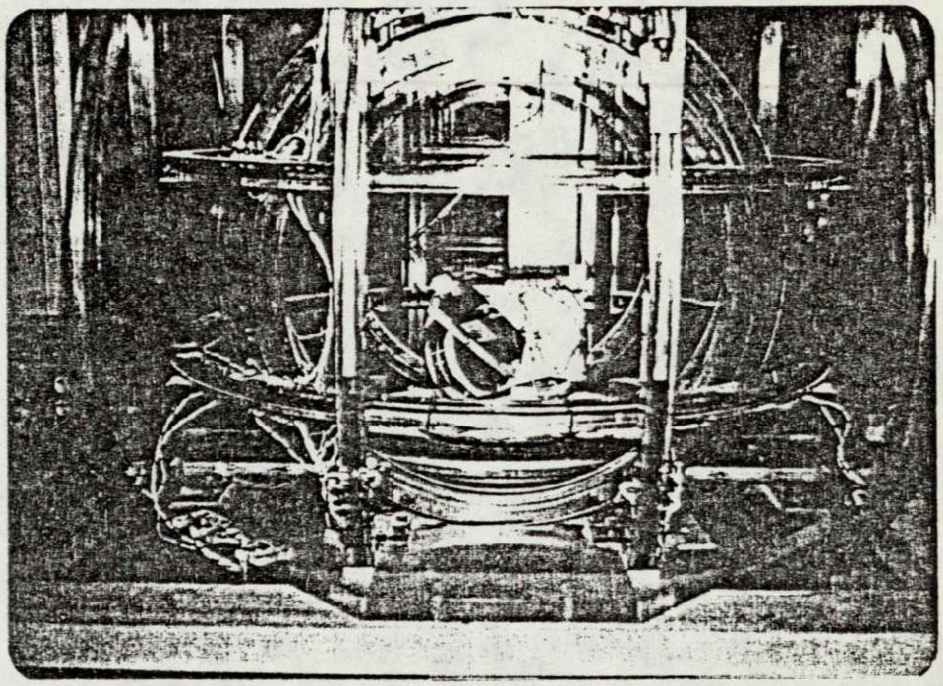

Photo 5-5 TEST FIXTURE MOUNTED IN HELMHOLTZ COIL ASSEMBLY

5-3 HEADING MEASUREMENTS WITH NO OFFSET CORRECTION

By maintaining heading of the text fixture constant (no rotation about the vertical axis) and varying both pitch and roll angle, the instrument display was observed to vary. This variation gave a direct measure of instrument error since a constant heading was maintained and a constant display was to be expected.

Data variations were recorded in Tables 5-1 and 5-2 and plotted on Figures 5-1 and 5-2. With only ± 10 degree variation in pitch combined with ± 30 degree variation in roll we note that the heading display varies 14 degrees. Obviously,

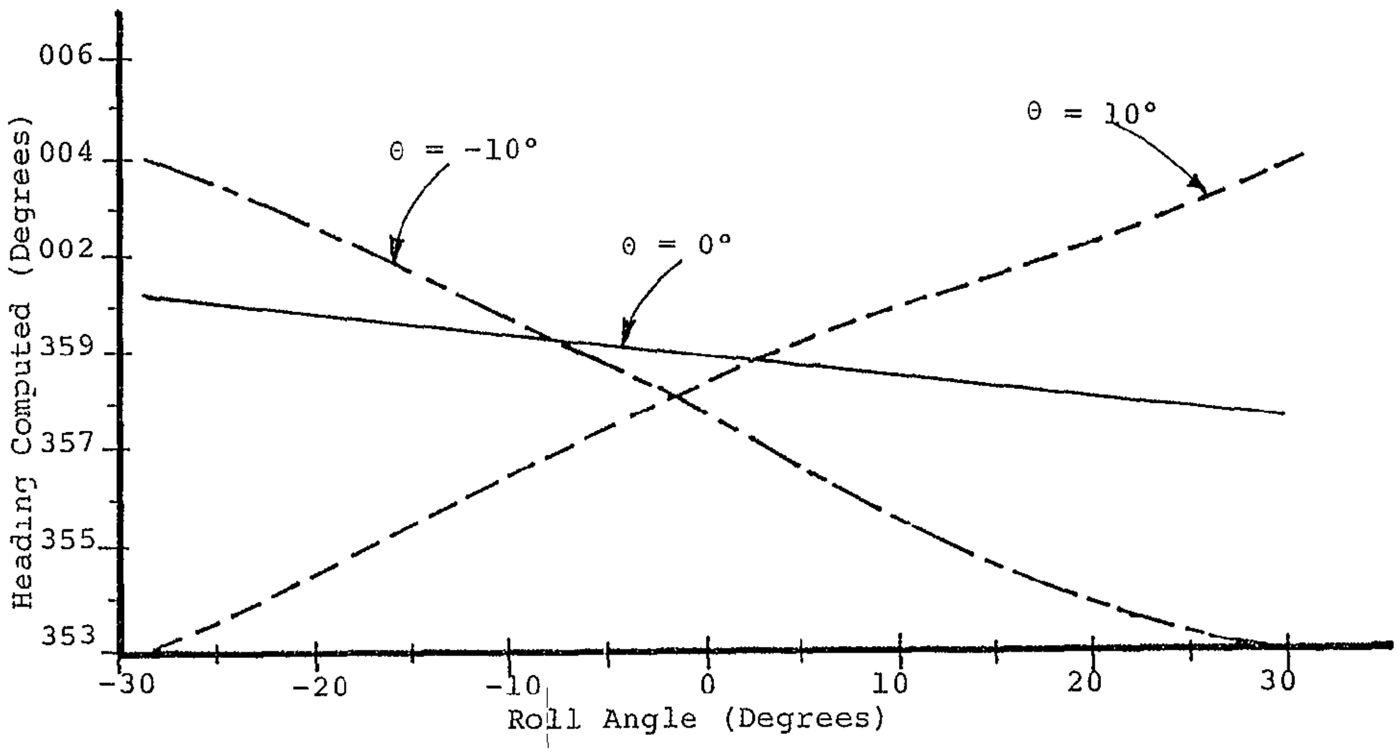

Fig. 5-1 HEADING COMPUTED AT A FIXED YAW ANGLE WITH VARYING θ AND Φ (NO OFFSET CORRECTION)

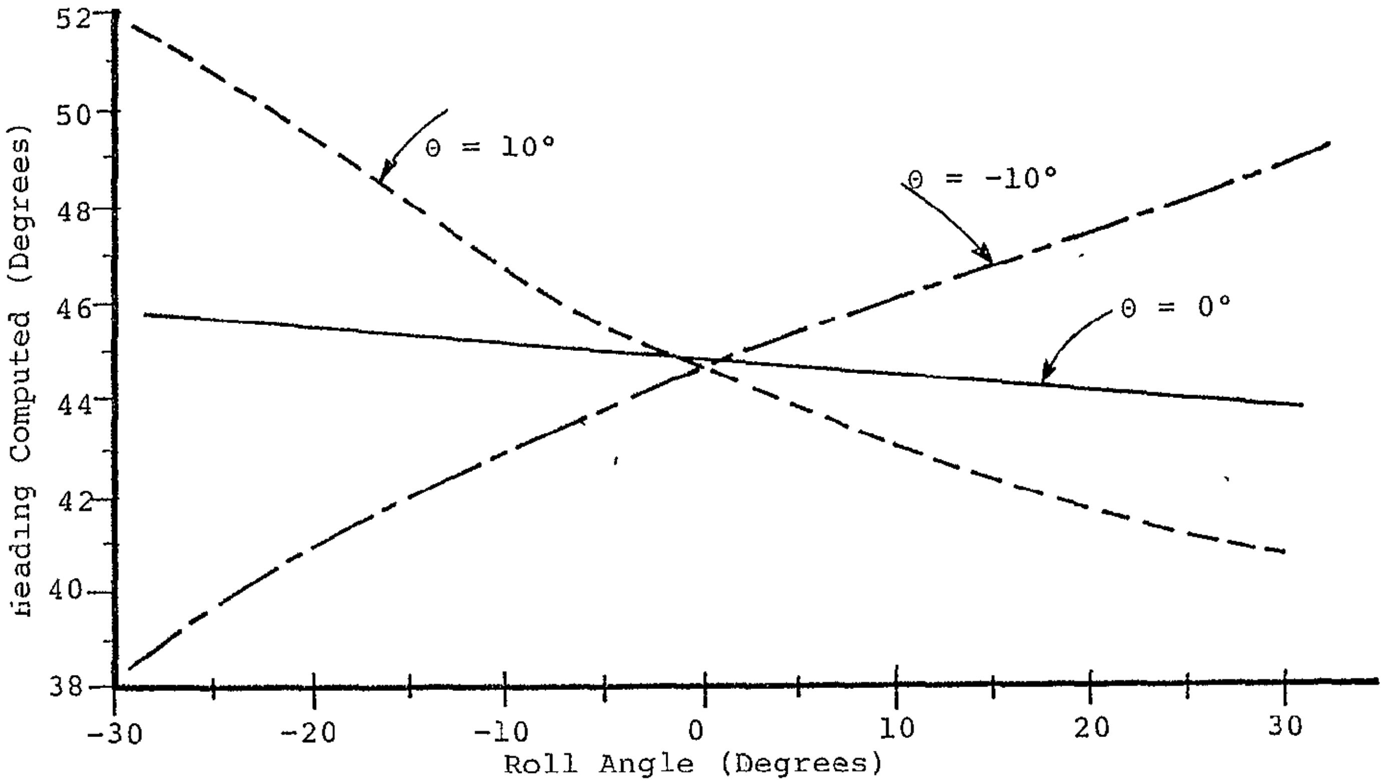

Fig. 5-2 HEADING COMPUTED AT A FIXED YAW ANGLE WITH VARYING
Θ AND Φ (NO OFFSET CORRECTION)

instrument operation indicated excessive error requiring more elaborate sensors or correction of a sensor inadequacy.

5-4 HEADING MEASUREMENTS TO INVESTIGATE ORTHOGONALITY ERROR

System performance was evaluated by initially aligning the sensors with zero pitch and roll angle. Sensor Z was positioned vertically with positive direction downwards. By observing the Z axis output[2] as the test fixture was rotated about the vertical axis, adjustments were made in pitch and roll angle to minimize coning of the Z axis. Angular measurements on the respective roll and pitch axis protractors were then made to establish the initial reference attitude angles.

Heading measurement accuracy was evaluated by rotating the test fixture in the horizontal plane until the display flickered between (XX9) and (XX9+1). The rotation was then continued a very small amount until a steady display (multiple of 10 degrees) was observed[3]. Measurements ranging from 0 to 350 degrees were made by recording angular position required to produce specific heading data displays. Sets of data were recorded at various combinations of pitch and roll then tabulated in Tables 5-3 through 5-8. Relative error was computed by determining angular position expected at each display value and then computing the difference in angular positions. Errors at the roll extremes of ± 44 degrees are plotted for pitch angles of plus and minus 20 degrees on Fig. 5-3 through 5-6 inclusive.

---

[2]A special subroutine was used to display Z axis data directly in BCD format on the seven bar output display.

[3]This measurement technique ensured that all heading measurements were made identically. In addition, error due to system imprecision was reduced.

Data in Tables 5-5, 5-6 and Fig. 5-3, 5-4 were recorded with no sensor orthogonality error correction implemented. Data in Tables 5-7, 5-8 and Fig. 5-5, 5-6 was recorded with the sensor orthogonality correction implemented. Comparison of these data indicate that considerable improvement in accuracy is achieved by correcting sensor orthogonality error.

5-5 CONCLUSIONS

Laboratory evaluation of the heading measurement instrument has shown that the algorithms developed in previous chapters are viable. Operation of the device in a laboratory environment has enabled empirical evaluation of the system under adverse combinations of noise, field gradient and sensor plus instrument error sources.

Test apparatus described in section 5-2 served to enable controlled simulation of roll, pitch and yaw rotations. The apparatus was nonmagnetic in nature and contributed insignificant error due to field pertebation. Mounting of protractors and pointers on the test apparatus made angular measurements possible to a precision of at least ± 0.5 degrees.

Effects of sensor offsets were evaluated in section 5-3 by recording system heading computations when only roll and pitch varied. Since the variations in Figures 5-1 and 5-2 prior to offset correction exceed the maximum excursions of Figures 5-3 and 5-4 by at least a factor of two (angular excursions in first set also less than in the record) and we note that offset errors were corrected prior to recording data in the second set of data, we conclude that offset in magnetometers can be a

PITCH ANGLE 0 DEGREES

ROLL ANGLE 0 DEGREES

Heading Displayed (Degrees)	Angular Position (Degrees)	Relative Error (Degrees)
10	275.3	0.3
30	295.2	0.2
50	315.4	0.4
70	335.5	0.5
90	355.5	0.5
130	34.8	-0.2
150	54.3	-0.7
170	74.0	-1.0
190	94.0	-1.0
210	114.4	-0.6
230	135.0	0.0
250	155.5	0.5
270	174.7	-0.3
290	195.5	0.5
310	215.2	0.2
330	235.2	0.2
350	254.7	-0.3

Table 5-3 REFERENCE DATA MEASUREMENTS OF HEADING TAKEN WITH NO ORTHOGONALITY CORRECTION

PITCH ANGLE 0 DEGREES
ROLL ANGLE 0 DEGREES

Heading Displayed (Degrees)	Angular Position (Degrees)	Relative Error (Degrees)
10	276.6	-0.4
30	296.6	-0.4
40	306.7	-0.3
50	316.7	-0.3
60	327.2	+0.2
70	337.0	0.0
90	355.9	-1.1
130	37.0	0.0
160	67.2	0.2
190	96.8	-0.2
220	126.9	-0.1
250	157.0	0.0
280	186.9	-0.1
310	216.6	-0.4
340	246.9	-0.1
350	256.4	-0.6

Table 5-4 HEADING MEASUREMENTS WITH OFFSET AND ORTHOGONALITY CORRECTIONS MADE

Heading Displayed (Degrees)	Roll = 44°		Roll = 20°		Roll = -20°		Roll = -44°	
	Angular Position	Error	Angular Position	Error	Angular Position	Error	Angular Position	Error
10	276.3	1.3	276.5	1.5	275.0	0.0	274.0	-1.0
30	296.3	1.3					293.6	-1.4
40			306.1	1.1	304.0	-1.0		
50							313.8	-1.2
60	325.8	0.8						
70			335.6	1.6	334.3	-0.7	333.8	-1.2
90	355.0	0.0	354.0	-1.0	353.1	-1.9	353.0	-2.0
130	34.3	0.7	34.3	-0.7	34.6	-0.4	34.4	-0.6
160	64.5	-0.5	64.0	-1.0	65.0	0.0	65.0	0.0
190	94.3	-0.7	94.6	-0.4	95.0	0.0	95.5	0.5
220	125.2	0.2	125.3	0.3	126.0	1.0	126.5	1.5
250	156.6	1.6	156.2	1.2	156.7	1.7	157.0	2.0
280	186.6	1.6	186.8	1.8	186.5	1.5		
310	216.8	1.8	216.8	1.8	215.9	0.9	215.9	0.9
340	246.0	1.0	246.8	1.8	245.0	0.0		
350							224.9	-0.1

TABLE 5-5 HEADING MEASUREMENTS AT PITCH = 20° WITH NO ORTHOGONALITY CORRECTION

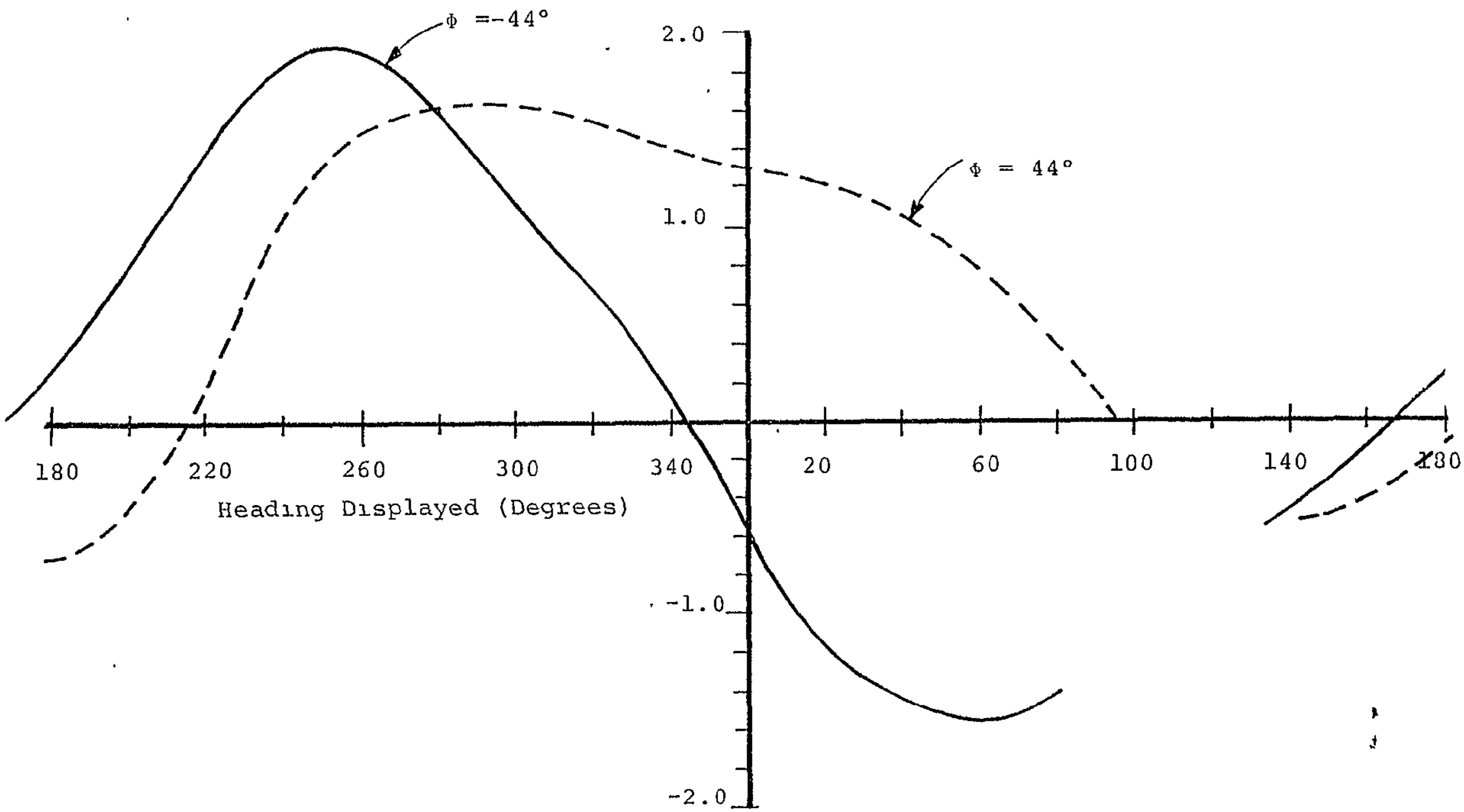

Fig. 5-3 HEADING MEASUREMENT ERROR AT PITCH = 20°
(NO ORTHOGONALITY CORRECTION)

Heading Displayed (Degrees)	Roll = 44°		Roll = 20°		Roll = -20°		Roll = -44°	
	Angular Position	Error	Angular Position	Error	Angular Position	Error	Angular Position	Error
10	276.1	1.1	275.1	0.1	274.2	-0.8	273.7	-1.3
30	296.2	1.2	295.9	0.9			293.6	-1.4
50	316.4	1.4	316.1	1.1			314.1	-0.9
70	336.5	1.5	336.4	1.4	335.5	0.5	334.6	-0.4
90	355.5	0.5	355.3	0.3	355.0	0.0	354.2	-0.8
130	36.0	1.0	36.4	1.4	135.7	0.7	135.7	0.7
150	55.3	0.3	55.9	0.9			55.8	0.8
170	74.5	-0.5	75.6	0.6			75.5	0.5
190	94.9	-0.1	95.3	0.3	95.5	0.5	95.5	0.5
210	115.0	0.0	115.4	0.4			115.6	0.6
220					125.5	0.5		
230	135.0	0.0	135.6	0.6			136.0	1.0
250	155.6	0.6	155.4	0.4	155.5	0.5	155.7	0.7
270	174.8	-0.2	174.8	-0.2			175.0	0.0
290	195.6	0.6	195.4	0.4			195.3	0.3
310	215.5	0.5	215.3	0.3	214.6	-0.4	214.5	-0.5
330	235.7	0.7	235.1	0.1			234.2	-0.8
350	255.6	0.6	255.2	0.2			253.8	-1.2

Table 5-6 HEADING MEASUREMENTS AT PITCH = -20° WITH NO ORTHOGONALITY CORRECTION

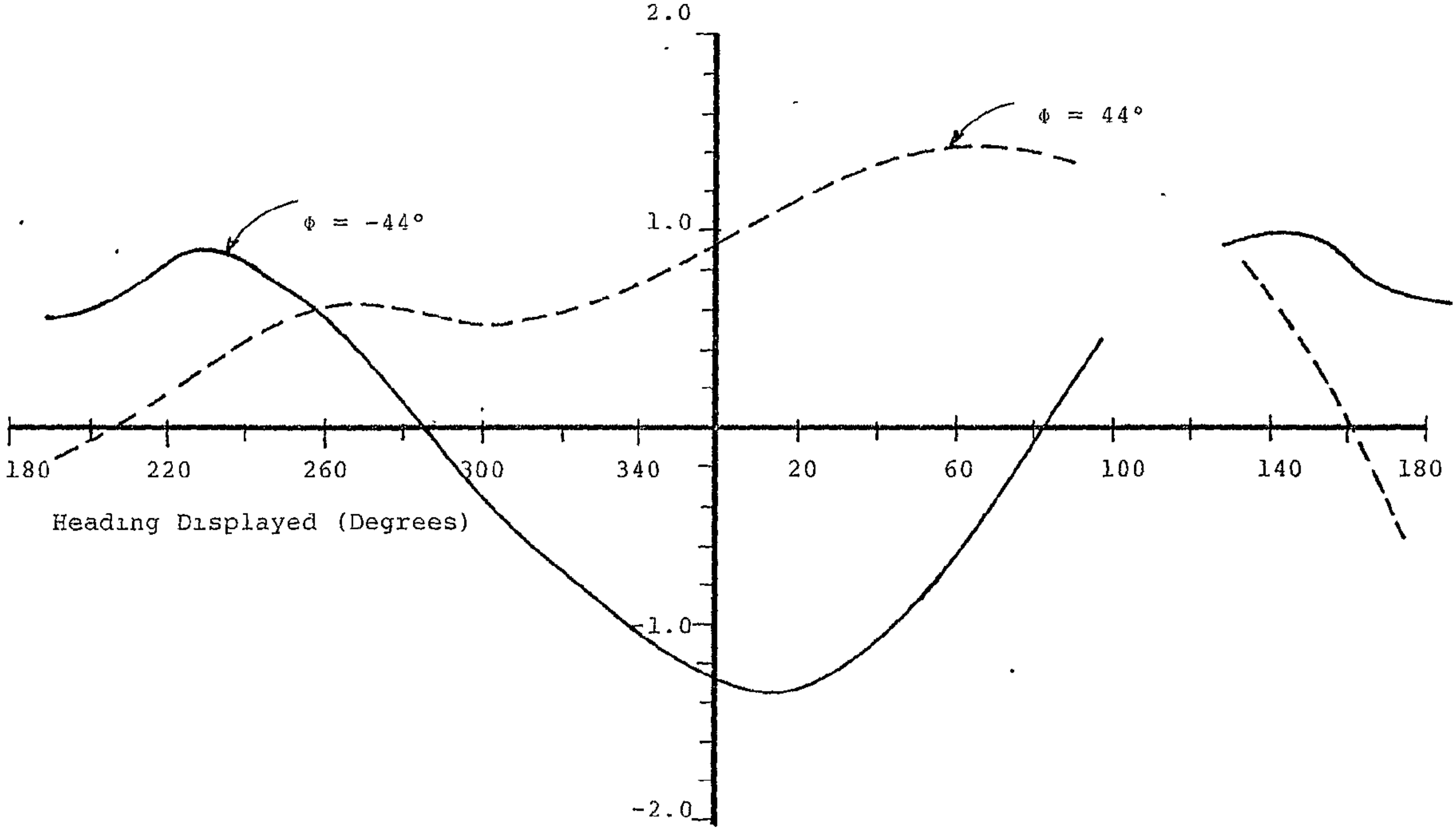

Fig. 5-4 HEADING MEASUREMENT ERROR AT PITCH = -20°
(NO ORTHOGONALITY CORRECTION)

Heading Displayed (Degrees)	Roll = 0° Angular Position	Error	Roll = 44° Angular Position	Error	Roll = -44° Angular Position	Error
20	287.3	0.3	287.5	0.3	286.3	-0.7
40	307.2	0.2	307.5	0.3	306.0	-1.0
60	327.0	0.0	327.9	0.7	325.9	-1.1
80	346.3	-0.7	347.5	0.3	345.6	-1.4
90	355.9	-1.1	357.0	0.2	356.2	-1.8
140	46.9	-0.1	47.0	-0.2	46.5	-0.5
160	67.0	0.0	67.3	0.1	67.1	0.1
180	86.6	-0.4	86.5	-0.7	87.0	0.0
200	107.0	0.0	107.3	0.1	108.1	1.1
220	127.6	0.6	127.3	0.1	128.3	1.2
240	147.2	0.2	147.4	0.2	148.5	1.5
260	167.0	0.0	167.1	-0.1	168.5	1.5
280	187.3	0.3	187.1	-0.1	188.5	1.5
300	207.2	0.2	207.1	-0.1	208.0	1.0
320	227.3	0.3	227.0	-0.2	227.5	0.5
340	247.4	0.4	247.3	+0.1	247.4	0.4
0	266.4	-0.6	267.0	-0.2	266.0	-1.0

Table 5-7 HEADING MEASUREMENTS AT PITCH = 20° WITH OFFSET AND ORTHOGONALITY CORRECTION MADE

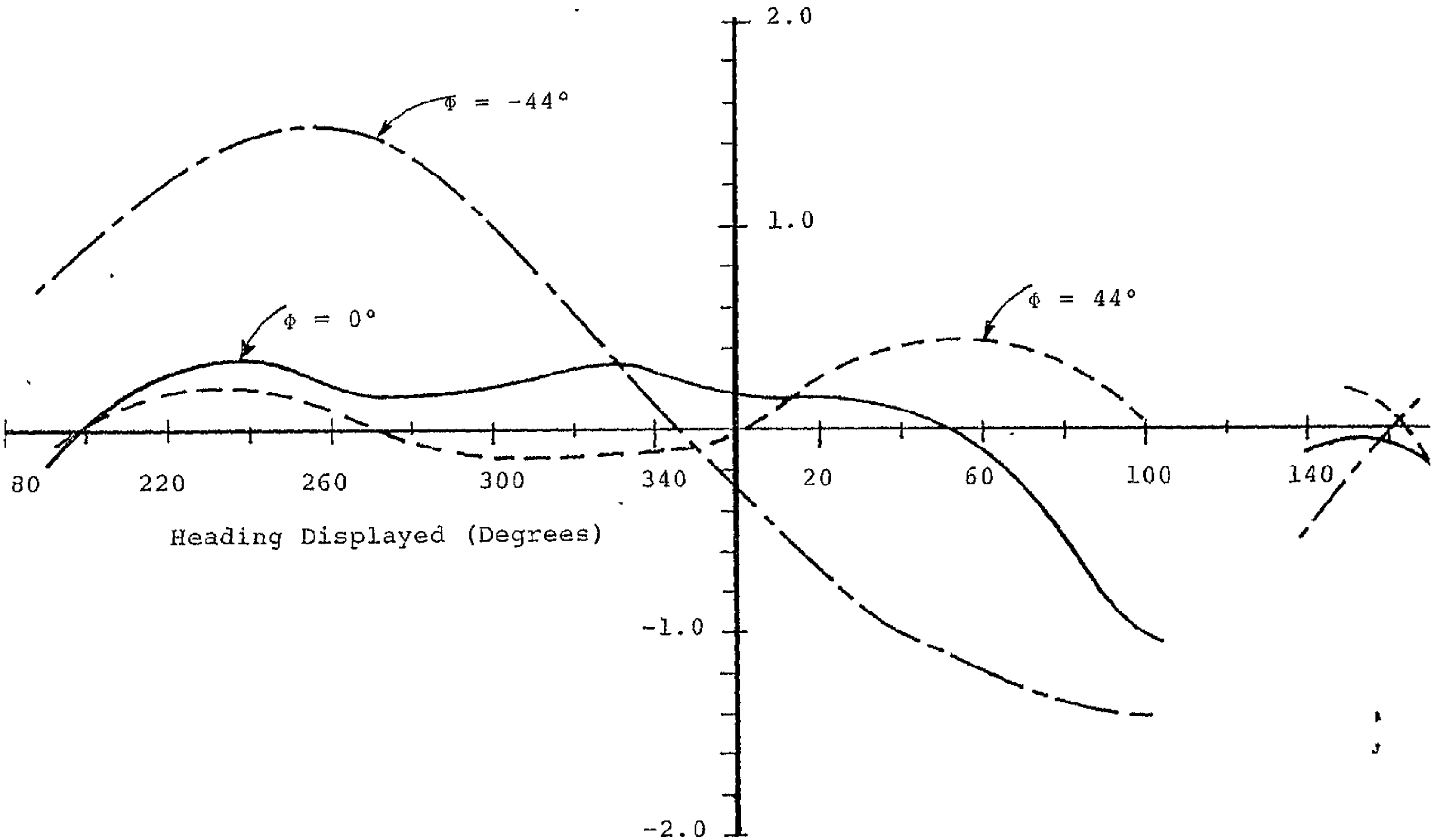

Fig. 5-5 HEADING MEASUREMENT ERROR AT PITCH - 20°
(OFFSET AND ORTHOGONALITY ERROR CORRECTED)

Heading Displayed (Degrees)	Roll = 44°		Roll = -44°	
	Angular Position	Error	Angular Position	Error
20	287.0	-0.4	286.5	-0.3
40	307.0	-0.4	306.7	-0.1
60	327.0	-0.4	326.8	0.0
80	347.0	-0.4	346.8	0.0
90	356.7	-0.7	355.6	-0.2
140	47.8	0.4	48.0	1.2
160	67.7	0.3	68.0	1.2
180	87.0	-0.4	87.8	1.0
200	107.6	0.2	108.0	1.2
220	127.7	0.3	128.0	1.2
240	147.8	0.4	147.4	0.6
260	167.6	0.2	167.2	0.4
280	187.6	0.2	187.0	0.2
300	207.1	-0.3	206.5	-0.3
320	227.1	-0.3	226.6	-0.2
340	247.1	-0.3	246.9	0.1
0	266.3	-0.9	266.0	-0.8

TABLE 5-8 HEADING MEASUREMENTS AT PITCH = -20° WITH OFFSET AND ORTHOGONALITY ERROR CORRECTED

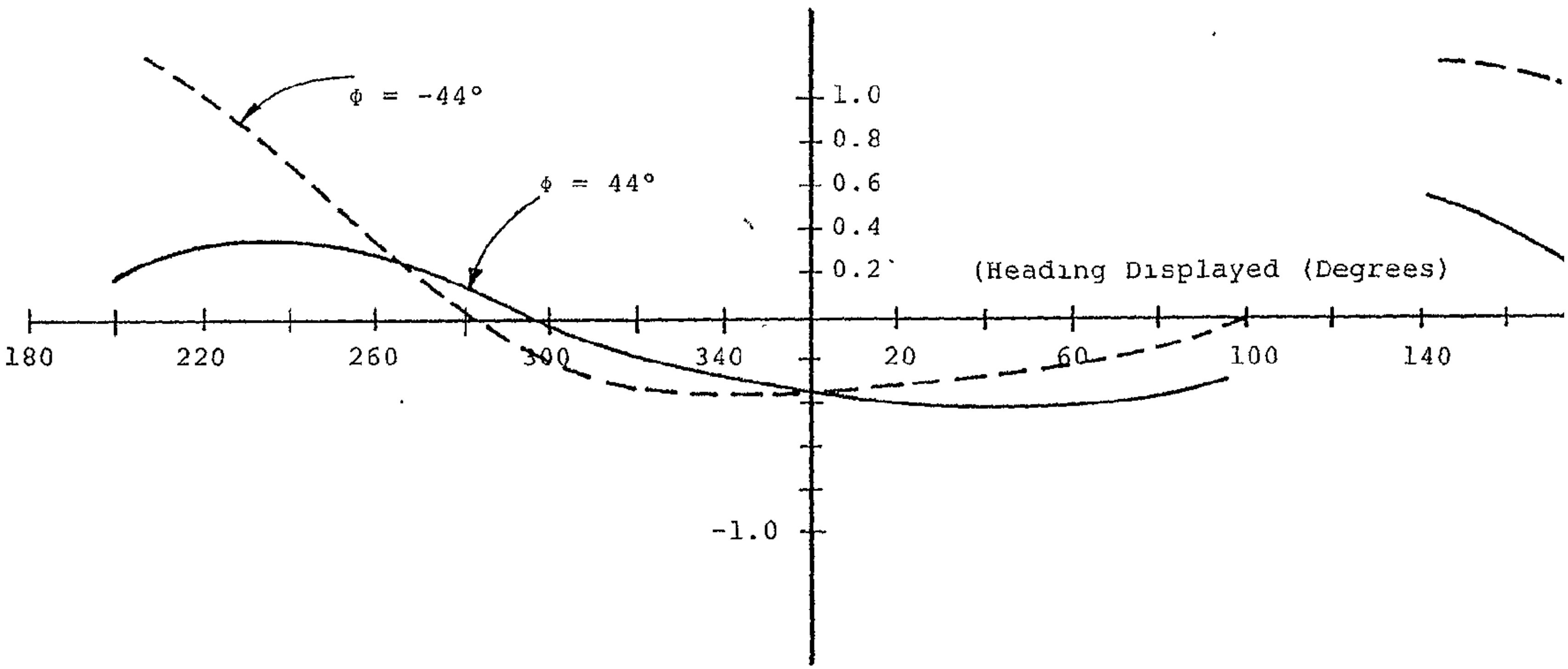

Fig. 5-6 HEADING MEASUREMENT ERROR AT PITCH = -20°
(OFFSET AND ORTHOGONALITY CORRECTED)

major error source[4]. Additionally, we note that the correction of offset error in sensors has been successful. Experimental results have verified that not only can offset errors be determinded (Chapter IV), but a suitable algorithm can be implemented in the computer to improve system operation. It is postulated that offset error correction can be extended to include correction of varying offset values (functions of temperature and supply voltage) by monitoring error causing variables (example temperature) and computing correction constants prior to offset correction as above.

Errors induced by sensor nonorthogonality were predicted in Chapter IVsection 4-2 and verified by plotting expected error along with measured error in Fig. 4-14. The curves of Fig. 4-14 were plotted for heading rotations with no pitch or roll angle. To evaluate system performance and the effect of orthogonality error with combined angular rotations, measurements of heading error were plotted in Fig. 5-3 thorugh 5-6 inclusive.

Comparison of these data indicate that maximum excursions of error as a function of heading are significantly less when orthogonality corrections are made. It is also postulated that data could be improved further by similarly correcting orthogonality error in te Z axis sensor[5].

In summary, the experimental evaluation has provided insight into the operation of an attitude independent remote magnetic indicator and heading computer in the "real world"

---

[4] This corroborates the observations predicted during error analysis in Chapter IV.

[5] We note that the error excursions are functions of pitch and roll and that Z axis data is used in the rotation algorithm.

environment complete with all contributing error sources. The error analysis evolved during development of the system has proven adequate in that an operational system was developed. Major error sources were measurable as predicted and the means of reducing their effects were successfully implemented. Correction of sensor offset and orthogonality error required an empirical evaluation of the respective sensor. These evaluations were performed, the errors characterized, correction coefficients determined, and correction algoritms implemented.

Successful implementation of these corrections was evidenced by significant reductions in system error. The correction methods presented can be extended in future with the net result that less demand is required of physical sensors if the sensor parameters can be established empirically prior to completion of instrument design. Utilization of a microprocessor in the instrument has added the computational flexibility required to facilitate accommodation of sensors with varying error magnitudes.

APPENDIX A

This appendix lists the instruction set of the Signetics 2650 microprocessor chip used to implement the heading instrument.

LOAD/STORE INSTRUCTIONS

			Length (bytes)
LODZ	r	Load Register Zero	1
LODI,r	v	Load Immediate	2
LODR,r	(*)a	Load Relative	2
LODA,r	(*)a(,X)	Load Absolute	3
STRZ	r	Store Register Zero	1
STRR,r	(*)a	Store Relative	2
STRA,r	(*)a(,X)	Store Absolute	3

ARITHMETIC INSTRUCTIONS

ADDZ	r	Add to Register Zero	1
ADDI,r	v	Add Immediate	2
ADDR,r	(*)a	Add Relative	2
ADDA,r	(*)a(,X)	Add Absolute	3
SUBZ	r	Subtract from Register Zero	1
SUBI,r	v	Subtract Immediate	2
SUBR,r	(*)a	Subtract Relative	2
SUBA,r	(*)a(,X)	Subtract Absolute	3

LOGICAL INSTRUCTIONS

ANDZ	r	And to Register Zero	1
ANDI,r	v	And Immediate	2
ANDR,r	(*)a	And Relative	2
ANDA,r	(*)a(,X)	And Absolute	3
IORZ	r	Inclusive or to Register Zero	1
IORI,r	v	Inclusive or Immediate	2
IORR,r	(*)a	Inclusive or Relative	2
IORA,r	(*)a(,X)	Inclusive or Absolute	3
EORZ	r	Exclusive or to Register Zero	1
EORI,r	v	Exclusive or Immediate	2
EORR,r	(*)a	Exclusive or Relative	2
EORA,r	(*)a(,X)	Exclusive or Absolute	3

COMPARISON INSTRUCTIONS

COMZ	r	Compare to Register Zero	1
COMI,r	v	Compare Immediate	2
COMR,r	(*)a	Compare Relative	2
COMA,r	(*)a(,X)	Compare Absolute	3

ROTATE INSTRUCTIONS

			Length (bytes)
RRR,r		Rotate Register Right	1
RRL,r		Rotate Register Left	1

BRANCH INSTRUCTIONS

BCTR,v	(*)a	Branch on Condition True Relative	2
BCFR,v	(*)a	Branch on Condition False Relative	2
BCTA,v	(*)a	Branch on Condition True Absolute	3
BCFA,v	(*)a	Branch on Condition False Absolute	3
BRNR,r	(*)a	Branch on Register Non-Zero Relative	2
BRNA,r	(*)a	Branch on Register Non Zero Absolute	3
BIRR,r	(*)a	Branch on Incrementing Register Relative	2
BIRA,r	(*)a	Branch on Incrementing Register Absolute	3
BDRR,r	(*)a	Branch on Decrementing Register Relative	2
BDRA,r	(*)a	Branch on Decrementing Register Absolute	3
BXA	(*)a(,x)	Branch Indexed Absolute Unconditional	3
ZBRR	(*)a	Zero Branch Relative, Unconditional	2

SUBROUTINE BRANCH/RETURN INSTRUCTIONS

BSTR,v	(*)a	Branch to Subroutine on Condition True, Relative	2
BSFR,v	(*)a	Branch to Subroutine on Condition False, Relative	2
BSTA,v	(*)a	Branch to Subroutine on Condition True Absolute	3
BSFA,v	(*)a	Branch to Subroutine on Condition False Absolute	3
BSNR,r	(*)a	Branch to Subroutine on Non Zero Register, Relative	2
BSNA,r	(*)a	Branch to Subroutine on Non Zero Register, Absolute	3
BSXA	(*)a(,x)	Branch to Subroutine Indexed Unconditional	3
RETC,v		Return From Subroutine Conditional	1
RETE,v		Return From Subroutine and Enable Interrupt, Conditional	1
ZBSR	(*),a	Zero Branch to Subroutine Relative, Unconditional	2

PROGRAM STATUS INSTRUCTIONS

LPSU		Load Program Status, Upper	1
LPSL		Load Program Status, Lower	1
SPSU		Store Program Status, Upper	1
SPSL		Store Program Status, Lower	1
CPSU	v	Clear Program Status, Upper Selective	2
CPSL	v	Clear Program Status, Lower Selective	2
PPSU	v	Preset Program Status, Upper Selective	2
PPSL	v	Preset Program Status Lower Selective	2
TPSU	v	Test Program Status Upper Selective	2
TPSL	v	Test Program Status Lower Selective	2

INPUT/OUTPUT INSTRUCTIONS

WRTD,r		Write Data	1
REDD,r		Read Data	1
WRTC,r		Write Control	1
REDC,r		Read Control	1
WRTE,r	v	Write Extended	2
REDE,r	v	Read Extended	2

MISCELLANEOUS INSTRUCTIONS

HALT		Halt Enter Wait State	1
DAR,r		Decimal Adjust Register	1
TMI,r	v	Test Under Mask Immediate	2
NOP		No Operation	1

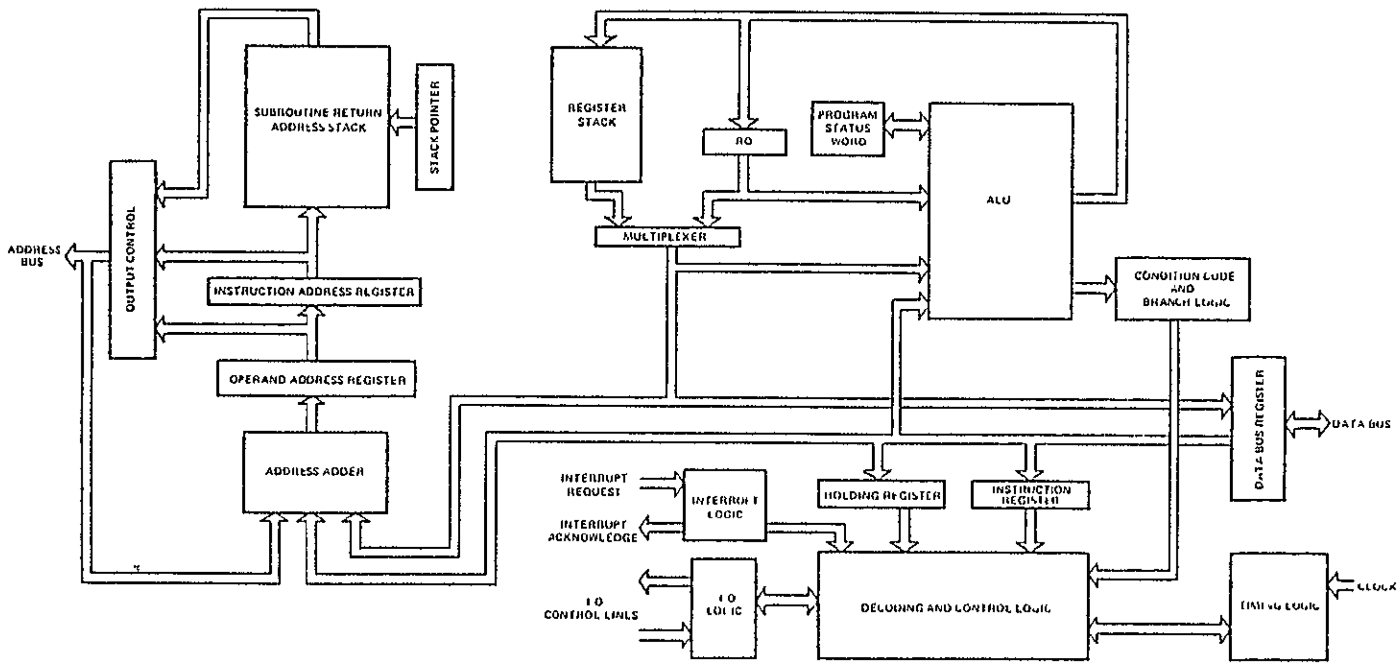

BLOCK DIAGRAM

APPENDIX B

This appendix contains alisting of the assembly language program used to implement the remote magnetic indicator heading algorithm. The program was assembled on the A2650 cross assembler program operational on the HP 2100 computer at the University of Santa Clara.

```
LINE  ADDR  LVHL  B1 B2 B3 B4 ERROR SOURCE

  3                                  ***************************************************
  4         0000                     R0     EQU     0
  5         0001                     R1     EQU     1
  6         0002                     R2     EQU     2
  7         0003                     R3     EQU     3
  8         0000                     UN     EQU     0
  9         0000                     Z      EQU     0
 10         0001                     P      EQU     1
 11         0002                     N      EQU     2
 12         0000                     EQ     EQU     0
 13         0001                     GT     EQU     1
 14         0001                     C      EQU     1
 15         0002                     LT     EQU     2
 16         0003                     UN     EQU     3
 17         0002                     COM    EQU     H'02'
 18         0010                     RS     EQU     H'10'
 19         0008                     WC     EQU     H'08'
 20         000F                     LOWR   EQU     H'0F'
 21         00F0                     UPPR   EQU     H'F0'
 22         0040                     FLAG   EQU     H'40'
 23         0020                     II     EQU     H'20'
 24         00FF                     NSAM   EQU     H'FF'
 25         0001                     MSB    EQU     1              OUTPUT
 26         0002                     LSB    EQU     2              OUTPUT
 27         0004                     THTA   EQU     4
 28         0008                     PHI    EQU     8
 29         0010                     SBIT   EQU     16
 30                                  ***************************************************
 31                                  ****   DATA STORAGE IN RAM    ****
 32                                         ORG     H'450'
 33         0450                     DATA   RES     10             RAW DATA
 34         045A                     DATM   RES     10             CORRECTED DATA
 35         0464                     LUPS   RES     1
 36         0465                     TEMP   RES     2
 37         0467                     SIND   RES     2
 38         0469                     SINR   RES     2
 39         046B                     HH2    RES     2              HH SQUARED DATA
 40         046D                     SIGN   RES     1
 41         046E                     HX2    RES     2              HX SQUARED DATA
 42         0470                     HY2    RES     2
 43         0472                     HZ2    RES     2
 44         0474                     QUAD   RES     1
 45         0475                     COSR   RES     2
 46         0477                     RSLT   RES     2
 47         0479                     OPR1   RES     2
 48         047B                     OPR2   RES     2
 49         047D                     STEM   RES     1
 50         047E                     SRES   RES     1
 51         047F                     DATX   RES     2
 52         0481                     DATY   RES     2
 53         0483                     DATZ   RES     2
 54         0485                     COST   RES     1
```

```
LINE  ADDR  LABL  B1 B2 B3 B4 ERROR SOURCE

 55          0446                         SIGX    RES      1
 56          0447                         SIGY    RES      1
 57          0448                         SIGZ    RES      1
 58          0449                         ABUF    RES      1
 59          044A                         BBUF    RES      1
 60          044B                         CBUF    RES      1
 61          044C                         DBUF    RES      1
 62          044D                         TBUF    RES      1
 63          044E                         OSET    RES      6
 64          0454                         SOST    RES      6
 65                                       ****************************************************
 66                                       ****    CONSTANTS IN ROM         ****
 67                                               ORG      H'500'
 68   0500   0500  00 01 03 04            SIN     DATA     H'00,01,03,04,06,07,09,0A,0C,0E,0F'
                   06 07 09 0A
                   0C 0E 0F
 69   050B         11 12 14 15                    DATA     H'11,12,14,15,17,19,1A,1C,1D,1F,20'
                   17 19 1A 1C
                   1D 1F 20
 70   0516         22 24 25 27                    DATA     H'22,24,25,27,28,2A,2B,2D,2E,30,31'
                   28 2A 2B 2D
                   2E 30 31
 71   0521         33 35 36 38                    DATA     H'33,35,36,38,39,3B,3C,3E,3F,41,42'
                   39 3B 3C 3E
                   3F 41 42
 72   052C         44 45 47 48                    DATA     H'44,45,47,48,4A,4B,4D,4E,50,51,53'
                   4A 4B 4D 4E
                   50 51 53
 73   0537         54 56 57 59                    DATA     H'54,56,57,59,5A,5C,5D'    61 DEG.
                   5A 5C 5D
 74   053E         5F 60 61 63                    DATA     H'5F,60,61,63,64,66,67,69,6A,6C,6D'
                   64 66 67 69
                   6A 6C 6D
 75   0549         6E 70 71 73                    DATA     H'6E,70,71,73,74,75,77,78,7A,7B,7C'
                   74 75 77 78
                   7A 7B 7C
 76   0554         7E 7F 80 82                    DATA     H'7E,7F,80,82,83,84,86,87,88,8A,8B,8C'
                   83 84 86 87
                   88 8A 8B 8C
 77   0560         8E 8F 90 92                    DATA     H'8E,8F,90,92,93,94,95,97,98,99,9B'
                   93 94 95 97
                   98 99 9B
 78   056B         9C 9D 9E 9F                    DATA     H'9C,9D,9E,9F,A1,A2,A3,A4,A6,A7,A8'
                   A1 A2 A3 A4
                   A6 A7 A8
 79   0576         A9 AA AB AD                    DATA     H'A9,AA,AB,AD,AE,AF,B0,B1,B2,B3,B5'
                   AE AF B0 B1
                   B2 B3 B5
 80   0581         B6 B7 B8 B9                    DATA     H'B6,B7,B8,B9,BA,BB,BC,BD,BF,C0,C1,C2'
                   BA BB BC BD
                   BF C0 C1 C2
 81   058D         C3 C4 C5 C6                    DATA     H'C3,C4,C5,C6,C7,C8,C9,CA,CB,CC,CD'
                   C7 C8 C9 CA
                   CB CC CD
```

```
LINE  ADDR  LABL  B1 B2 B3 B4 ERROR SOURCE

  82  0598        CE CF D0 D1                  DATA      H'CE,CF,D0,D1,D2,D3,D3,D4,D5,D6,D7'
                  D2 D3 D3 D4
                  D5 D6 D7
  83  05A3        D8 D9 D9 DA                  DATA      H'D8,D9,D9,DA,DB,DC,DD,DD,DE,DF,E0'
                  DB DC DD DD
                  DE DF E0
  84  05AE        F1 E1 E2 E3                  DATA      H'E1,E1,E2,E3,E3,E4,E5,E6,E6,E7,E8'
                  E3 E4 E5 E6
                  E6 E7 E8
  85  05B9  05B9  FF FF FF FF            COS   DATA      H'FF,FF,FF,FF,FF,FF,FF,FF,FF,FF'
                  FF FF FF FF
                  FF FF
  86  05C3        FF FF FF FF                  DATA      H'FF,FF,FF,FF,FF,FE,FE,FE,FE,FE'
                  FF FF FE FF
                  FE FE
  87  05CD        FE FD FD FD                  DATA      H'FE,FD,FD,FD,FD,FC,FC,FC,FC,FB'
                  FD FC FC FC
                  FC FB
  88  05D7        FB FB FB FA                  DATA      H'FB,FB,FB,FA,FA,FA,F9,F9,F9,F8'
                  FA FA F9 F9
                  F9 F8
  89  05E1        F8 F7 F7 F7                  DATA      H'F8,F7,F7,F7,F6,F6,F5,F5,F4,F4'
                  F6 F6 F5 F5
                  F4 F4
  90  05EB        F4 F3 F3 F2                  DATA      H'F4,F3,F3,F2,F2,F1,F1,F0,EF,EF'
                  F2 F1 F1 F0
                  EF EF
  91  05F5        EE EF FD ED                  DATA      H'EE,FE,ED,ED,EC,EB,EB,EA,EA,E9,E8,E8'
                  EC EB EB EA
                  EA E9 E8 E8
  92  0601        E7 E6 E6 E5                  DATA      H'E7,E6,E6,E5,E4,E3,E3,E2,E1,E1'
                  E4 E3 E3 E2
                  E1 E1
  93  060B        E0 DF DE DD                  DATA      H'E0,DF,DF,DD,DD,DC,DB,DA,D9,D9'
                  DD DC DB DA
                  D9 D9
  94  0615        D8 D7 D6 D5                  DATA      H'D8,D7,D6,D5,D4,D3,D3,D2,D1,D0'
                  D4 D3 D3 D2
                  D1 D0
  95  061F        CF CF CD CC                  DATA      H'CF,CE,CD,CC,CB,CA,C9,C8,C7,C6'
                  CB CA C9 C8
                  C7 C6
  96  0629        C5 C4 C3 C2                  DATA      H'C5,C4,C3,C2,C1,C0,BF,BE,BD,BC'
                  C1 C0 BF BE
                  BD BC
  97  0633        BB BA B9 B8                  DATA      H'BB,BA,B9,B8,B7,B6,B5,B3,B2,B1'
                  B7 B6 B5 B3
                  B2 B1
  98  063D        B0 AF AE AD                  DATA      H'B0,AF,AE,AD,AB,AA,A9,A8,A7,A6,A4'
                  AB AA A9 A8
                  A7 A6 A4
  99  0648        A3 A2 A1 9F                  DATA      H'A3,A2,A1,9F,9E,9D,9C,9B,99,98,97,95'
                  9E 9D 9C 9B
                  99 98 97 95
```

```
LINE  ADDR  LABL  B1 B2 B3 B4 ERROR SOURCE

 100  0654        94 93 92 90                 DATA    H'94,93,92,90,8F,8E,8C,8B,8A,88'
                  8F 8E 8C 8B
                  8A 88
 101  065E        87 86 84 83                 DATA    H'87,86,84,83,82,80,7F,7E,7C,7B'
                  82 80 7F 7E
                  7C 7B
 102  0668        7A 78 77 75                 DATA    H'7A,78,77,75,74,73,71,70,6E,6D,6C'
                  74 73 71 70
                  6E 6D 6C
 103  0673        6A 69 67 66                 DATA    H'6A,69,67,66,64,63,61,60,5F,5D,5C'
                  64 63 61 60
                  5F 5D 5C
 104  067E        5A 59 57 56                 DATA    H'5A,59,57,56,54,53,51,50,4F,4D'
                  54 53 51 50
                  4E 4D
 105  0688        4B 4A 48 47                 DATA    H'4B,4A,48,47,45,44,42,41,3F,3E,3C'
                  45 44 42 41
                  3F 3E 3C
 106  0693        3B 39 38 36                 DATA    H'3B,39,38,36,35,33,31,30,2E,2D'
                  35 33 31 30
                  2E 2D
 107  069D        2B 2A 28 27                 DATA    H'2B,2A,28,27,25,24,22,20,1F,1D'
                  25 24 22 20
                  1F 1D
 108  06A7        1C 1A 19 17                 DATA    H'1C,1A,19,17,15,14,12,11,0F,0E'
                  15 14 12 11
                  0F 0E
 109  06B1        0C 0A 09 07                 DATA    H'0C,0A,09,07,06,04,03,01,00'
                  06 04 03 01
                  00
 110  06BA  06BA  7F 7B 77 72           COSM  DATA    H'7F,7B,77,72,6E,69,65,61,5C,58,54'
                  6E 69 65 61
                  5C 58 54
 111  06C5        50 4C 47 43                 DATA    H'50,4B,47,43,3F,3C,38,34,31,2D,2A'
                  3F 3C 38 34
                  31 2D 2A
 112  06D0        27 23 20 1D                 DATA    H'27,23,20,1D,1B,18,15,13,11,0E,0C'
                  1B 18 15 13
                  11 0F 0C
 113  06DB        0B 09 07 06                 DATA    H'0B,09,07,06,04,03,02,01,01,00,00,00,00'
                  04 03 02 01
                  01 00 00 00
                  00
 114  06E8  06FB  FF 8B 12 9F           COSL  DATA    H'FF,8B,12,9E,2F,C5,63,08,B7,72,38,0C'
                  2F C5 63 0A
                  B7 72 38 0C
 115  06F4        F0 E3 F8 FF                 DATA    H'F0,E3,EB,FF,2B,6C,C3,32,B9,59,15,EC'
                  2B 6C C3 32
                  B9 59 15 EC
 116  0700        F0 F2 22 72                 DATA    H'E0,F2,22,72,E2,73,26,FB,F4,10,52,B8'
                  E2 73 26 FB
                  F4 1  52 BA
```

```
LINE ADDR LABL  B1 B2 B3 B4 ERROR SOURCE

     070C        43 F5 CD CC              DATA      H'43,F5,CD,CC,F1,3E,B3,4F,13,00'
                 F1 3E B3 4F
                 13 00
     0716  0716  01 02 04 08        BCD   DATA      H'01,02,04,08,16,32,64,00'
                 16 32 64 00
     071E  071E  03                 SINE  DATA      H'03'
                                    ****************************************************
                                          ORG       H'750'
                                    ****************************************************
                                    *  INIALIZATION OF THE INSTRUMENT                 *
                                    *  PARAMETERS AFFECTED INCLUDE:                   *
                                    *  (1) PR. STATUS LOWER/UPPER                     *
                                    *  (2) CONTENTS OF REGS. C&D ON CPU BOARD         *
                                    ****************************************************
                                    ****  INITIALIZE                  ****
     0750        76 21                    PPSU      II          INHIBIT INTERRUPTS
     0752        75 FF                    CPSL      H'FF'       CLEAR ALL
     0754        77 02                    PPSL      COM         LOGICAL COMPARISONS
     0756        04 FF                    LODI,R0   NSAM
     0758        F0                       WRTD,R0               NO SAMPLE/HLD OR MUX
     0759        74 FF                    CPSU      H'FF'       CLEAR ALL
                                    **
                                    ****  START MAIN PROGRAM          ****
     075B  075B  3F 07 80           MAIN  BSTA,UN   SAMP        SAMPLE ALL DATA CHANNELS
     075E        3F 0A E6                 BSTA,UN   ROTX        CORRECT HX DATA
     0761        3F 0A 71                 BSTA,UN   ROTY        CORRECT HY DATA
     0764        3F 0A 09                 BSTA,UN   HVEC        COMPUTE HORIZ. VECTOR
     0767        3F 07 70                 BSTA,UN   WICH        CALC. HEADING & O/P
     076A        3F 08 97                 BSTA,UN   OUTA        O/P ROLL &PITCH
     076D        1F 07 5B                 BCTA,UN   MAIN        LOOP FOREVER
                                    ****************************************************
                                    *
                                    *
     0770  0770  77 02              WICH  PPSL      COM
     0772        0C 04 70                 LODA,R0   HY2
     0775        EC 04 6E                 COMA,R0   HX2
     0778        1D 08 14                 BCTA,GT   COSY
     077B        1E 08 2B                 BCTA,LT   SINY
     077E        0C 04 71                 LODA,R0   HY2+1       LS BITS
     0781        EC 04 6F                 COMA,R0   HX2+1
     0784        1D 08 14                 BCTA,GT   COSY
     0787        1F 08 2B                 BCTA,UN   SINY
                                    ****************************************************
```

```
LINE  ADDR  LABL  B1 B2 B3 B4 ERROR SOURCE

                                               ORG       H'07B0'
                                        ************************************************
                                        * A SUBROUTINE TO SAMPLE DATA FROM ALL SENSORS   *
                                        *  REGISTER "D" CONTROLS SAMPLE/HOLD & MUX       *
                                        *   BITS 0,1,&2 SELECT HX,HY,HZ,THETA,PHI        *
                                        * DATA IS STORED IN DOUBLE PRECISION FORM        *
                                        * BEGINNING AT "DATA" WITH HX(MSB) FOLLOWED BY   *
                                        *      HX(LSB),HY,HZ,PITCH,ROLL.                 *
                                        *    (1) CONVERTS A/D DATA TO SIGN MAGNITUDE     *
                                        *    (2) CHANGES SIGN OF HY & HZ(ORIENTATION)    *
                                        *    (3) CORRECTS FOR OFFSET ERROR               *
                                        *   EXIT WITH CORRECTED DATA IN TABLE "DATM"     *
                                        ************************************************
                                        ****   BEGIN SUBROUTINE           ****
      07B0  07B0  05 FF                 SAMP   LODI,R1   -1             DATA INDEX
      07B2        06 05                        LODI,R2   5              LOOP COUNTER
      07B4        07 01                        LODI,R3   1              1ST SAMPLE
      07B6        75 09                        CPSL      C+WC
      07B8  07B8  F3                    NEXT   WRTC,R3                  SELECT & SAMPLE DATA
      07B9        67 80                        IORI,R3   H'80'          READY TO HOLD
      07BB        F3                           WRTC,R3                  HOLD DATA
      07BC        04 80                        LODI,R0   H'80'
      07BE        B0                           WRTC,R0                  RESET A/D
      07BF        20                           EORZ      R0
      07C0        B0                           WRTC,R0                  START A/D
      07C1  07C1  70                    TEST   REDD,R0                  READ LSB
      07C2        F4 01                        TMI,R0    H'01'
      07C4        1A 7B                        BCTR,N    TEST           BRANCH BACK IF EOC=1
      07C6        24 FF                        EORI,R0   H'FF'
      07C8        44 F0                        ANDI,R0   UPPR           STRIP OFF 4 LS BITS
      07CA        CD 24 51                     STRA,R0   DATA+1,R1,+    STORE LS 1/3
      07CD        30                           REDC,R0                  READ MS 2/3
      07CF        24 FF                        EORI,R0   H'FF'
      07D0        CD 24 4F                     STRA,R0   DATA-1,R1,+    STORE MSB
      07D3        87 01                        ADDI,R3   1              POINT TO NEXT DATA
      07D5        47 0F                        ANDI,R3   LOWR           POINT TO CHAN. ONLY
      07D7        FA 5F                        BDRR,R2   NEXT           TEST LOOP COUNTER
                                        ************************************************
                                        *   CONVERT TO SIGN MAGNITUDE
      07D9        77 08                        PPSL      WC             ENABLE CARRY
      07DB        06 FF                        LODI,R2   -1             INDEX
      07DD        07 07                        LODI,R3   7              LOOP COUNTER
      07DF  07DF  0E 24 50     -        CONT   LODA,R0   DATA,R2,+      GET MSB OF DATA
      07E2        1A 13                        BCTR,N    RSTU           BR. IF SIGN=1
      07E4        C1                           STRZ      R1
      07E5        20                           EORZ      R0             CLEAR R0
      07E6        77 01                        PPSL      C              SET UP FOR SUBT.
      07E8        AE 24 50                     SUBA,R0   DATA,R2,+      SUB. LS BITS
      07EB        CE 64 5A                     STRA,R0   DATM,R2        STORE NEW DATA
      07EE        20                           EORZ      R0
      07EF        A1                           SUBZ      R1             SUB. MS BITS
      07F0        64 80                        IORI,R0   H'80'          SET SIGN=1 (NEG)
```

```
LINE  ADDR  LABL  B1 B2 B3 B4 ERROR SOURCE

      07F2        CE 64 59                     STRA,R0   DATM-1,R2   STORE MS BITS
      07F5        18 08                        BCTR,UN   FINI
      07F7  07F7  44 7F                RSTO    ANDI,R0   H'7F'       SIGN BIT = 0
      07F9        CE 64 5A                     STRA,R0   DATM,R2     STORE NEW DATA
      07FC        0E 24 50                     LODA,R0   DATA,R2,+   GET  LS DATA
      07FF        CE 64 5A                     STRA,R0   DATM,R2     STORE AS NEW DATA
      0802  0802  F8 58                FINI    BDRR,R3   CONT
                                       *   CHANGEBSIGN OF HY &HZ (SENSOR ORIENTATION)
      0804        0C 04 5C                     LODA,R0   DATM+2      CHANGE SIGN OF HY & HZ
      0807        0D 04 5E                     LODA,R1   DATM+4
      080A        24 80                        EORI,R0   H'80'
      080C        25 80                        EORI,R1   H'80'
      080E        CC 04 5C                     STRA,R0   DATM+2
      0811        CD 04 5E                     STRA,R1   DATM+4
                                       *   CORRECT FOR OFFSET ERROR IN HX,HY, & HZ CHANNELS
      0814        07 00                        LODI,R3   0           DO HX 1ST
      0816        3F 08 2A                     BSTA,UN   OFST
      0819        07 02                        LODI,R3   2           HY
      081B        3F 08 2A                     BSTA,UN   OFST
      081E        07 04                        LODI,R3   4           HZ
      0820        3F 08 2A                     BSTA,UN   OFST
      0823        C0                           NOP
      0824        07 07                        LODI,R3   7
                                       *   CORRECT FOR ORTHOGONALITY ERROR IN HX AXIS
      0826        3F 0F 88                     BSTA,UN   ORTH
      0829        17                           RETC,UN
                                       ***********************************************
```

```
LINE  ADDR  LABL  B1 B2 B3 B4 ERROR SOURCE

                                   **************************************************
                                   **************************************************
      082A  082A  0F 64 5A         OFST   LODA,R0    DATM,R3     MS BYTE OF DATA
      082D        C1                      STRZ       R1
      082E        44 7F                   ANDI,R0    H'7F'       STRIP SIGN
      0830        45 80                   ANDI,R1    H'80'       SAVE SIGN
      0832        CC 04 77                STRA,R0    RSLT
      0835        CD 04 7F                STRA,R1    SRES
      0838        0F 64 5B                LODA,R0    DATM+1,R3   LS BYTE OF DATA
      083B        CC 04 78                STRA,R0    RSLT+1
      083E        0F 64 8E                LODA,R0    OSET,R3     MS BYTE OF OFFSET
      0841        CC 04 65                STRA,R0    TEMP
      0844        0F 64 8F                LODA,R0    OSET+1,R3
      0847        CC 04 66                STRA,R0    TEMP+1
      084A        0F 64 94                LODA,R0    SOST,R3
      084D        CC 04 70                STRA,R0    STE1
      0850        75 02                   CPSL       COM
      0852        77 10                   PPSL       RS          BANK=1
      0854        3F 09 98                BSTA,UN    SADD
      0857        75 10                   CPSL       RS          BANK=0
      0859        0C 04 77                LODA,R0    RSLT
      085C        CF 64 5A                STRA,R0    DATM,R3
      085F        0C 04 78                LODA,R0    RSLT+1
      0862        CF 64 5B                STRA,R0    DATM+1,R3
      0865        17                      RETC,UN
                                   **************************************************
                                   *      BINARY MULT. FOR A TWO-BYTE INTEGER       *
                                   *      MULT. BY A SINGLE BYTE INTEGER            *
                                   *      MULTIPLIER IS IN OPR1+1                   *
                                   *      MULTIPLICAND IS IN OPR2,OPR2+1            *
                                   *      RESULT WILL BE IN RSLT,RSLT+1             *
                                   *      (2 BYTES ARE DISCARDED )                  *
                                   **************************************************

                                   ****   BEGIN SUBROUTINE        ****
      0866  0866  77 0A            SMPY   PPSL       WC          SET MODE
      0868        20                      EORZ       R0
      0869        CC 04 77                STRA,R0    RSLT        CLEAR RESULT
      086C        CC 04 78                STRA,R0    RSLT+1      CLEAR RESULT+1
      086F        CC 04 79                STRA,R0    OPR1
      0872        07 08                   LODI,R3    8           LOAD COUNT
      0874  0874  0E 04 7A         LOC0   LODA,R2    OPR1+1      GET MULTIPLIER
      0877  0877  52               LOOO   RRR,R2                 ROT. RIGHT WITH CARRY
                                   *  THIS ROTATES MULTIPLIER BY 1 BIT TO GET LSB INTO CARRY
      0878        20                      EORZ       R0          CLEAR R0
      0879        D0                      RRL,R0                 GET CARRY INTO LSB
      087A        FB 00                   BDRR,R0    LOC4        BRANCH IF C=0
      087C  087C  05 02            LOC1   LODI,R1    2           INDEX
      087E  087E  0D 64 76         LOC2   LODA,R0    RSLT-1,R1   ADD MULTIPLICAND TO PRODUCT
      0881        8D 64 7A                ADDA,R0    OPR2-1,R1
      0884        CD 64 76                STRA,R0    RSLT-1,R1
      0887        F9 75                   BDRR,R1    LOC2        FINISH THE ADD
```

```
PIP ASSEMBLER VERSION SCU LEVEL 1 HEADING INSTRUMENT ASSEMLY PROGRAM  1976 PAGE  10

ADDR  LABL  B1 B2 B3 B4 ERROR SOURCE

0889  0889  05 FE          LOC4   LODI,R1    -2          ROT. THE PRODUCT
088B  088B  0D 63 79       LOC5   LODA,R0    RSLT-256+2,R1
088E        50                    RRR,R0
088F        CD 63 79              STRA,R0    RSLT-256+2,R1
0892        D9 77                 BIRR,R1    LOC5
0894        FB 61                 BDRR,R3    LOOP        FINISH THE LOOP
                           ***********************************************
0896        17                    RETC,UN
                           ***********************************************
                           *   A SUBROUTINE TO OUTPUT PITCH & ROLL DATA    *
                           *   CALLED BY MAIN PROG. , FETCHES CONVERTED DATA*
                           *   FROM TABLE "DATM" THEN O/P'S BCD ANGLE + SIGN*
                           ***********************************************
0897  0897  0C 04 60       OUTA   LODA,R0    DATM+6      FETCH THETA (MSB)
089A        C3                    STRZ       R3
089B        44 80                 ANDI,R0    H'80'       SAVE SIGN
089D        1A 16                 BCTR,N     NTH         BR. ON NEG THETA
089F        2C 04 62              EORA,R0    DATM+8      COMPARE SIGNS
08A2        1A 06                 BCTR,N     NPHI
08A4        04 07                 LODI,R0    7
08A6        04 10                 WRTE,R0    SRIT        BOTH POSITIVE
08A8        1B 14                 BCTR,UN    AGL
08AA  08AA  20             NPHI   EORZ       R0
08AB        04 10                 WRTE,R0    SRIT        PHI NEG.
08AD        1B 0F                 BCTR,UN    AGL
08AF  08AF  2C 04 62       NTH    EORA,R0    DATM+8
08B2        19 06                 BCTR,P     NPH
08B4        04 03                 LODI,R0    3
08B6        04 10                 WRTE,R0    SRIT        PITCH NEG.& ROLL POS.
08B8        1B 04                 BCTR,UN    AGL
08BA  08BA  04 08          NPH    LODI,R0    8
08BC        04 10                 WRTE,R0    SRIT        BOTH NEGATIVE
08BE  08BE  3F 08 CC       AGL    BSTA,UN    LOD         FORM ANGLE (BCD)
08C1        05 04                 WRTE,R1    THTA        OUTPUT PITCH
08C3        0F 04 62              LODA,R3    DATM+8      FETCH ROLL
08C6        3F 08 CC              BSTA,UN    LOD         ANGLE(BCD)
08C9        05 08                 WRTE,R1    PHI         OUTPUT PHI
08CB        17                    RETC,UN
                           ***********************************************
08CC  08CC  47 7F          LOD    ANDI,R3    H'7F'
08CE        CF 04 7C              STRA,R3    OPR2+1      MULTIPLICAND
08D1        20                    EORZ       R0
08D2        CC 04 7B              STRA,R0    OPR2        CLEAR LS BYTE
08D5        04 5A                 LODI,R0    H'5A'       FACTOR(.35156)
08D7        CC 04 7A              STRA,R0    OPR1+1      MULTIPLIER
08DA        3F 04 66              BSTA,UN    SMPY        BINARY ANGLE
08DD        0C 04 7B              LODA,R0    RSLT+1      ANGLE
08E0        3F 0C 64              BSTA,UN    BCDA        ANGLE(BCD)
08E3        25 FF                 EORI,R1    H'FF'
08E5        17                    RETC,UN
                           ***********************************************
```

```
LINE  ADDR  LABL  B1 B2 B3 B4 ERROR SOURCE

                                       ************************************************
                                       *   S.R. ROTX TO CORRECT HX'DATA USING ALGORITHM *
                                       *        HX=HX**COS(PITCH)+SIN(PITCH)*(HYM*SIN(  *
                                       *                ROLL)+HZM*COS(ROLL))             *
                                       *   ENTER WITH "RAW DATA" IN TABLE DATM           *
                                       *   EXIT WITH MODIFIED HX IN "DATX"               *
                                       *   CALLS S.R. H7R1                               *
                                       *   CALLS S.R.S. "SADD" & "SMPY" TO DO             *
                                       *   SIGNED MAGNITUDE ADD/SUBT AND MULTIPLY         *
                                       ************************************************
      08E6  08E6  77 08                ROTX    PPSL     WC+C        ARITH WITH CARRY, C=1
      08E8        0C 04 60                     LODA,R0  DATM+6      THETA (PITCH)
      08EB        C1                           STRZ     R1
      08EC        C3                           STRZ     R3
      08ED        45 7F                        ANDI,R1  H'7F'       STRIP OFF SIGN
      08EF        47 80                        ANDI,R3  H'80'       SAVE SIGN
      08F1        CF 04 67                     STRA,R3  SINO        SIGN THETA
      08F4        0D 65 00                     LODA,R0  SIN,R1      SIN(THETA)
      08F7        CC 04 68                     STRA,R0  SINO+1
      08FA        0D 65 89                     LODA,R0  COS,R1      COS(THETA)
      08FD        CC 04 65                     STRA,R0  COST
      0900        CC 04 7A                     STRA,R0  OPR1+1      MULTIPLIER
      0903        0C 04 5A                     LODA,R0  DATM        HX MSBITS
      0906        C1                           STRZ     R1
      0907        44 7F                        ANDI,R0  H'7F'       STRIP OFF SIGN
      0909        45 80                        ANDI,R1  H'80'       SAVE SIGN
      090B        CC 04 7B                     STRA,R0  OPR2        MULTIPLICAND
      090E        CD 04 86                     STRA,R1  SIGA
      0911        0C 04 5B                     LODA,R0  DATM+1
      0914        CC 04 7C                     STRA,R0  OPR2+1
      0917        3F 06 66                     BSTA,UN  SMPY        FORM HX* COS (THETA)
      091A        0C 04 77                     LODA,R0  RSLT        MOVE PRODUCT
      091D        CC 04 8B                     STRA,R0  CBUF
      0920        0C 04 78                     LODA,R0  RSLT+1
      0923        CC 04 8C                     STRA,R0  DBUF
      0926        3F 0F 40                     BSTA,UN  H7R1
      0929        0C 04 68                     LODA,R0  SINO+1      SIN (THETA)
      092C        CC 04 7A                     STRA,R0  OPR1+1      MULTIPLIER
      092F        3F 06 66                     BSTA,UN  SMPY        HZ*SIN(THETA)
      0932        0C 04 67                     LODA,R0  SINO        SIGN OF THETA
      0935        CC 04 7E                     STRA,R0  SGES        FOR USE BY SADD
      0938        0D 04 86                     LODA,R1  SIGA
      093B        CD 04 7D                     STRA,R1  STEM
      093E        0C 04 8B                     LODA,R0  CBUF
      0941        0D 04 8C                     LODA,R1  DBUF
      0944        CC 04 65                     STRA,R0  TEMP
      0947        CD 04 66                     STRA,R1  TEMP+1
      094A        75 02                        CPSL     COM         FLAG = ADD
      094C        3F 04 98                     BSTA,UN  SADD        FORM NEW HX
      094F        0C 04 78                     LODA,R0  RSLT+1      MOVE NEW HX
      0952        CC 04 40                     STRA,R0  DATX+1
      0955        0C 04 77                     LODA,R0  RSLT
```

```
LINE  ADDR  LABL  B1 B2 B3 B4 ERROR SOURCE

394   0958        CC 04 7F                  STRA,R0   DATX
395   095B        17                        RETC,UN
396                                   ***********************************************
397                                   *  SUBROUTINE TO SQUARE TWO 2 BYTE VALUES      *
398                                   *  ENTER WITH VALUE  IN R1(MSB) & R2(LSB)      *
399                                   *  EXIT WITH 2 MSB IN RSLT & RSLT+1            *
400                                   ***********************************************
401                                   ****      BEGIN                  ****
402   095C  095C  77 08               SOU       PPSL      WC
403   095E        20                            EORZ      R0
404   095F        CC 04 77                      STRA,R0   RSLT         CLEAR TEMP STORAGE
405   0962        CC 04 78                      STRA,R0   RSLT+1
406   0965        07 10                         LODI,R3   16           COUNTER
407   0967        45 7F                         ANDI,R1   H'7F'
408   0969        CD 04 7B                      STRA,R1   OPR2
409   096C        CE 04 7C                      STRA,R2   OPR2+1
410   096F  096F  51                  ROTA      RRR,R1                 ROTATE MULTIPLIER
411   0970        52                            RRR,R2
412   0971        20                            EORZ      R0
413   0972        D0                            RRL,R0                 GET LS BIT INTO R0
414   0973        F8 12                         BDRR,R0   NOAD         NO ADD IF C=0
415   0975        0C 04 78                      LODA,R0   RSLT+1
416   0978        8C 04 7C                      ADDA,R0   OPR2+1
417   097B        CC 04 78                      STRA,R0   RSLT+1
418   097E        0C 04 77                      LODA,R0   RSLT
419   0981        8C 04 7B                      ADDA,R0   OPR2
420   0984        1F 09 8A                      BCTA,UN   NOAD+3
421   0987  0987  0C 04 77            NOAD      LODA,R0   RSLT
422   098A        50                            RRR,R0
423   098B        CC 04 77                      STRA,R0   RSLT
424   098E        0C 04 78                      LODA,R0   RSLT+1
425   0991        50                            RRR,R0                 ROTATE LS 1/2 RESULT
426   0992        CC 04 78                      STRA,R0   RSLT+1
427   0995        F8 5B                         BDRR,R3   ROTA         CONT. MULT. IF REQ.
428                                   ***********************************************
429   0997        17                            RETC,UN                END OF SUBROUTINE
```

PIP ASSEMBLER VERSION SCU LEVEL 1 HEADING INSTRUMENT ASSEMBLY PROGRAM 1976 PAGE 13

```
LINE  ADDR  LABL  B1 B2 B3 B4 ERROR SOURCE

 431                                    ***************************************************
 432                                    *    S.R. SADD TO PERFORM DOUBLE PRECISION          *
 433                                    *    SIGN & MAGNITUDE ADD/SUBT                      *
 434                                    *    ADDEND (SUBT-AHEND) IN TEMP, TEMP+1            *
 435                                    *    AUGEND (MINUEND) IN RSLT, RSLT+1               *
 436                                    *    STEM = SIGN OF TERM IN TEMP SRES = SIG         *
 437                                    *    COM BIT IS FLAG ((0=ADD; 1= SUBT)              *
 438                                    *    SIGNED TOT L LEFT IN RSLT, RSLT+1              *
 439                                    ***************************************************
 440  099A  099A  77 09                 SADD   PPSL     WC+C         ARITH WITH CARRY; SET CARRY
 441  099A        07 02                        LODI,R3  2            INDEX
 442  099C        B5 02                        TPSL     COM          TEST FLAG
 443  099E        1C 0A 18                     BCTA,UN  SSUB         BR. IF SUBT.
 444                                    *   START ADD HERE
 445  09A1        0F 04 70                     LODA,R3  STEM         SIGN OF TEMP
 446  09A4        03                           LODZ     R3           EX. OR WITH SIGN RESULT
 447  09A5        2C 04 7E                     EORA,R0  SRES
 448  09A8        1E 09 CA                     BCTA,N   DIFR         BR. IF SIGNS DIFR
 449  09AB        75 01                        CPSL     C
 450  09AD        0C 04 66                     LODA,R0  TEMP+1       FORM SUM
 451  09B0        8C 04 78                     ADDA,R0  RSLT+1
 452  09B3        CC 04 78                     STRA,R0  RSLT+1
 453  09B6        0C 04 65                     LODA,R0  TEMP
 454  09B9        8C 04 77                     ADDA,R0  RSLT
 455  09BC        9C 09 F9                     BCFA,Z   RTRN
 456  09BF        0D 04 78                     LODA,R1  RSLT+1       GET LS BITS
 457  09C2        9C 09 F9                     BCFA,Z   RTRN
 458  09C5        20                           EORZ     R0
 459  09C6        CC 04 77                     STRA,R0  RSLT         ZERO RSLT = POS
 460  09C9        17                           RETC,UN
 461  09CA  09CA  06 02                 DIFR   LODI,R2  2            CTR/INDEX
 462  09CC        03                           LODZ     R3
 463  09CD        1E 0A 02                     BCTA,N   XNEG         BR. IF RX = NEG
 464  09D0  09D0  0E 64 64              SUP1   LODA,R0  TEMP-1,R2    FORM TEMP - RSLT
 465  09D3        AE 64 76                     SUBA,R0  RSLT-1,R2
 466  09D6        CE 64 76                     STRA,R0  RSLT-1,R2
 467  09D9        FA 75                        BDRR,R2  SUP1
 468  09DB        B5 01                        TPSL     C
 469  09DD        1C 0A 12                     BCTA,UN  TZER         BR. IF C = 1
 470  09E0  09E0  77 01                 TNEG   PPSL     C
 471  09E2        06 02                        LODI,R2  2            INDEX/CTR
 472  09E4  09E4  20                    SUP2   EORZ     R0           FORM 2'S COMPLEMENT
 473  09E5        AE 64 76                     SUBA,R0  RSLT-1,R2    IF C = 0
 474  09E8        CE 64 76                     STRA,R0  RSLT-1,R2
 475  09EB        FA 77                        BDRR,R2  SUP2
 476  09ED        C1                           STRZ     R1
 477  09EE        9C 09 FE                     BCFA,Z   NRES
 478  09F1        0D 04 78                     LODA,R1  RSLT+1
 479  09F4        9C 09 FE                     BCFA,Z   NRES
 480  09F7        18 01                        BCTR,UN  NOW
 481  09F9  09F9  63                    RTRN   IORZ     R3
 482  09FA  09FA  CC 04 77              NOW    STRA,R0  RSLT
```

```
     PIP ASSEMBLER VERSION SCU LEVEL 1 HEADING INSTRUMENT ASSEMLY PROGRAM  1976 PAGE    1

LINE  ADDR  LABL ' B1 B2 B3 B4 ERROR SOURCE

 483  09FD         17                           RETC,UN
 484  09FE  09FE   64 80                 NRES   IORI,R0    H'80'
 485  0A00          18 7A                        BCTR,UN    NOW
 486                                      *   START HERE IF TERM IN "TEMP" IS NEGATIVE
 487  0A02  0A02   0E 64 76              XNEG   LODA,R0    RSLT-1,R2   FORM DIFFERENCE
 488  0A05         AE 64 64                     SUBA,R0    TEMP-1,R2
 489  0A08         CE 64 76                     STRA,R0    RSLT-1,R2
 490  0A0B         FA 75                        BDRR,R2    XNEG        LOOP ONCE
 491  0A0D         B5 01                        TPSL       C
 492  0A0F         9C 09 F0                     BCFA,UN    TNEG
 493  0A12  0A12   44 7F                 TZER   ANDI,R0    H'7F'       RESULT IS POS
 494  0A14         CC 04 77                     STRA,R0    RSLT
 495  0A17         17                           RETC,UN
 496                                      ****************************************************
 497                                      *   START HERE IF SUBTRACTION IS REQUIRED
 498                                      *   I.E. (RSLT.RSLT+1) - (TEMP, TEMP+1)
 499  0A18  0A18   0C 04 7E              SSUB   LODA,R0    SRES        SIGN OF RESULT
 500  0A1B         C3                           STRZ       R3
 501  0A1C         06 02                        LODI,R2    2
 502  0A1E         2C 04 7D                     EORA,R0    STEM
 503  0A21         9E 0A 36                     BCFA,N     SUBR        BR. IF SIGNS SAME
 504  0A24         75 01                        CPSL       C
 505  0A26  0A26   0E 64 64              SLUP   LODA,R0    TEMP-1,R2
 506  0A29         8E 64 76                     ADDA,R0    RSLT-1,R2
 507  0A2C         CE 64 76                     STRA,R0    RSLT-1,R2
 508  0A2F         FA 75                        BDRR,R2    SLUP
 509  0A31         63                           IORZ       R3
 510  0A32         CC 04 77                     STRA,R0    RSLT
 511  0A35         17                           RETC,UN
```

```
LINE  ADDR  LABL  B1 B2 B3 B4 ERROR SOURCE

                                  *    START HERE IF BOTH TERMS SAME SIGN
      0A36  0A36  77 01          SUBR  PPSL       C             C=1
      0A38  0A38  0E 64 76       BLUP  LODA,R0    RSLT-1,R2     RSLT = TEMP - RSLT
      0A3B        AE 64 64             SUBA,R0    TEMP-1,R2
      0A3E        CE 64 76             STRA,R0    RSLT-1,R2
      0A41        FA 75                BDRR,R2    BLUP
      0A43        B5 01                TPSL       C             TEST CARRY
      0A45        1C 0A 5F             BCTA,UN    FINS
      0A48        06 02                LODI,R2    2             START 2'S COMPL
      0A4A        77 01                PPSL       C
      0A4C  0A4C  20             CLUP  EORZ       R0            LOOP TO DO
      0A4D        AE 64 76             SUBA,R0    RSLT-1,R2     2'S COMPL.
      0A50        CE 64 76             STRA,R0    RSLT-1,R2
      0A53        FA 77                BDRR,R2    CLUP
      0A55        0D 04 7E             LODA,R1    SVES          TEST SIGN
      0A58        16                   RETC,N                   RTN IF NEG.
      0A59        64 80                IORI,R0    H'80'
      0A5B        CC 04 77             STRA,R0    RSLT
      0A5E        17                   RETC,UN
      0A5F  0A5F  C1             FINS  STRZ       R1
      0A60        9C 0A 6A             BCFA,Z     FAN
      0A63        0D 04 78             LODA,R1    RSLT+1
      0A66        9C 0A 6A             BCFA,Z     FAN
      0A69        17                   RETC,UN
      0A6A  0A6A  63             FAN   IORZ       R3            SIGN = STEM
      0A6B        CC 04 77             STRA,R0    RSLT
      0A6E        77 02                PPSL       COM
      0A70        17                   RETC,UN
                                 ************************************************
```

```
LINE  ADDR  LABL  B1 B2 B3 B4 ERROR SOURCE

                                    **************************************************
                                    *   S.R. ROTY TO ADJUST HY DATA USING ALGORITHM  *
                                    *        HY=HYM*COS(ROLL)-HZM*SIN(ROLL)          *
                                    *   USES SIGN AND MAGNITUDE DATA FROM TABLE DATM *
                                    *   STORES NEW DATA INTO DATY, DATY+1            *
                                    *   CALLS S.R.S. "SADD" & "SMPY" TO PERFORM SIGNED*
                                    *   MAGNITUDE ARITHMETIC                         *
                                    **************************************************
      0A71  0A71  77 09             ROTY    PPSL     WC+C
      0A73        0C 04 62                  LODA,R0  DATM+H     GET ROLL ANGLE PHI
      0A76        C1                        STRZ     R1
      0A77        45 7F                     ANDI,R1  H'7F'      STRIP OFF SIGN
      0A79        2C 04 5E                  EORA,R0  DATM+4     DETERMINE SIGN OF PROD.
      0A7C        44 80                     ANDI,R0  H'80'
      0A7E  0A7E  CC 04 7D          AHED    STRA,R0  STEM
      0A81        0D 65 19                  LODA,R0  COS,R1     COS (PHI)
      0A84        CC 04 75                  STRA,R0  COSR
      0A87        0D 65 10                  LODA,R0  SIN,R1     SIN (PHI)
      0A8A        CC 04 7A                  STRA,R0  OPR1+1     MULTIPLIER
      0A8D        0C 04 5E                  LODA,R0  DATM+4     GET HZ
      0A90        44 7F                     ANDI,R0  H'7F'      STRIP SIGN
      0A92        CC 04 7B                  STRA,R0  OPR2       MULTIPLICAND
      0A95        0C 04 5F                  LODA,R0  DATM+5
      0A98        CC 04 7C                  STRA,R0  OPR2+1
      0A9B        3F 08 66                  BSTA,UN  SMPY       FORM Z2$SIN(PHI)
      0A9E        0C 04 77                  LODA,R0  RSLT       MOVE PRODUCT
      0AA1        CC 04 65                  STRA,R0  TEMP
      0AA4        0C 04 78                  LODA,R0  RSLT+1
      0AA7        CC 04 66                  STRA,R0  TEMP+1
                                    *   BEGIN FORMING 2ND TERM
      0AAA        0C 04 5C                  LODA,R0  DATM+2     GET HY MS BITS
      0AAD        C1                        STRZ     R1
      0AAE        45 7F                     ANDI,R1  H'7F'      STRIP SIGN
      0AB0        CD 04 7B                  STRA,R1  OPR2       MULTIPLICAND
      0AB3        44 80                     ANDI,R0  H'80'      SAVE SIGN
      0AB5        CC 04 7F                  STRA,R0  SRES       SIGN OF RESULT
      0AB8        0C 04 5D                  LODA,R0  DATM+3     HY LS BITS
      0ABB        CC 04 7C                  STRA,R0  OPR2+1
      0ABE        0C 04 75                  LODA,R0  COSR
      0AC1        CC 04 7A                  STRA,R0  OPR1+1     MULTIPLIER
      0AC4        3F 08 66                  BSTA,UN  SMPY
                                    *   NOW FORM NEW HY
      0AC7        77 02                     PPSL     COM
      0AC9        3F 0? 78                  BSTA,UN  SADD
      0ACC        0C 04 77                  LODA,R0  RSLT       MOVE ROTATED HY
      0ACF        CC 04 ?1                  STRA,R0  DATY
      0AD2        0C 04 78                  LODA,R0  RSLT+1
      0AD5        CC 04 ?2                  STRA,R0  DATY+1
      0AD8        17                        RETC,UN
```

```
LINE  ADDR  LABL  B1 B2 B3 B4 ERROR SOURCE

 593                                 ****************************************************
 594                                 *   S.R. HVEC TO COMPUTE HORIZ. FIELD VECTOR        *
 595                                 *   HH2 = HX (HORIZ)!2 + HY (HORIZ) !2              *
 596                                 *   GETS HX & HY FROM (DATX,DATX+1) & (DATY,DATY+1) *
 597                                 *   RESULT INTO HH2,HH2+1                           *
 598                                 ****************************************************
 599  0AD9  0AD9  77 08              HVEC   PPSL     WC
 600  0ADB        0D 04 7F                  LODA,R1  DATX         GET ROTATED HX
 601  0ADE        0E 04 80                  LODA,R2  DATX+1
 602  0AE1        3F 09 5C                  BSTA,UN  SQU          SQUARE HX
 603  0AE4        0C 04 77                  LODA,R0  RSLT         MOVE RESULT
 604  0AE7        CC 04 6E                  STRA,R0  HX2
 605  0AEA        0C 04 78                  LODA,R0  RSLT+1
 606  0AED        CC 04 6F                  STRA,R0  HX2+1
 607  0AF0        0D 04 81                  LODA,R1  DATY         GET HY (ROTATED)
 608  0AF3        0E 04 82                  LODA,R2  DATY+1
 609  0AF6        3F 09 5C                  BSTA,UN  SQU          SQUARE HY
 610  0AF9        06 02                     LODI,R2  2
 611  0AFB  0AFB  0E 64 76           LUPF   LODA,R0  RSLT-1,R2    MOVE HY2
 612  0AFE        CE 64 6F                  STRA,R0  HY2-1,R2
 613  0B01        FE 0A FB                  BDRA,R2  LUPF
 614  0B04        75 01                     CPSL     C
 615  0B06        06 02                     LODI,R2  2
 616  0B08  0B08  0E 64 6D           LUPH   LODA,R0  HX2-1,R2     SUM HX!2+HY!2
 617  0B0B        8E 64 76                  ADDA,R0  RSLT-1,R2
 618  0B0E        CE 64 6A                  STRA,R0  HH2-1,R2
 619  0B11        FA 75                     BDRR,R2  LUPH
 620  0B13        17                        RETC,UN
 621                                 ****************************************************
 622                                 *  S.R. TO COMPUTE YAW1 = ANGLE FROM THE HORIZ.     *
 623                                 *                         VECTOR COMP. HH          *
 624                                 *  ENTER WHEN MAGN(HX)< MAGN(HY)                    *
 625                                 *    YAW1 = ARCOS(HX!2/HH!2)                        *
 626                                 *   HH2= DIVIS R      OPR1...= HX2...= DIVIDEND     *
 627                                 *   RSLT= QUOTIENT                                  *
 628                                 ****************************************************
 629                                 ****   BEGIN
 630  0B14  0B14  05 02              COSY   LODI,R1  2            INDEX
 631  0B16  0B16  0D 64 6D           LUPE   LODA,R0  HX2-1,R1     LOAD OPR1+1,OPR1
 632  0B19        CD 64 70                  STRA,R0  OPR1-1,R1
 633  0B1C        F9 78                     BDRR,R1  LUPE         LOOP ONCE
 634  0B1E        3F 08 6A                  BSTA,UN  DIVI         FORM HX2/HH2
 635  0B21        3F 08 7B                  BSTA,UN  ANGL         FIND ARCOS
 636  0B24        3F 0C 64                  BSTA,UN  BCDA         CONVERT TO BCD
 637  0B27        3F 0C 7C                  BSTA,UN  HDG          COMPUTE HEADING
 638  0B2A        17                        RETC,UN
 639                                 ****************************************************
```

```
LINE  ADDR  LABL  B1 B2 B3 B4 ERROR SOURCE

 641                                       ******************************************************
 642                                       *  A SUBROUTINE TO COMPUTE HEADING WHEN              *
 643                                       *  ( +/-)135 < YAW <(+/-)45 DEGREES                  *
 644                                       ******************************************************
 645  0B2B  0B2B  05 02                    SINY    LODI,R1    2            INDEX
 646  0B2D  0B2D  0D 64 6F                 LUP     LODA,R0    HY2-1,R1     LOAD OPR1+1,OPR1
 647  0B30        CD 64 78                         STRA,R0    OPR1-1,R1
 648  0B33        F9 7B                            BDRR,R1    LUP
 649  0B35        20                               EORZ       R0
 650  0B36        3F 0B 4A                         BSTA,UN    DIVI         FORM HY2/HH2
 651  0B39        3F 0B 9B                         BSTA,UN    ANGL         FORM ARCOS(HY2/HH2)
 652  0B3C        3F 0C 64                         BSTA,UN    BCDA         CONVERT TO BCD
 653  0B3F        04 90                            LODI,R0    H'90'        CALC. 90-ANGLE
 654  0B41        77 09                            PPSL       C+WC
 655  0B43        A1                               SUBZ       R1
 656  0B44        94                               DAR,R0
 657  0B45        C1                               STRZ       R1
 658  0B46        3F 0C 7C                         BSTA,UN    HDG
 659  0B49        17                               RETC,UN
 660                                       ******************************************************
```

```
LINE  ADDR  LABL  B1 B2 B3 B4 ERROR SOURCE

                                   ************************************************
                                   *  A SUBROUTINE TO DIVIDE HX2/HH2 OR HY2/HH2   *
                                   *  ENTER WITH HX2 OR HY2 IN OPR1 & OPR1+1      *
                                   *  EXIT WITH QUOTIENT IN RSLT,RSLT+1           *
                                   ************************************************
      0B4A  0B4A  20               DIVI   EORZ      R0
      0B4B        CC 04 77                STRA,R0   RSLT         CLR QUOTIENT
      0B4E        CC 04 78                STRA,R0   RSLT+1
      0B51        07 11                   LODI,R3   17           CTR.
      0B53        0E 04 6C                LODA,R2   HH2+1
      0B56        0D 04 6B                LODA,R1   HH2
      0B59  0B59  77 0B            LUP1   PPSL      COM+C+WC     LOGICAL COMP.,C=1, WITH C
      0B5B        E5 00                   COMI,R1   0
      0B5D        1C 0B 93                BCTA,Z    ZER
      0B60        ED 04 79                COMA,R1   OPR1
      0B63        19 19                   BCTR,GT   GTD          BR. IF HH'2>HX'2
      0B65        1A 05                   BCTR,LT   LTD          BR. IF HH'2<HX'2
      0B67        EE 04 7A                COMA,R2   OPR1+1
      0B6A        19 12                   BCTR,GT   GTD          BR. IF HH>HX (LS BITS)
                                   ****   HERE IF HH<HX OR HH=HX (ALL BITS)
      0B6C  0B6C  0C 04 7A         LTD    LODA,R0   OPR1+1
      0B6F        A2                      SUBZ      R2           FORM DIVIDEND-DIVISOR
      0B70        CC 04 7A                STRA,R0   OPR1+1
      0B73        0C 04 79                LODA,R0   OPR1
      0B76        A1                      SUBZ      R1
      0B77        CC 04 79                STRA,R0   OPR1
      0B7A        77 01                   PPSL      C
      0B7C        1B 02                   BCTR,UN   JMP
      0B7E  0B7E  75 01            GTD    CPSL      C
      0B80  0B80  0C 04 78         JMP    LODA,R0   RSLT+1
      0B83        D0                      RRL,R0                 LSB=1 OR 0
      0B84        CC 04 78                STRA,R0   RSLT+1       STR. QUOTIENT  (C=0)
      0B87        0C 04 77                LODA,R0   RSLT
      0B8A        D0                      RRL,R0                 LSB=1 OR 0
      0B8B        CC 04 77                STRA,R0   RSLT         STR. QUOTIENT  (C=0)
      0B8E        51                      RRR,R1                 ROT. DIVISOR WITH C
      0B8F        52                      RRR,R2
      0B90        FB 47                   BDRR,R3   LUP1         CONT. UNTIL DONE
                                   ****   HERE RSLT=COS(YAW1)
      0B92        17                      RETC,UN
      0B93  0B93  E6 00            ZER    COMI,R2   0
      0B95        9C 0B 60                BCFA,Z    LUP1+7
      0B98        1F 0B 7E                BCTA,UN   GTD
                                   ************************************************
                                   ************************************************
                                   *  A SUBROUTINE TO CALCULATE THE ARCUS FUNCTION *
                                   *  THE ALGORITHM USES SUCCESSIVE APPROXIMATION  *
                                   *       & TABLE LOOK-UP TO ITERATE TO THE SOLUTION*
                                   *  BEGIN WITH ARG. IN RSLT,RSLT+1               *
                                   *  EXIT WITH ARCOS(ARG) IN R0                   *
                                   ************************************************
      0B9B  0B9B  77 0B            ANGL   PPSL      C+WC+COM
```

```
LINE  ADDR  LABL  B1 B2 B3 B4 ERROR SOURCE

714   0B9D        0E 04 77                   LODA,R2    RSLT         MS BYTE OF ARG.
715   0BA0        05 17                      LODI,R1    23           1ST ESTIMATE
716   0BA2        07 17                      LODI,R3    23           TWICE 1ST INCREMENT
717   0BA4  0BA4  0D 66 8A             LUPA  LODA,R0    COSM,R1      COS(EST.)
718   0BA7        75 01                      CPSL       C            MODIFY & TEST CTR.
719   0BA9        53                         RRR,R3
720   0BAA        18 1F                      BCTR,Z     LAST
721   0BAC        E2                         COMZ       R2
722   0BAD        19 0D                      BCTR,GT    ELTA         BR. IF EST. < ANGLE
723   0BAF        1A 12                      BCTR,LT    EGTA         BR. IF EST. > ANGLE
724   0BB1  0BB1  E4 01                EQL1  COMI,R0    1
725   0BB3        1D 0C 43                   BCTA,GT    QUIT
726   0BB6        1C 0C 49                   BCTA,EQ    ONE
727   0BB9        1F 0C 27                   BCTA,UN    ITLS         MS BITS ARE EQU. & < 1
728   0BBC  0BBC  75 01                ELTA  CPSL       C            INCR. EST.
729   0BBE        01                         LODZ       R1
730   0BBF        83                         ADDZ       R3
731   0BC0        C1                         STRZ       R1
732   0BC1        1B 61                      BCTR,UN    LUPA         CONTINUE LOOPING
733   0BC3  0BC3  77 01                EGTA  PPSL       C            DECR. EST.
734   0BC5        01                         LODZ       R1
735   0BC6        A3                         SUBZ       R3
736   0BC7        C1                         STRZ       R1
737   0BC8        1B 5A                      BCTR,UN    LUPA         LOOP BACK
738   0BCA  0BCA  07 0A                LAST  LODI,R3    10           LAST ITERATIONS
739   0BCC  0BCC  0D 66 8A             LUPB  LODA,R0    COSM,R1
740   0BCF        F2                         COMZ       R2
741   0BD0        19 05                      BCTR,GT    ELT
742   0BD2        1A 09                      BCTR,LT    EGT
743   0BD4        1F 0B B1                   BCTA,UN    EQL1         TEST VS QUTY 1
744   0BD7  0BD7  75 01                ELT   CPSL       C
745   0BD9        85 01                      ADDI,R1    1
746   0BDB        1B 04                      BCTR,UN    TSTR
747   0BDD  0BDD  77 01                EGT   PPSL       C
748   0BDF        A5 01                      SUBI,R1    1
749   0BE1  0BE1  FB 69                TSTR  BDRR,R3    LUPB         LOOP IF R3≠0
750                                    *   BEGIN INTERPOLATING USING MSBITS
751   0BE3        0D 66 8A                   LODA,R0    COSM,R1
752   0BE6        E2                         COMZ       R2
753   0BE7        19 18                      BCTR,GT    IGT
754                                    *   START IF COS(EST.) < ARG.
755   0BE9        C3                         STRZ       R3           TEMP ST. COS(EST.)
756   0BEA        0D 66 89                   LODA,R0    COSM-1,R1
757   0BED        77 01                      PPSL       C
758   0BEF        A3                         SUBZ       R3
759   0BF0        75 01                      CPSL       C
760   0BF2        50                         RRR,R0
761   0BF3        75 01                      CPSL       C
762   0BF5        83                         ADDZ       R3
763   0BF6        F2                         COMZ       R2           INTERP. VALUE VS ARG
764   0BF7        1E 0C [illegible]          BCTA,LT    QUIT
765   0BFA        77 01                      PPSL       C
```

REPRODUCIBILITY OF THE ORIGINAL PAGE IS POOR

```
ADDR  LABL  B1 B2 B3 B4 ERROR SOURCE

0BFC        85 01                          SUBI,R1   1
0BFF        1F 0C 43                       BCTA,UN   QUIT
                                   *   START HERE IF COS(EST.) > ARG.
0C01  0C01  E4 02                  IGT     COMI,R0   2
0C03        98 07                          BCFR,EQ   NEQ2         BR. IF COS(EST) # 2
0C05        75 01                          CPSL      C
0C07        85 01                          ADDI,R1   1
0C09        1F 0C 43                       BCTA,UN   QUIT
0C0C  0C0C  0D 66 E8               NEQ2    LODA,R0   COS+1,R1
0C0F        C1                             STRZ      R1
0C10        0D 66 8A                       LODA,R0   COS,R1
0C13        77 01                          PPSL      C
0C15        A3                             SUBZ      R3
0C16        75 01                          CPSL      C
0C18        50                             RRR,R0
0C19        75 01                          CPSL      C
0C1B        83                             ADDZ      R3
0C1C        E2                             COMZ      R2
0C1D        1E 0C 43                       BCTA,LT   QUIT
0C20        75 01                          CPSL      C
0C22        85 01                          ADDI,R1   1
0C24        1F 0C 43                       BCTA,UN   QUIT
                                   *   EXAMINE LS BITS
0C27  0C27  75 01                  ITLS    CPSL      C            BEGIN ITERATION ON LSBITS
0C29        05 2A                          LODI,R1   42           ESTIMATE OF ADDRESS
0C2B        0E 0A 78                       LODA,R2   RSLT+1
0C2F        F6 81                          COMI,R2   H'81'        1ST ESTIMATE
0C30        1D 0C 43                       BCTA,GT   QUIT
0C33        85 01                          ADDI,R1   1
0C35        F6 31                          COMI,R2   H'31'         2ND EST.
0C37        1D 0C 43                       BCTA,GT   QUIT
0C3A        85 01                          ADDI,R1   1
0C3C        F6 09                          COMI,R2   H'09'        3D EST.
0C3F        1D 0C 43                       BCTA,GT   QUIT
0C41        85 01                          ADDI,R1   1
0C43  0C43  01                     QUIT    LODZ      R1
0C44        75 01                          CPSL      C
0C46        84 20                          ADDI,R0   45
                                   ***********************************************
0C48        17                             RETC,UN
0C49  0C49  05 28                  ONE     LODI,R1   40
0C4B        0D 66 E9                       LODA,R0   COSL+1,R1
0C4E        C3                             STRZ      R3
0C4F        0D 66 E8                       LODA,R0   COSL,R1
0C52        77 01                          PPSL      C
0C54        A3                             SUBZ      R3
0C55        75 01                          CPSL      C
0C57        50                             RRR,R0
0C58        75 01                          CPSL      C
0C5A        83                             ADDZ      R3
0C5B        FC 0A 78                       COMA,R0   RSLT+1
0C5F        1A 63                          BCTR,LT   QUIT
```

```
LINE  ADDR  LABL  B1 B2 B3 B4 ERROR SOURCE

      0C60        05 29                       LODI,R1   41
      0C62        18 5F                       BCTR,UN   QUIT
                                        ************************************************
                                        ************************************************
                                        *  A SUBROUTINE TO CONVERT BINARY ANGLE TO BCD  *
                                        *  ENTR WITH R0=ANGLE(BIN) & EXIT R1= BCD EQUIV. *
                                        ************************************************
      0C64  0C64  07 07                 BCDA  LODI,R3   7            CTR.
      0C66        05 00                       LODI,R1   0            CLR TOTAL
      0C68  0C68  75 01                 BRCH  CPSL      C            CLR. C
      0C6A        D0                          RRL,R0
      0C6B        C2                          STRZ      R2           MOVE RESULT
      0C6C        9A 08                       BCFR,N    NINC         BR. IF MS BIT=0
      0C6E        01                          LODZ      R1
      0C6F        75 01                       CPSL      C
      0C71        84 66                       ADDI,R0   H'66'        BCD ADD 2 BYTES
      0C73        8F 67 15                    ADDA,R0   BCD-1,R3     INCR. BCD TOTAL
      0C76        94                          DAR,R0
      0C77        C1                          STRZ      R1
      0C78        02                          LODZ      R2           RESULT TO R0
      0C79  0C79  FB 6D                 NINC  BDRR,R3   BRCH         GO BACK TIL DONE
                                        ****  LEAVE WITH BCD EQUIV. OF YAW1 IN R1
      0C7B        17                          RETC,UN
                                        ************************************************
```

```
LINE  ADDR  LABEL  B1 B2 B3 B4 ERROR SOURCE

                                         **********************************************
                                         *  A SUBROUTINE TO CALCULATE HEADING & OUTPUT  *
                                         *      THREE BCD DIGITS PLUS SIGN              *
                                         **********************************************
      0C7C  0C7C   77 09                 HDG     PPSL      WC+C
      0C7E         0C 04 7F                      LODA,R0   DATX         SIGN OF HX ?
      0C81         1A 1B                         BCTR,N    YAW0         BR. IF NEG
                                         *  SOLVE FOR HEADING (BCD FORM)
      0C83         0C 04 81                      LODA,R0   DATY         GET HY
      0C86         1A 10                         BCTR,N    HYN          BR. ON HY=NEG.
                                         *
                                         * START HERE O  POS. HY & HX
      0C88         F5 00                         COMI,R1   0
      0C8A         18 0C                         BCTR,EQ   HYN
      0C8C         04 60                         LODI,R0   H'60'
      0C8E         A1                            SUBZ      R1
      0C8F         94                            DAR,R0
      0C90         C3                            STRZ      R3
      0C91         06 03                         LODI,R2   H'03'
      0C93         A6 00                         SUBI,R2   0
      0C95         96                            DAR,R2
      0C96         1B 27                         BCTR,UN   FINE
                                         *
                                         * ENTER HERE IF HX=POS. & HY=NEG.
      0C98  0C98   06 00                 HYN     LODI,R2   H'00'
      0C9A         01                            LODZ      R1
      0C9B         C3                            STRZ      R3
      0C9C         1B 21                         BCTR,UN   FINE
                                         *
                                         *  ENTER HERE HX=NEG & HY= +/-
      0C9E  0C9E   0C 04 81              YAW0    LODA,R0   DATY         TEST SIGN OF HY
      0CA1         1A 12                         BCTR,N    NHY
```

```
LINE  ADDR  LABL  B1 B2 B3 B4 ERROR SOURCE

                                   *  ENTER HERE IF HX=NEG & HY=POS
      0CA3        04 80                     LODI,R0   H'80'
      0CA5        75 01                     CPSL      C
      0CA7        84 66                     ADDI,R0   H'66'
      0CA9        81                        ADDZ      R1
      0CAA        94                        DAR,R0
      0CAB        C3                        STRZ      R3
      0CAC        06 01                     LODI,R2   H'01'
      0CAE        86 66                     ADDI,R2   H'66'
      0CB0        86 00                     ADDI,R2   0
      0CB2        96                        DAR,R2
      0CB3        1B 0A                     BCTR,UN   FINE
                                   *  ENTER HERE IF HX & HY = NEG
      0CB5  0CB5  04 80            NHY      LODI,R0   H'80'
      0CB7  0CB7  A1               DO       SUBZ      R1          SUB. YAW1 LSB
      0CB8        94                        DAR,R0
      0CB9        C3                        STRZ      R3
      0CBA        06 01                     LODI,R2   H'01'
      0CBC        A6 00                     SUBI,R2   0
      0CBF        96                        DAR,R2
                                   *
                                   *
                                   ****  READOUT OF DATA   ***********
      0CBF  0CBF  26 FF            FINE     EORI,R2   H'FF'
      0CC1        06 01                     WRTE,R2   MSB         MSB OUT
      0CC3        27 FF                     EORI,R3   H'FF'
      0CC5        07 02                     WRTE,R3   LSB         LSB OUT
      0CC7        17                        RETC,UN
                                   ***************************************************
                                            ORG       H'E40'
                                   ***************************************************
                                   *   S.R. TO CALC. THE HZ COMPONENT IN X-Z PLANE   *
                                   *       HZ=HY*SIN(PHI) + HZ*COS(PHI)              *
                                   *   EXIT WITH HZ IN OPR2,OPR2+1                   *
                                   ***************************************************
      0E40  0E40  0D 04 62         HZR1     LODA,R1   DATM+8      GET PHI
      0E43        0E 04 62                  LODA,R2   DATM+8
      0E46        45 80                     ANDI,R1   H'80'       SAVE SIGN
      0E48        46 7F                     ANDI,R2   H'7F'       STRI SIGN
      0E4A        CD 04 8D                  STRA,R1   TAUF        HOLD SIGN
      0E4D        0E 65 00                  LODA,R0   SIN,R2      SIN(PHI)
      0E50        CC 04 69                  STRA,R0   SINR
      0E53        0E 65 89                  LODA,R0   COS,R2      COS(PHI)
      0E56        CC 04 7A                  STRA,R0   OPR1+1
      0E59        0C 04 5E                  LODA,R0   DATM+4      HZ
      0E5C        0D 04 5F                  LODA,R1   DATM+5
      0E5F        CC 04 7B                  STRA,R0   OPR2
      0E62        CD 04 7C                  STRA,R1   OPR2+1
      0E65        3F 08 66                  BSTA,UN   SMPY        HZ*COS(PHI)
      0E68        0C 04 77                  LODA,R0   RSLT
      0E6B        0D 04 78                  LODA,R1   RSLT+1
      0E6F        CC 04 89                  STRA,R0   ABUF
```

```
ADDR  LABL  B1 B2 B3 B4 ERROR SOURCE

0E71        CD 04 8A                    STRA,R1   BBUF
0E74        0C 04 69                    LODA,R0   SINR
0E77        CC 04 7A                    STRA,R0   OPR1+1
0E7A        0C 04 5C                    LODA,R0   DATM+2     HY
0E7D        0D 04 5D                    LODA,R1   DATM+3
0E80        C2                          STRZ      R2
0E81        44 7F                       ANDI,R0   H'7F'
0E83        46 80                       ANDI,R2   H'80'
0E85        2E 04 8D                    EORA,R2   TBUF       DETERMINE SIGN
0E88        CC 04 7B                    STRA,R0   OPR2
0E8B        CD 04 7C                    STRA,R1   OPR2+1
0E8E        CE 04 7E                    STRA,R2   SRES
0E91        3F 08 66                    BSTA,UN   SMPY       HY*SIN(PHI)
0E94        0C 04 89                    LODA,R0   ABUF
0E97        0D 04 8A                    LODA,R1   BBUF
0E9A        CC 04 65                    STRA,R0   TEMP
0E9D        CD 04 66                    STRA,R1   TEMP+1
0EA0        75 02                       CPSL      COM        ADD
0EA2        20                          EORZ      R0
0EA3        CC 04 7D                    STRA,R0   STEM       HZ*COS(PHI)=POS.
0EA6        3F 09 98                    BSTA,UN   SADD
0EA9        0C 04 77                    LODA,R0   RSLT
0EAC        0D 04 78                    LODA,R1   RSLT+1
0EAF        CC 04 7B                    STRA,R0   OPR2
0EB2        CD 04 7C                    STRA,R1   OPR2+1
0EB5        77 02                       PPSL      COM
0EB7        17                          RETC,UN
```

```
LINE  ADDR  LABL  B1 B2 B3 B4 ERROR SOURCE

 956                                        ****************************************************
 957                                        *  S.R. TO CORRECT NONORTHOGONALITY ERRORS IN HX *
 958                                        *   ENTER ONCE EACH SAMPLE CORRECTING HX SAMPLE  *
 959                                        *        HX=HX(MEAS) + HY(MEAS)*SIN(ERROR)       *
 960                                        *   LOCATE SIN(ERROR) IN SINE                    *
 961                                        *   USES "SMPY" TO FORM PRODUCT & "SADD" TO SUM  *
 962                                        *   EXIT WITH MODIFIED HX IN DATM,DATM+1         *
 963                                        ****************************************************
 964  0EB8  0EB8  75 01                     ORTH   CPSL      C
 965  0EBA        0C 04 5C                         LODA,R0   DATM+2     HY MSB
 966  0EBD        0D 04 5D                         LODA,R1   DATM+3     HY LSB
 967  0EC0        0E 07 1E                         LODA,R2   SINE       SIN(ERROR)
 968  0EC3        C3                               STRZ      R3
 969  0EC4        44 7F                            ANDI,R0   H'7F'      STRIP SIGN
 970  0EC6        47 80                            ANDI,R3   H'80'      SAVE  SIGN
 971  0EC8        CC 04 7B                         STRA,R0   OPR2
 972  0ECB        CD 04 7C                         STRA,R1   OPR2+1
 973  0ECE        CE 04 7A                         STRA,R2   OPR1+1
 974  0ED1        CF 04 7E                         STRA,R3   SRES       SIGN OF HY*SIN(ERR)
 975  0ED4        3F 08 66                         BSTA,UN   SMPY       FORM PROD.
 976  0ED7        0C 04 5A                         LODA,R0   DATM       HX MSB
 977  0EDA        0D 04 5B                         LODA,R1   DATM+1     HX LSB
 978  0EDD        C2                               STRZ      R2
 979  0EDE        44 7F                            ANDI,R0   H'7F'
 980  0EE0        46 80                            ANDI,R2   H'80'
 981  0EE2        CC 04 65                         STRA,R0   TEMP
 982  0EE5        CD 04 66                         STRA,R1   TEMP+1
 983  0EE8        CE 04 70                         STRA,R2   STEM
 984  0EEB        75 02                            CPSL      COM
 985  0EED        3F 09 98                         BSTA,UN   SADD       FORM SUM
 986  0EF0        0C 04 77                         LODA,R0   RSLT
 987  0EF3        0D 04 78                         LODA,R1   RSLT+1
 988  0EF6        CC 04 5A                         STRA,R0   DATM       MODIFIED HX
 989  0EF9        CD 04 5B                         STRA,R1   DATM+1
 990  0EFC        77 02                            PPSL      COM
 991  0EFE        17                               RETC,UN
 992                                        ****************************************************
 993                                               END


TOTAL ASSEMBLER ERRORS =     0
```

APPENDIX C

The transcendental functions used throughout the heading computation algorithm were implemented using a table look up procedure. To generate the respective look up tables in computer memory data was first generated using algol programs. This technique expedited modifications to tabular data and provided output data in a convenient (hexadecimal) format.

Programs that calculated Cos (Θ) and Cos^2 (Θ) to eight bit and sixteen bit resolution respectively are included.

PAGE 001

```
00000 HPAL,L,"RP"
00000 BEGIN
00001 &*****************************************************;
00001 &    A PROGRAM TO GENERATE A COS*COS TABLE FOR A      *
00001 &       MICROPROCESSOR BASED SYSTEM                   ;
00001 &   ADDRESS, ANGLE , COS(ANGLE), AND DATA IN          .
00001 &       BOTH BINARY AND HEX FORMAT IS TABULATED       ;
00001 &*****************************************************;
00001 INTEGER A,B,C,D,E,F;
00010 REAL THETA,STHETA,AR,BSTH;
00020 REAL ARRAY AN(0:256,0:15);
21070 INTEGER ARRAY VAL[0:15]:="0","1","2","3","4","5",
              "6","7","8","9","A",
              "B","C","D","E","F";
21114 INTEGER ARRAY MULT[0:3]:=8,4,2,1;
21124 INTEGER ARRAY HEX[0:256,0:3];
23136 WRITE (6,#(1H));
23175 WRITE (6,#(//,9X,"A",5X,"THETA",4X,"COS*COS",5X,
              "BINARY",14X,"HEX",//));
23242 WRITE (6,#(5X,"(ADDR.)",3X,"(DEG)",18X," DATA ",//));
23276 FOR A:= 45 TO 90 DO
23304      BEGIN
23304      AR:=A;
23310      THETA:= AR*PI/180;
23316      STHETA:=((COS(THETA))^2);
23330      B :=0;
23332      BSTH:=STHETA;
23336      WHILE B<17 DO
23341        BEGIN
23342        BSTH:= 2*BSTH;
23350       IF BSTH>1 THEN
23355          BEGIN
23355         AN(A,B]:=1;
23367          BSTH :=BSTH-1;
23375         END ELSE  AN[A,B]:=0;
23435       B:=B+1;
23440       END;
23441       D:=0;
23443       FOR C :=0 TO 3 DO
23451          BEGIN
23451          D :=4*C;
23455         F:=0;
23457         FOR E:=0 TO 3 DO
23465           BEGIN
23465           F:=F+MULT[E]*AN[A,D+E];
23520           HEX[A,C]:= VAL[F];
23533         END;
23537         END;
23543      THETA:= THETA*180/PI;
23553     WRITE (6,#(5X,I5,2(3X,F8.6),3X,16I1 ,5X,4A2),A,
             THETA,STHETA,  FOR B:= 0 TO 15 DO
             AN[A,B], FOR D:= 0 TO 3 DO HEX[A,D]);
23653     END;
23657 END$
```

PROGRAM= 023663 ERRORS=000

A (ADDR.)	THETA (DEG)	COS*COS	BINARY DATA	HEX
45	45.00000	.500000	0111111111111111	7 F F F
46	46.00000	.482550	0111101110001000	7 8 8 8
47	47.00000	.465122	0111011100010010	7 7 1 2
48	48.00000	.447736	0111001010011110	7 2 9 E
49	48.99999	.430413	0110111000101111	6 E 2 F
50	50.00000	.413176	0110100111000101	6 9 C 5
51	51.00000	.396044	0110010101100011	6 5 6 3
52	52.00001	.379039	0110000100001000	6 1 0 8
53	53.00000	.362181	0101110010110111	5 C 8 7
54	54.00000	.345491	0101100001110010	5 8 7 2
55	55.00000	.328990	0101010000111000	5 4 3 8
56	56.00000	.312697	0101000000001100	5 0 0 C
57	57.00000	.296632	0100101111110000	4 B F 0
58	58.00000	.280814	0100011111100011	4 7 E 3
59	58.99999	.265264	0100001111101000	4 3 E 8
60	60.00001	.250000	0011111111111111	3 F F F
61	61.00000	.235040	0011110000101011	3 C 2 B
62	62.00000	.220403	0011100001101100	3 8 6 C
63	63.00000	.206107	0011010011000011	3 4 C 3
64	64.00000	.192169	0011000100110010	3 1 3 2
65	65.00000	.178606	0010110110111001	2 D B 9
66	66.00000	.165435	0010101001011001	2 A 5 9
67	66.99998	.152671	0010011100010101	2 7 1 5
68	68.00000	.140330	0010001111101100	2 3 E C
69	69.00000	.128427	0010000011100000	2 0 E 0
70	70.00000	.116978	0001110111110010	1 D F 2
71	71.00000	.105995	0001101100100010	1 B 2 2
72	72.00000	.095491	0001100001110010	1 8 7 2
73	73.00000	.085481	0001010111100010	1 5 E 2
74	73.99998	.075476	0001001101110011	1 3 7 3
75	75.00000	.066987	0001000100100110	1 1 2 6
76	76.00000	.058526	0000111011111011	0 E F B
77	77.00002	.050603	0000110011110100	0 C F 4
78	78.00000	.043227	0000101100010000	0 B 1 0
79	79.00000	.036408	0000100101010010	0 9 5 2
80	80.00000	.030154	0000011110111000	0 7 B 8
81	81.00000	.024472	0000011001000011	0 6 4 3
82	82.00000	.019369	0000010011110101	0 4 F 5
83	83.00000	.014852	0000001111001101	0 3 C D
84	84.00002	.010926	0000001011001100	0 2 C C
85	84.99998	.007596	0000000111110001	0 1 F 1
86	86.00000	.004866	0000000100111110	0 1 3 E
87	87.00000	.002739	0000000010110011	0 0 B 3
88	88.00000	.001218	0000000001001111	0 0 4 F
89	89.00000	.000305	0000000000010011	0 0 1 3
90	90.00000	.000000	0000000000000000	0 0 0 0

PAGE 001

```
00000 HPAL,L,"RP"
00000 HFGIN
00001 &*************************************************;
00001 &   A PROGRAM TO GENERATE A COS TABLE FOR A       *
00001 &      MICROPROCESSOR HASED SYSTEM                ;
00001 &  ADDRESS, ANGLE , COS(ANGLE), AND DATA IN       ;
00001 &      BOTH HINARY AND HEX FORMAT IS TABULATFD    ;
00001 &*************************************************;
00001 INTFGER A,B,C,D,E,F;
00010 RFAL THETA,STHETA,AR,BSTH;
00020 RFAL ARRAY AN[0'256,0:16];
21070 INTFGER ARRAY VAL[0:15]:="0","1","2","3","4","5",
21102          "6","7","8","9","A",
21107          "B","C","D","E","F";
21114 INTFGER ARRAY MULT[0:3]:=8,4,2,1;
21124 INTFGFR ARRAY HEX[0:256,0:3];
23136 WRITE (6,#(1H));
23175 WRITE (6,#(//,9X,"A",5X,"THETA",4X,"COS(THETA)",2X, "BINARY",6X,"HEX",
23240          /));
23243 WRITE (6,#(5X,"(ADDR.)",3X,"(DEG)",18X," DATA ",//));
23277 FOR A = 45 TO 90 DO
23305     BEGIN
23305     AR:=A;
23311     THETA:= AR*PI/180;
23317     STHETA:= COS(THETA);
23323     B:=0;
23325     BSTH:=STHETA;
23331     WHILE B<9  DO
23334       BEGIN
23335       BSTH:= 2*BSTH;
23343       IF BSTH>1 THEN
23350         BEGIN
23350         AN[A,B]:=1;
23362         BSTH:=BSTH-1;
23370         END ELSE  AN[A,B]:=0;
23403       B:=B+1;
23406       END;
23407       D:=0;
23411       FOR C:=0 TO 3 DO
23417         BEGIN
23417         D:=4*C;
23450         F:=0;
23452         FOR E:=0 TO 3 DO
23460           BEGIN
23460           F :=F+MULT[E]*AN[A,D+E];
23513           HEX[A,C]:= VAL[F];
23526         END;
23532         END;
23536      THETA = THETA*180/PI;
23546     WRITE (6,#(5X,I5,2(3X,F8.6),3X,8F1.0,5X,2A2),A,THETA,STHETA,
23605          FOR B:=0 TO 7 DO AN[A,B],FOR D:=0 TO 1 DO HEX[A,D]);
23646     END;
23652 END;
```

PROGRAM= 023656 ERRORS=000

A (ADDR.)	THETA (DEG)	COS(THETA)	BINARY DATA	HEX
45	45.00000	.707107	1.11.1.1	8 5
46	46.00000	.694659	1.11...1	8 1
47	47.00000	.681998	1.1.111.	A E
48	48.00000	.669131	1.1.1.11	A B
49	48.99999	.656059	1.1..111	A 7
50	50.00000	.642788	1.1..1..	A 4
51	51.00000	.629320	1.1....1	A 1
52	52.00001	.615662	1..111.1	9 D
53	53.00000	.601815	1..11.1.	9 A
54	54.00000	.587785	1..1.11.	9 6
55	55.00000	.573576	1..1..1.	9 2
56	56.00000	.559193	1...1111	8 F
57	57.00000	.544639	1...1.11	8 B
58	58.00000	.529919	1....111	8 7
59	58.99999	.515038	1.....11	8 3
60	60.00001	.500000	.1111111	7 F
61	61.00000	.484810	.11111..	7 C
62	62.00000	.469471	.1111...	7 8
63	63.00000	.453991	.111.1..	7 4
64	64.00000	.438371	.111....	7 0
65	65.00000	.422618	.11.11..	6 C
66	66.00000	.406737	.11.1...	6 8
67	66.99998	.390731	.11..1..	6 4
68	68.00000	.374607	.1.11111	5 F
69	69.00000	.358368	.1.11.11	5 B
70	70.00000	.342020	.1.1.111	5 7
71	71.00000	.325568	.1.1..11	5 3
72	72.00000	.309017	.1..1111	4 F
73	73.00000	.292372	.1..1.1.	4 A
74	73.99998	.275637	.1...11.	4 6
75	75.00000	.258819	.1....1.	4 2
76	76.00000	.241922	..1111.1	3 D
77	77.00002	.224951	..111..1	3 9
78	78.00000	.207912	..11.1.1	3 5
79	79.00000	.190809	..11....	3 0
80	80.00000	.173648	..1.11..	2 C
81	81.00000	.156435	..1.1...	2 8
82	82.00000	.139173	..1...11	2 3
83	83.00000	.121869	...11111	1 F
84	84.00002	.104528	...11.1.	1 A
85	84.99998	.087156	...1.11.	1 6
86	86.00000	.069757	...1...1	1 1
87	87.00000	.052336	....11.1	0 D
88	88.00000	.034900	....1...	0 8
89	89.00000	.017452	.....1..	0 4
90	90.00000	-.000000	....	0 0

BIBLIOGRAPHY

[1-1] C. C. Kalweit, "The ESRO 1 attitude measurement system," *IEEE Trans. Aerosp. Electron. Syst.*, vol. AES-7, pp. 132-141, Jan. 1971.

[1-2] G. A. Korn and T. M. Korn, *Mathematical Handbook for Scientists and Engineers*. New York: McGraw-Hill, 1961, sec. 14.10-2.

[1-3] E. V. Condon and H. Odishaw, *Handbook of Physics*, 2nd ed., 1967, ch. 2-3.

[1-4] S. H. Crandall, *Dynamics of Mechanical and Electromechanical Systems*. New York: McGraw-Hill, 1968, pp. 42-152.

[1-5] M. Kayton and W. Fried, *Avionics Navigation Systems*. New York: Wiley, 1969.

[1-6] S. Chapman and J. Bartel, *Geomagnetism*, vol. II, New York: Oxford Univ. Press, 1940.

[1-7] Vestine *et al.*, "The geomagnetic field, its description and analysis," Dept. Terrestrial Magnetism, Carnegie Inst. Technol., Pittsburgh, PA., publ. 580, ch. 2, 1947.

[1-8] E. Irving, *Paleomagnetism and Its Application to Geology and Geophysical Problems*. New York: Wiley, 1964, ch. 3.

[1-9] F. D. Stacey, *Physics of the Earth*. New York: Wiley, 1969, ch. 5.

[1-10] D. R. Hartman, D. J. Tskey, and G. L. Friedberg, "A system for digital aeromagnetic interpretation," *Geophysics*, vol. 36, pp. 891-918, Oct. 1971.

[1-11] M. L. Hill, "Introducing the electrostatic autopilot", *Astronaut. Aeronaut.*, pp. 24-31, Nov. 1972.

[1-12] R. Markson, "Practical aspects of electrostatic stabilization," *Astronaut. Aeronaut.*, pp. 44-49, Apr. 1974.

BIBLIOGRAPHY (Continued)

[2-1] R. Pietila and W. R. Dunn, Jr., "A Vector Autopilot System," *IEEE Transactions on Aerospace and Electronic Systems,"* vol. AES-12, No. 3, May, 1976.

[2-2] G. A. Korn and T. M. Korn, *Electronic Analog Computer*, McGraw-Hill, 2nd ed., 1956.

[2-3] E. A. Parrish, Jr., and Y. C. Lee, "A microcomputer preprocessor/postprocessor for analog signals," *IEEE Trans. on Industrial Electronics and Control Instrumentation,* vol. IECI-21, No. 1, Feb. 1974, pp. 38-41.

[3-1] R. Allan, "Components: Microprocessors Galore," *IEEE Spectrum,* vol. 13, no. 1, Jan. 1976, pp. 50-56.

[3-2] G. Kaplon, "Industrial Electronics to Boost Productivity," *IEEE Spectrum,* vol. 13, no. 1, Jan. 1976, pp. 87-90.

[3-3] H. Falk, "Computers: Poised for Progress", *IEEE Spectrum,* vol. 13, no. 1, Jan. 1976, pp 44-49.

[3-4] D. Christianson, "Technology '76", *IEEE Spectrum,* vol. 13, no. 1, Jan. 1976, pp 42-43.

[3-5] W. Myers, "Key Developments in Computer Technology: A Survey", *Computer, IEEE Computer Society,* vol 9, no. 11, Nov. 1976, pp 48-77.

[3-6] E. A. Terrero, "Focus on Microprocessors", *Electronic Design 7,* March 29, 1976, pp 58-64.

[3-7] R. Noyce, "From Relays to MPU's", *Computer, IEEE Computer Society,* vol. 9, no. 12, Dec. 1976, pp 26-29.

[3-8] E. R. Garren, "Applying Microprocessors and Microcomputers", *Modern Data,* Feb. 1975, pp. 54-57.

[3-9] D. N. Kaye, "How to Pick a Microprocessor, a Mini or Anything in Between", *Electronic Design 16,* Aug. 1975, pp. 26-30.

BIBLIOGRAPHY (Continued)

[3-10] T. A. Seim, "Microprocessors Aid Experimentation in Scientific Laboratory", *Computer Design*, Sept. 1976, pp. 83-89.

[3-11] M. Teener and W. Liles, "Microcomputers, Where the Action Really is", *Modern Data*, Feb. 1975, pp. 49-53.

[3-12] H. D. Scott and R. A. Smoak, "A Microcomputer Controller for a Nuclear Pool Reactor", *IEEE Trans. on Industrial Electronics and Control Instrumentation*, vol. IECI-22, no. 1, Feb. 1975, pp. 15-18.

[3-13] A. Osbourne and Associates, "*An Introduction to Microcomputers*", Adam Osbourne and Associates, Inc., Berkeley, CA. 1975.

[3-14] M. H. Lewin, "Integrated Microprocessors", *IEEE Trans. on Circuits and Systems"*, Vol. CAS-22, no. 7, July 1975, pp. 577-585.

[3-15] R. K. Jurgen, "The Microprocessor: In the Driver's Seat", *IEEE Spectrum*, vol. 12, no. 6, June 1975, pp. 73-77.

[3-16] C. Newcombe, "How to Evaluate Microprocessor Instruments", *IEEE Spectrum*, vol. 13, no. 4, April 1976, pp. 38-55.

[3-17] S. Sheikh, "A Programmable Digital Control System for Copying Machines", *IEEE Trans. on Industrial Electronics and Control Instrumentation*, vol. IECI-21, no. 1. Feb. 1974, pp. 25-33.

[3-18] D. L. Smith, "The Problem with Programmable Controllers", *IEEE Trans. on Industrial Electronics and Control Instrumentation*, vol. IECI-21, no. 2, May 1974. pp. 50-52.

[3-19] H. Falk, "Self Contained Microcomputers Ease System Implementation", *Computer, IEEE Spectrum*, vol. 11, no. 12, Dec. 1974, pp. 53-54.

[3-20] A. R. Ward, "LSI Microprocessors and Microcomputers: A Bibliography", *Computer, IEEE Computer Society*, vol. 7, no. 7, July 1974.

BIBLIOGRAPHY (Continued)

[3-21] A. R. Ward "LSI Microprocessors and Microcomputers: A Bibliography Continued", *Computer, IEEE Computer Society*, vol. 9, no. 1, Jan. 1976, pp. 42-53.

[3-22] *Signetics 2650 Microprocessor Manual*, Signetics Corporation, Sunnyvale, CA. 1975.

[3-23] A.V.Oppenheim and R.W.Schafer, *Digital Signal Processing*, Prentice Hall, N.J., 1975.

[3-24] C.E.Shannon, "Communication in the Presence of Noise", *Proc. IRE*, vol. 37, No. 1 (Jan. 1949), pp 10-21.

[3-25] *Engineering Product Handbook (A/D and D/A Converters)*, Datel Systems Incorporated, 2nd Printing. Canton, Massachusetts.

[3-26] *Analog-Digital Converter Data Sheets*, Analog Devices, Inc., Norwood, Massachusetts.

[3-27] *Analog-Digital Converter Data Sheets*, Burr-Brown Research Corp., Tucson, AZ.

[3-28] User's Guide to A/D Converters. *Electronic Products*, Dec. 1976.

[3-29] T.R.Blakeslee, *Digital Design with Standard MSI and LSI*, Wiley=Interscience Pub.,John Wiley & Sons,1975.

[3-30] J. B. Peatman, *The Design of Digital Systems*, McGraw-Hill, 1972.

[3-31] H. W. Gschwind, *Design of Digital Computers*, Springer-Verlag, N.Y., 1967.

[3-32] The Signetics 2650 Assembler Version SCU Level 1 (Signetics part number 2650 AS1000/1100) operational on the HP2100 computer at the University of Santa Clara.

[3-33] C.McGowan "Structured Programming:A Review of Some Practical Concepts",*IEEE Computer*,Vol 8,No.6,June,1975

[3-34] *Three Axis Fluxgate Magnetometer Specification*, Model 9200C. Develco, Inc., Mountain View, CA.

[3-35] *Analog to Digital Converter Specification*, Model ADC-MA12B2B. Datel Systems, Inc., Canton, Mass.

BIBLIOGRAPHY (Continued)

[3-36] Telephone conversations with Dr. Opher of Develco Inc., during summer of 1976.

[3-37] G. Dahlquist and A.Bjorck, *Numerical Methods*, Prentice Hall, 1974.

[3-38] C.V.Ramamoorthy, J.R.Goodman and K.H.Kim, "Some Properties of Iterative Square-Rooting Methods Using High Speed.

[4-1] Telephone conversation with Develco magnetometer project engineer, Ronald Warkentine, November 3, 1976.

[4-2] P.E. Gise, "A Cylindrical Thin-Film Magnetometer Sensor", PhD Thesis, University of Santa Clara, 1976.

[4-3] Telephone Conversation with Ronald Warkentine (project engineer) at Develco, November 24, 1976.

[4-4] J.A. Cadzow, *Discrete Time Systems*, Prentice-Hall, Inc., Englewood Cliffs, New Jersey, 1973.

[4-5] A.V.Oppenheim, R.W.Schafer, *Digital Signal Processing*, Prentice-Hall, Inc., Englewood Cliffs, N.J., 1975.

[4-6] S.Mason and H.J. Zimmerman, *Electronic Circuits, Signals and Systems*, John Wiley & Sons, Inc., New York, 1960.

[4-7] Model MM-8, *8 Channel Analog Multiplexer Data Sheets*, Datel Systems, Inc., Canton, Mass., 1975

[4-8] B.A.Barry, *Engineering Measurements*, J. Wiley, & Sons, Inc., N.Y., 1964.

[4-9] M.B.Stout, *Basic Electrical Measurements*, Prentice-Hall, Inc., N.J., 1960.

[4-10] Model SHM-IC-1, *Sample and Hold Integrated Circuit*, Datel Systems, Inc., Canton, Mass., 1975.

[4-11] Model ADC-MA12B1B, *Analog to Digital Converter Data Sheets*, Datel Systems, Inc., Canton, Mass., 1974.

[4-12] G.Dahlquist, *Numerical Methods*, Prentice-Hall, Inc., Englewood Cliffs, N.J., 1974.

Section III

Earth Electric Field Research -
& Field Model of Cumulonimbus Cloud

TABLE OF CONTENTS

I. INTRODUCTION

The fact that the Earth has a surrounding electric field has been known for centuries, but the study of the effect of clouds on this electric field is a fairly new area of study. Ideally the earth's electric field is a perfect vertical, however since clouds are not electrically neutral, their presence distorts the earth's field; nearly neutral clouds causing slight perturbations while heavily charged clouds actually reverse the direction of the resultant field. The most highly charged clouds belong to the cumulonimbus family.

The report evaluates various electrical models of cumulonimbus clouds. The resultant field of each model is compared with actual readings of the earth's electric field in the presence of a cumulonimbus cloud at various heights and distances from the cloud. Using the actual field readings, this report will develop a new electrical model of a cumulonimbus cloud.

This paper also reviews the electrical properties of the atmosphere, particularly of clouds and suggests some possible uses of the knowledge of the field around a cumulonimbus cloud.

II. ATMOSPHERIC ELECTRICITY

Atmospheric electricity is defined by Dolezalek [1] as "the science of everything electric in the atmosphere between the solid and liquid surface of the earth to the lower regions of the ionosphere, including the boundary layers of both."

Like every science, atmospheric electricity has its own sign conventions. Distance is measured positively upward. Current flow to the earth is considered positive. Electric potential is measured relative to earth. The terms "field" and "potential gradient" are in general used to denote the same quantity, i.e. the partial derivative of voltage with respect to height. The units used are the MKSA system.

All lines of force commence on a positive charge and end on a negative charge. The density of lines of force across any area gives a measure of the field. If the line of force terminates on the earth's surface, it must enter vertically. Any change in space charge will immediately effect the lines of force and thus, the electric field.

As space charge appears, a potential gradient is produced immediately at the ground. The air-earth current will change as will the lines of force. To determine the potential gradient change produced due to the appearance of the space charge, one must know the relaxation time, ε/λ, of the air where ε is the permittivity of the air and λ is the conductivity. Near the earth's surface the relaxation time generally ranges between 5 to 40 minutes depending to a great extent on the pollution level. The higher the pollution level, the lower the conductivity and, therefore, the higher the relaxation time. At an altitude of 18km the relaxation time is about 4 seconds while at 70km it is on the order of 10^{-8} seconds. At the earth's surface it is 10^{-6} seconds or less. The potential gradient at some time after a change in space charge can be given by the equation [2]

$$E = E_1 e^{-t/\tau} + E_2 (1 - e^{-t/\tau}) \tag{1}$$

where E_1 is the potential gradient immediately after the change, E_2 is the potential gradient when the conditions are again quasistatic, τ is the relaxation time and E is the potential gradient in the intervening time.

Ions are relatively rare when compared to the total number of molecules in the atmosphere. A cubic meter of clean land air will contain approximately 800 million ions out of 10^{25} molecules. The conductivity of the atmosphere may be written as [1]

$$\lambda = \Sigma n_i^+ e_i^+ k_i^+ + \Sigma n_j^- e_j^- k_j^- \tag{2}$$

where n_i^+ is the number of positive ions with a charge of e_i^+ and a mobility of k_i^+, n_j^- is the number of negative ions with a charge of e_j^- and a mobility of k_j^-, and λ is the conductivity. The mobility is computed from the potential gradient E and the velocity of the particle v by

$$k = v / E \tag{3}$$

or the velocity acquired in a potential gradient of 1 volt/meter. The mobility is highly dependent on physical properties of the ion such as size and shape.

Since the air-earth current is continually bringing positive charges to the earth there must be some restoring component which will complete the circuit carrying the positive charges upward again. The most popular theory on the generation and continuation of the electrical characteristics of the atmosphere is the condenser theory. [1,3] In this theory the ionosphere is positively charged with respect to the earth. The air-earth current tends to continually discharge this global condenser. However, this process is compensated by thunderstorms which act as the generator restoring positive charge to the ionosphere. Figure 1 shows the schematic of this global circuit. The lower portion of a thunderstorm is negatively charged while the upper portion is positive. The world wide occurrence of thunderstorms also corresponds to the diurnal variation of the earth's electric field.

The study of atmospheric electricity is divided into two quite different divisions, fair weather and disturbed weather. Disturbed weather is defined by Dolezak as "when we have hydrometers in the atmosphere - fog, rain, snow - or when we have high winds, in particular in

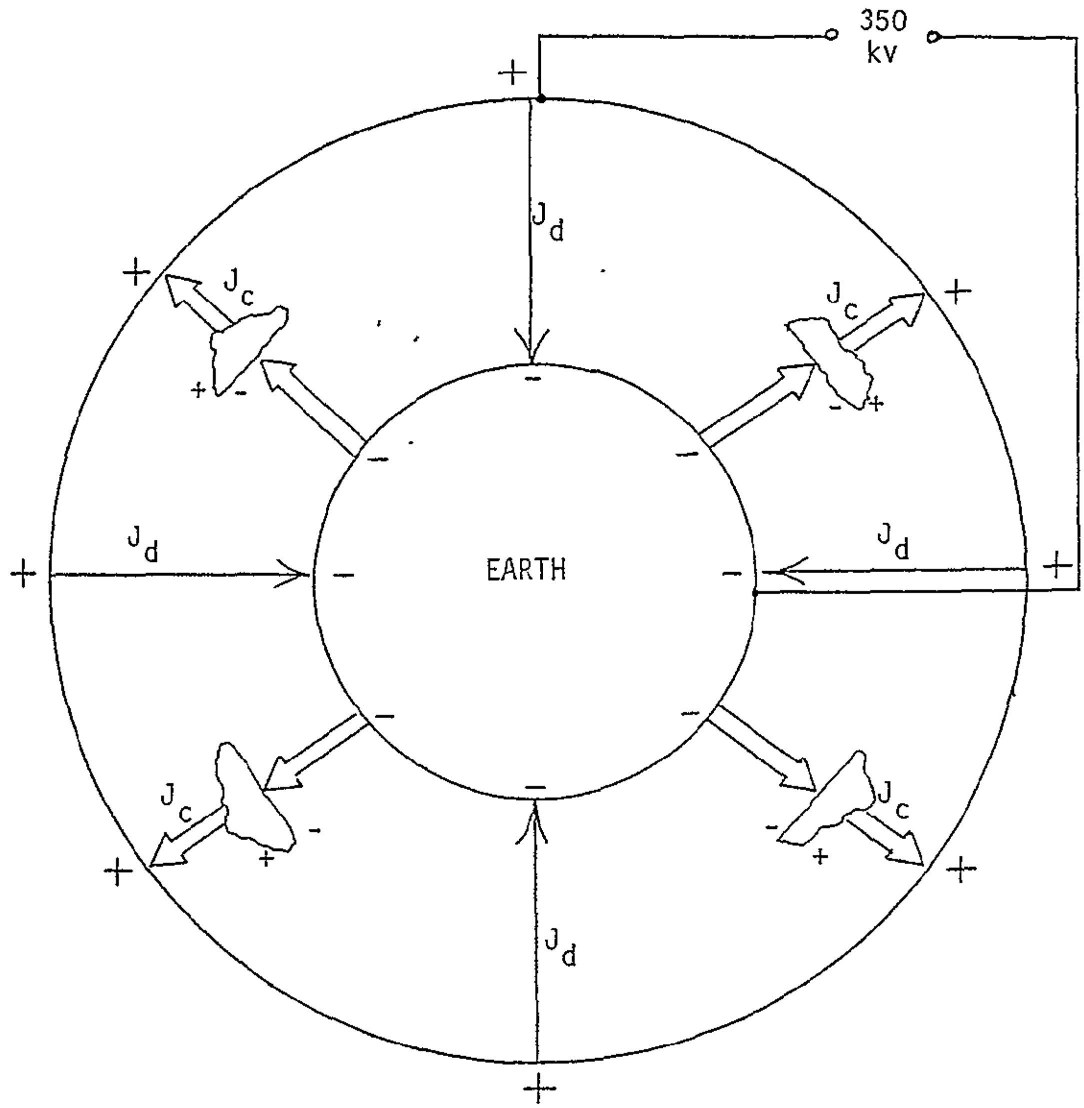

J_d Discharging Currents

J_c Charging Currents

Figure 1

(from IEEE Spectrum [3])

connection with blown-up dust or snow, or when we have much of the sky covered by substantial clouds." [1] The absence of these phenomena is considered fair weather. Fair weather conditions are predictable and one can assume a quasistatic state to determine its properties, while disturbed weather conditons can alter rapidly and a quasistatic state cannot be applied.

Fair weather conditions have several characteristic quantities. Voltage increases with height. The potential gradient is positive and essentially vertical. It is constant for the first few meters and shows a progressive decrease with height at approximately 100 meters. The conductivities are also constant for the first few meters, then show a marked increase with height at approximately 100 meters due to an increase with altitude of ionization by cosmic rays and a decrease in pollution. The current density is the same at all levels and is equal to the voltage of the ionosphere with respect to earth divided by the resistance of a $1m^2$ column of air from the earth to the ionosphere. Tables 1 and 2 list fair weather parameters as compiled by Dolezelek. [1]

The disturbed weather phenomena is much harder to typify. The potential gradient can have horizontal variations of large magnitude. There are added currents carried by precipitation and lightning. Constant changes in conductivity occur due to fresh charges. It is in this still unsolved phenomena that much of the current work is being performed.

Part of Atmosphere for which the Values are Calculated	Currents, I, in A; and current densities, i, in A/m^2	Potential Differences, U, in V; field strength E in V/m	Resistances, R, in Ω; Columnar res., R_c, in Ωm^2 Resistivities, ρ, in Ωm
Volume element at about sea level, one cubic meter	$i=3x10^{-12}$	$E_o=1.2x10^2$	$\rho_o=4x10^{13}$
Lower column of 1 m^2 cross section - sea-level to 2 km	same as above	at upper end: $U_1=1.8x10^5$	$R_{c1}=6x10^{16}$
Volume element at about 2 km height, 1 m^3	same as above	$E_2=6.6x10^1$	$\rho_2=2.2x10^{13}$
Center column of 1 m^2 cross section - 2 to 12 km	same as above	at upper end: $U_m=3.15x10^5$.	$R_{cm}=4.5x10^{16}$
Volume element at about 12 km height, 1 m^3	same as above	$E_{12}=4.2x10^0$	$\rho_{12}=1.3x10^{12}$
Upper column of 1 m^2 cross section - 12 to 65 km	same as above	at upper end: $U_u=3.5x10^5$	$R_{cu}=1.5x10^{16}$
Whole column of 1 m^2 cross section - 0 to 65 km	same as above	at upper end: $U=3.5x10^5$	$R_c=1.2x10^{17}$
Total spherical capacitor area: $5x10^{14}$ m^2	$I=1.5x10^3$	$U = 3.5x10^5$	$R=2.4x10^2$

Table 1

Part of Atmosphere for which the Values are Calculated	Conductances, G, in Ω^{-1}; Col. conductances G_c, in $\Omega^{-1}m^{-2}$; total cond. Λ, in $\Omega^{-1}m^{-1}$	Capacitances, C, in F; Col. capacitances C_c, in Fm^{-2}; Capacitivities ε, in Fm^{-1}	Relaxation Times τ, in seconds
Volume element at about sea level, one cubic meter	$\Lambda_o=2.5x10^{-14}$	$\varepsilon_o=8.9x10^{-12}$	$\tau_o=3.6x10^2$
Lower column of 1 m^2 cross section - sea level to 2 km	$G_{c1}=1.7x10^{-17}$	$C_{c1}=4.4x10^{-15}$	$\tau_{c1}=2.6x10^2$
Volume element at about 2 km height, 1 m^3	$\Lambda_2=4.5x10^{-14}$	$\varepsilon_2=8.9x10^{-12}$	$\tau_2=2x10^2$
Center column of 1 m^2 cross section - 2 to 12 km	$G_{cm}=5x10^{-17}$	$C_{cm}=8.8x10^{-16}$	$\tau_{cm}=1.8x10^1$
Volume element at about 12 km height, 1 m^3	$\Lambda_{12}=4.0x10^{-13}$	$\varepsilon_{12}=8.9x10^{-12}$	$\tau_{12}=1.2x10^1$
Upper column of 1 m^2 cross section - 12 to 65 km	$G_{cu}=2.5x10^{-17}$	$C_{cu}=1.67x10^{-16}$	$\tau_{cu}=6.7x10^0$
Whole column of 1 m^2 cross section - 0 to 65 km	$G_c=8.3x10^{-18}$	$C_c=1.36x10^{-16}$	$\tau_c=1.64x10^1$
Total spherical capacitor area: $5x10^{14}$ m^2	$G=4.2x10^{-3}$	$C=6.8x10^{-2}$	$\tau=1.64x10^1$

Table 2

III. METEOROLOGY

The nomenclature for the various sections of the atmosphere are not agreed upon by all who study the atmosphere, however the divisions and their names as used by Dobson [4] are shown in Figure 2.

The lowest cloud in the troposphere is known as fog. This occurs when the ground is within a few degrees of the dew point. Fog can be produced three ways. Radiation fog is created on clear nights if the earth cools greatly since without a cloud cover the heat radiates into the upper atmosphere. A slight breeze will then bring the earth to the dew point. Advection fog is caused by warm moist air blowing over a colder surface and becoming chilled to its dew point. Frontal fog may be produced when cold air mixes with warm moist air. Other cloud types are summarized in Table 3.

The cloud names come from four basic words: cirrus, cumulus, stratus and nimbus. Cirrus clouds are composed of ice crystals and are delicate and curly in appearance. Sun shines through them without a shadow. Cumulus clouds are lumpy or billowing forms. The sheetlike cloud layers are stratus clouds. Nimbus clouds are stratus or cumulus that develop a "head" or thickness. "Alto" is also used as a prefix to indicate clouds at intermediate heights.

When two air masses of differing temperatures, pressures and relative humidities mix, a front is formed. The colder air mass sits

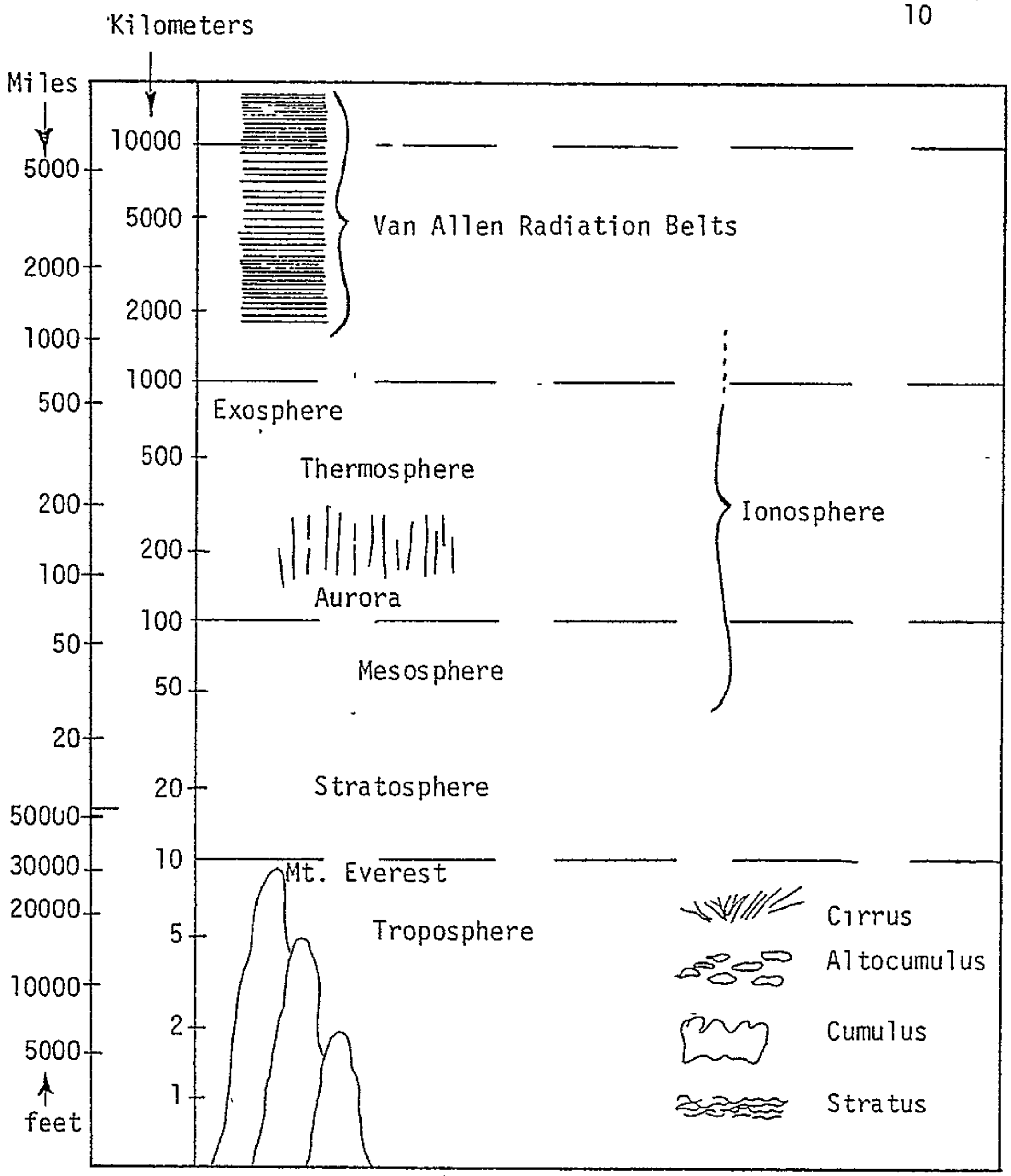
Kilometers
Miles
10000
5000
5000
2000
2000
1000
1000
500
Van Allen Radiation Belts
Exosphere
500
Thermosphere
200
Ionosphere
200
100
Aurora
100
50
Mesosphere
50
20
Stratosphere
20
50000
30000
10
Mt. Everest
20000
5
Troposphere
Cirrus
Altocumulus
10000
2
Cumulus
5000
1
Stratus
feet

Figure 2

CLOUD NAME	AVERAGE HEIGHT AND RANGE IN HEIGHT
	High Clouds
Cirrus	30,000 ft. (10,000 to 50,000 ft.)
Cirro-cumulus	20,000 ft. (8,000 to 36,000 ft.)
Cirro-stratus	35,000 ft. (15,000 to 45,000 ft.)
	Middle Clouds
Alto-cumulus	12,000 ft. (3,000 to 27,000 ft.)
Alto-stratus	15,000 ft. (5,000 to 35,000 ft.)
	Low Clouds
Strato-cumulus	5,000 ft. (1,000 to 15,000 ft.)
Stratus	2,000 ft. (50 to 6,000 ft.)
Nimbo-stratus	2,500 ft. (200 to 18,000 ft.)
	Clouds with Vertical Development
Cumulus	2,500 ft. (1,000 to 10,000 ft.) Tops may extend to 20,000 ft.
Cumulo-nimbus	2,500 ft. (500 to 10,000 ft.) Tops may extend to over 35,000 ft.

Table 3

(from Aerology for Pilots [5])

wedgelike under the warmer air mass. The air that is displacing another air mass gives its name to the front; thus, if cold air is displacing warm air it is known as a cold front. Likewise, in a warm front warm air displaces the colder air. An occluded front exists when two colder air masses trap a third air mass between them forcing the third air mass aloft until it dissipates. Figure 3 shows cross sections of the warm and cold types of fronts and the clouds associated with them.

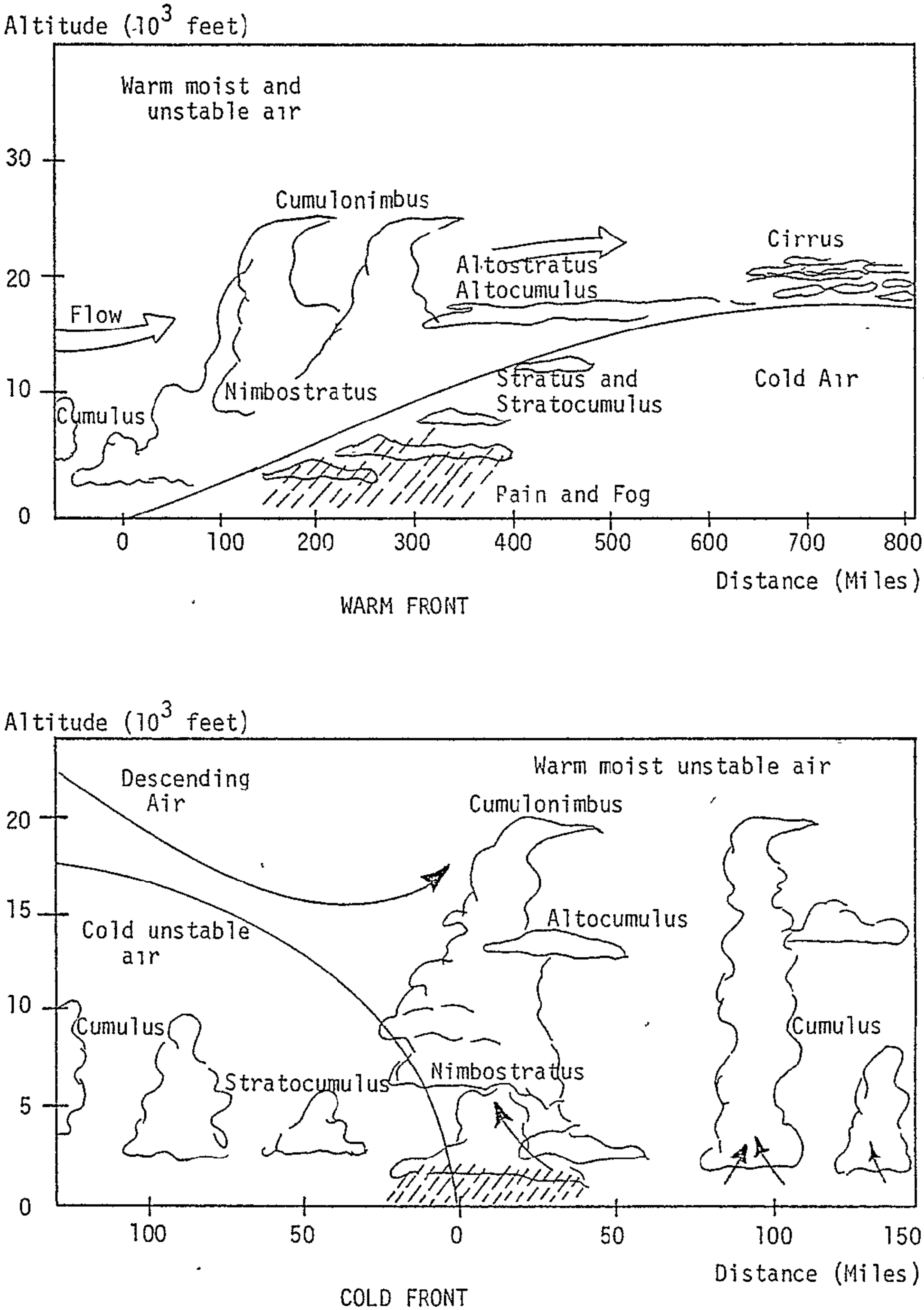

Figure 3

(from Introduction to Aviation [6])

IV. EXISTING MODELS

The cumulonimbus cloud differs from other types of clouds in its rate of accumulation of charge. A collection of charges, such as a cloud, in a conductive medium will attract an equal but oppositely charged screening layer and, therefore, cause no appreciable change in the electric field. However, since the rate of increase of charge in a cumulonimbus cloud within the time constant of the surrounding atmosphere approximately doubles the amount of charge [7], an effective screening layer can not be generated and, therefore, the cloud effects the neighboring electric field. Models of cumulonimbus clouds can eliminate the screening layer and simply use the net increase in charge as the only charge present.

Experimentors have been attempting for years to gather data on the electric field in the vicinity of a thundercloud, i.e. a cumulonimbus cloud, in order to generate a valid electrical model for the cloud. The measurements were originally made at ground level but more recently include airborne measurements in, around and above thunderclouds.

In 1948 O.H. Gish and G.R. Wait [8], in an effort to show that thunderclouds could supply the negative current flow necessary to maintain the general electrification of the earth, gathered measurements of the electric field strength above thunderstorms. Their findings were as follows: Of 87 traverses across thunderstorms, in 22 data was incomplete or unsatisfactory, 31 profiles corresponded well to a bipolar model while the remaining 34 were of a more complicated nature where a bipolar model was only a good first approximation, additional dipoles would be required for an accurate model.

A model was proposed using the data gathered on a flight an an altitude of 43,000 feet on October 28, 1948. This data was typical of a storm when little lightning activity was present. The data and associated model are shown in Figure 4. A complete mapping of the electric field in an area 21km in horizontal distance from the cloud's charge concentrations and to a height of 16km is shown in Figure 5.

Israel [9] lists two other proposed electrical models for a thundercloud, one from Simpson and Robinson and the other from D.J. Malan. The model proposed by Simpson and Robinson is often referred to as the "Classical Model." It consists of a positive charge of 24 coulombs at a height of 6km, a charge of -20 coulombs at 3km and a charge of 4 coulombs at 1.5 km. The Malan model has a charge of 40 coulombs at approximately 10km, -40 coulombs at about 5km and 10 coulombs at about 2km. The electric field map for the Simpson and Robinson model is shown in Figure 6 and for the Malan model in Figure 7.

The program used to generate the data used in Figures 5, 6 and 7 and the data listings from the program are contained in Appendix A. The charge system for each of the three models used as inputs to the program are shown in Figure 10, utilizing the method of electrical images as described in the next section.

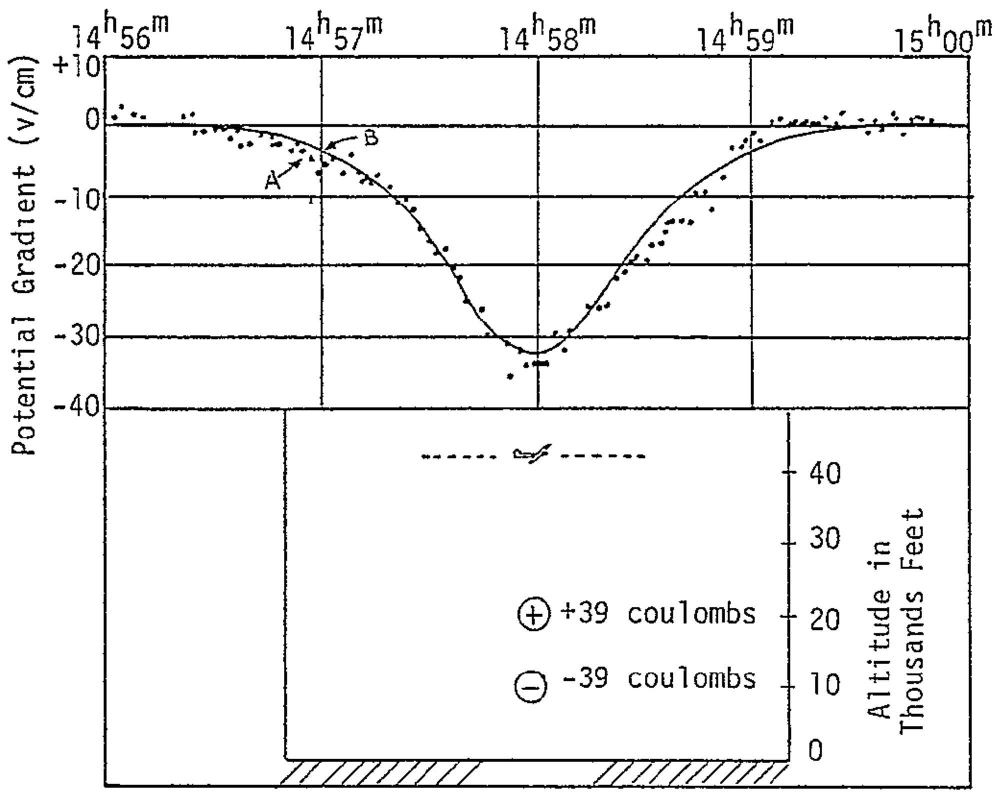

POTENTIAL GRADIENT (VERTICAL COMPONENT) OVER THUNDERSTORM, OCTOBER 28, 1948, STORM NO. 1, TRAVERSE NO. 8, (A) OBSERVED, (B) CALCULATED FOR MODEL SHOWN

Figure 4

(from Gish and Wait [8])

Scale: 1 In. = 4000 v/m

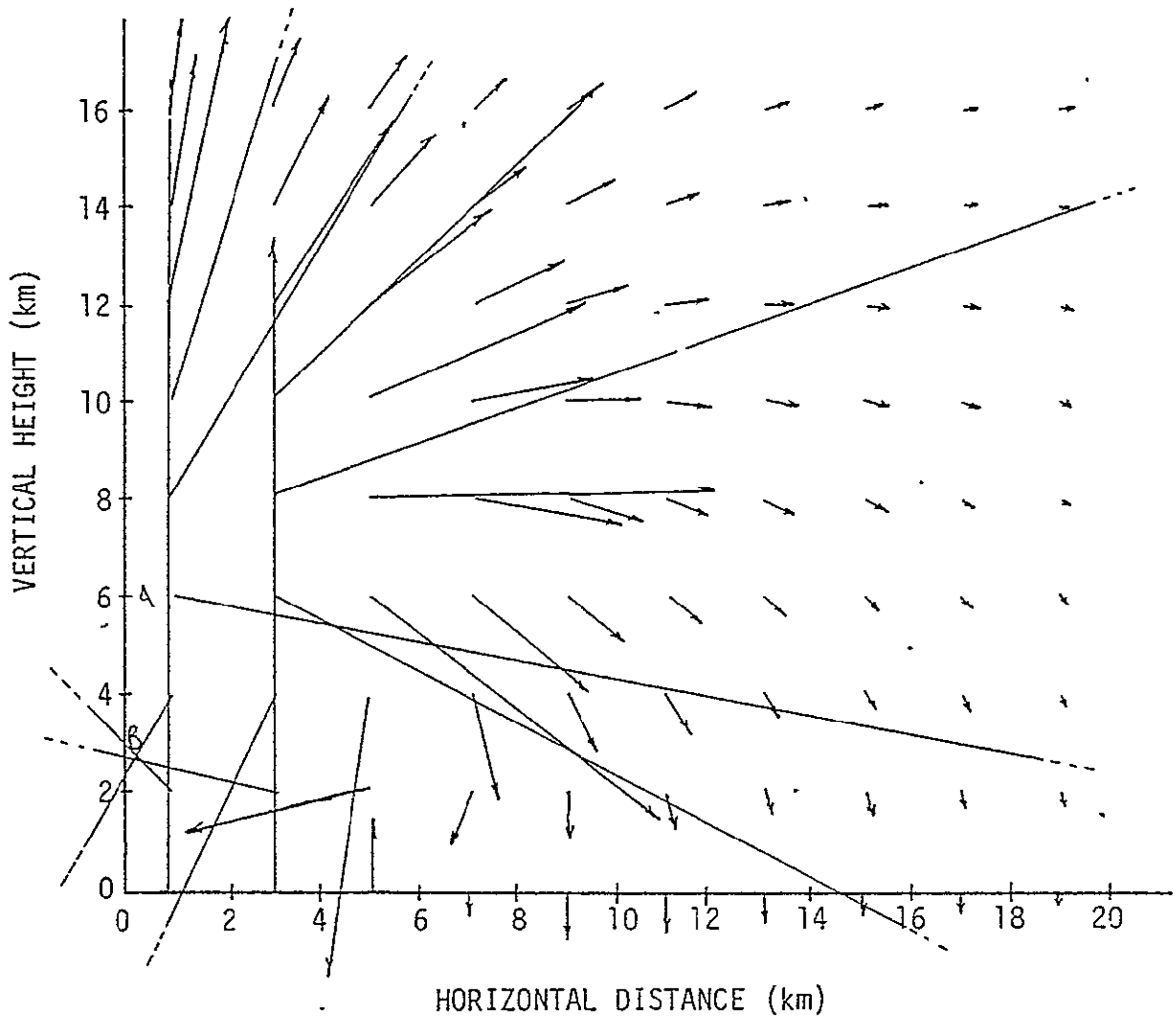

A = 39 coulombs
B = -39 coulombs

ELECTRIC FIELD MAP FOR
GISH AND WAIT MODEL

Figure 5

Scale: 1 in. = 4000 v/m

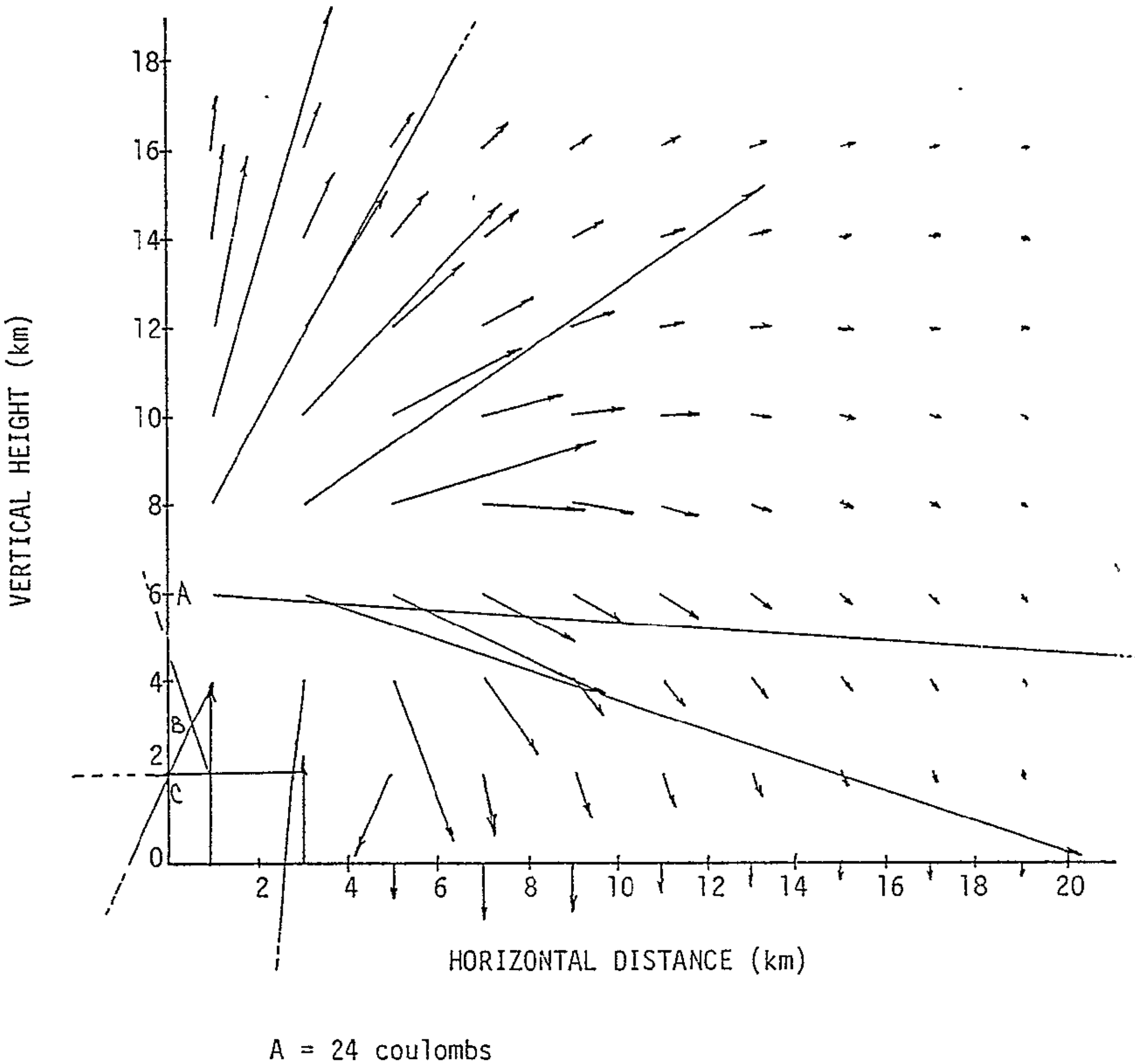

A = 24 coulombs
B =-20 coulombs
C = 4 coulombs

ELECTRIC FIELD MAP FOR

SIMPSON AND ROBINSON MODEL

Figure 6

Scale: 1 In. = 4000 v/m

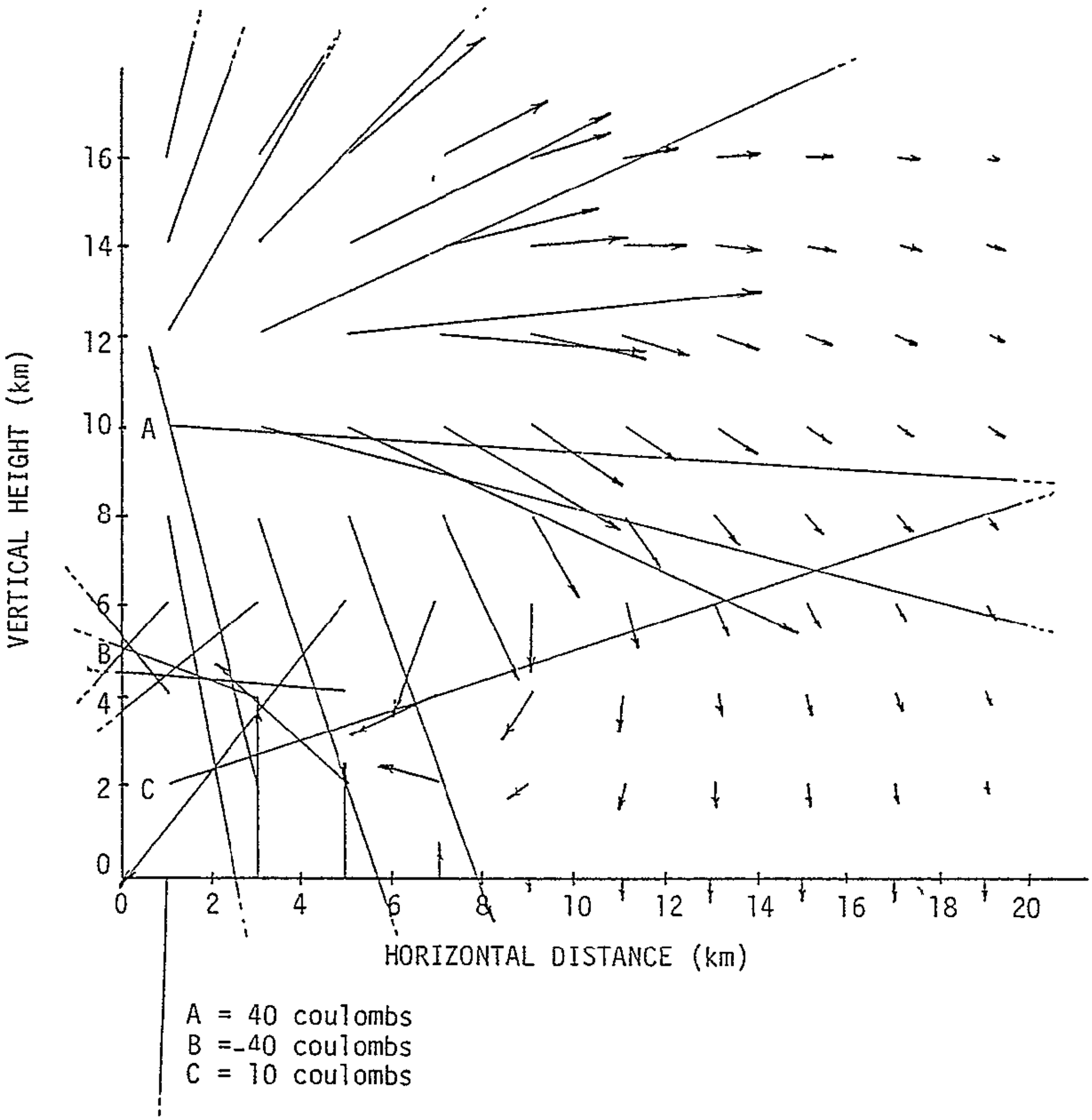

A = 40 coulombs
B =-40 coulombs
C = 10 coulombs

ELECTRIC FIELD MAP FOR
MALAN MODEL

Figure 7

a-3

V. GENERAL NEAR-FIELD MODEL

The field at any point in space due to a single point charge Q can be computed from Guass's law,

$$\oint \vec{D} \cdot d\vec{s} = \int_{v} \zeta \, dV \qquad (4)$$

where $\vec{D}$ is the electric flux density, V is the volume enclosed by the surface S and ζ is the charge density within V. If one considers S to be a spherical surface with its center at Q (Q being the only charge within S), the equation becomes

$$\vec{D} = (Q \,/\, 4\pi r^2)\ \vec{r} \qquad (5)$$

Since $\vec{D} = \varepsilon\vec{E}$ where ε is the permittivity of the substance then

$$\vec{E} = (Q \,/\, 4\pi r^2 \varepsilon)\ \vec{r} \qquad (6)$$

The direction of $\vec{E}$ is radially outward if Q is positive and radially inward if Q is negative. See Figure 8 where Q is a positive charge. The magnitude of E is inversely proportional to the square of the distance to Q. If the permittivity is constant over all space concerned, the field created at a point P due to more than a single point charge may be computed by the vector addition

$$\vec{E} = \frac{1}{4\pi\varepsilon}\left(\frac{Q_1}{r_{1P}^2}\,\vec{r}_{1P} + \frac{Q_2}{r_{2P}^2}\,\vec{r}_{2P} + \dots + \frac{Q_N}{r_{NP}^2}\,\vec{r}_{NP}\right) \qquad (7)$$

where Q_J is the charge located at a point J and r_{JP} is the distance between Q_J and P. The permittivity used for this problem is that of free space, i.e. 8.854×10^{-12} farads per meter.

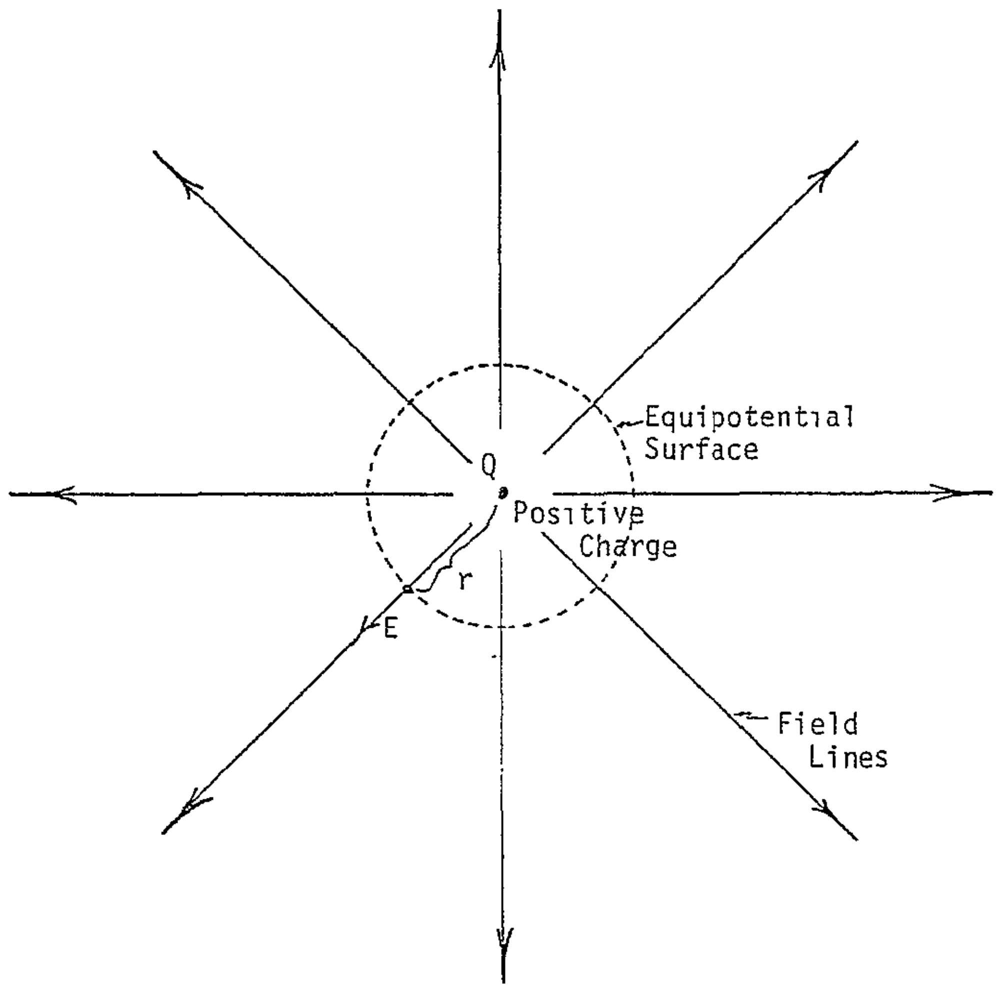

Figure 8

The earth, here considered flat over the area under consideration is an equipotential. To produce an equipotential surface one can use the method of electrical images, where an imaginary distribution of charges inside a conducting body of an electrostatic system is determined which would produce exactly the same field outside the body as that produced by the induced free charges over its surface. For the system of a conducting plane, one can look at a simplified problem of a single positive charge located above the plane. See Figure 9. As shown in the figure, an equal but oppositely charged point is placed an equal distance below the plane as the positive charge is above the plane. Now if the plane is removed, the field above the plane would remain unchanged. Therefore, the field produced by all the charges induced on the conducting plane may be reduced to the field produced by the single point, -Q. This method can be expanded to include an oppositely charged point below the plane for each charged point above the plane in a more complex system. The systems suggested as thundercloud electrical models by Simpson and Robinson, Gish and Wait, and Malan are shown in Figure 10 using the method of electrical images.

Each of these models was derived using the data collected by the particular experimentor under a particular set of conditions. The models fit the individual data, yet they vary considerably in the overall field maps as shown in Figures 5, 6 and 7. For example,

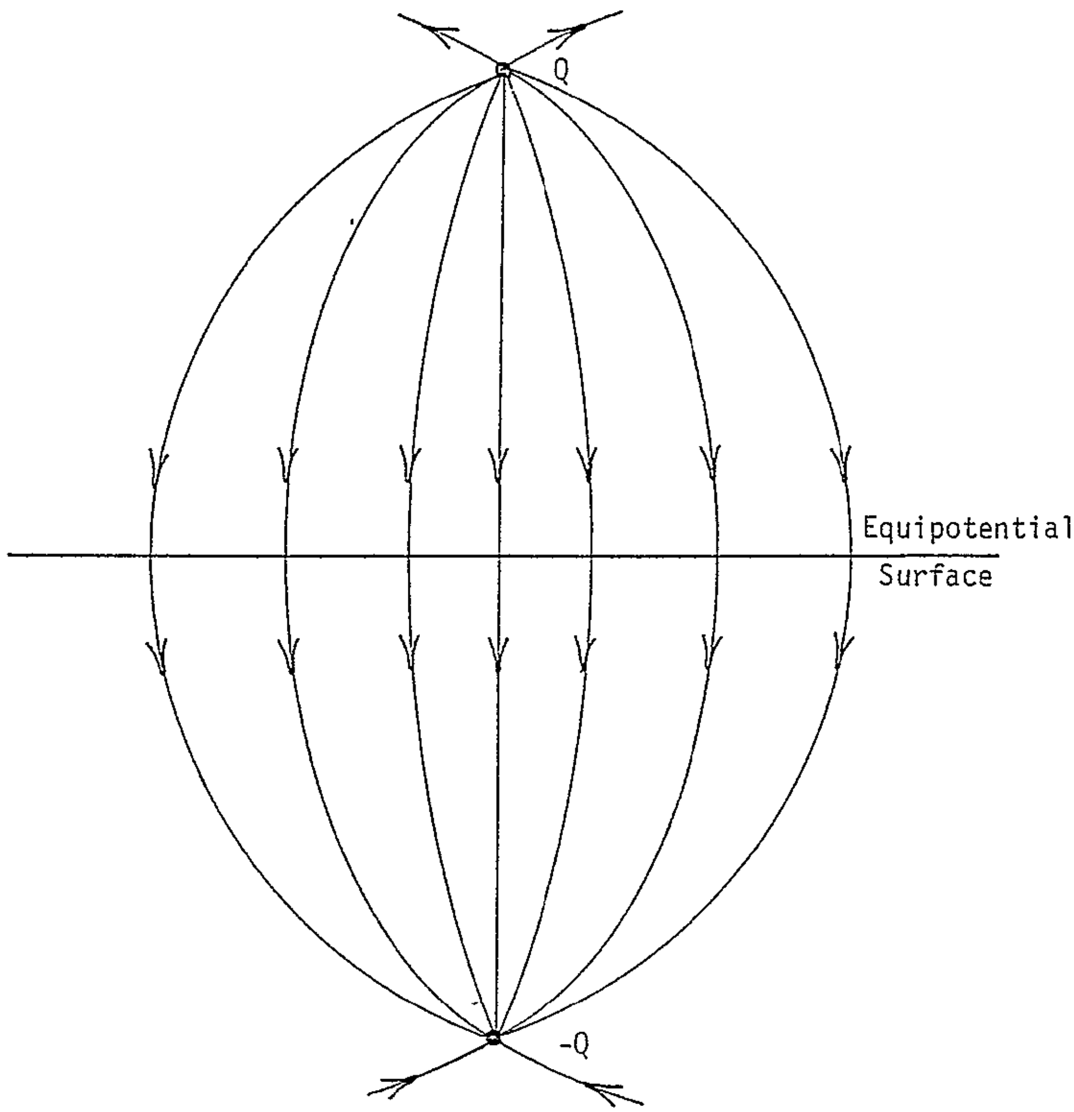

Figure 9

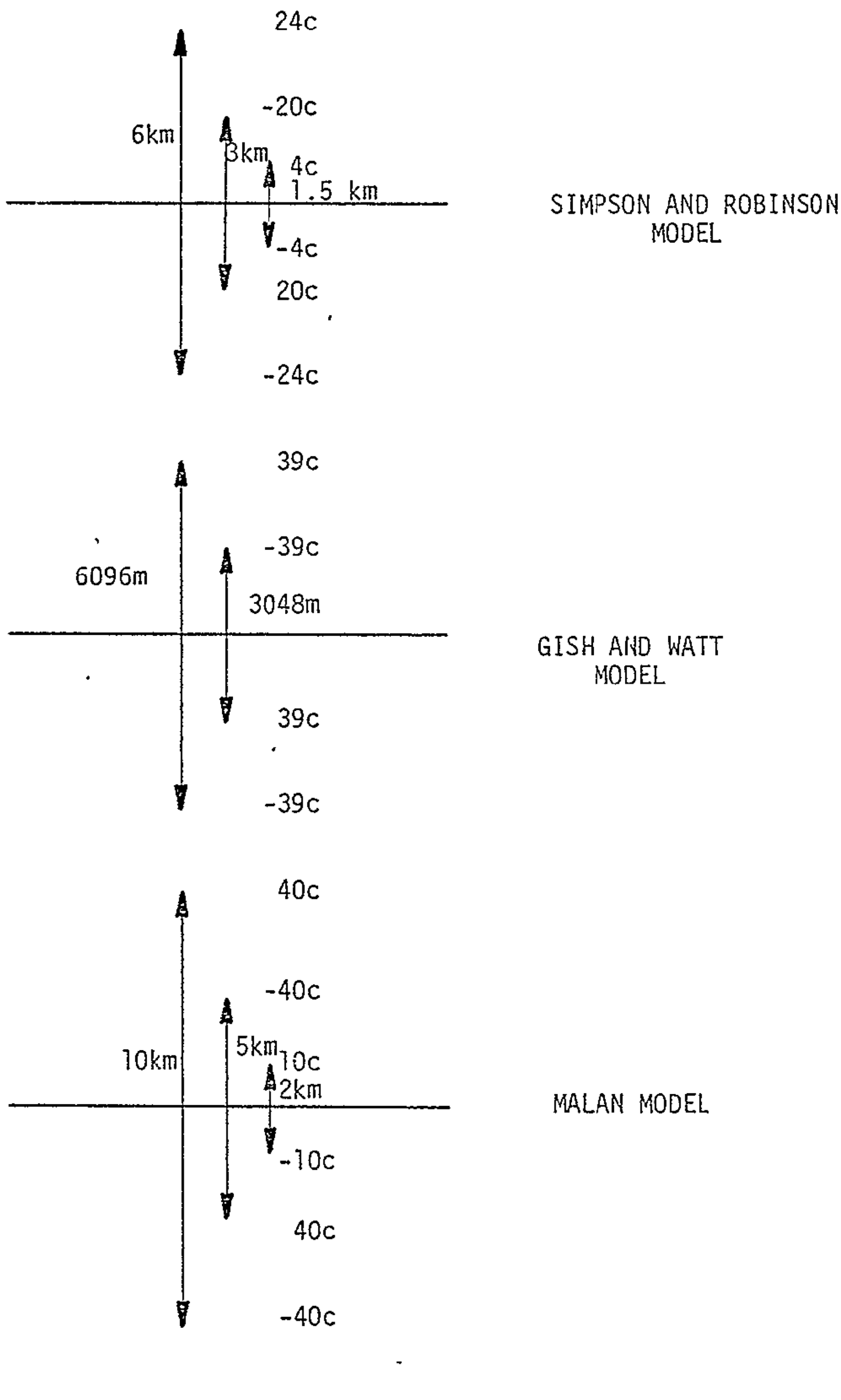
24c
-20c
6km
3km
4c
1.5 km
SIMPSON AND ROBINSON MODEL
-4c
20c
-24c
39c
-39c
6096m
3048m
GISH AND WATT MODEL
39c
-39c
40c
-40c
10km
5km
10c
2km
MALAN MODEL
-10c
40c
-40c

Figure 10

at 500 meters horizontally from the charge centers and at gound level, the Simpson and Robinson model yields a field with a magnitude of 938 volt/meter, the Gish and Wait model yields a magnitude of 26122 volts/meter, while Malan's model has a magnitude of 19991 volts/meter at that location. If a model could be generated to best fit a combination of various field readings taken at different heights and different times under a variety of conditions, the result would be a more universal model of a thundercloud.

The model developed in this paper is found by starting with the charge center values and locations determined by Simpson and Robinson, Gish and Wait, and Malan. The field strength is calculated for selected locations using one model at a time and compared to actual values measured by various experimentors. The measured values used for the comparison and the source of each value are shown in Table 4. The readings from Wormell [10] are average potential gradients taken over all directions from the charge centers at ground level immediately before a lightning discharge.

The calculated value of the field using Equation 7 at location I, EFLD(I), is subtracted from the measured value, EF(I), and the percentage of variation computed as

$$\frac{EF(I) - EFLD(I)}{EF(I)} \quad 100 \qquad (8)$$

	DISTANCE FROM CHARGE CENTERS (METERS)	MEASURED FIELD STRENGTH* (VOLTS/M)	SOURCE
1	2500	- 1310	Wormell [10]
2	5000	- 1160	"
3	7500	- 760	"
4	10000	- 460	"
5	12500	- 260	"
6	15000	- 135	"
7	17500	- 60	"
8	20000	0	"
9	13100	33000	Gish & Wait [8]

Note: 1 through 8 are horizontal distance with measurements made at ground level. 9 is a vertical height directly above the charge centers.

*due to cloud only.

Table 4

The resulting value is then squared. The square of the percentage of variation is computed for each location in Table 4 and added together to produce a quantity ESQRT. The amount of charge at one of the charge centers is now varied in increments of .01 coulombs until a minimum is found for ESQRT. The process of calculating the fields and computing ESQRT is begun again with this new charge quantity replacing the old value for the selected charge center and a different charge center quantity is varied until a new minimum is found for ESQRT. The program continues to vary one charge center quantity at a time, each time finding the minimum ESQRT, until ESQRT is less than or equal to 100 or until ESQRT reaches a local minimum. The program listing and resulting output from the program are contained in Appendix B.

The resulting field maps of the Simpson and Robinson; Gish and Wait, and Malan models, after being modified by the program shown in Appendix B, are shown in Figures 11, 12 and 13 respectively. The progressive evaluation of the charge center values are shown in the output listings in Appendix B. The charge center values used for the modified Simpson and Robinson model are 4.6 coulombs at 6km, -11.3 coulombs at 3km and 5.97 coulombs at 1.5km. ESQRT had a value of 5.22×10^2 at these values. The charge centers for the modified Gish and Wait model are 1.52 coulombs at 6096 meters and -2.64 coulombs at 3048 meters; ESQRT equals 6.24×10^2. The charge centers for the modified Malan model are 20.1 coulombs, -36.8 coulombs and 12.7 coulombs at 10km, 5km and 2km respectively; ESQRT equals 7.99×10^2 at this point.

1 In. = 400 v/m

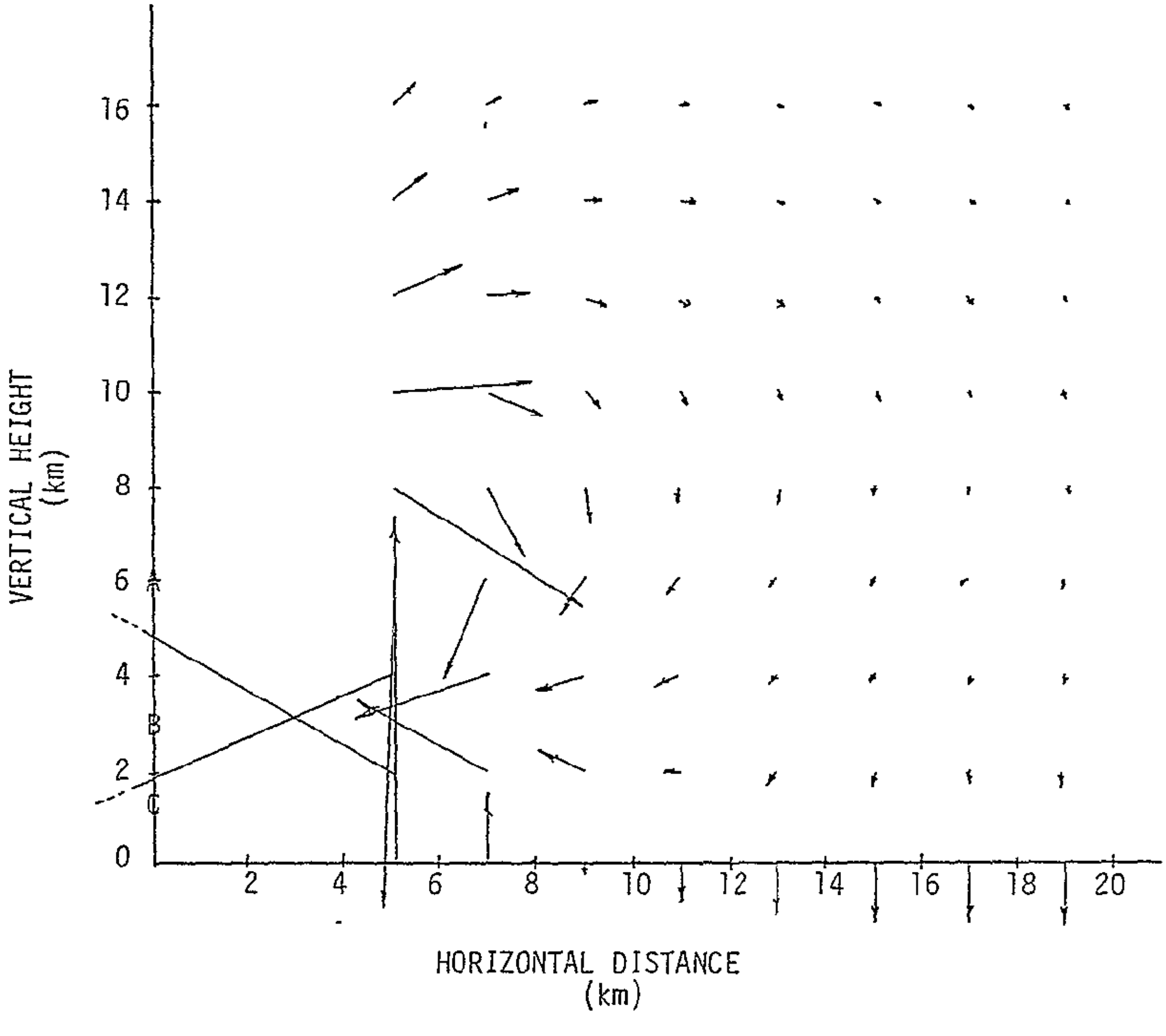

A = 4.6 coulombs
B =-11.3 coulombs
C = 5.97 coulombs

ELECTRIC FIELD MAP FOR
MODIFIED SIMPSON AND ROBINSON MODEL

Figure 11

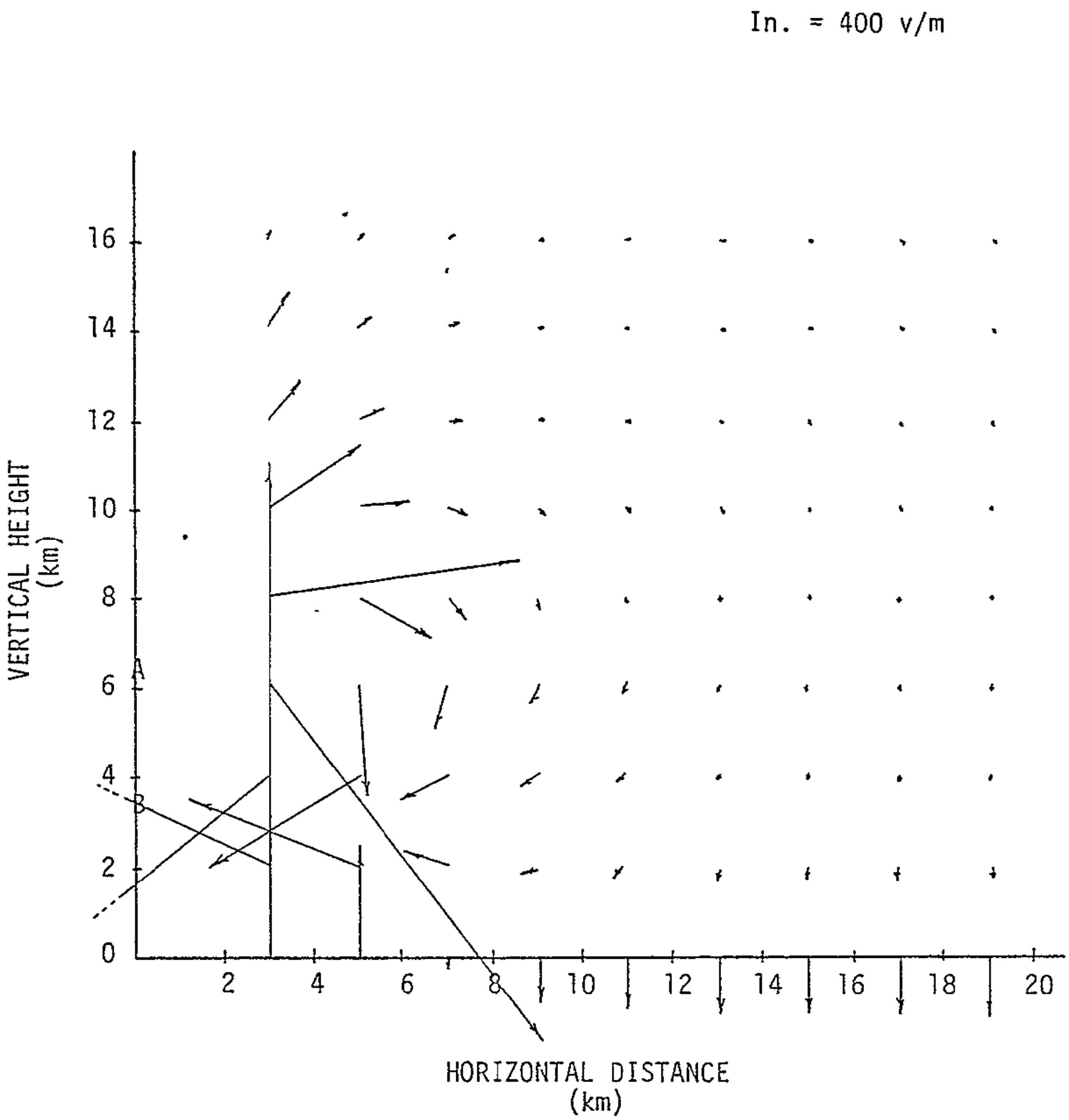

A = 1.52 coulombs
B =-2.64 coulombs

ELECTRIC FIELD MAP FOR
MODIFIED GISH AND WAIT MODEL

Figure 12

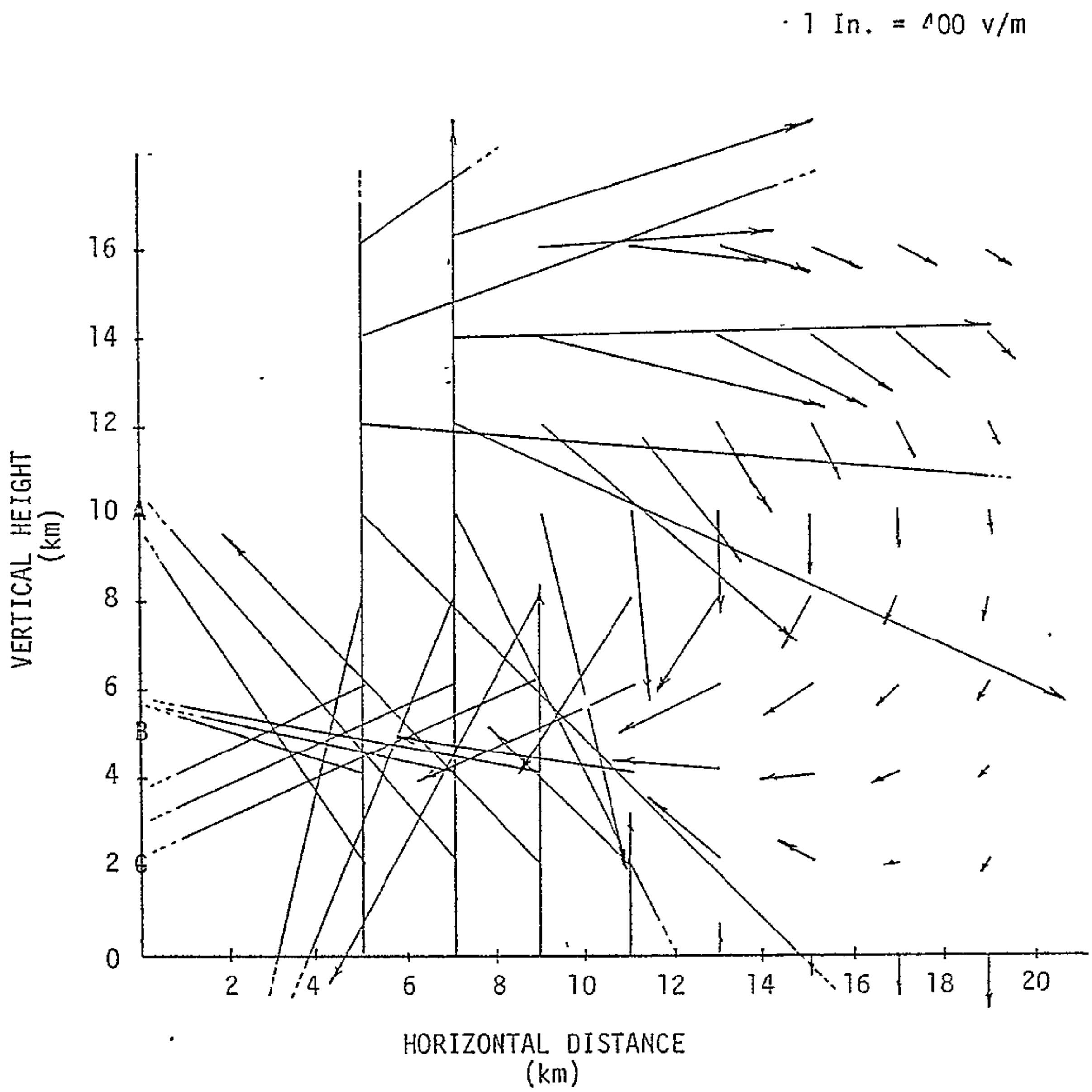

A = 20.1 coulombs
B =-36.8 coulombs
C = 12.7 coulombs

ELECTRIC FIELD MAP FOR
MODIFIED MALAN MODEL

Figure 13

VI. CONCLUSION

In order to select the model which most closely approximates a typical thundercloud, one must use more than the values of ESQRT which were generated. The modified models come closer to fitting the electric field values measured at ground level by Wormell and the values Gish and Wait measured to 40,000 feet than the original models as shown in Figures 14 and 15, yet the final model should most nearly conform to all electric field measurements made in the vicinity of a thundercloud without lightning present.

R. Markson [11] states that thunderclouds, not considering lightning flashes, can effect the electric field within 50km or more. In order to evaluate the ability of the modified models to meet this requirement, one can note the effect the various models have on the electric field at the farthest distance evaluated, i.e. 21km. Using an expression for the approximate electric field given by Dolezalek [1], h being the height in km,

$$E = 81.8 \exp(-4.52h) + 38.6 \exp(-.375h) + 10.27 \exp(-.121h) \quad (9)$$

the field values at 4km, 10km and 16km are 4.59 v/m, .640 v/m and .119 v/m respectively. The values at 21km horizontal distance from the charge centers at these heights are 16.53 v/m at 73° from the vertical, 6.77 v/m at -12° from vertical and 4.24 v/m at -47° from vertical for the modified Simpson and Robinson model. The modified Gish and Wait model yields 15.8 v/m at -0.1°, 5.18 v/m at -10° and 2.53 v/m at -36° and

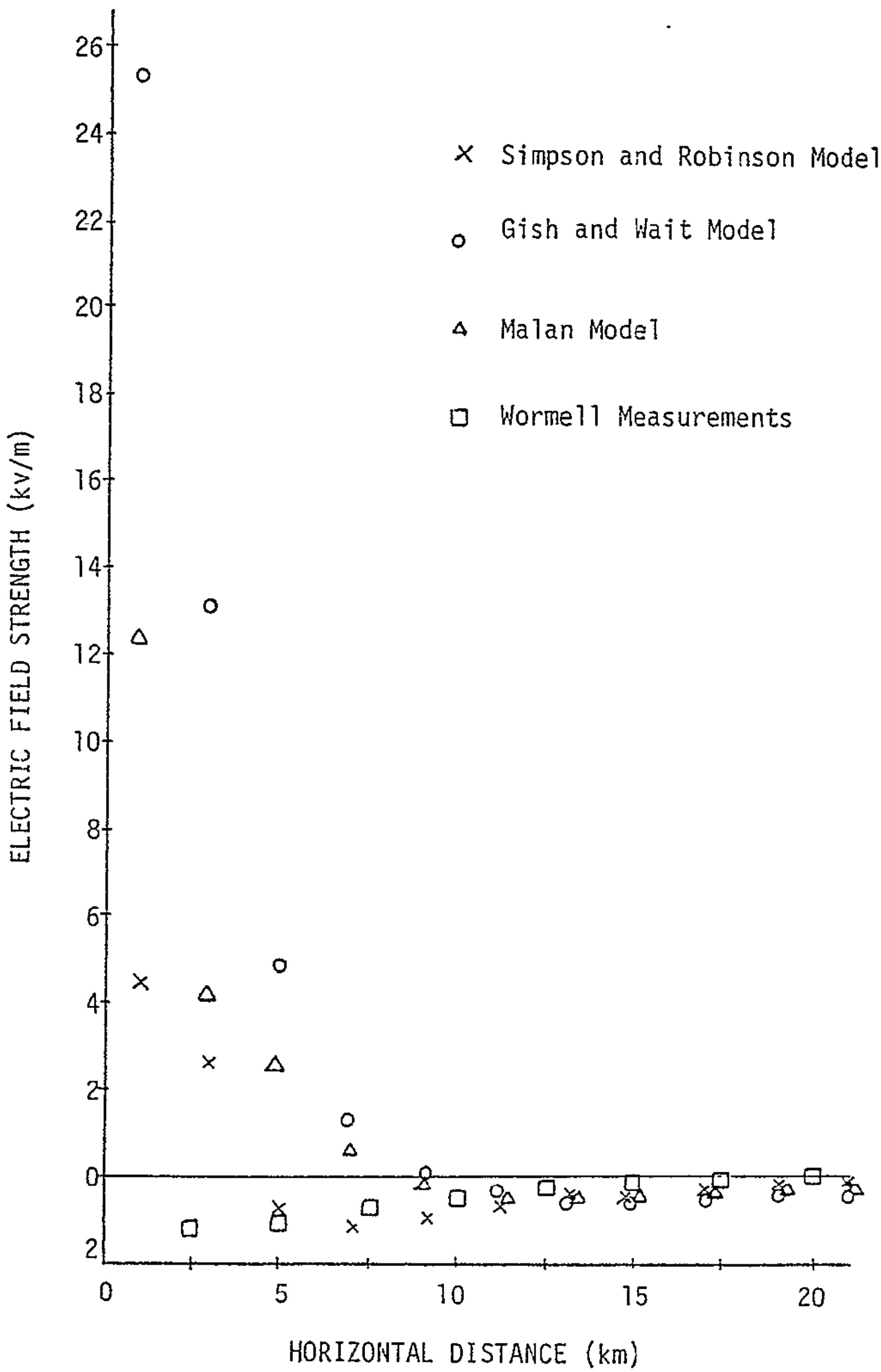

ELECTRIC FIELD STRENGTH AT GROUND LEVEL FOR ORIGINAL MODELS

Figure 14

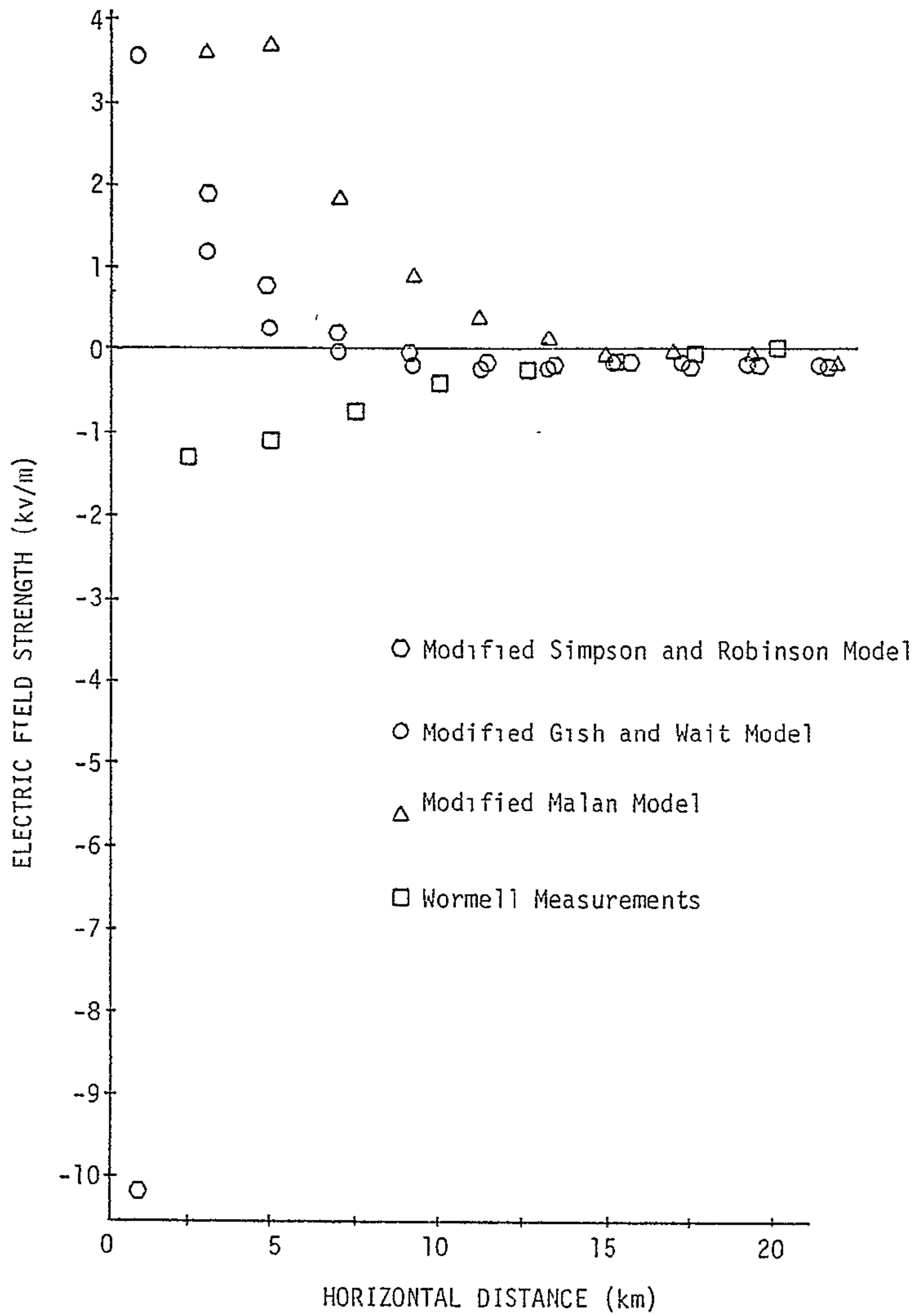

ELECTRIC FIELD STRENGTH AT GROUND LEVEL FOR THE MODIFIED MODELS

Figure 15

34.42 v/m at 20°, 45.2 v/m at -12° and 51.15 v/m at -56° for the modified Malan model. Since these values are for 21km and the field is to be effected within 50km or more, the largest resultant field values at the greatest angles must be chosen as being the closest fit. Here the modified Malan model is the best fit, followed by the modified Simpson and Robinson model, then the modified Gish and Wait model.

D.R. Lane-Smith [12] states that "tropical thunderstorms have been observed to produce negative electric fields of 3000 v/m or higher." All three modified models qualify under this criterion, Simpson and Robinson having a negative field as high as 47,000 v/m at a distance and height of 1km and 4 km, Gish and Wait producing 13,000 v/m at 1km and 4km height, and Malan producing 179,000 v/m at 1km and 10km height.

C.G. Stergis, G.C. Kein and T. Kangas [13] in balloon flights over thunderclouds made the measurements shown in Figures 16 and 17 The electric field measurements at a horizontal distance of 1km and a height of 16km for the three modified models are 85.17 v/m for Simpson and Robinson, 33.05 v/m for Gish and Wait and 2886.61 v/m for Malan. Because the value of the field strength will decrease as the height increases to that of the readings in Figures 16 and 17, i.e. above 21 km, the modified Malan model is the only one which could possibly satisfy these readings.

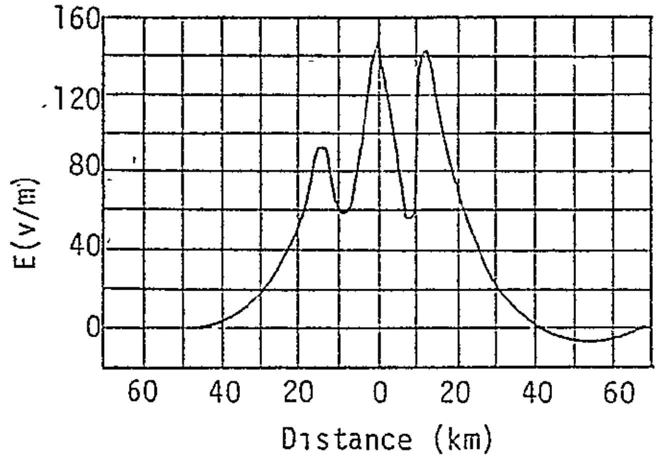

Flight at an altitude of 70,000 Feet
on 21 July 1956

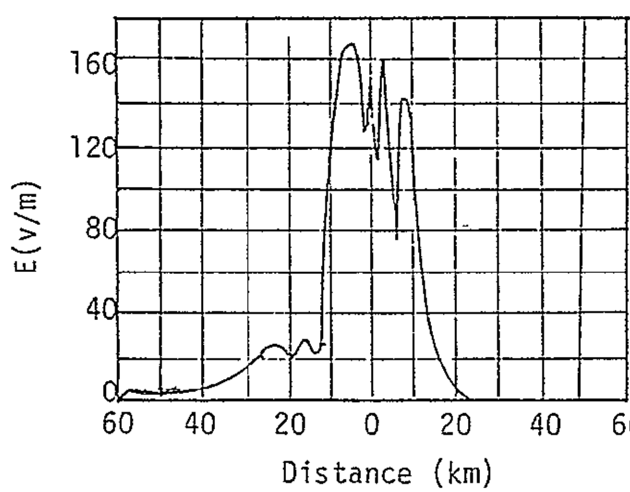

Flight at an altitude of 71,000 Feet
on 30 July 1956

ELECTRIC FIELD MEASUREMENTS ABOVE
THUNDERCLOUDS

Figure 16

(from Stergis, Rein and Kangas [13])

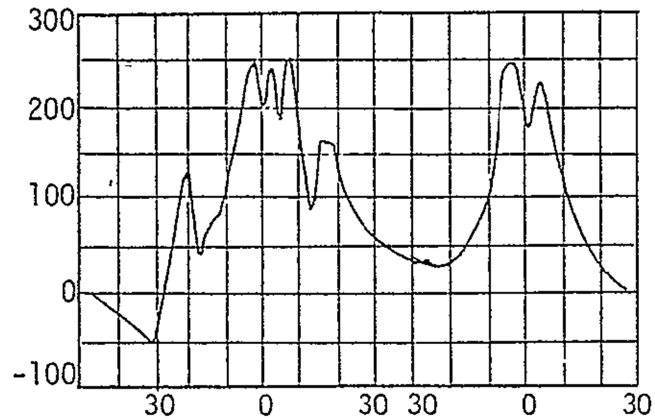

Distance (km)

Flight at an altitude of 76,000 Feet
on 3 August 1956

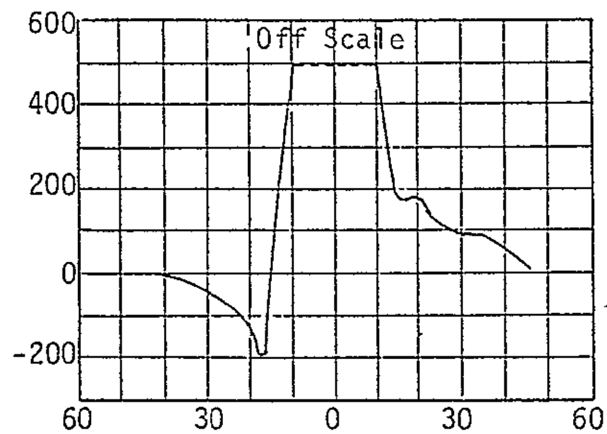

Distance (km)

Flight at an altitude of 76,000 Feet
on 20 July 1956

ELECTRIC FIELD MEASUREMENTS ABOVE
THUNDERCLOUDS

Figure 17
(from Stergis, Rein and Kangas [13])

Height above the thundercloud where E was measured,	0-100	100-300	300-500	500-1000	1,000
E_{max}, v/m	13,300	3,700	3,400	2,000	2,500
Number of measurements	34	29	40	24	13

DEPENDENCE OF E_{MAX} ON HEIGHT ABOVE THUNDERCLOUD

Table 5
(From Shvarts [14])

Similarly, Ya. M. Shvarts [14] gives the mean values of the maximum vertical component of the electric field at various distances above thunderclouds as shown in Table 5. In the modified Simpson and Robinson model the highest charge center is at 6km, the top of the cloud could therefore be considered to be somewhat below 8km. The vertical component of the electric field reading at 1km horizontal distance and the 8km height is 4821 v/m and, therefore, within the range of values in Table 5. The modified Gish and Wait model has its highest charge center also near 6km. In this case the vertical component of the electric field reading at 1km and 8km height is 1822 v/m. This is somewhat lower than the values in Table 5. The uppermost charge center of the modified Malan model is at 10km. The top of the cloud could be considered to be near 13km. Therefore, using the reading at 1km and 14km height, the vertical component is 7239 v/m. This is slightly high yet still within the range shown by Shvarts.

When considering the electrical specifications for a typical thunderstorm as described in the last two sections, the modified Malan model appears to be the best fit. The new electrical model of a cumulonimbus cloud has a charge of 20.1 coulombs at 10km, -36.8 coulombs at 5km and 12.7 coulombs at 2km.

The knowledge of the electric field surrounding a typical thundercloud has some practical uses and some limitations. Low cost avionics such as the field measuring device as described by M.L. Hill [14] and later by R. Markson [11] would be able to detect a field mapping of a thundercloud and therefore warn the pilot to avoid such an area. Yet, this model is only of a typical thundercloud; any specific thundercloud could exhibit quite different electric field characteristics, particularly during lightning, which has not been accounted for in this model. A model which would include lightning would demand an exceedingly complex system of which this model is only a beginning.

APPENDIX A

The following program, written for the HP2100 computer, is used to produce a field map for a system of three charge centers of values Q(1), Q(2) and Q(3) at the corresponding heights of Y(1), Y(2) and Y(3). The output lists the X and Y locations, X field value, Y field value, total field and the angle in radians of the total field at the location (X,Y). X is incremented by 2000m from 1000m to 21000m;Y is incremented by 2000m from ground level to 16000m.

```
     PROGRAM EMAP
    REAL NX,NY,KNY
    DIMENSION Y(6), Q(6)
 20 READ (5,1) Y(1),Y(2),Y(3),Q(1),Q(2),Q(3)
  1 FORMAT (6F10.2)
    IF (Y(1)) 22,22,21
 21 Y(4)=-Y(3)
    Y(5)=-Y(2)
    Y(6)=-Y(1)
    Q(4)=-Q(3)
    Q(5)=-Q(2)
    Q(6)=-Q(1)
    READ (5,4) A1,A2,A3,A4,A5,A6,A7
  4 FORMAT (7A4)
    WRITE (6,5) A1,A2,A3,A4,A5,A6,A7
  5 FORMAT (1H1,45X,7A4,//,3X,"CHARGE CENTER 1",5X,"CHARGE CENTER 2",5
   1X,"CHARGE CENTER 3",/,2X,"HEIGHT",3X,"COULOMBS",3X,"HEIGHT",3X,"CO
   2ULOMBS",3X,"HEIGHT",3X,"COULOMBS")
    WRITE (6,2) Y(1),Q(1),Y(2),Q(2),Y(3),Q(3)
  2 FORMAT (1H,6F10.2)
    WRITE (6,6)
  6 FORMAT (//,3X,"X",5X,"Y",4X,"X FIELD",3X,"Y FIELD",4X,"TOTAL",5X,"
   1THETA")
    CONST =4.*3.1416*8.854*(10.**(-12))
    DO 10 NNY=0,16,2
    NY=NNY*1000.
    DO 10 NNX=10,210,20
    NX=NNX*100.
    EXSUM=0.
    EYSUM=0.
    DO 11 N=1,6,1
    EXSUM=EXSUM +Q(N)*NX/(CONST*(NX**2+(NY-Y(N))*(NY-Y(N)))**1.5)
 11 EYSUM=EYSUM+Q(N)*(NY-Y(N))/(CONST*(NX**2+(NY-Y(N))*(NY-Y(N)))**1.5
   1)
    KNY=NY/1000.
    EYSUM=EYSUM-81.8*EXP(-4.52*KNY)-38.*EXP(-.375*KNY)-10.27*EXP(- 121
   1*KNY)
    IF (EXSUM) 15,13,12
 12 THETA=ATAN(EYSUM/EXSUM)
 16 ETOTL=SQRT(EXSUM*EXSUM+EYSUM*EYSUM)
 14 WRITE (6,3) NX,NY,EXSUM,EYSUM,ETOTL,THETA
  3 FORMAT(2I6,3F10.2,F10.4)
 10 CONTINUE
    GO TO 20
 15 PI=3.1416
    ANGLE=SIGN(PI,EYSUM)
    THETA=ANGLE+ATAN(EYSUM/EXSUM)
    GO TO 16
 13 ANGLE=3.1416/2.
    THETA=SIGN(ANGLE,EYSUM)
    ETOTL=EYSUM
    GO TO 14
 22 END
```

SIMPSON AND ROBINSON MODEL

CHARGE CENTER 1		CHARGE CENTER 2		CHARGE CENTER 3	
HEIGHT	COULOMBS	HEIGHT	COULOMBS	HEIGHT	COULOMBS
6000.00	24.00	3000.00	-20.00	1500.00	4.00

X	Y	X FIELD	Y FIELD	TOTAL	THETA
1000	0	.00	4066.83	4066.83	1.5708
3000	0	.00	2559.72	2559.72	1.5708
5000	0	.00	-881.20	-881.20	-1.5708
7000	0	.00	-1285.40	-1285.40	-1 5708
9000	0	.00	-1054.19	-1054.19	-1.5708
11000	0	.00	-797.06	-797.06	-1.5708
13000	0	.00	-605.92	-605.92	-1.5708
15000	0	.00	-474.12	-474.12	-1.5708
17000	0	.00	-383.90	-383.90	-1.5708
19000	0	.00	-321.34	-321.34	-1.5708
21000	0	.00	-277.11	-277.11	-1.5708
1000	2000	-34552.17	64956.74	73574.67	2.0597
3000	2000	-7460.80	-123.11	7451.82	-3.1251
5000	2000	-787.46	-1881.66	2039.79	-1.9671
7000	2000	245.10	-1399.23	1420.54	-1.3974
9000	2000	306.39	-967.06	1014.43	-1.2640
11000	2000	229.31	-675.36	713.22	-1.2435
13000	2000	157.24	-483.80	508.71	-1.2566
15000	2000	106.70	-356.71	372.33	-1.2801
17000	2000	73.30	-270.68	280.43	-1.3063
19000	2000	51.36	-211.07	217.23	-1.3321
21000	2000	36.75	-168.81	172.76	-1 3564
1000	4000	-42327.79	-97247.95	106060.39	-1.9813
3000	4000	-1222.37	-13244.89	13301.17	-1.6628
5000	4000	1358.17	-3666.89	3910.34	-1.2161
7000	4000	1077.23	-1591.73	1921.99	-.9758
9000	4000	714.07	-902.53	1150.84	-.9015
11000	4000	463.20	-589.46	749.68	-.9048
13000	4000	303.79	-415.05	514.35	-.9390
15000	4000	203.43	-305.87	367.34	-.9839
17000	4000	139.51	-232.83	271.43	-1.0310
19000	4000	97.98	-181.91	206.62	-1.0767
21000	4000	70.38	-145.35	161.49	-1.1199
1000	6000	210423 44	-15336.63	210981.59	-.0728
3000	6000	17672.71	-6032.24	18673.86	-.3289
5000	6000	4772.50	-2261.52	5281.21	- 4425
7000	6000	2042.89	-1072.73	2307.41	-.4835

X	Y	X FIELD	Y FIELD	TOTAL	THETA
9000	6000	1093.99	-631.81	1263.32	-.5237
11000	6000	655.36	-427.21	782.31	-.5777
13000	6000	418.42	-311.83	521.84	-.6405
15000	6000	278.75	-237.61	366.28	-.7059
17000	6000	191.85	-186.06	267.25	-.7701
19000	6000	135.65	-148.64	201.24	-.8310
21000	6000	98.18	-120.74	155.62	-.8881
1000	8000	18077.88	32606.24	37282.39	1.0646
3000	8000	11414.12	5261.37	12568.38	.4319
5000	8000	4725.81	563.86	4759.33	.1188
7000	8000	2246.16	-134.77	2250.20	-.0599
9000	8000	1229.38	-226.77	1250.12	-.1824
11000	8000	742.58	-215.60	773.25	-.2826
13000	8000	478.86	-187.20	514.15	-.3727
15000	8000	323.02	-158.48	359.85	-.4564
17000	8000	225.34	-133.35	261.84	-.5343
19000	8000	161.45	-112.08	196.54	-.6068
21000	8000	118.28	-94.50	151.40	-.6741
1000	10000	2631.71	9182.00	9551.70	1.2917
3000	10000	4116.18	4404.92	6028.78	.8193
5000	10000	2896.25	1547.05	3283.54	.4906
7000	10000	1777.12	483.03	1841.60	.2654
9000	10000	1102.76	111.90	1108.42	.1011
11000	10000	712.94	-20.71	713.24	-.0290
13000	10000	479.75	-67.37	484.45	-.1395
15000	10000	333.74	-80.73	343.37	-.2373
17000	10000	238.55	-80.62	251.80	-.3259
19000	10000	174.38	-75.18	189.90	-.4071
21000	10000	129.96	-67.94	146.64	-.4817
1000	12000	748.58	3825.96	3898.50	1.3776
3000	12000	1598.30	2610.45	3060.89	1.0214
5000	12000	1556.23	1395.26	2090.12	.7309
7000	12000	1199.36	662.58	1370.21	.5047
9000	12000	860.01	291.66	908.12	.3270
11000	12000	609.46	112.35	619.73	.1823
13000	12000	435.98	26.07	436.76	.0597
15000	12000	316.79	-15.06	317.14	-.0475
17000	12000	234.00	-33.81	236.43	-.1435
19000	12000	175.57	-41.23	180.35	-.2307
21000	12000	133.65	-42.89	140.36	-.3106
1000	14000	296.39	1984.18	2006.20	1.4225
3000	14000	723.55	1573.04	1731.51	1.1396
5000	14000	845.55	1044.32	1343.71	.8902
7000	14000	767.55	620.30	986.87	.6797
9000	14000	623.99	344.12	712.58	.5040
11000	14000	484.45	179.98	516.81	.3557

X	Y	X FIELD	Y FIELD	TOTAL	THETA
13000	14000	370.29	85.95	380.14	.2281
15000	14000	282.64	32.89	284.55	.1159
17000	14000	216.82	3.36	216.84	.0155
19000	14000	167.62	-12.68	168.10	-.0755
21000	14000	130.74	-20.94	132.41	-.1588
1000	16000	142.35	1173.79	1182.39	1.4501
3000	16000	372.18	1004.45	1071.18	1.2160
5000	16000	483.71	754.30	896.07	1.0006
7000	16000	490.83	515.07	711.48	.8095
9000	16000	440.14	329.57	549.85	.6427
11000	16000	370.05	200.88	421.06	.4973
13000	16000	301.17	116.66	322.98	.3696
15000	16000	241.51	63.21	249.64	.2560
17000	16000	192.67	29.86	194.97	.1537
19000	16000	153.74	9.36	154.03	.0608
21000	16000	123.08	-3.00	123.12	-.0244

GISH AND WAIT MODEL

CHARGE CENTER 1		CHARGE CENTER 2		CHARGE CENTER 3	
HEIGHT	COULOMBS	HEIGHT	COULOMBS	HEIGHT	COULOMBS
6096.00	39.00	3048.00	-39.00	.00	.00

X	Y	X FIELD	Y FIELD	TOTAL	THETA
1000	0	-.00	46473.19	46473.19	1.5708
3000	0	.00	13560.42	13560.42	1.5708
5000	0	-.00	1791.56	1791.56	1.5708
7000	0	.00	-672.18	-672.18	-1.5708
9000	0	.00	-966.69	-966.69	-1.5708
11000	0	.00	-841.81	-841.81	-1.5708
13000	0	.00	-676.21	-676.21	-1.5708
15000	0	.00	-541.02	-541.02	-1.5078
17000	0	.00	-440.81	-440.81	-1.5708
19000	0	-.00	-368.09	368.09	-1.5708
21000	0	.00	-315.17	-315.17	-1.5708
1000	2000	-108718.89	109432.34	154257.06	2.3529
3000	2000	-21174.68	4780.39	21707.59	2.9196
5000	2000	-3802.59	-948.36	3919.07	-2.8972
7000	2000	-504.58	-1243.51	1341.98	-1.9563
9000	2000	114.77	-1006.48	1013.00	-1 4573
11000	2000	187.85	-757.27	780.22	-1.3276
13000	2000	157.06	-565.07	586.50	-1.2997
15000	2000	116.66	-426.54	442.21	-1.3038
17000	2000	84.33	-328.00	338.67	-1.3191
19000	2000	61.00	-257.49	264.62	-1.3382
21000	2000	44.61	-206.39	211.15	-1.3579
1000	4000	-104554.09	-181997.62	209892.09	-2.0922
3000	4000	-10832.73	-23238.61	25639.44	-2.0070
5000	4000	-803.15	-5802.10	5857.43	-1.7084
7000	4000	509.48	-2232.55	2289.94	-1.3464
9000	4000	578.85	-1172.51	1307.61	-1.1122
11000	4000	452.19	-741.18	868 24	-1.0230
13000	4000	325.58	-516 84	610.84	-1.0087
15000	4000	230.37	-380.52	444.82	-1.0264
17000	4000	163.69	-290.07	333.07	-1.0570
19000	4000	117.79	-226.91	255.66	-1.0920
21000	4000	86.10	-181.33	200.73	-1.1275
1000	6000	334420.31	-65541.23	340782.31	-.1935
3000	6000	25453.36	-13660.82	28887.57	-.4926
5000	6000	5864.96	-4583.87	7443.76	-.6634

REPRODUCIBILITY OF THE ORIGINAL PAGE IS POOR

X	Y	X FIELD	Y FIELD	TOTAL	THETA
7000	6000	2295.37	-1901.85	2980.90	-.6919
9000	6000	1211.50	-984.07	1560.81	-.6822
11000	6000	738.83	-607.15	956.30	-.6879
13000	6000	483.46	-420.12	640.50	-.7154
15000	6000	329.47	-311.14	453.16	-.7568
17000	6000	231.05	-240.02	333.16	-.8044
19000	6000	165.83	-190.20	252.34	-.8537
21000	6000	121.47	-153.73	195.93	-.9021
1000	8000	32652.30	54711.66	63714.52	1.0327
3000	8000	18372.59	6858.57	19611.02	.3573
5000	8000	6873.42	65.88	6873.74	.0096
7000	8000	3002.36	-547.50	3051.88	-.1804
9000	8000	1557 87	-467.76	1626.58	-.2917
11000	8000	917.97	-357.29	985.05	-.3712
13000	8000	587.85	-277.19	649.92	-.4406
15000	8000	397.35	-220.69	454.52	-.5070
17000	8000	278.74	-179.23	331.39	-.5714
19000	8000	201.04	-147.64	249.43	-.6334
21000	8000	418.25	-122.96	192.61	-.6924
1000	10000	4416.47	14565.66	15220.50	1.2764
3000	10000	6586.64	6468.16	9231.52	.7763
5000	10000	4350.91	1974.11	4777 82	.4259
7000	10000	2512.04	481.38	2557.75	.1893
9000	10000	1485.50	37.40	1485.97	.0252
11000	10000	930.13	-90.61	934.53	-.0971
13000	10000	614.63	-122.40	626.70	-.1966
15000	10000	423.93	-123.41	441.53	-.2833
17000	10000	302.16	-114.40	323.09	-.3619
19000	10000	220.97	-102.57	243 62	-.4346
21000	10000	165.01	-90.60	188.25	-.5021
1000	12000	1196.20	5814.28	5936 05	1.3679
3000	12000	2491.73	3826.18	4566.00	.9936
5000	12000	2333.49	1919.59	3021.59	.6884
7000	12000	1724.09	839.38	1917 56	.4531
9000	12000	1190.52	332.74	1236.15	.2725
11000	12000	819.34	107.33	826.34	.1303
13000	12000	574.33	7.58	574.38	.0132
15000	12000	412.00	-36.05	413.58	-.0873
17000	12000	302.12	-53.86	306.89	-.1764
19000	12000	225.87	-59.41	233.56	-.2572
21000	12000	171.73	-59.08	181.61	-.3313
1000	14000	456.98	2925.56	2961.03	1.4158
3000	14000	1099.50	2273.60	2525.50	1.1204
5000	14000	1253.13	1456.99	1921.76	.8605
7000	14000	1104.81	827.48	1380 34	.6429
9000	14000	873.05	436.67	976.17	.4638

X	Y	X FIELD	Y FIELD	TOTAL	THETA
11000	14000	661.57	215.99	695.94	.3156
13000	14000	496.24	95.67	505.37	.1905
15000	14000	373.66	30.78	374.92	.0822
17000	14000	284.04	-3.87	284.06	-.0136
19000	14000	218.33	-21.90	219.43	-.1000
21000	14000	169.73	-30.69	172.48	-.1789
1000	16000	213.59	1693.36	1706.78	1.4453
3000	16000	553.23	1431.78	1534.94	1.2021
5000	16000	707.20	1052.13	1267.72	.9790
7000	16000	703.10	698.73	991.25	.7823
9000	16000	617.32	433.55	754.35	.6123
11000	16000	509 07	256.01	569.82	.4660
13000	16000	407.65	143.80	432.27	.3391
15000	16000	322.76	74.81	331.31	.2278
17000	16000	255.06	32.95	257.18	.1285
19000	16000	202.18	7.85	202.34	.0388
21000	16000	161.14	-6.94	161.28	-.0431

MALAN MODEL

CHARGE CENTER 1		CHARGE CENTER 2		CHARGE CENTER 3	
HEIGHT	COULOMBS	HEIGHT	COULOMBS	HEIGHT	COULOMBS
10000.00	40.00	5000.00	-40.00	2000.00	10.00

X	Y	X FIELD	Y FIELD	TOTAL	THETA
1000	0	.00	-12251.73	12251.73	-1.5708
3000	0	-.00	4015.52	4015.52	1.5708
5000	0	.00	2591.42	2591.52	1.5708
7000	0	-.00	632.48	632.48	1.5708
9000	0	.00	-247.33	-247.33	-1.5708
11000	0	.00	-537.95	-537.95	-1.5708
13000	0	.00	-587.30	-587.30	-1.5708
15000	0	.00	-551.52	-551.52	-1.5708
17000	0	.00	-492.79	-492.79	-1.5708
19000	0	.00	-433.99	-433.99	-1.5708
21000	0	.00	-382.39	-382.39	-1.5708
1000	2000	78723.22	28109.79	83591.31	.3430
3000	2000	-2692.49	10027.17	10382.37	1.8331
5000	2000	-3037.11	2608.98	4003.85	2.4319
7000	2000	-1313.15	320.30	1351.65	2.9024
9000	2000	-449.35	-366.78	580.04	-2.4570
11000	2000	-102.73	-530.26	540.12	-1.7622
13000	2000	21.59	-520.62	521.07	-1.5294
15000	2000	58.41	-459.97	463.67	-1.4445
17000	2000	62.82	-391.33	396.34	-1.4116
19000	2000	56.43	-328.87	333.68	-1.4009
21000	2000	47.45	-276.16	280.20	-1.4006
1000	4000	-117514.45	133725.22	178022.72	2.2918
3000	4000	-24778.07	8331.59	26141.32	2.8172
5000	4000	-6751.43	-378.73	6762.04	-3.0856
7000	4000	-2037.31	-1102.32	2316.41	-2.6456
9000	4000	-540.37	-954.34	1096.70	-2.0860
11000	4000	-42.81	-754.78	756.00	-1.6275
13000	4000	111.29	-595.46	605.77	-1.3860
15000	4000	144.15	-474.77	496.17	-1.2760
17000	4000	135.96	-382.97	406.39	-1.2297
19000	4000	116.25	-312.38	333.31	-1.2145
21000	4000	95.57	-257.55	274.71	-1.2155
1000	6000	-120686.14	-142335.00	186612.97	-2.2741
3000	6000	-23275.31	-19824.02	30573.39	-2.4361
5000	6000	-4897.77	-6664.76	8270.87	-2.2046

X	Y	X FIELD	Y FIELD	TOTAL	THETA
7000	6000	-976.07	-2978.22	3134.08	-1.8875
9000	6000	16.83	-1586.22	1586.31	-1.5602
11000	6000	265.29	-969.45	1005.09	-1.3037
13000	6000	297.59	-657.70	721.90	-1.1459
15000	6000	266.77	-480.23	549.35	-1.0637
17000	6000	222.12	-368.41	430.91	-1.0282
19000	6000	179.59	-292.18	342.97	-1.0197
21000	6000	143.60	-237.19	277.27	-1.0264
1000	8000	21198.36	-95907.80	98222.58	-1.3533
3000	8000	9820.07	-27568.87	29265.62	-1.2286
5000	8000	3454.41	-8824.13	9475.19	-1.1977
7000	8000	1714.37	-3563.27	3954.23	-1.1224
9000	8000	1067.79	-1741.09	2042.45	-1.0207
11000	8000	742.80	-990.34	1237.95	-.9273
13000	8000	544.33	-634.98	836.36	-.8621
15000	8000	409.54	-445.56	604.19	-.8275
17000	8000	313.02	-333.47	457.35	-.8170
19000	8000	241.97	-260.99	355.90	-.8232
21000	8000	188.84	-210.66	282.91	-.8399
1000	10000	356977.94	-12116.47	357183.50	-.0339
3000	10000	34966.09	-7850.73	35836.60	-.2209
5000	10000	9876.40	-4179.14	10724.20	-.4003
7000	10000	3963.03	-2198.17	4531.83	-.5064
9000	10000	1994.93	-1232.97	2345.20	-.5536
11000	10000	1175.08	-753.90	1396.13	-.5704
13000	10000	768.44	-502.01	917.89	-.5787
15000	10000	537.57	-359.77	646.85	-.5898
17000	10000	392.89	-273.12	478.49	-.4076
19000	10000	295.74	-216.30	366.40	-.6315
21000	10000	227.34	-176.57	287.85	-.6604
1000	12000	31233.70	58117 42	65978.62	1.0777
3000	12000	20824.47	10466.50	23306.79	.4657
5000	12000	9037.53	1317.70	9133.19	.1448
7000	12000	4310.54	-266.50	4316.48	-.0525
9000	12000	2316.31	-417.18	2353.58	-.1782
11000	12000	1381.88	-368.39	1430.15	-.2605
13000	12000	895.93	-295.87	943.52	-.3190
15000	12000	618.29	-236.96	662.14	-.3660
17000	12000	446.61	-193.30	486.64	-.4085
19000	12000	333.48	-160.96	370.29	-.4497
21000	12000	255.22	-136.36	289.36	-.4907
1000	14000	4700.79	16794.50	17439.98	1.2979
3000	14000	7520.32	8299.14	11199.60	.8346

X	Y	X FIELD	Y FIELD	TOTAL	THETA
5000	14000	5424.10	3011.47	6204.01	.5068
7000	14000	3362.94	961.95	3497.82	.2786
9000	14000	2082.60	243.79	2096.82	.1165
11000	14000	1341.62	-2.14	1341.62	-.0016
13000	14000	905.85	-83.00	909.65	-.0914
15000	14000	638.60	-105.42	647.24	-.1636
17000	14000	466.70	-107.03	478.82	-.2254
19000	14000	351.07	-101.35	365.41	-.2810
21000	14000	270.20	-93.40	285.89	-.3328
1000	16000	1366.02	7108.68	7238.74	1.3809
3000	16000	2945.49	4908.01	5724.03	1.0303
5000	16000	2903.74	2666.07	3942.04	.7428
7000	16000	2255.76	1287.59	2597.37	.5187
9000	16000	1621.80	584 09	1723.78	.3457
11000	16000	1150.72	246.31	1176.79	.2109
13000	16000	826.67	85.77	831.11	.1034
15000	16000	606.64	9.07	606.71	.0150
17000	16000	455.31	-27.59	456.15	-.0605
19000	16000	348.89	-44.61	351.73	-.1272
21000	16000	272.20	-51.70	277.07	-.1877

MODIFIED SIMPSON AND ROBINSON MODEL

CHARGE CENTER 1		CHARGE CENTER 2		CHARGE CENTER 3	
HEIGHT	COULOMBS	HEIGHT	COULOMBS	HEIGHT	COULOMBS
6000.00	4.60	3000.00	-11.30	1500.00	5.97

X	Y	X FIELD	Y FIELD	TOTAL	THETA
1000	0	.00	-10538.48	-10538.48	-1.5708
3000	0	.00	1939.86	1939.85	1.5708
5000	0	-.00	770.68	770.68	1.5708
7000	0	-.00	177.66	177.66	1.5708
9000	0	.00	-20.31	-20.31	-1.5708
11000	0	-.00	-88.79	88.79	-1.5708
13000	0	-.00	-114.33	114.33	-1.5708
15000	0	-.00	-124.48	124.48	-1.5708
17000	0	.00	-218.68	-128.68	-1.5708
19000	0	.00	-130.42	-130.42	-1.5708
21000	0	-.00	-131.11	131.11	-1.5708
1000	2000	2650.72	52024.13	52091.62	1.5199
3000	2000	-3226.18	2930.23	4358.27	2.4042
5000	2000	-918.40	537.89	1064.33	2.6118
7000	2000	-279.52	153.89	319.08	2.6383
9000	2000	-93.95	41.60	102.75	2.7247
11000	2000	-34.56	.63	34.56	3.1235
13000	2000	-13.63	-15.77	20.84	-2.2837
15000	2000	-5.63	-22.64	23.33	-1.8145
17000	2000	-2.35	-25.57	25.68	-1.6630
19000	2000	-.96	-26.79	26.81	-1.6066
21000	2000	-.34	-27.25	27.25	-1.5832
1000	4000	-29521.43	-36532.12	46969.25	-2.2505
3000	4000	-4359.65	-2692.04	5123.83	-2.5884
5000	4000	974.39	-440.09	1069.16	-2.7174
7000	4000	-304.88	-102.55	321.66	-2.8171
9000	4000	-111.29	-34.15	116.41	-2.8439
11000	4000	-44.17	-19.65	48.34	-2.7231
13000	4000	-18.43	-16.91	25.02	-2.3993
15000	4000	-7.89	-16.60	18.38	-2.0143
17000	4000	-3.35	-16.64	16.97	-1.7693
19000	4000	-1.32	-16.62	16.67	-1.6502
21000	4000	-.41	-16.52	16.53	-1.5956
1000	6000	38668.84	-7161.18	39326.34	-.1831
3000	6000	1607.50	-2427.45	2911.46	-.9859
5000	6000	-21.39	-690.32	690.65	-1.6018
7000	6000	-90.12	-220.81	238.49	-1.9583
9000	6000	-53.42	-82.80	98.54	-2.1438

X	Y	X FIELD	Y FIELD	TOTAL	THETA
11000	6000	-26.85	-37.86	46.42	-2.1877
13000	6000	-12.78	-21.92	25.37	-2.0985
15000	6000	-5.82	-15.78	16.81	-1.9240
17000	6000	-2.44	-13.17	13.39	-1.7544
19000	6000	-.83	-11.92	11.95	-1.6404
21000	6000	-.08	-11.23	11.23	-1.5778
1000	8000	3119.30	4820.74	5741.91	.9965
3000	8000	1548.54	188.47	1559.96	.1211
5000	8000	381.93	-235.11	448.49	-.5518
7000	8000	80.84	-145.22	167.08	-1.0658
9000	8000	12.37	-74.57	75.59	-1.4065
11000	8000	-.95	-39.09	39.10	-1.5951
13000	8000	-2.06	-22.69	22.79	-1.6615
15000	8000	-1.10	-15.06	15.10	-1.6439
17000	8000	-.20	-11.36	11.36	-1.5885
19000	8000	.34	-9.46	9.47	-1.5350
21000	8000	.60	-8.41	8.43	-1.5000
1000	10000	389.07	1106.02	1172.46	1.2325
3000	10000	525.92	367.35	641.52	.6097
5000	10000	277.42	19.99	278.14	.0719
7000	10000	113.39	-46.45	122 53	-.3888
9000	10000	43.38	-41.14	59.79	-.7589
11000	10000	16 93	-27.92	32.65	-1.0257
13000	10000	7.27	-18.44	19.82	-1.1950
15000	10000	3.73	-12.78	13.31	-1.2868
17000	10000	2.36	-9.55	9.84	-1.3285
19000	10000	1.76	-7.71	7.90	-1.3468
21000	10000	1.43	-6.62	6.77	-1.3583
1000	12000	93.86	377.89	389.37	1.3274
3000	12000	181.48	210.26	277.75	.8587
5000	12000	145.99	66.95	160.61	.4300
7000	12000	86.33	3.99	86.42	.0462
9000	12000	45.34	-13.40	47.28	-.2873
11000	12000	23.26	-14.64	27.48	-.5617
13000	12000	12.34	-12.05	17.24	-.7734
15000	12000	7.04	-9.38	11.72	-.9270
17000	12000	4.40	-7.41	8.61	-1.0351
19000	12000	3.00	-6.08	6.78	-1.1119
21000	12000	2.21	-5.22	5.66	-1.1707
1000	14000	31.83	164.82	167.86	1.3800
3000	14000	72.40	114.53	135.50	1.0071
5000	14000	73.86	56.83	93.20	.6558
7000	14000	55.56	19.21	58.78	.3328
9000	14000	36.16	1.52	36.20	.0419
11000	14000	22.20	-4.80	22.71	-.2130

X	Y	X FIELD	Y FIELD	TOTAL	THETA
13000	14000	13.54	-6.19	14.89	-.4291
15000	14000	8.48	-5.88	10.32	-.6067
17000	14000	5.56	-5.18	7.60	-.7499
19000	14000	3.84	-4.51	5.92	-.8656
21000	14000	2.79	-3.98	4.86	-.9603
1000	16000	13.30	84.13	85.17	1.4140
3000	16000	33.00	65.71	73.53	1.1054
5000	16000	38.80	40.76	56.27	.8100
7000	16000	34.25	20.22	39.77	.5332
9000	16000	26.01	7.43	27.05	.2784
11000	16000	18.29	.87	18.31	.0476
13000	16000	12.47	-1.98	12.63	-.1578
15000	16000	8.50	-2.99	9.01	-.3378
17000	16000	5.90	-3.18	6.71	-.4942
19000	16000	4.22	-3.07	5.22	-.6293
21000	16000	3.11	-2.88	4.24	-.7463

MODIFIED GISH AND WAIT MODEL

CHARGE CENTER 1		CHARGE CENTER 2		CHARGE CENTER 3	
HEIGHT	COULOMBS	HEIGHT	COULOMBS	HEIGHT	COULOMBS
6096.00	1.52	3048.00	-2.64	.00	.00

X	Y	X FIELD	Y FIELD	TOTAL	THETA
1000	0	.00	3545.22	3545.22	1.5708
3000	0	-.00	1187.98	1187.98	1.5708
5000	0	.00	250.43	250.43	1.5708
7000	0	.00	-13.31	-13.31	-1.5708
9000	0	-.00	-91.15	91.15	-1.5708
11000	0	.00	-116.55	-116.55	-1.5708
13000	0	.00	-125.58	-125.58	-1.5708
15000	0	.00	-128.98	-128.98	-1.5708
17000	0	.00	-130.27	-130.27	-1.5708
19000	0	.00	-130.73	-130 73	-1.5708
21000	0	.00	-130.86	-130.86	-1.5708
1000	2000	-7475.19	8083.68	11010 19	2.3171
3000	2000	-1617.19	741.00	1778.87	2.7119
5000	2000	-385.38	158.82	416.83	2.7507
7000	2000	-108.76	35.33	114.35	2.8275
9000	2000	-34.87	-3.81	35.07	-3.0328
11000	2000	-12.29	-18.04	21.83	-2.1690
13000	2000	-4.62	-23.54	23.99	-1.7645
15000	2000	-1.78	-25.71	25.77	-1.6399
17000	2000	-.66	-26.54	26.55	-1.5958
19000	2000	-.21	-26.82	26.83	-1.5785
21000	2000	-.02	-26.87	26.87	-1.5716
1000	4000	-7871.57	-10551.76	13164.40	-2.2117
3000	4000	-1323.56	-1069.44	1701.62	-2.4620
5000	4000	-335.01	-203.10	391.77	-2.5966
7000	4000	-108.12	-56.04	121.78	-2.6634
9000	4000	-39.01	-25.36	46.53	-2.5651
11000	4000	-14.98	-18.42	23.74	-2.2536
13000	4000	-5.93	-16.76	17.78	-1.9109
15000	4000	-2.32	-16.30	16.46	-1.7123
17000	4000	-.83	-16.09	16.12	-1.6224
19000	4000	-.21	-15.94	15.94	-1.5838
21000	4000	.05	-15.80	15.80	-1.5677
1000	6000	12714.70	-3423.76	13167.60	-.2630

X	Y	X FIELD	Y FIELD	TOTAL	THETA
3000	6000	621.85	-834.46	1040.68	-.9304
5000	6000	17.03	-256.63	257.19	-1.5045
7000	6000	-24.18	-89.68	92.89	-1.8342
9000	6000	-15.81	-38.13	41.28	-1.9639
11000	6000	-7.83	-20.88	22.30	-1.9297
13000	6000	-3.46	-14.62	15.02	-1.8032
15000	6000	-1.33	-12.12	12.20	-1.6801
17000	6000	-.35	-11.01	11.02	-1.6024
19000	6000	.08	-10.44	10.45	-1.5631
21000	6000	.25	-10.11	10.12	-1.5462
1000	8000	1201.91	1821.65	2182.42	.9876
3000	8000	580.59	79.03	585.95	.1353
5000	8000	151.69	-83.67	173.24	-.5041
7000	8000	36.74	-56.27	67.20	-.9924
9000	8000	8.45	-31.35	32.47	-1.3076
11000	8000	1.92	-18.54	18.64	-1.4675
13000	8000	.66	-12.49	12.51	-1.5183
15000	8000	.53	-9.61	9.63	-1.5156
17000	8000	.57	-8.19	8.21	-1.5011
19000	8000	.58	-7.43	7.45	-1.4925
21000	8000	.55	-7.00	7.02	-1.4919
1000	10000	147.57	420.51	445.66	1.2333
3000	10000	199.73	141.81	244.95	.6174
5000	10000	107.87	9.84	108.32	.0909
7000	10000	46.23	-17.46	49.42	-.3612
9000	10000	19.05	-16.94	25.49	-.7270
11000	10000	8.28	-12.67	15.13	-.9921
13000	10000	4.05	-9.39	10.23	-1.1635
15000	10000	2.32	-7.38	7.74	-1.2658
17000	10000	1.54	-6.21	6.40	-1.3272
19000	10000	1.14	-5.52	5.64	-1.3677
21000	10000	.89	-5.11	5.18	-1.3982
1000	12000	35.78	144.76	149.11	1.3285
3000	12000	69.59	81.26	106.99	.8626
5000	12000	56.88	26.50	62.75	.4360
7000	12000	34.59	1.73	34.64	.0499
9000	12000	18.92	-5.70	19.76	-.2928
11000	12000	10.21	-6.73	12.23	-.5828
13000	12000	5.75	-6.07	8.36	-.8129
15000	12000	3.47	-5.24	6.28	-.9853
17000	12000	2.27	-4.58	5.11	-1.1104
19000	12000	1.59	-4.12	4.42	-1.2015
21000	12000	1.18	-3.81	3.99	-1.2695
1000	14000	12.26	63.59	64.76	1.3803
3000	14000	28.05	44.40	52.52	1.0074
5000	14000	28.97	22.21	36.51	.6540

X	Y	X FIELD	Y FIELD	TOTAL	THETA
7000	14000	22.23	7.46	23.45	.3237
9000	14000	14.87	.26	14.87	.0178
11000	14000	9.44	-2.52	9.77	-.2606
13000	14000	5.98	-3.31	6.83	-.5054
15000	14000	3.89	3.36	5.14	-.7120
17000	14000	2.64	-3.19	4.14	-.8794
19000	14000	1.87	-2.99	3.53	-1.0117
21000	14000	1.39	-2.83	3.15	-1.1152
1000	16000	5.18	32.64	33.05	1.4133
3000	16000	12.92	25.55	28.63	1.1025
5000	16000	15.35	15.88	22.08	.8024
7000	16000	13.75	7.81	15.81	.5162
9000	16000	10.66	2.66	10.98	.2445
11000	16000	7.68	-.09	7.68	-.0118
13000	16000	5.38	-1.37	5.55	-.2500
15000	16000	3.78	-1.90	4.22	-.4653
17000	16000	2.69	-2.06	3.39	-.6541
19000	16000	1.97	-2.09	2.87	-.8137
21000	16000	1.48	-2.05	2.53	-.9455

MODIFIED MALAN MODEL

CHARGE CENTER 1		CHARGE CENTER 2		CHARGE CENTER 3	
HEIGHT	COULOMBS	HEIGHT	COULOMBS	HEIGHT	COULOMBS
10000.00	20.10	5000.00	-36.80	2000.00	12.70

X	Y	X FIELD	Y FIELD	TOTAL	THETA
1000	0	.00	-19578.95	19578.95	-1.5708
3000	0	-.00	3637.27	3637.27	1.5708
5000	0	-.00	3716.05	3716.05	1.5708
7000	0	-.00	1895.86	1895.86	1.5708
9000	0	.00	834.24	834.24	1.5708
11000	0	-.00	318.36	318.36	1.5708
13000	0	-.00	74.38	74.38	1.5708
15000	0	-.00	-41.76	41.76	-1.5708
17000	0	.00	-97.60	-97.60	-1 5708
19000	0	.00	-124.44	-124.44	-1.5708
21000	0	-.00	-137.05	137.05	-1.5708
1000	2000	103233.12	27386.64	106804.06	.2593
3000	2000	-220.84	11093.19	11095.39	1.5907
5000	2000	-2687.20	4168.82	4959.85	2.1434
7000	2000	-1469.13	1723.87	2264.96	2.2766
9000	2000	-694.81	750.14	1022.49	2.3179
11000	2000	-323.74	326.33	459.67	2.3522
13000	2000	-152.78	131.82	201.79	2.4297
15000	2000	-73.20	39.62	83.24	2.6456
17000	2000	-35.29	-4.78	35.62	-3.0069
19000	2000	-16.79	-26.07	31.01	-2.1430
21000	2000	-7.61	-35.92	36.72	-1.7795
1000	4000	-106052.11	132575 97	169774.69	2.2455
3000	4000	-22433 32	12080.09	25479.06	2.6476
5000	4000	-6881.11	2186.94	7220.28	2.8339
7000	4000	-2651.36	604.03	2719.30	2.9176
9000	4000	-1133.96	219.37	1154.98	2.9505
11000	4000	-514.44	83.59	521.19	2.9805
13000	4000	-242.18	22.49	243.22	3.0490
15000	4000	-116.43	-7.75	116.69	-3.0752
17000	4000	-56.17	-22.75	60.60	-2.7568
19000	4000	-26.49	-29.72	39.81	-2.2988
21000	4000	-11.62	-32.40	34.42	-1.9151
1000	6000	-112747.42	-120485.62	165011.41	-2.3230
3000	6000	-24307.53	-12275.94	27231.50	-2.6739
5000	6000	-6793.48	-3155.99	7490.77	-2.7067

X	Y	X FIELD	Y FIELD	TOTAL	THETA
7000	6000	-2468.76	-1113.56	2708.28	-2.7179
9000	6000	-1045.96	-455.83	1140.97	-2.7306
11000	6000	-481.72	-211.68	526.18	-2.7276
13000	6000	-231.42	-113.86	257.91	-2.6844
15000	6000	-112.84	-72.00	133.85	-2.5737
17000	6000	-54.37	-52.51	75.59	-2.3736
19000	6000	-24.85	-42.35	49.10	-2.1015
21000	6000	-9.82	-36.26	37.57	-1.8354
1000	8000	6212.02	-60396.07	60714.70	-1.4683
3000	8000	-268.39	-18165.98	18167.96	-1.5856
5000	8000	-1294.72	-5611.02	5758.46	-1.7976
7000	8000	-840.03	-2057.74	2222.60	-1.9584
9000	8000	-468.22	-867.77	986.04	-2.0656
11000	8000	-251.55	-408.78	479.98	-2.1225
13000	8000	-131.84	-212.91	250.42	-2.1252
15000	8000	-66.51	-122.65	319.53	-2.0677
17000	8000	-31.09	-78.18	84.14	-1.9493
19000	8000	-12.11	-54.75	56.07	-1.7885
21000	8000	-2.16	-41.49	41.54	-1.6227
1000	10000	178385.59	-10509.62	178694.91	-.0588
3000	10000	15647.43	-6656.05	17004.27	-.4022
5000	10000	3283.88	-3374.60	4708.69	-.7990
7000	10000	794.46	-1638.40	1802.85	-1.1193
9000	10000	188.63	-817 80	839.28	-1 3441
11000	10000	36.77	-428.97	430.54	-1.4853
13000	10000	3.73	-238.40	238.43	-1.5552
15000	10000	1.04	-141.21	141.22	-1.5634
17000	10000	4.47	-89.55	89.66	-1.5209
19000	10000	7.70	-60.86	61.35	-1.4449
21000	10000	9.56	-44.18	45.20	-1.3577
1000	12000	15343.80	27077 87	31123.04	1.0553
3000	12000	9643.77	3652.56	10312.30	.3621
5000	12000	3639.16	-331 55	3654.24	-.0909
7000	12000	1391.71	-660.15	1540.34	-.4429
9000	12000	562.67	-487.56	744 52	-.7140
11000	12000	244.91	-314.33	398.48	-.9089
13000	12000	117.72	-198.32	230.62	-1.0351
15000	12000	64.31	-127.23	142.56	-1.1028
17000	12000	40.48	-84.50	93.70	-1.1241
19000	12000	28.86	-58.65	65.36	-1.1135
21000	12000	22.48	-42.67	48.23	-1.0860
1000	14000	2204.57	7239.22	7567.46	1.2752
3000	14000	3376.22	3169.39	4630.75	.7538
5000	14000	2220.67	792.93	2357.99	.3430
7000	14000	1197.03	16.01	1197.14	.0134
9000	14000	620.33	-159.92	640.61	-.2523
11000	14000	327.34	-162.03	365.25	-.4596
13000	14000	181.07	-127.25	221.31	-.6126

X	Y	X FIELD	Y FIELD	TOTAL	THETA
15000	14000	106.90	-93.18	141.81	-.7170
17000	14000	67.96	-67.41	95.72	-.7814
19000	14000	46.49	-49.41	67.85	-.8158
21000	14000	33.92	-37.15	50.31	-.8308
1000	16000	604.37	2822.63	2886.61	1.3599
3000	16000	1259.94	1806.48	2202.46	.9618
5000	16000	1160.41	819.86	1420.81	.6151
7000	16000	815.26	271.42	859.25	.3214
9000	16000	516.19	39.06	517.67	.0755
11000	16000	317.21	-40.16	319.74	-.1259
13000	16000	196.48	-57.73	204.79	-.2858
15000	16000	125.36	-54.10	136.53	-.4074
17000	16000	83.34	-45.11	94.76	-.4961
19000	16000	57.98	-36.24	68.37	-.5586
21000	16000	42.17	-28.97	51.16	-.6010

APPENDIX B

The following program, written for the HP2100 computer, is used to minimize the percentage of variation as shown in Equation 8 by varying the values of three charge centers A, B and C which are located at YA, YB and YC. One charge center is modified at a time beginning with A, then B, then C, back to A and so on until an oscillation is noticed in the percentage of variation. At that point, the value of INC can be decreased and the program restarted using the A, B and C values which were computed as the oscillation began. The output gives the values of A, B and C in coulombs and the corresponding sum of the squares of the percentage of variations.

The initial value of INC was 0.1. Oscillation using this value of INC occurred at A = 6.8, B = 13.8 and C = 3.4 for the Simpson and Robinson model. ESQRT equalled .187 x 10^4. Oscillation in the Gish and Wait model occurred at A = 2.7 and B = 5 with ESQRT equalling .813 x 10^3 while in the Malan model it occurred at A = 22.9, B = -40, C = 10 and ESQRT = .269 x 10^4.

Changing INC to equal .01 and using the A, B and C values found in the previous step resulted in the following values for the modified models:

MODIFIED MODEL	A	B	C	ESQRT
Simpson & Robinson	4.6	-11.3	5.97	522
Gish & Wait	1.52	- 2.64	0.0	624
Malan	20.1	-36.8	12.7	799

```
      PROGRAM FIELD
      REAL INC,MULT
      DIMENSION EFLD(9),X(9),EF(9),Y(9)
   11 READ (5,3) A,B,C,YA,YB,YC
    3 FORMAT (6F10.1)
      IF (A) 13,12,13
   13 READ (5,4) A1,A2,A3,A4,A5,A6,A7
    4 FORMAT (7A4)
      WRITE (6,5) A1,A2,A3,A4,A5,A6,A7
    5 FORMAT (1H1,45X,7A4,//,3X,"CHARGE CENTER A",5X,"CHARGE CENTER B", 5
     1X,"CHARGE CENTER C",/,2X,"HEIGHT",3X,"COULOMBS",3X,"HEIGHT",3X,"CO
     2ULOMBS",3X,"HEIGHT",3X,"COULOMBS")
      WRITE (6,3) YA,A,YB,B,YC,C
      VALUE=A
      INC=.1
      J=1
      EF(1)=-1310.
      EF(2)=-1160.
      EF(3)=-760.
      EF(4)=-460.
      EF(5)=-260.
      EF(6)=-135.
      EF(7)=-60.
      EF(8)=1.
      EF(9)=33000.
      X(1)=2500.
      X(2)=5000.
      X(3)=7500.
      X(4)=10000.
      X(5)=12500.
      X(6)=15000.
      X(7)=17500.
      X(8)=20000.
      X(9)=13100.
      MULT=1./(4.*3.1415*8.854*(10.**(-12)))
  131 II=1
      K=1
  130 EXQRT=0.
      DO 10 I=1,8,1
      EFLD(I)=MULT*((2.*YA*A/(X(I)**2.+YA**2.)**1.5)+(2.*YB*B/(X(I)**2.+
     1YB**2.)**1.5)+(2.*YC*C/(X(I)**2.+YC**2.)**1.5))
      ESQRT=ESQRT+(EF(I)-EFLD(I))*(EF(I)-EFLD(I))/(EF(I)*EF(I))
   10 CONTINUE
      EFLD(9)=MULT*(A/(Y(9)-YA)**2.-A/(Y(9)+YA)**2.+B/(Y(9)-YB)**2.-B/(Y
     1(9)+YB)**2.+C/(Y(9)-YC)**2.-C/(Y(9)+YC)**2.)
```

```
      ESQRT=ESQRT+(EF(9)-EFLD(9))*(EF(9)-EFLD(9))/(EF(9)*EF(9))
      ESQRT=ESQRT*100.
      IF (II-1) 20,20,30
 20   ESMIN=ESQRT
      GO TO 40
 30   IF (ESQRT-ESMIN) 20,20,50
 50   IF (II-2) 60,60,70
 60   K=-K
      VALUE=VALUE+K*INC
 40   II=II+1
      VALUE=VALUE+K*INC
      IF (ESMIN-100.) 180,180,80
 80   IF (J-1) 90,90,100
 90   A=VALUE
      GO TO 130
100   IF (J-2) 110,110,120
110   B=VALUE
      GO TO 130
120   C=VALUE
      GO TO 130
 70   IF (J-1) 140,140,150
140   A=VALUE
      VALUE=B
      J=2
      GO TO 190
150   IF (J-2) 160,160,170
160   B=VALUE
      VALUE=C
      J=3
      GO TO 190
170   C=VALUE
      VALUE=A
      J=1
190   WRITE (6,2) A,B,C,ESMIN
  2   FORMAT (4E10.3)
      GO TO 131
180   WRITE (6,6)
  6   FORMAT(//,1X,"CHARGE A",2X,"CHARGE B",2X,"CHARGE C",3X,"EFLD(1)",3
     1X,"EFLD(2)",3X,"EFLD(3)",3x,"EFLD(4)",3X,"EFLD(5)",3X,"EFLD(6)",3X
     2,"EFLD(7)",3X,"EFLD(8)",3X,"EFLD(9)")
      WRITE (6,1) A,B,C,EFLD(1),EFLD(2),EFLD(3),EFLD(4),EFLD(5),EFLD(6),
     1EFLD(7),EFLD(8),EFLD(9)
  1   FORMAT (12E10.3)
      GO TO 11
 12   END
```

Bibliography

1. Dolezalek, H. A Brief Introduction to Atmospheric Electricity. Notes from a course at Chautauqua. August-October, 1972.

2. Chalmers, J.A. Atmospheric Electricity. Pergamon Press, Oxford, 1967.

3. Tilson, S. "Electricity and Weather Modification," IEEE Spectrum, April 1969, pp. 26-45.

4. Dobson, G.M.B. Exploring the Atmosphere. Clarendon Press, Oxford, 1963.

5. Aerology for Pilots. McGraw-Hill, New York, 1943.

6. Introduction to Aviation. Aero Education Associates, California, 1970.

7. Imyanitov, I.M., Chubarina, Ye.V. and Shvarts, Ya.M. Electricity of Clouds, NASA Technical Translation TTF-718, June, 1972.

8. Gish, O.H. and Wait,G.R., "Thunderstorms and the Earth's General Electrification," Journal of Geophysical Research, V55, 1950, pp. 473-484.

9. Israil, H. Atmospheric Electricity, Keter Press, Jerusalem, 1973.

10. Wormell, T.W. "The Effects of Thunderstorms and Lightning Discharges on the Earth's Electric Field," Phil. Trans. R. Soc., VA238, pp. 249-303.

11. Markson, R. "Practical Aspects of Electrostatic Stabilization," Astronautics and Aeronautics, April 1974, pp. 44-49.

12. Lane-Smith, D.R. "The Influence of Point Discharge Current and Precipitation on the Vertical Profile of Potential Gradient," Journal of Geophysical Research, April 20, 1972, pp.2147-2150.

13. Stergis, C.G., Rein, G.C., and Kangas, T. "Electric Field Measurements Above Thunderstorms," Journal of Atmospheric and Terrestrial Physics, 1957, Vol. 11, pp. 83-90.

14. Shvarts, Ya.M. "Calculation of the Electrical Structure of Thunderclouds," Studies in Atmospheric Electricity, Keter Press, Jerusalem, 1974

15. Hill, M.L. "Introducing the Electrostatic Autopilot," Astronautics and Aeronautics, Nov. 1972, pp. 24-31.

16. Mason, B.J. The Physics of Clouds, Clarendon Press, Oxford, 1971.

Section IV

Aircraft Noise Suppression -

Electronic Acoustic Noise Suppression

TABLE OF CONTENTS

INTRODUCTION

An alternative to passive sound insulation is active electronic control. In the approach, described earlier by Olson [1,2] and others [3,4], one connects a microphone, an inverting amplifier, and a loudspeaker in a negative feedback fashion to reduce noise. In this system (figure 1), the electric signal produced by the microphone from an incident sound pressure P_i, is amplified by an inverting amplifier with a gain of $-K_a$. The amplifier drives the loudspeaker, producing an output pressure P_o. This pressure is summed acoustically with the incident sound pressure P_i. The resulting pressure at the microphone is the sound pressure error signal, P_ε;

$$P_\varepsilon = P_i + P_o$$

The resulting sound pressure level P_ε at the microphone has been shown to be less than the incident sound pressure level P_i, [1,2,5]. If the microphone is placed near one's ear, a considerable reduction in the noise level is observed. However, airborne noise reduction through active electronic control is confined to a fairly narrow range of frequencies.

This treatise will show that signal time delays from wave propagation through the acoustic medium and inherent transducer delay are responsible for this narrow bandwidth limitation. A classical method of lag-lead compensation will be used to improve the bandwidth of airborne-noise-reduction systems developed in the references [1,2,5]. Finally, lag-lead compensation using maximally-flat (Butterworth) and equal-ripple (Chebyshev) polynomials will be developed to further extend the bandwidth.

MATH MODEL

The active compensation system of figure 1 is depicted schematically by the block diagram in figure 2. Here, $-K_a$ represents the gain of an ideal amplifier. $G_m(s)$, $G_f(s)$, and $G_s(s)$ are the transfer functions of the microphone, filter, and loudspeaker respectively, in the s domain. (The transfer function $G_f(s)$ is the principle topic of this paper and is discussed below in detail.) System time delay τ is represented by $e^{-S\tau}$. T' is transformation from the time domain to the frequency domain has been accomplished according to the Laplace shift theorem:

$$L\{y(t-\tau)\ U_\tau(t)\} = e^{-S\tau}\ Y(s), \quad \text{where } U_\tau(t) = \begin{cases} 0 & t<\tau \\ 1 & t\geq\tau \end{cases} \tag{2}$$

$$\tau = \tau_p + \tau_t, \quad \text{where } \tau_p = \text{wave propagation delay}, \quad \text{and } \tau_t = \text{total transducer delay}. \tag{3}$$

Time delay τ is the sum of transducer delay and acoustic wave propagation delay. When time delay is present in a feedback control system, numerical analysis of that system is difficult because of the introduction of the transcendental function $e^{-S\tau}$, in the transfer function. However, a graphical approach is often adequate for stability analysis of feedback systems with time delay. This is the method used here.

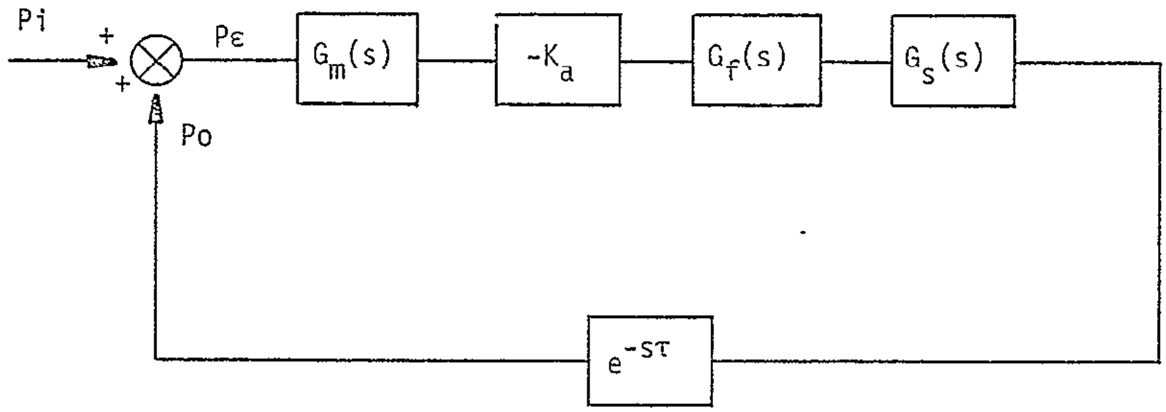

Block diagram representation

Figure 2

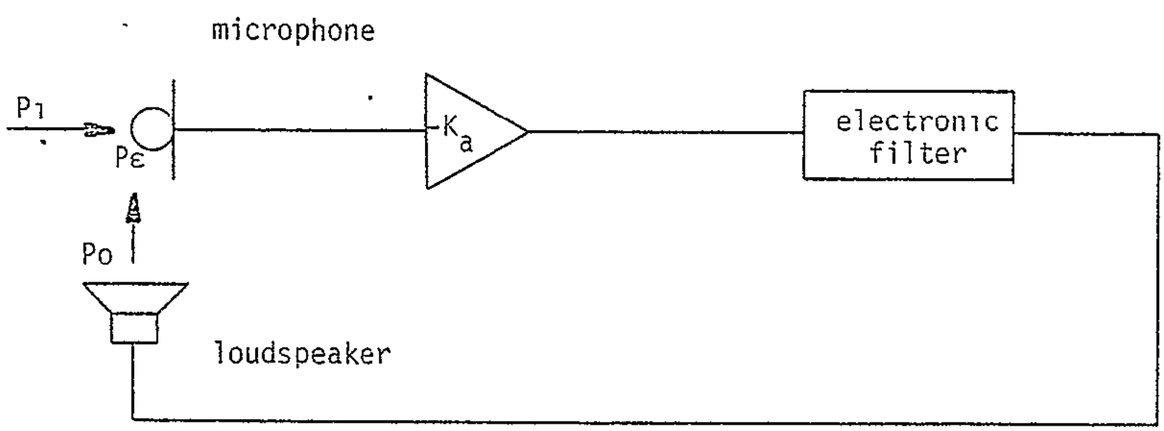

Active compensation scheme

Figure 1

The open-loop response (where $G_f(s) \equiv 1$) of an active electronic airborne-noise controller are shown in figures 3a and 3b. At the higher frequencies, the phase-frequency relationship becomes linear, indicating the presence of time delay. This is graphically illustrated in figure 4. Note that the system phase is the sum of the phase associated with two poles and the phase that represents pure time delay. At high frequencies, for which all phase associated with poles and zeros can be considered a constant, the delay τ of equation (4) is simply the slope of the system phase function.

$$\angle e^{-j\omega\tau} = -\omega\tau \tag{4}$$

For the system represented in figures 3a, 3b, and 4 a time delay of 49 μsecs is determined. Meeker [5] achieved this result with a microphone-speaker separation of 3.1 mm (.125 inch), which accounts only for 9 μsecs of signal delay due to acoustic wave propagation (with an acoustic wave velocity of 347 meters/sec.) Approximately 40 μsecs of delay must be attributed to the transducers. This conclusion is substantiated by the work of C.A. Ewaskio and O.K. Mawardi [6]. Their measurements of phase shift in loudspeakers indicated time delays of the magnitude found above. Transducer delay τ_t in equation (3) is equal to 40 μsecs for the system of figures 3a and 3b.

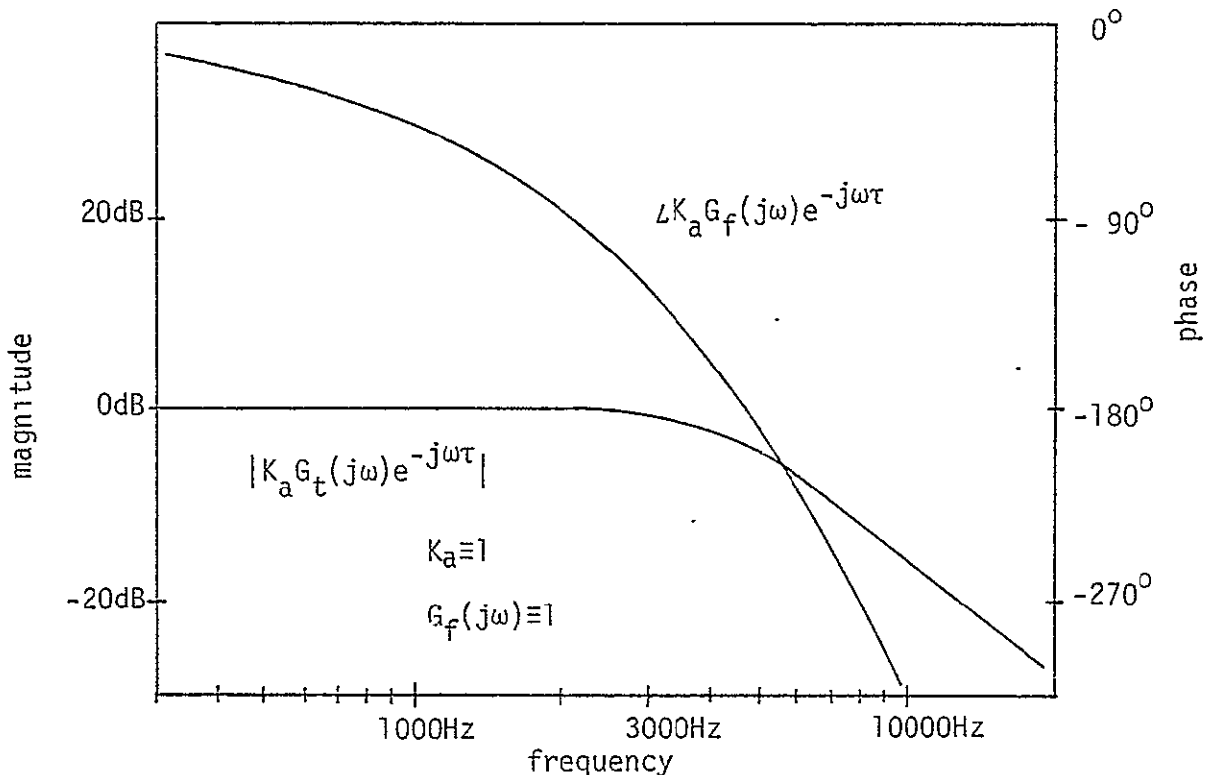

Open-loop frequency response of an airborne-noise controller

Figure 3a

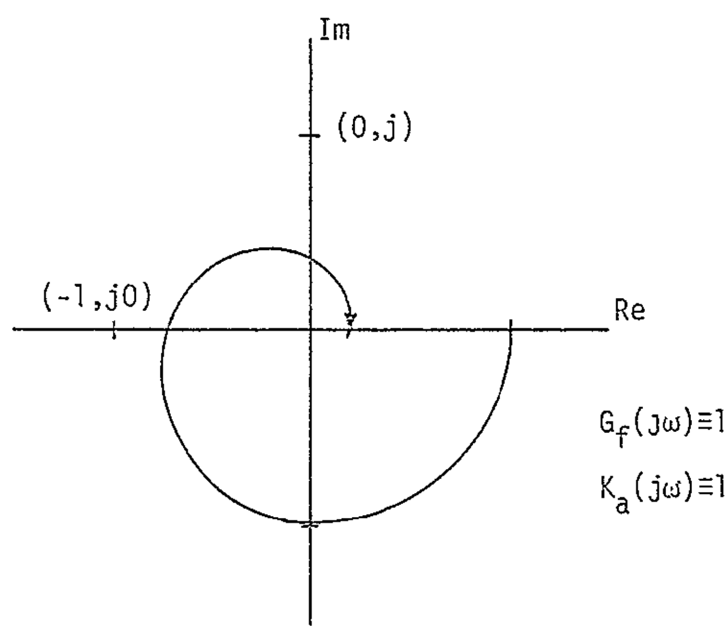

nyquist diagram of figure 3a

Figure 3b

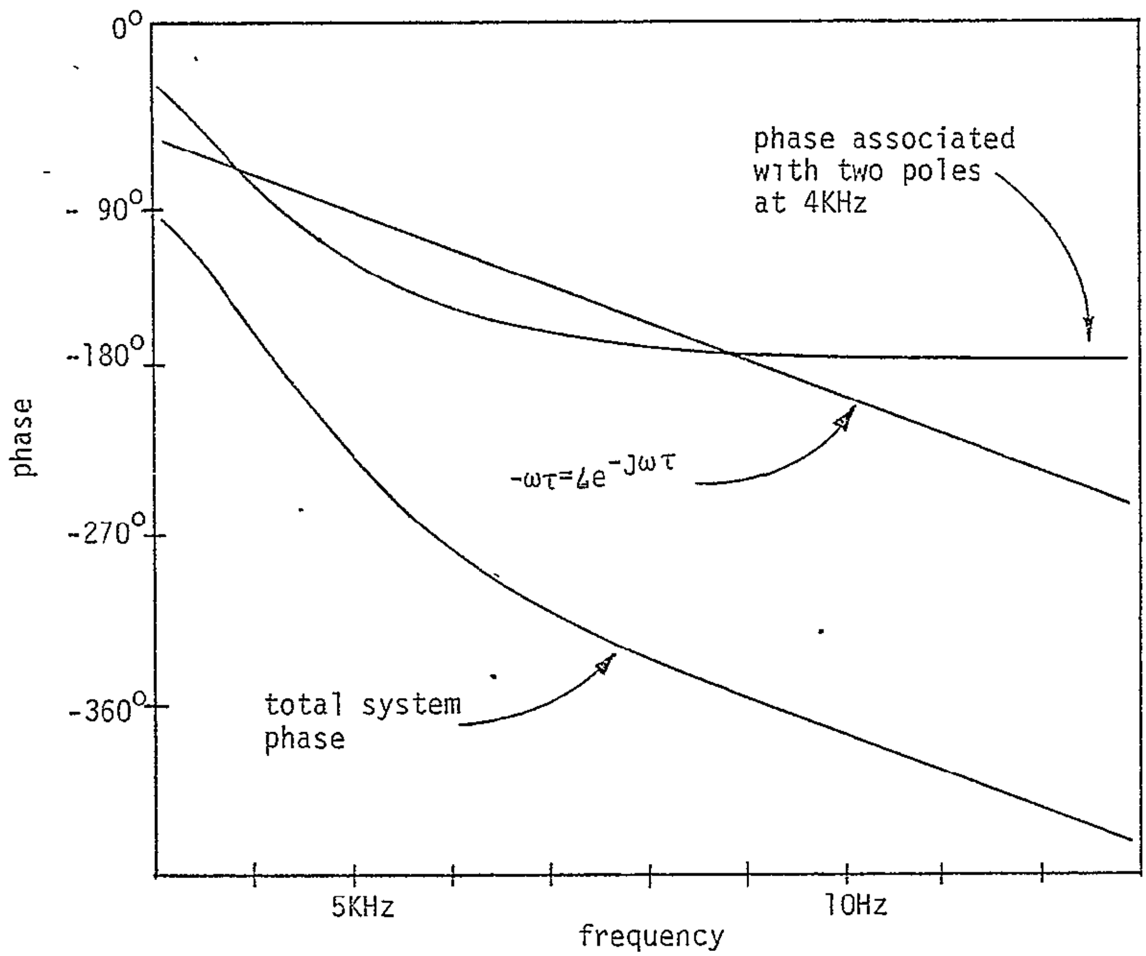

Open-loop phase with $G_f(j\omega) \equiv 1$

Figure 4

The magnitude function in figure 3a indicates a bandwidth of 4 KH_z, at which point it rolls-off at -12 dB/octave. For this sytem to achieve stability without compensation, the open-loop gain must be made less than unity.

Lowering the gain of the system, however, decreases its effectiveness. The acoustic noise intensity I_r is calculated by comparing the sound pressure error signal P_ε with the original incident sound pressure P_i. I_r in decibels is:

$$I_r(j\omega) = 20 \log_{10} \frac{P_i(j\omega)}{P_\varepsilon(j\omega)} \tag{5}$$

The sound pressure is measured at the microphone's diaphragm, P_ε is measured with the active electronic control functioning, P_i is measured with the system off.

From the block diagram (figure 2), P_ε for real frequencies is,

$$P_\varepsilon(j\omega) = \frac{P_i(j\omega)}{1+K_a G_t(j\omega) e^{-j\omega\tau}} \; , \tag{6}$$

$$\text{where } G_t(j\omega) \stackrel{\Delta}{=} G_m(j\omega)G_f(j\omega)G_s(j\omega).$$

Substituting into equation (5), I_r becomes

$$I_r(j\omega) = 20 \log_{10} \left| 1+K_a G_t(j\omega)\, e^{-j\omega\tau} \right|. \tag{7}$$

For those real frequencies ω, where the open-loop gain is much greater than unity, $|K_a G_t(j\omega)\ e^{-j\omega\tau}| >> 1$, the reduction in the acoustic noise intensity at the microphone's diaphragm is approximately equal to the system's open-loop gain.

$$I_r(j\omega) \cong 20 \log_{10} |K_a G_t(j\omega)|,\ \text{since}\ |e^{-j\omega\tau}| \equiv 1. \quad (8)$$

Thus, for maximum noise reduction, the open-loop gain should be kept as high as possible.

SYSTEM DESIGN

To obtain both stability and high gain, bandwidth of the system must be sacrificed. This conclusion will be made clear through graphical stability analysis in the form of a Nyquist diagram. A polor plot of the open-loop frequency response of $K_a G_t(j\omega)e^{-j\omega\tau}$ for $-\infty \leq \omega \leq \infty$ is constructed. This plot is referred to as a Nyquist diagram of $K_a G_t(j\omega)e^{-j\omega\tau}$, see figure 3b. A minimal-phase (no right half-plane zeros) closed-loop system is stable if and only if the Nyquist diagram of $K_a G_t(j\omega)e^{-j\omega\tau}$ does not encircle the $(-1, j0)$ critical point on the complex plane.

Olson [1,2] and Meeker [5] used lag compensation to obtain stability, simultaneously obtaining high open-loop gain over a narrow range of frequencies, see figures 5a and 5b. To obtain a gain of 20dB, the bandwidth had to be lowered to 200Hz. The compensated noise-reducing system of figure 4a has a filter $G_f(j\omega)$, where

$$G_f(j\omega) = \frac{1}{j\omega/1250 + 1}. \quad (9)$$

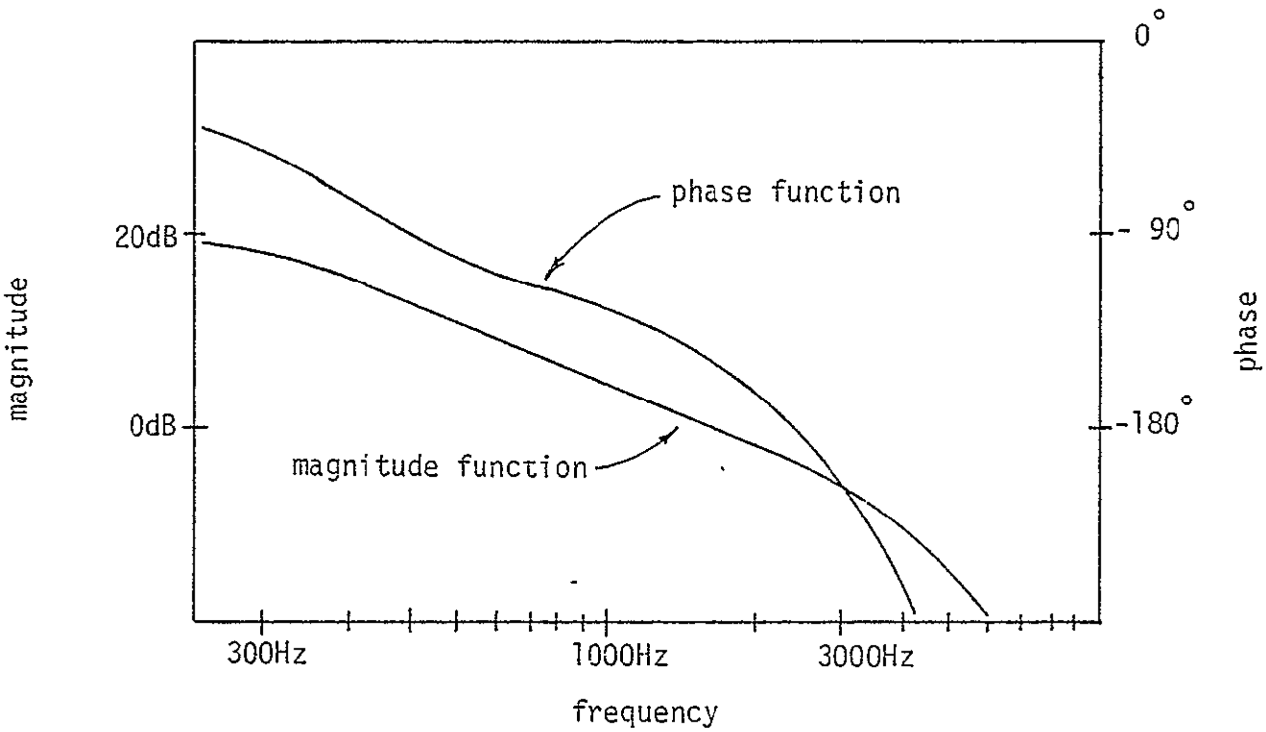

System developed by Olson [1,2]

Figure 5a

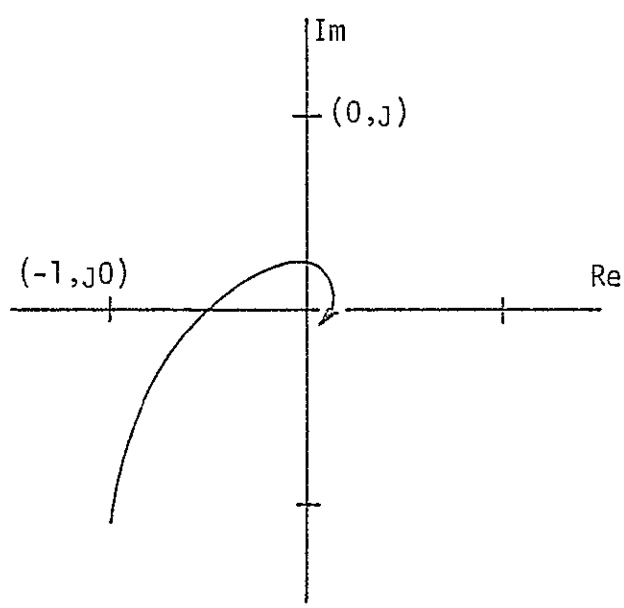

Nyguist diagram of Figure 5a

Figure 5b

The filter $G_f(j\omega)$ has one pole at 200 Hz. Thus, the Nyquist diagram avoids encirclement of the (-1,j0)critical point, producing a stable system.

From equation (8) and figure 5a, reduction in the noise intensity is found to be approximately 20dB up to a frequency of 200 Hz. To increase the bandwidth of the system in figures 4a and 4b one would like to raise the crossover frequency ω_{-180} of $\angle e^{-j\omega\tau}$. (ω_{-180} is defined to be the frequency where $\angle e^{-j\omega\tau}$ is equal to -180 degrees). One would like to move ω_{-180} to infinity, that is eliminate the time delay; however, this is not physically realizable. In the airborne-noise-reduction system investigated, a large percentage of the time delay is associated with transducers. With present state-of-the-art transducers, little can be done to reduce the inherent time delay. Therefore, to avoid encirclement of the (-1,j0) point on the Nyquist diagram, the magnitude function must be less than unity before the frequency ω_{-180}. Consequently, this frequency, ω_{-180} must be considered the upper limit on an airborne-noise-reduction system's bandwidth.

If the bandwidth is to be increased, it must be done through manipulation of the magnitude function. An increase in the bandwidth may be realized if the magnitude function is made to roll-off at a greater rate than that of the one-pole filter in figure 5a. This allows the -3dB bandwidth to move closer to the upper limit, ω_{-180}. In a minimal-phase system increased roll-off is always accompanied by additional phase. Hence, trade-offs must be made.

Lag-lead compensation is commonly used to reduce gain while minimizing excess phase. The transfer function of a lag-lead compensator consists of a simple pole-zero pair:

$$G_f(j\omega) = \frac{1+j\omega/\omega_z}{1+j\omega/\omega_p} \quad . \tag{10}$$

The pole is always nearer the origin of the s plane than the zero. Note that the magnitude function, $G_f'(j\omega)$, has an initial gain of unity. As ω approaches infinity, the gain becomes ω_p/ω_z. Moreover, the phase function returns to zero as ω goes to infinity. Lag-lead compensation allows the magnitude function to decrease while introducing smaller amounts of excess phase than lag compensation.

The use of a first-order (both denominator and numerator are first order polynomials) lag-lead compensator in the airborne-noise-reduction systems of the references [1,2,5] would extend the bandwidth to 300Hz, see figures 6a and 6b. The pole-zero location of the compensator have been determined graphically and found to be

$$G_f'(j\omega) = \frac{1+j\omega/2.51\text{x}10^4}{1+j\omega/1880} \tag{11}$$

A graphical approach for finding the pole and zero locations of a lag-lead compensator is quite adequate for a single-input, single-output closed-loop system. The location of the pole and zero is left to the designer. The

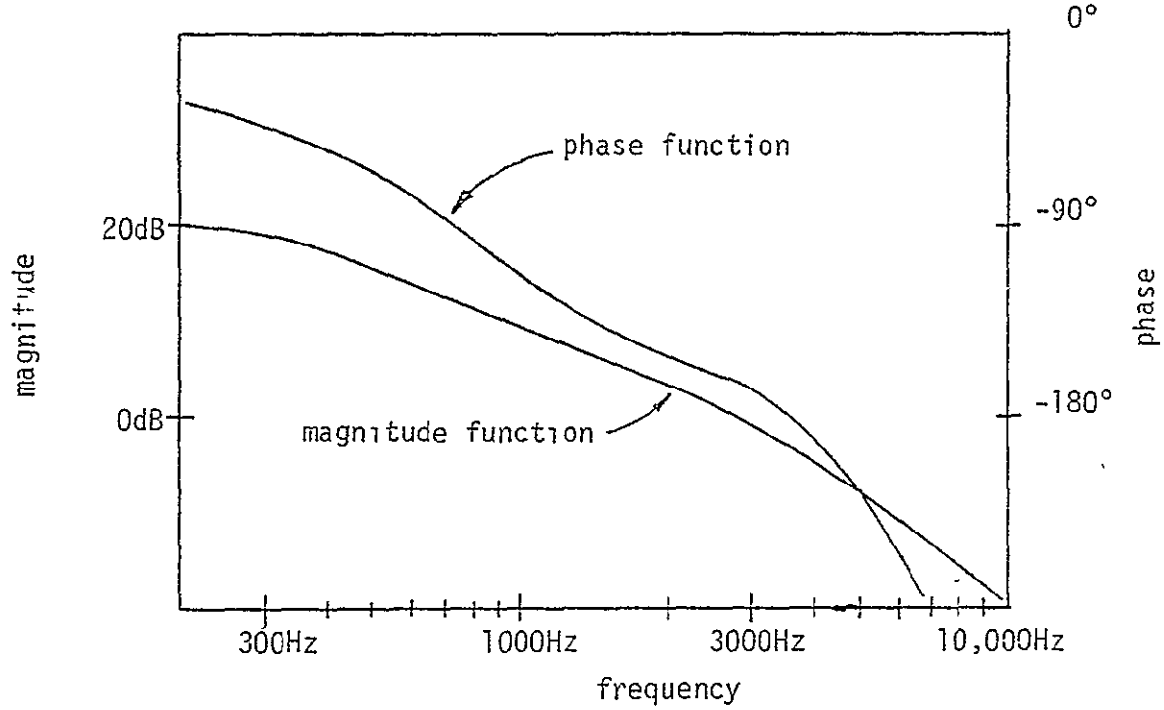

Olson's system with first-order lag-lead compensation

Figure 6a

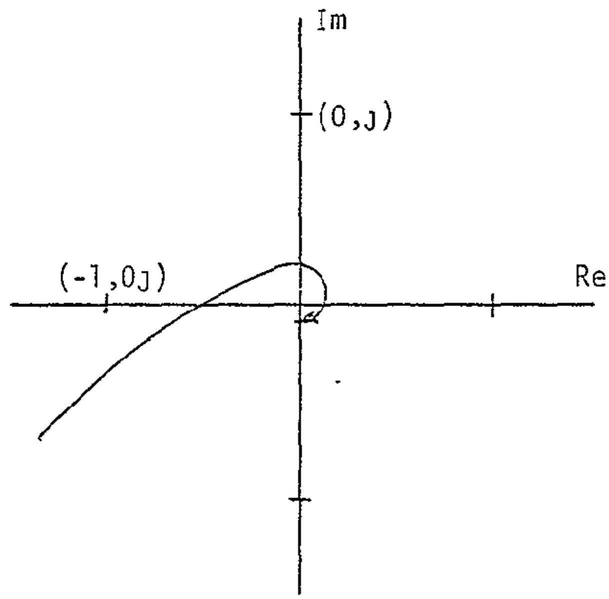

Nyquist diagram of Figure 6a

Figure 6b

proper phase and gain margins may then be selected for desired overshoot and damping. Insofar as the noise-reduction system can be approximated by a second-order system, the phase-gain margin concept will be a graphical convenience which can provide approximate closed-loop analysis by inspection. Criteria for phase and gain margins will not be discussed, except for the statement that phase margin greater than 55 degrees and a gain margin greater than 6dB are desirable. This gives an approximate closed-loop damping >.55.

The ideal normalized (the -3dB bandwidth frequency, defined as ω_{-3dB}, is equal to one) lag-lead compensator is characterized by a magnitude that is unity for frequencies, $\omega \leq 1$ and can be represented by $1/K_f$, for frequencies $\omega > 1$. These ideal properties are not attainable with constant, lumped, and linear networks, therefore the requirements imposed by the ideal characteristics can be only approximated. This is done by allowing the magnitude and phase to stay within prescribed limits of the ideal, see figures 7a and 7b.

It is evident from the magnitude function graphed in figures 8a and 8b that cascading more than one first-order lag-lead compensator results in a magnitude function $|G_f'(j\omega)|$ that tends away from the ideal. Also from figure 8b, it is evident that excess phase is increased with increased number of cascaded filters.

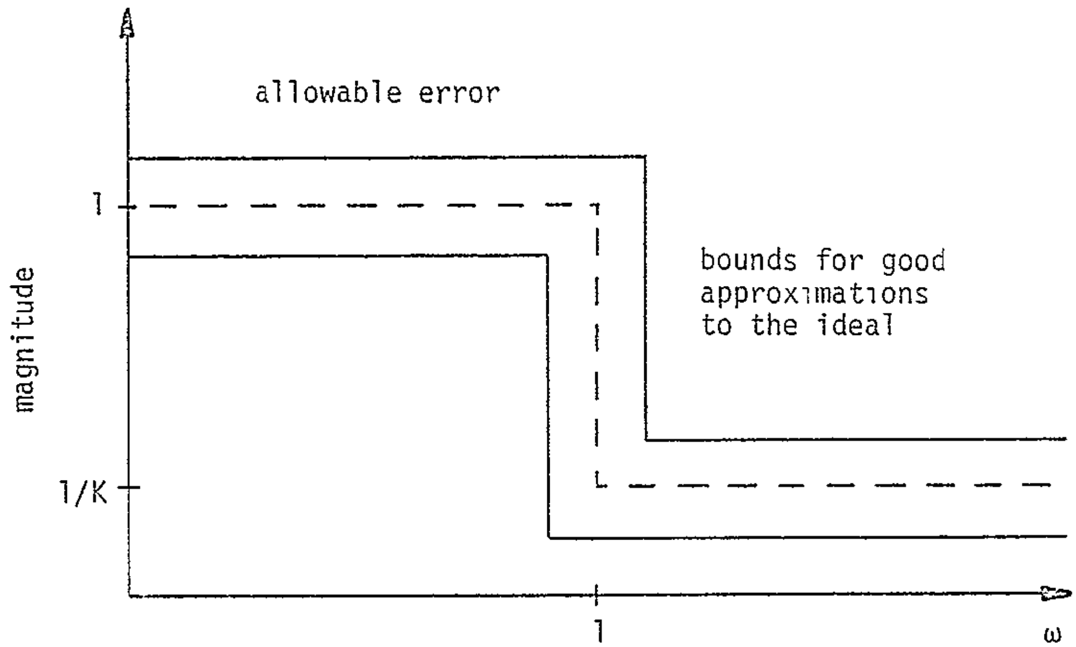

Ideal log-lead magnitude function

Figure 7a

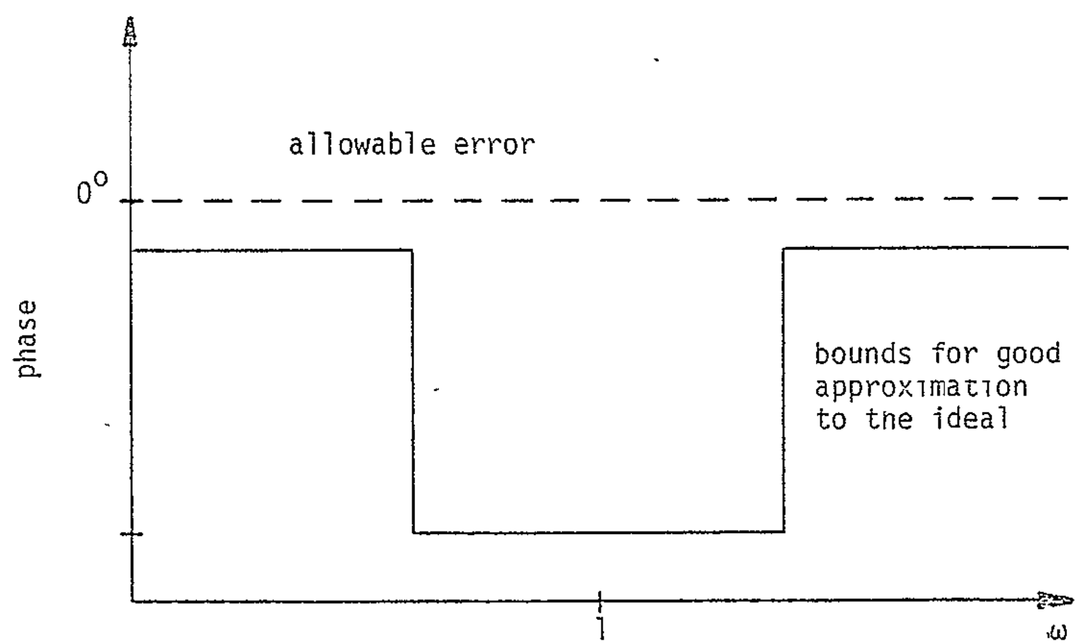

Ideal lag-lead phase function

Figure 7b

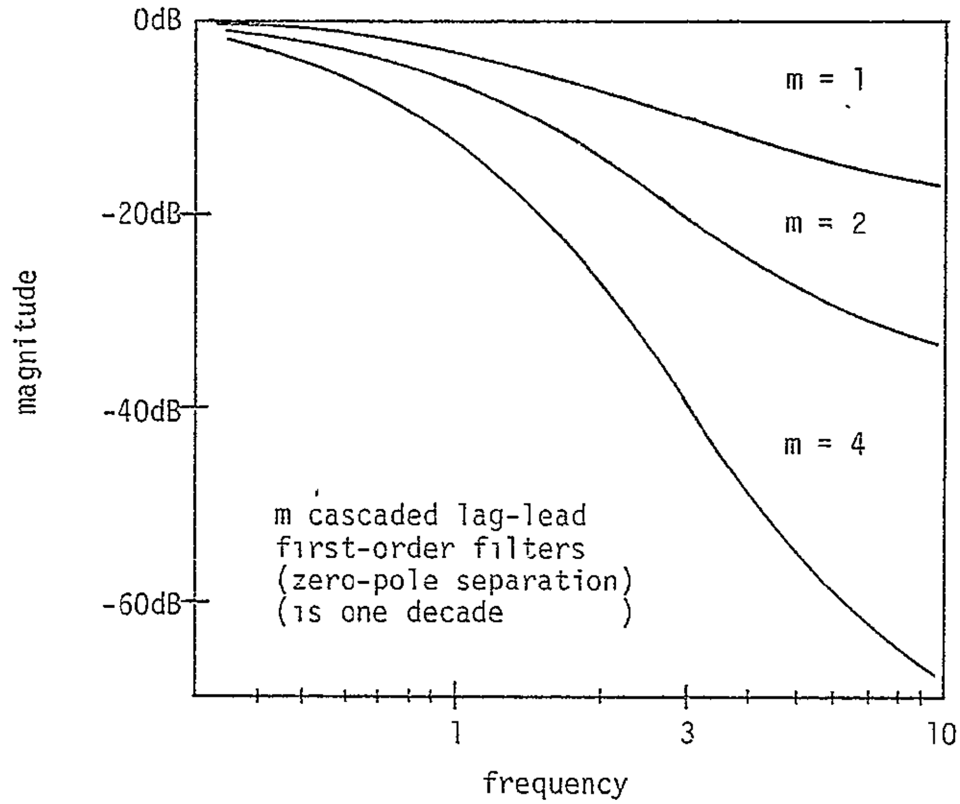

Figure 8a

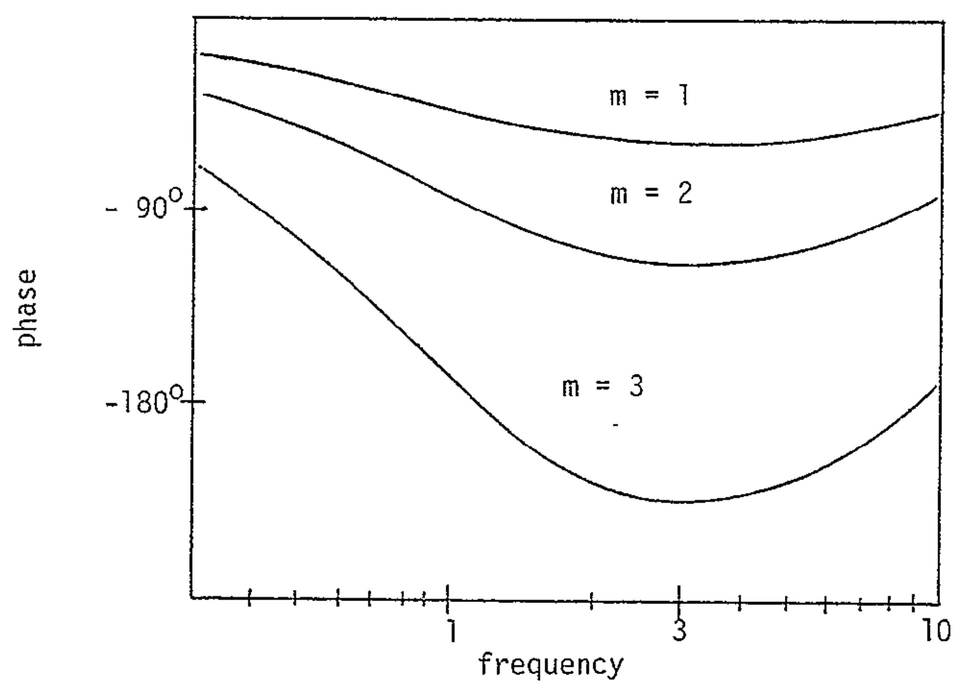

Figure 8b

BUTTERWORTH-CHEBYSHEV LAG-LEAD COMPENSATION

Functions of the form

$$G_f(s) = \frac{N(s)}{D(s)} , \tag{12}$$

which obey the specified constraints of figures 7a and 7b, represent approximations to the ideal lag-lead filter. Combinations of the maximally-flat (Butterworth) and the equal-ripple (Chebyshev) polynomials provide candidate approximations to the ideal.

The excess phase associated with the maximally-flat function increases with frequency at a much smaller rate than that of the equal-ripple polynomial, see figure 9a and 9b. Of the four ratio combinations, representing the equal-ripple polynomial by N(s) (which contributes positive phase) and the maximally-flat polynomial by D(s) (which contributes relative little negative phase) yields the most desirable phase function.

A suitable representation of this lag-lead compensator can be obtained by starting with the general expression of the magnitude-squared function. Let

$$|G_f''(j\omega)|^2 = \frac{N(\omega^2)}{D(\omega^2)} , \tag{13}$$

for real frequencies ω.

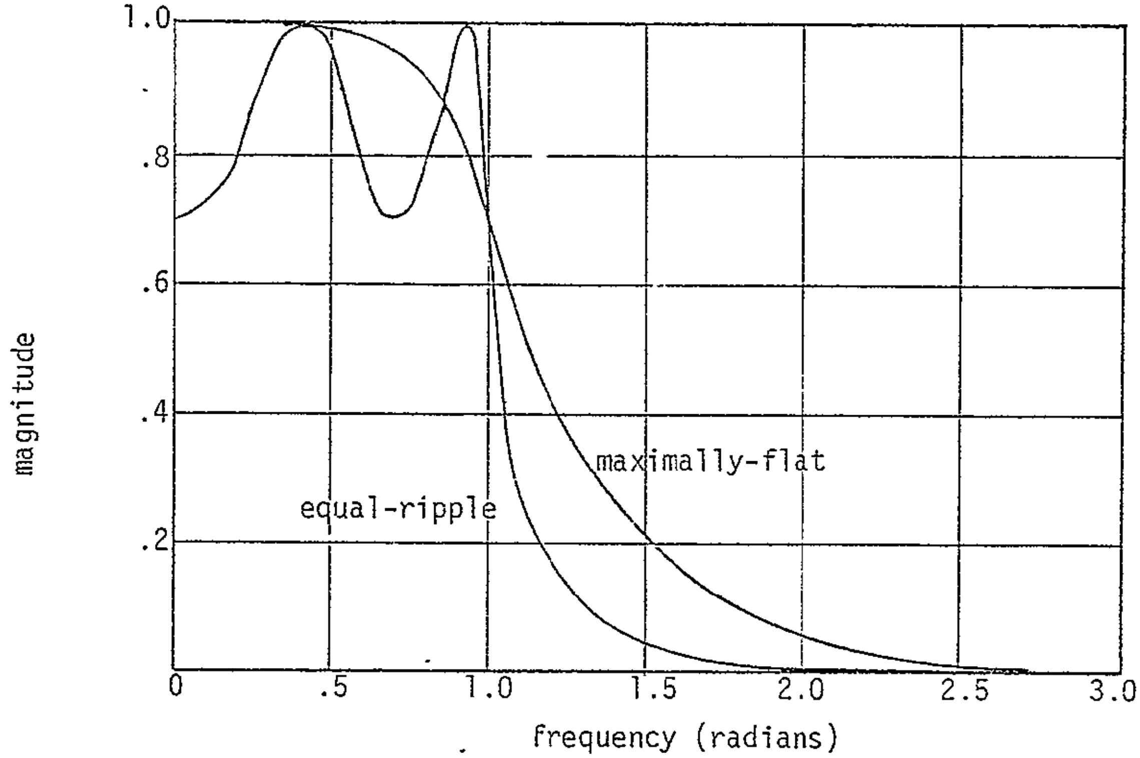

Fourth-order Butterworth and Chebyshev magnitude function

Figure 9a

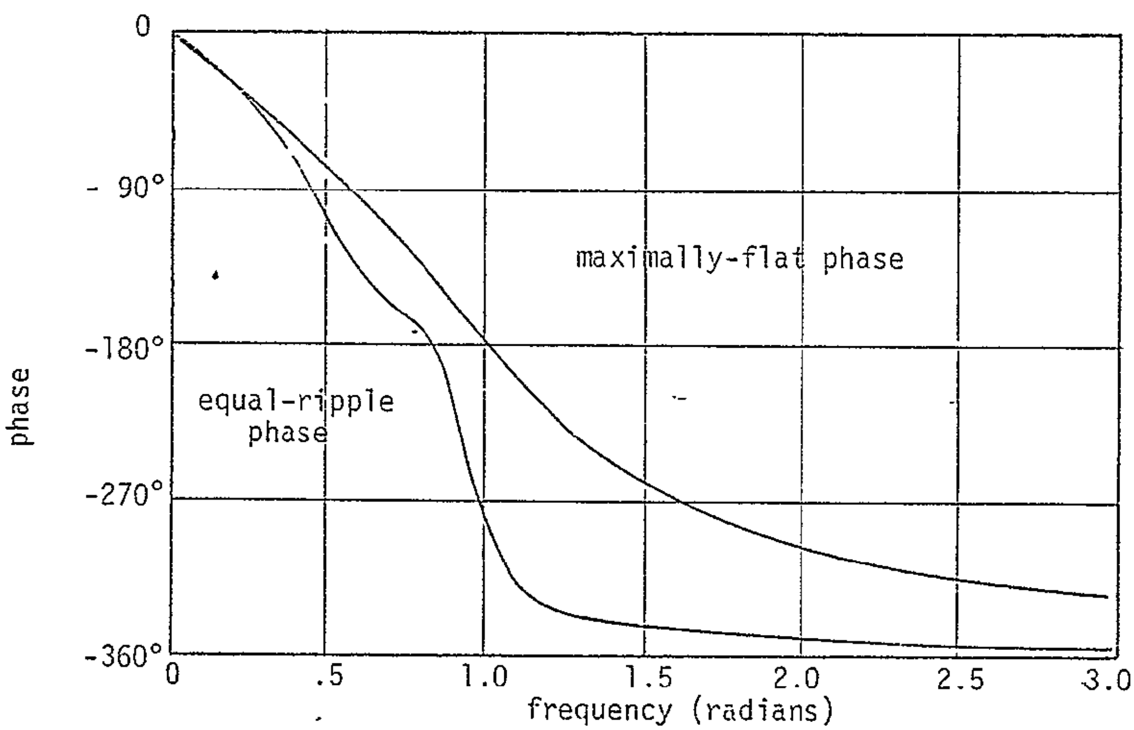

Fourth-order Betterworth and Chebyshev phase function

Figure 9b

For frequencies $\omega \leq 1$ the magnitude-squared function of the normalized filter $G_f(j\omega)$ should be approximately unity. For frequencies $\omega > 1$ the function should not depart appreciably from $1/K_f^2$. The filter design to be discussed in detail is

$$|G_f''(j\omega)|^2 = \frac{1+\varepsilon^2 C_n^2\left(\frac{1}{\alpha\omega}\right)}{K^2+\varepsilon^2 \dfrac{2^{2(n-1)}}{(\alpha\omega)^{2n}}}, \tag{14}$$

where the $C_n(x)$ are called the Chebyshev polynomials.

$$C_n^2\left(\frac{1}{\alpha\omega}\right) = \cos^2\left(n \cos^{-1} \frac{1}{\alpha\omega}\right) \tag{15a}$$

$$= \cosh^2\left(n \cosh^{-1} \frac{1}{\alpha\omega}\right). \tag{15b}$$

Although either form of $C_n^2(1/\alpha\omega)$ can be employed, it is convenient to use equation (15a) for frequencies $1/\alpha\omega \leq 1$ and equation (15b) for $1/\alpha\omega \geq 1$.

It will presently be shown that $|G_f''(j\omega)|^2$ is a ratio of an equal-ripple polynomial $(N(\omega^2))$ to a maximally-flat polynomial $(D(\omega^2))$

For real frequencies ω, when $\omega \to 0$,

$$|G_f''(j\omega)|^2_{\omega\to 0} \cong \frac{\varepsilon^2 C_n^2\left(\frac{1}{\alpha\omega}\right)}{\varepsilon^2 \dfrac{2^{2(n-1)}}{(\alpha\omega)^{2n}}} = 1 \tag{16a}$$

because

$$\cosh^2\left(n \cosh^{-1} \frac{1}{\alpha\omega}\right) \cong 2^{2(n-1)}\left(\frac{1}{\alpha\omega}\right)^{2n}, \text{ for } \frac{1}{\alpha\omega} > 1 \tag{16b}$$

For real frequencies ω, when $\omega \to \infty$,

$$|G_f''(j\omega)|^2_{\omega\to\infty} \cong \begin{cases} 1/K^2 & \text{for } n \text{ odd} \\ (1+\varepsilon^2)/K^2 & \text{for } n \text{ even,} \end{cases} \tag{17a}$$

when n is the order of the polynomial.

This is true because

$$\cos^2(n\cos^{-1}\frac{1}{\alpha\omega}) = \cos^2(n\frac{\pi}{2}), \text{ for } \frac{1}{\alpha\omega} \ll 1. \tag{17b}$$

For frequencies $\omega > 1/\alpha$, $C_n^2(1/\alpha\omega)$ is a cosine-squared function. Therefore

$$0 \leq |C_n^2(1/\alpha\omega)| \leq 1. \tag{18}$$

The magnitude characteristic of $N(\omega^2)$ is equal-ripple in nature, the numerator of $|G_f''(j\omega)|^2$ will swing between 1 and $1+\varepsilon^2$ exactly n times, for $\omega > 1/\alpha$.

Note that

$$|N(\omega^2)| = 1 \qquad \text{when } C_n^2(1/\alpha\omega) = 0.$$

This occurs when $\omega = \frac{1}{\alpha} \sec\frac{\pi k}{2n}$ (where $k = 1,3,5,\cdots$).

Also,

$$|N(\omega^2)| = 1+\varepsilon^2 \qquad \text{when } C_n^2(\frac{1}{\alpha\omega}) = 1.$$

This occurs when $\omega = \frac{1}{\alpha}\sec\frac{\pi k}{n}$ (where $k=0,1,2,\cdots$).

Because the parameter ε controls the amount of ripple for $\omega > 1/\alpha$, it is called the ripple factor.

All filter designs discussed will be normalized about the filter's -3dB frequency, ω_{-3dB}; thus $\omega_{-3dB} = 1$. The normalizing parameter α is the value for which

$$|G_f''(j\omega_{-3dB})|^2 = \frac{1}{2} \tag{19}$$

The value of α must be solved by a successive-approximation. The value of α as a function of K_f/ε for different n is shown in figure 10. If the approximation (16b) is valid for ω=1, then

$$C_n^2(\frac{1}{\alpha}) \cong 2^{2(n-1)} \frac{1}{(\alpha)^{2n}}, \text{ for } \frac{1}{\alpha} > 1.$$

Substituting for $C_n^2(1/\alpha)$ in equation (14),

$$|G_f''(j\omega)|^2_{\omega=1} = \frac{\varepsilon^2\, 2^{2(n-1)} \frac{1}{\alpha^{2n}}}{K_f^2 + \varepsilon^2 \frac{2^{2(n-1)}}{\alpha^{2n}}} = \frac{1}{2}.$$

Solving for the normalizing parameter α,

$$\alpha = \left(\frac{\varepsilon}{K_f}\right)^{1/n} 2^{(n-1)/n} < 1. \tag{20}$$

This result is displayed in figure 10, where it is compared with the calculated value of the normalizing parameter α. Note that equation (20) is valid for α less than unity, because cosh(x) in the Chebyshev polynomial may be approximated by $e^x/2$. Therefore, equation (20) can be considered valid when

$$\frac{K_f}{\varepsilon} > 2^{n-1}. \tag{21}$$

Also of interest is the frequency $\omega = 1/\alpha$. $|G''_f(j\omega)|^2$ becomes

$$|G''_f(j\omega)|^2_{\omega=\frac{1}{\alpha}} \cong \frac{1+\varepsilon^2}{K_f^2+\varepsilon^2 2^{2(n-1)}} \quad . \tag{22}$$

However, if inequality (21) is valid, then from (22)

$$|G''_f(j\omega)|^2_{\omega=\frac{1}{\alpha}} \cong \frac{1+\varepsilon^2}{K_f^2} \quad . \tag{23}$$

The denominator D(s) becomes a better approximation to K_f^2 for $\omega > 1/\alpha$. Since the numerator N(s) for these frequencies swings between 1 and $1+\varepsilon^2$ (see equation (18)). the magnitude-squared function $|G''_f(j\omega)|^2$ will swing $1/K_f^2$ and $(1+\varepsilon^2)/K_f^2$, n times. This ripple effect begins at $\omega=1/\alpha$ which may be considered the corner frequency of the numerator. The above characteristics are diagrammatically illustrated in figure 11.

Heretofore, just the magnitude function has been studied, because phase information cannot be obtained from magnitude-squared functions. To acquire the phase functions, the roots of the equal-ripple and maximally-flat polynomials must be found. Expressing the magnitude-squared function as

$$|G_f(j\omega)|^2 = G_f(j\omega)G_f(-j\omega) \tag{24a}$$

or

$$|G_f(j\omega)|^2_{-s^2=\omega^2} = G_f(s)G_f(-s) \quad , \tag{24b}$$

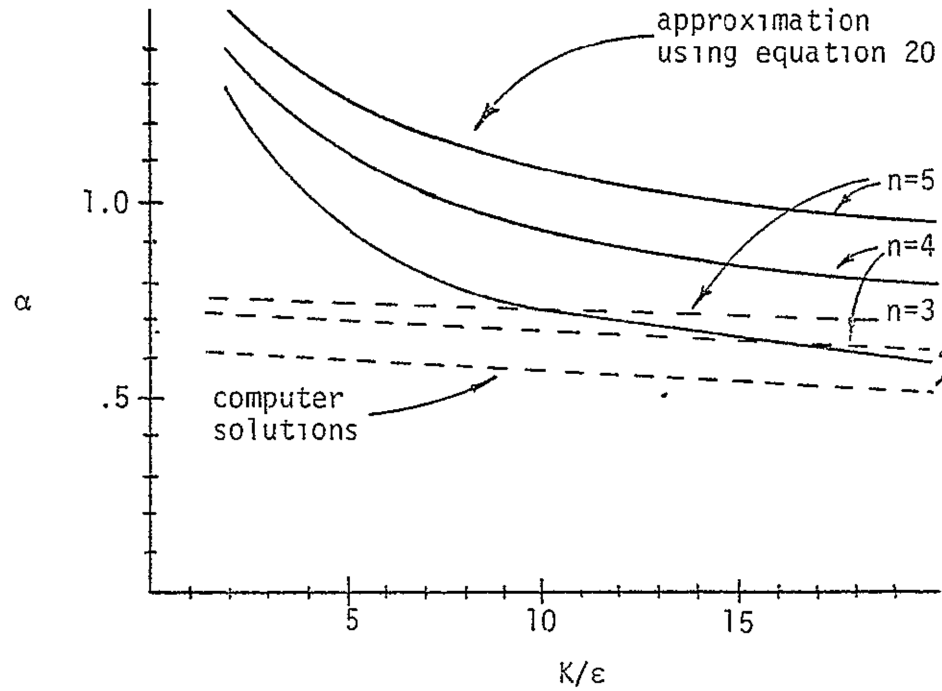

Figure 10

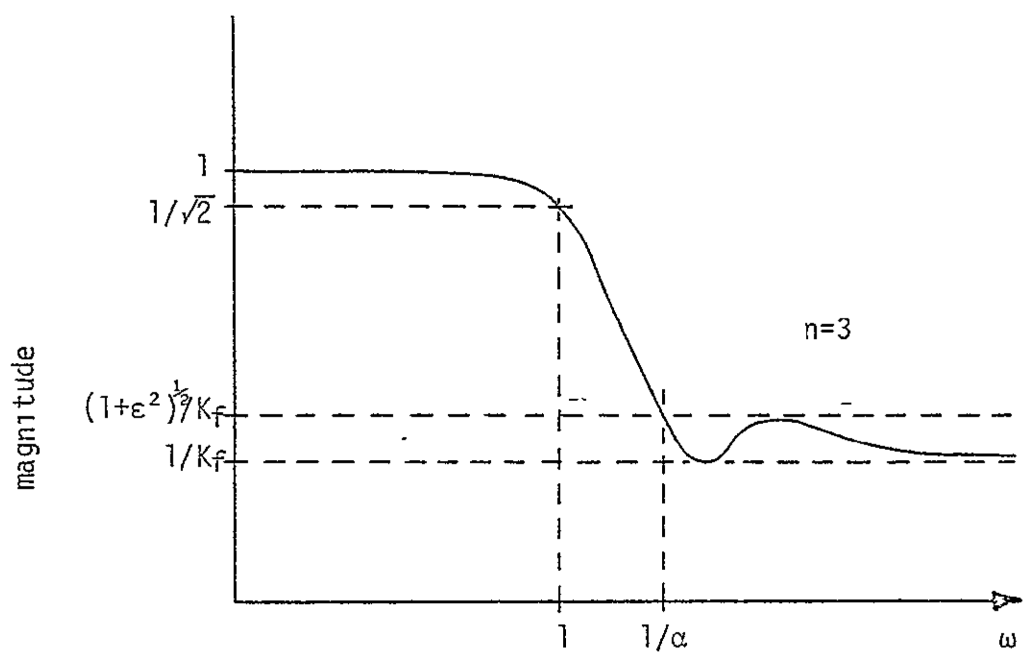

Figure 11

$G_f(s)$ may be found. It should be remembered that although the notation is in terms of the imaginary variable $j\omega$, the variable which appears in the function is the real variable ω^2 (for example see (14)). The desired generalization is made by substituting s/j for ω. The remaining problem is to separate equation (24b) into its two constituents, $G_f(s)$ and $G_f(-s)$. This is done by realizing that $G_f(s)G_f(-s)$ contains the poles and zeros of $G_f(j\omega)$ and their mirror images with respect to the $j\omega$ axis. Therefore, to assure a stable minimal-phase system one assigns all the left half-plane roots to $G_f(j\omega)$.

Solving the denominator of equation (14) by substituting s/j for ω, $D(s)D(-s)$ becomes

$$D(s)D(-s) \;=\; K_f^2 + \varepsilon^2 \frac{2^{2(n-1)}}{(-1)^n \alpha^{2n} s^{2n}} \;=\; 0 \,. \tag{25a}$$

To simplify the computation, a new variable p is defined: $p=1/s$. Substituting into (25a),

$$p^{2n} \;=\; (-1)^n \frac{\alpha^{2n} K_f^2}{\varepsilon^2 2^{2(n-1)}} \,. \tag{25b}$$

Solving for the 2n roots,

$$p_m = \sqrt[n]{\frac{2^n K_f}{\varepsilon 2^{n-1}}}\; e^{j\,\frac{\pi}{2}\left(1+\frac{2m-1}{n}\right)} \quad \text{, where m } 1,2,3,\cdots,2n. \tag{25c}$$

The n left half-plane roots, p_k, may be found from (25c) to be

$$p_k = \sqrt[n]{\frac{\alpha^n K_f}{\varepsilon 2^{n-1}}}\ [-\sin\frac{\pi}{2n}(2k-1) + j\cos\frac{\pi}{2n}(2k-1)] \qquad (25d)$$

, where $k=1,2,\cdots,n$.

The roots p_k lie on a circle of radius $\sqrt[n]{\frac{\alpha^n K_f}{\varepsilon 2^{n-1}}}$. Note that if the normalizing parameter α is approximated by (20) the circle becomes a unit circle.

The function D(s) is found by replacing p with 1/s;

$$D(s) = C_o[D(p)\,|_{s=\frac{1}{p}}]. \qquad (25e)$$

Since D(s) is constructed from the roots, and the roots solve all polynomials that are multiples of D(p), the constant C_o is needed. The constant C_o is found by equating D(s) with the square root of equation (25a) for any ω.

Solving for the roots of the numerator of equation (14) is more difficult. Substituting s/j for ,

$$N(s)N(-s) = 1+\varepsilon^2 C_n^2\ (j/\alpha s) = 0. \qquad (26a)$$

Again utilizing p=1/s for simplification, equation (26a) can be written

$$1+\varepsilon^2 C_n^2\ (\frac{jp}{\alpha}) = 0. \qquad (26b)$$

With equation (15a),

$$C_n^2\left(\frac{jp}{\alpha}\right) = \cos\left(n\cos^{-1}\frac{jp}{\alpha}\right) = \pm j\,\frac{1}{\varepsilon}\,. \tag{26c}$$

In solving for p, the complex variable w is introduced,

$$w = u+jv = \cos^{-1}\frac{jp}{\alpha}\,. \tag{26d}$$

Substituting and equating real and imaginary parts,

$$\begin{aligned} \cos n\,w &= \cos(nu+jnv) \\ &= \cos(nu)\cosh(nv) - j\sin(nu)\sinh(nv) = \pm j\frac{1}{\varepsilon} \end{aligned} \tag{26e}$$

Hence,

$$\cos(nu)\cosh(nv) = 0$$

and

$$\sin(nu)\sinh(nv) = \pm\frac{1}{\varepsilon}\,. \tag{26f}$$

Cosh(nv) cannot be equal to zero for real v; therefore, cos(nu) = 0. The solutions for u are

$$u_m = \frac{\pi}{2n}(2m-1)\ , \text{ where } m = 1,2,\cdots,2n. \tag{26g}$$

For u_m, $\sin(nu_m)$ is equal to one. Solving the remaining equation of (26f),

$$\sinh(nv) = \pm\frac{1}{\varepsilon},\ \text{it follows that } v = \frac{1}{n}\sinh^{-1}\frac{1}{\varepsilon}\,. \tag{26h}$$

Rearranging equation (26d)

$$\frac{jp_m}{\alpha} = \cos w = \cos(u_m+jv), \quad \text{where } m=1,2,\cdots,2n. \tag{26i}$$

The n left half-plane roots are,

$$p_k = \alpha(-\sin(u_k)\sinh(v)+j\cos(u_k)\cosh(v)), \qquad (26j)$$

where k= 1,2,...,n.

The function N(s) is found by

$$N(s) = C_1[N(p) \mid_{s=\frac{1}{p}}].$$

The constant C_1 is needed for the same reasons that C_o was used in equation (25e).

To realize the benefit of the filter design, one must apply the above results to the noise-reduction systems in the references [1,2,5]. For comparison with [1,2,5] the amplifier gain in figure 2 will be 20dB The $G_f'''(j\omega)$ used for this example will be a third-order filter, having a filter gain, K_f, of -17dB and a ripple of 1.5dB. To obtain the value of ε, $\sqrt{1+\varepsilon^2}$ must be made 1.5dB greater than 1, that is

$$.\ 20 \log_{10} \frac{\sqrt{1+\varepsilon^2}}{1} = 1.5\text{dB}. \qquad (27)$$

Here ε is found to be .6423.

For a filter gain of -17dB, K_f from equation (17a) is

$$-17d_B = 20 \log_{10} \frac{1}{K_f} \qquad (28)$$

where K_f is found to be 7.079.

In this example, inequality (21) will be considered adequate; then from (20) α is found to be .7133.

These four parameters $(n,\alpha,\varepsilon,K_f)$ provide a good idea of what the normalized magnitude function $|G_f'''(j\omega)|$ will look like; the -3dB bandwidth frequency is at $\omega=1$; the corner frequency, where the ripple effect begins is at $\omega=1/\alpha$; magnitude function will swing between $1/K_f=.1413$ and $\sqrt{1+\varepsilon^2}/K_f = .1679$ exactly n=3 times. These characteristics are illustrated in figure 11.

Starting with equation (25d) the roots of the D(s) are found to be

$$p_1 = -.500 + j.866, \quad P_2 = -1.00, \quad P_3 = -.500 - j.866.$$

Multipling the roots together to form D(p),

$$\begin{aligned} D(p) &= (p+1.00)[(P+.500)^2+.866^2] \\ &= p^3+2.00p^2+2.00p+1. \end{aligned}$$

Using (25e),

$$D(p)\Big|_{s=\frac{1}{p}} = \frac{1}{s^3} + \frac{2.00}{s^2} + \frac{2.00}{s} + 1. \tag{29}$$

Before finding D(s), C_o of equation (25e) must be determined. As $\omega\to\infty$ for real frequencies $D(p)|_{s=1/p} \to 1$ (see (29)) but, $|D(s)|\to K_f$ (from the square foot of (25a)). Therefore, C_o must be equal to K_f (see (25e)). It follows that

$$D(s) = 7.079[\frac{1}{s^3} + \frac{2.00}{s^2} + \frac{2.00}{s} + 1]. \tag{30}$$

Using equation (26j) the roots are found to be

$$p_1 = -.1495+j.6696,\ P_2 = -.2990,\ P_3 = -.1495-j.6696.$$

Multipling the roots together to form N(p),

$$\begin{aligned} N(p) &= (p+.2990)[(p+.1495)^2+.6696^2] \\ &= p^3+.5980p^2+.5601p+.1407. \end{aligned}$$

Using (26k)

$$N(p)\Big|_{s=\frac{1}{p}} = \frac{1}{s^3} + \frac{.5980}{s^2} + \frac{.5601}{s} + .1407 \qquad (31)$$

As C_0 was evaluated C_1 is found to be K_f. Thus

$$N(s) = \frac{7.079}{s^3} + \frac{4.250}{s^2} + \frac{3.981}{s} + 1 \qquad (32)$$

Finally,

$$G_f'''(s) = \frac{s^3+3.981s^2+4.250s+7.079}{7.079s^3+14.16s^2+14.16s+7.079} \qquad (33)$$

The magnitude and phase functions of $G_f'''(j\omega)$ for real frequencies ω are shown in figure 12.

$G_f'''(s)$ is now used in the noise-reducing system in figures 3a and 3b (with amplifer gain K_a=20dB) to reduce the open-loop gain from K_a to K_a/K_f. Because the phase of $G_f'''(s)$ (for large n) can shift beyond -180 degrees for some frequencies, the open-loop gain $|K_aG_t|$ must be kept greater than unity until the open-loop phase returns to above -180 degrees. This is necessary to avoid encirclment of the (-1,j0) critical

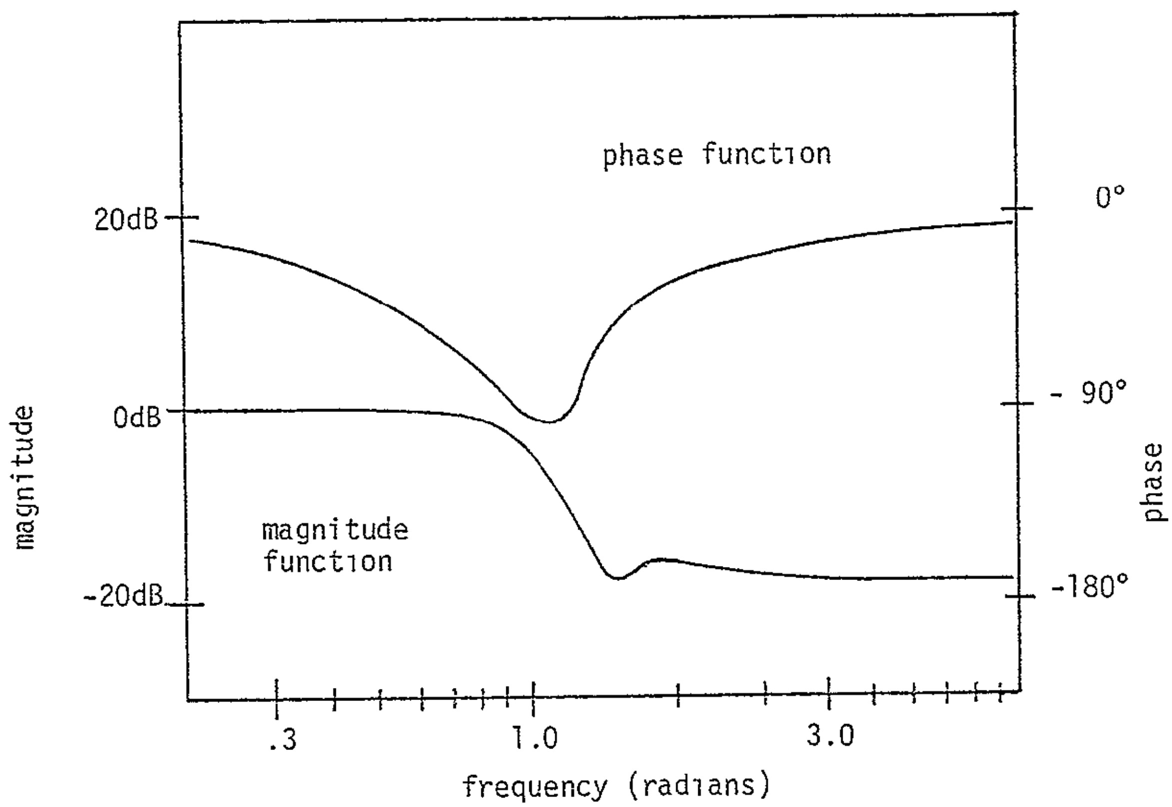

Third-order Butterworth-Chebyshev Filter

Figure 12

point on the Nyquist diagram. Subsequently, the magnitude must become less than unity before the open-loop phase function, which reflects the increasing negative phase of the time delay, returns below -180 degrees, see 13a and 13b.

This magnitude characteristic is not always guaranteed by $G_m(s)G_s(s)$. In this case, an additional lag pole will be necessary.

Through graphical manipulation (using figures 3a,3b,12a,12b), the open-loop transfer function characteristics in figure 13a and 13b were constructed. Here, the -3dB frequency ω_{-3dB} of $G_f'''(j\omega)$ is found to be 1.0KHz. The normalized filter function (33) is translated to the actual frequencies by replacing s in (33) by $s/2\pi(1000)$:

$$G_f'''(s)\Big|_{\omega_{-3dB}=2000\pi} = \frac{4.030\times10^{-12}s^3+1.01\times10^{-8}s+6.76\times10^{-4}s+7.079}{2.85\times10^{-12}s^3+3.59\times10^{-7}s^2+2.25\times10^{-3}s+7.079} \qquad (34)$$

Also, from figures 13a and 13b, it can be seen that a pole is needed near 2.2KHz to bring the magnitude function below unity. Now the open-loop transfer function in s for figures 13a and 13b is

$$|K_aG_t(s)| = 10\left[G_f'''(s)\Big|_{\omega_{-3db}=2000\pi}\right] \frac{1}{7.23\times10^{-5}s+1} \; \frac{1}{(3.98\times10^{-5}s+1)^2} \qquad (35)$$

In the above example the bandwidth was extended to 1000Hz with a third-order, maximally-flat, equal-ripple, lag-lead filter.

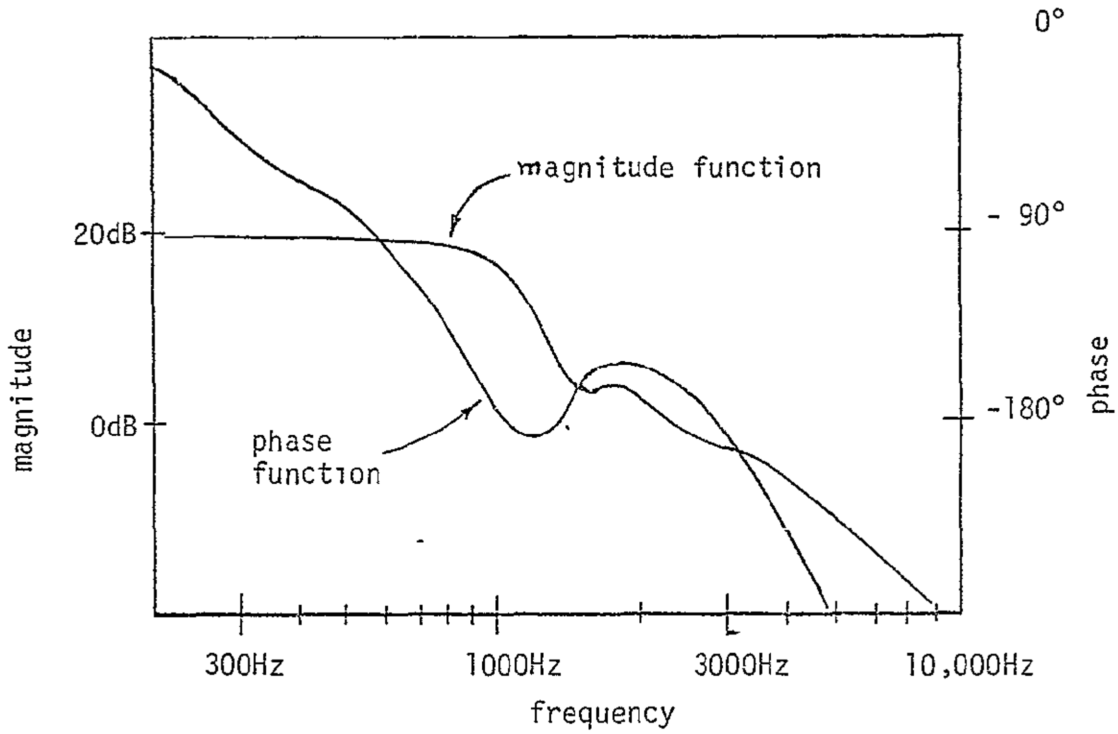

Olson's system with Butterworth-Chebyshev Compensation

Figure 13a

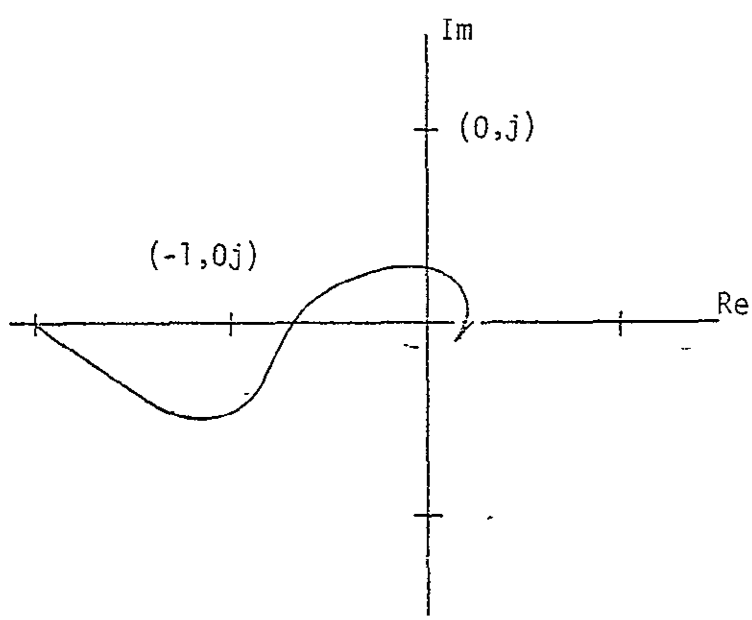

Nyguist diagram of Figure 13a

Figure 13b

CONCLUSION

The work reported upon here showed that, by using additional electronic filtering, the bandwidth of an active electronic noise reduction system could be increased by two octaves. This improvement was achieved through the use of the algebraically tractable Butterworth and Chebyshev functions. Also, filter parameters $(n,\alpha,\varepsilon,K_f)$ were chosen such that significant filter characteristics could be determined by inspection. Hence, by employing such an easily designed electronic filter, a significant improvement in active electronic noise reduction systems was realized.

For further improvements in system bandwidth, higher-order filter functions could be tried, in addition to types other than Butterworth and Chebyshev. Moreover, improvements which would reduce time delay in other system components should be investigated.

BIBLIOGRAPHY

1. H.F. Olson and E.G. May, "Electronic Sound Absorber", J. Acoust. Soc. Am. 25, 1130-1136 (1953).

2. H.F. Olson, "Electronic Control of Noise, Vibration, and Reverberation," J. Acoust. Soc. Am. 28, 966-972 (1956).

3. O. Bschorr, "Verminderung des Fluglarms durch gesteuerte Interferenz," Messerschitt-Bolkow-Blohm Gmbh, MBB Bericht Nr: BB-55-71 (1971), (in German).

4. G. Canevert and N. Jessel, "Les Absorbeurs Acoustiques Actif," 7th Internat. Congress on Acoustics, Budapest, 20 E 5, (1971), (In French).

5. W.F. Meeker, "Active Ear Defender System. Development of a Laboratory Model," NASA Contract No. AF 33(616)-3051, WADC Technical Report 57-368, (1960).

6. C.A. Ewaskio and O.K. Mawardi, "Electroacoustic Phase Shift in Loudspeakers", J. Acoust. Soc. Am., 444-448, (1950).